University of Naples Federico II

Department of Structures for Engineering and Architecture

(Di.St.)

PhD Program in Industrial Product and Process Engineering

(XXXIII cycle)

Coordinator: Prof. Andrea D'Anna

Francesca Autiero

PhD thesis

MULTISCALE APPROACH TOWARD THE ASSESSMENT AND CONSERVATION OF ARCHAEOLOGICAL HERITAGE AT POMPEII

Tutor: Prof. Andrea Prota

Co-tutor: Prof. Marco Di Ludovico

year 2021

ACKNOWLEDGEMENTS

Most of the work in this thesis was conducted at the Department of Structures for Engineering and Architecture of the University of Naples Federico II (DiSt), whereas an important part of the investigations was conducted *in situ* at the Archaeological Park of Pompeii (PAP). Moreover, a period of work (5 months) was conducted at the University of Minho (Guimaraes, Portugal), Institute for Sustainability and Innovation in Structural Engineering (ISISE).

First, I want to express my gratitude to Prof. Andrea Prota, supervisor of the thesis, for giving me the possibility of carrying out this research, which was for me a path of personal and professional growth. I owe a special thanks to Prof. Marco Di Ludovico, co-tutor of the thesis, for his continuous support and guidance. I also want to thank all the people at DiSt (colleagues, collaborators and friends) who, in different ways, significantly contributed and supported me during this journey.

I am grateful for the willingness and support from PAP, particularly Prof. Massimo Osanna, Arch. Annamaria Mauro, Arch. Bruno De Nigris, Dr. Alberta Martellone, and Eng. Vincenzo Calvanese, who allowed conducting all necessary inspections and surveys and provided precious information and documentation. I want to extend my gratitude to all the people I met and who supported me during *in situ* activities.

A special thank goes to Prof. Miguel Azenha and Prof. Paulo B. Lourenco from ISISE, Meera, Carolina and all the wonderful people I met in Portugal, who left their mark, both from a scientific and personal point of view.

Finally, this work would not be possible without my family, my friends and all those who accompanied me and believed in me. My deepest thank goes to them.

ABSTRACT

The protection and promotion of heritage structures must be addressed by following fundamental principles of compatibility, reversibility, distinguishability, and minimum intervention for the protection of both the material asset and intangible values. To do that, conservation, reinforcement, and restoration interventions of architectural heritage require multi-disciplinary approaches. Indeed, the achievement of comprehensive and detailed knowledge of the structural behavior and material characteristics of heritage structures is an essential part of the conservation and restoration process. The archaeological site of Pompeii was listed as a World Heritage Site for the outstanding value of its tangible and intangible heritage. The protection of this exceptional site set special challenges related to its great extension, the fragility of its built asset, and a large number of visitors hosted every day. Moreover, from a structural point of view, technical and conservation restrictions limit the possibility to perform extensive and in-depth investigation campaigns to characterize basic mechanical properties. This study was based on scientific cooperation between the Department of Structures for Engineering and Architecture (DiSt), of the University of Naples Federico II, and the authority of the Archaeological Park of Pompeii (PAP).

The research programme developed in this thesis aimed at providing fundamental mechanical information, which was still lacking in the literature, and suitable diagnostic methodologies, mainly based on non-destructive techniques and correlations with destructive test outcomes, to support structural assessment and conservation. For this purpose, the study was developed through multiscale diagnostic approaches and involved different types of activities and methodologies: extensive surveys; archival research; *in situ* inspections; in situ and laboratory testing involving both non-destructive and destructive methods; and numerical simulations. The research mainly focused on two typical constructive elements of ancient Pompeian architecture, among those most representative and vulnerable of the site: rubble stone masonry structures, traditionally known as *opus incertum;* and free-standing multridrum tuff columns.

The study of rubble stone masonry was developed through three main stages from the scale of the building materials to the scale of the masonry assemblages: i) the mechanical characterization of typical building materials (i.e. archeological stone units and mortars), which involved destructive tests (i.e. compression tests) and non-destructive tests (i.e. sclerometric tests and ultrasonic pulse velocity tests) performed on the stone units; ii) the characterization of archaeological masonry structures through *in situ* non-destructive tests, namely sonic pulse velocity tests; iii) the construction and characterization through non-destructive (i.e. sonic pulse velocity tests) and destructive tests (i.e. *in situ* diagonal compression tests and laboratory axial compression tests) of masonry panels reproducing the archaeological *opus incertum*. These were constructed by carefully following the ancient technique found at Pompeii and using original stone units and compatible mortar. Considering the impossibility of performing minor destructive tests or destructive tests on the archaeological materials, the extended and articulated investigation programme provided unique information on a very common masonry typology in heritage contexts.

As regards the study of the multidrum columns, it involved two main stages: i) extensive surveys and analyses of their geometrical features and the most widespread forms of degradation, affecting their stability and seismic response, which included an analysis of past structural interventions and their effects on the current state of preservation of the columns; ii) the numerical modeling of these elements and simulation of their seismic response, under different real seismic inputs. Systematic and detailed knowledge of the geometrical properties and state of preservation of a considerable number of free-standing multidrum columns allowed identifying columns being potentially more vulnerable than others; moreover, approximate formulations for a primary estimation of the stability of multidrum columns towards the seismic risk were derived from the numerical simulations.

In addition to that, a comprehensive and accurate research programme was developed for the design and characterization of a suitable repair mortar for structural interventions on archaeological structures. This part of the research was developed within a research visit at the University of Minho (Guimaraes, Portugal), Institute for Sustainability and Innovation in Structural Engineering (ISISE), and the research stay was coordinated and supervised by Prof. Eng. Miguel Azenha and Prof. Eng. Paulo B. Lourenco for ISISE. The mixture was prepared following traditional mix design and using raw materials as similar as possible to the ancient ones. In particular, precious and rarely available natural pozzolan from the Phlegrean area (i.e. the same volcanic region where the ancient Roman builders collected their pozzolan) was used. The experimental programme and the adopted methodologies were accurately controlled to monitor fundamental mechanical and physical properties of the mortar from the first days after the preparation up to 200 days, to provide useful information which is still lacking in the literature.

This study aimed at supporting the conservation and valorization of heritage assets of immeasurable value, by contributing to achieving adequate knowledge from a structural point of view. The attainment of that objective was intended based on the development of investigation approaches that are: i) compatible with conservation requirements; ii) repeatable and comparable with experimental campaigns carried out in other contexts; iii) representative of the vast built heritage of the site. The achieved information could represent a useful tool for the definition of appropriate choices and new methodologies for the design and planning of suitable interventions on the heritage structures.

Keywords

Archeological Pompeii Site, Rubble Stone Masonry, Multidrum Columns, Lime Putty and Phlegrean Pozzolan Mortar, Non-Destructive Tests (NDTs), Destructive Tests (DTs).

TABLE OF CONTENTS

LIST OF FIGURES

LIST OF TABLES

INTRODUCTION

The preservation of heritage structures requires the definition of restoration interventions that meet the principles of compatibility, reversibility, distinguishability and minimum intervention for the protection of both the tangible and intangible assets. To that aim, a comprehensive and interdisciplinary approach is needed to achieve an adequate knowledge of the structural properties of the ancient structures and their components (D'Agostino et al. 2009; ICOMOS 2003; Italian Ministry of Cultural Heritage and Activities 2010). The International Council of Monuments and Sites, ICOMOS, is a non-governmental international organization advisory body of UNESCO having the mission of promoting the conservation, protection, use and enhancement of monuments, built complexes and sites and providing charters and doctrinal documents for the definition of related principles and guidelines. A specific reference for the conservation and structural restoration of the architectural heritage is the ICOMOS Charter ratified by the ICOMOS 14th General Assembly in Victoria Falls, Zimbabwe, in 2003, *Principles for the analysis, conservation and structural restoration of architectural heritage* (hereafter be referred to as "the ICOMOS Charter"). In that document, the necessity to define specific recommendations concerning the conservation and restoration of the architectural heritage, addressing the limitations of technical codes defined for new and existing unprotected structures is stated. Among the main principles provided in the ICOMOS Charters for the conservation, reinforcement and restoration of architectural heritage are: i) the need for a multidisciplinary approach; ii) the necessity of implementing comprehensive and precisely defined methods, with an organization similar to those used in the medicine (i.e. anamnesis, diagnosis, therapy and controls); iii) the need of achieving the cost-effectiveness and minimal impact of all the process and consequently the possibility of repeating the phases of the method in an iterative process; iv) the prominence of an understanding of the structural and material properties of the building, achieved through historical, qualitative and quantitative methods; v) the importance of documenting all the phases; vi) the execution of interventions that should be indispensable, minimized, distinguishable, reversible, compatible and durable; vi) the preference for preventive maintenance rather than reparation and reparation rather than substitution; vii) the importance of checks and monitoring during and after the process.

As regards the national legislative framework, the Legislative Decree of 22 January 2004, no. 42, *Codice dei beni culturali e del paesaggio, ai sensi dell'articolo 10 della legge 6 luglio 2002, n. 137* (hereafter be referred to as "the Code") and subsequent modifications, represents the main regulatory framework in Italy as concerns the conservation, fruition and enhancement of cultural heritage. In the Code are now recognized as "cultural heritage" all the "immovable and movable things" "which have an artistic, historical, archaeological or ethnic anthropological interest" (D.Lgs 42 2004, Art. 10). According to Article 4 of the Code, the protection of the Italian artistic and cultural heritage is under the responsibility of the Italian Ministry of Cultural Heritage and Activities and Tourism (*Ministero per i beni e le attività culturali e per il turismo*, MiBACT). MiBACT has the responsibility to define "guidelines, technical standards, criteria and models of intervention regarding the conservation of cultural heritage" (Code, Art. 29). Therefore, MiBACT has provided guidelines and technical regulations to promote correct approaches to the prevention and reduction of risks and emergency management. The main technical reference is the Directive of the President of the Council of Ministers of 9 February 2011, *Direttiva del Presidente del Consiglio dei Ministri 9 febbraio 2011. Linee guida per la valutazione e la riduzione del rischio sismico del patrimonio culturale con riferimento alle nuove Norme tecniche per le costruzioni di cui al decreto del Ministero delle infrastrutture e di trasporti del 14 gennaio 2008* (hereafter be referred to as "the Guidelines"), although it has not been updated to the new version of the Italian Technical Standard of 2018. The Guidelines intend to define a path of knowledge, methodological approach for the definition of the safety level concerning the seismic risk (in consideration of the high level of seismic activity in Italy) and appropriate possible interventions, by adapting the principles defined for new and existing unprotected structures. Afterward, further prominent documents regarding the prevention and reduction of the seismic risk for the cultural heritage were provided based on the principles of the Guidelines: Circular no. 15 of 30 April 2015, *Disposizione in materia di tutela del patrimonio architettonico e mitigazione del rischio sismico*, by the General

Secretariat of MiBACT regarding the preservation of the structures, considered as "heritage of techniques and materials" and the Circular no. 15 of 5 April 2018, *Linee di indirizzo relative agli interventi afferenti al settore prevenzione del rischio sismico – Indicazioni tecniche,* other than specific documents concerning areas damaged by the earthquake of 24 August 2016 in the center of Italy (www.uss-sisma2016.beniculturali.it). A key part of the Guidelines is focused on the knowledge of the building is considered to be the fundamental prerequisite for both a reliable evaluation of the current seismic safety level and for the choice of effective seismic improvement interventions, as also pointed out by the ICOMOS Charter. According to the objectives of the interventions, different levels of knowledge can be achieved, depending on the accuracy of survey operations, historical researches and experimental investigations and all or just a part of the building can be involved. The process of knowledge is defined in the Guidelines in the following steps: i) identification of the building, taking into account the localization in areas subjected to specific seismic risk, the relationship with the surrounding urban context and the identification of any valuable elements which can affect the level of risk; ii) geometric survey of the building in its current state, including any cracking and deformation phenomena; iii) identification of the evolution of the building with the sequence of its transformation during the history and the definition of its hypothetical original configuration; iv) identification of the structural elements and the relative construction techniques, with particular attention to the constructive details and the connections between the elements; v) identification of the materials, their state of degradation and current mechanical properties; vi) investigation of the subsoil and condition of the foundation structures.

Despite different testing methods are available for the investigation of the mechanical properties of existing building materials and structures, involving destructive tests (DTs), minor-destructive tests (MDTs) and non-destructive tests (NDTs), adequate knowledge of typical constructive techniques and their mechanical properties in historical and archaeological contexts is still lacking. From the structural point of view, these data are generally incomplete related to the constraints to perform standard DTs and MDTs and still limited dataset related to NDTs. The limitations for the execution of DTs and MDTs are due to: i) conservation restrictions, preventing the execution of tests resulting in damage of the old structure of requiring the collection of large volume specimens; ii) technical limitations, for which it is complicated to obtain undamaged specimens. The limited information derived from NDTs are related to: i) studies and classifications of materials and construction techniques traditionally conducted with a different purpose; ii) lack of NDT methods that provide direct information on mechanical properties of materials and structures; iii) need to calibrate the results for the specific testing conditions and specimen typologies.

The importance to achieve adequate knowledge of cultural heritage structures by promoting the involvement of different expertise, methodologies and testing methods (with special attention to non-destructive and minor destructive methods) is not only highlighted by major legislative and recommendation of the field, but it was the main motivation of extensive research in recent years. These include major European projects among which: ONSITEFORMASONRY, PROHITECH, PERPETUATE, NIKER and STANDFORHERITAGE (www.cordis.europa.eu). In almost all of these, Italian institutions have been extensively involved, related to a great cultural heritage available in the country and the need to make a continuous effort to protect it. ONSITEFORMASONRY project (On-site investigation techniques for the structural evaluation of historic masonry buildings) had the main objective to develop methodologies for the structural evaluation of historic masonry structures, by promoting a diagnostic methodology based on NDTs and MDTs and combination of them intended to better analyze, predictand early prevent environmental damages of cultural heritage (caused by ageing, microclimate, seismic and traffic vibrations and by dead load) (www.ndt.net). The project has been developed between 2001 and 2004 and coordinated by the Federal Institute for Material Research and Testing (Germany) with the participation of thirteen European bodies, among which five Italian ones. The research particularly focused on the following testing methods: ground penetrating radar (GPR), ultrasonics, impact-echo and sonics (particularly sonic tomography) as NDTs, and endoscopy, flat-jack and core-drilling and MDTs. The investigations involved both real case studies and masonry specimens constructed to represent historical typologies. The other projects mentioned above particularly focused on the protection of cultural heritage from seismic risk, taking into account the intense seismic activity of the Mediterranean area. PROHITECH project (Seismic Protection of Historical Buildings by Reversible Mixed Technologies) aimed at developing sustainable methodologies for the seismic protection of existing structures and particularly heritage structures by promoting reversible mixed technologies. These latter concern the combined use of different innovative materials and special devices, in the respect of the principle of reversibility of interventions. The project has been developed between 2004 and 2008 and coordinated by the University of Naples Federico II (Italy) with the participation of fourteen European bodies, among which three Italian ones. PERPETUATE project (Performance-based approach to the earthquake protection of cultural heritage in European and Mediterranean countries), on the other hand, addressed the evaluation and mitigation of seismic risk to cultural heritage assets, particularly focusing on the need to improve methods of analysis and assessment procedures rather than intervention techniques. The project has been developed between 2010 and 2012 and coordinated by the University of Genoa (Italy) with the participation of ten European bodies, among which four Italian ones. The research resulted in European guidelines for the seismic preservation of cultural heritage assets structured on three main steps: i) assessment of the seismic input; ii) modeling the seismic response; and, iii) rehabilitation decisions. NIKER project (New integrated knowledge-based approaches to the protection of cultural heritage from earthquake-induced risk) (www.niker.eu) aimed at developing a new integrated methodology for the protection of cultural heritage structures from the seismic risk based on a multidisciplinary approach for the development of innovative materials and systems for low-intrusiveness, compatible interventions. It looked at the concept of optimized intervention, in the respect of the principles of “minimum intervention”, authenticity and compliance with the original structural concept. The project resulted in a comprehensive database linking earthquake-induced failure mechanisms, construction types, materials, interventions and assessment techniques. It has been developed between 2010 and 2012 and coordinated by the University of Padua (Italy) with the participation of seventeen European bodies, among which two Italian ones. Finally, STAND4HERITAGE project (New STANDards for seismic assessment of built cultural HERITAGE) started in 2019 and is still ongoing (it will end in 2024), being hosted by the University of Minho (Portugal) (www.stand4heritage.org). It is particularly focused on the development of approaches for seismic response prediction of masonry structures, involving both numerical and analytical studies and shaking-table experimentations.

Within this framework, archaeological contexts still require a specific research effort, to define proper investigation and assessment methodologies taking into account the particular fragility and stratification of this type of assets. In particular, the preservation of archaeological heritage at the Pompeii site set a special issue as regards the protection of material and intangible testimonies of inestimable value and the huge number of visitors hosted every day. From 2012, a general plan of intervention started with the *Great Pompeii Project* (GPP). The project aimed to improve the conservation conditions of the archaeological structures based on an in-depth knowledge programme (De Nigris and Previti 2017). Moreover, multidisciplinary studies were developed in the last decades within the site aimed at defining new, suitable and comprehensive diagnostic approaches. Among these is the project “Pompei - *Insula* del Centenario (IX, 8)” developed between 1999 and 2006 by the University of Bologna, Alma Mater Studiorum, which investigated the *Insula* through accurate archaeological and archaeometrical analyses. The research also involved structural analyses based on numerical modeling of the masonry structures for their structural assessment in the current conditions and with possible interventions. However, an experimental programme for the mechanical characterization of materials and structures was not involved in the project and the structural analyses were based on the results of geometrical surveys and material mechanical properties from the literature and guidelines prescriptions. The “Villa of Diomedes project” as a part of the ANR RECAP programme between 2015 and 2019 (RECAP: Rebuilding after an earthquake: Ancient experiences and innovations in Pompeii) coordinated by the École Normale Supérieure (France) (www.villadiomede.huma-num.fr). The project involved several disciplines: archaeology, structural engineering, computer science, 3D modeling, Earth science. A qualitative structural assessment of the Villa was based on non-destructive methods involving visual inspections, sonic pulse velocity tests and tomography, video endoscope, and dynamic identification (Dessales et al. 2020). The project of the University of Padua MACH (Multidisciplinary methodological Approaches to the knowledge, conservation and valorization of Cultural Heritage: application to archeological sites) studied between

2015 and 2017 the Sarno Bath (*Regio* VIII, *Insula* 2), involving the university departments of structural engineering, cultural heritage and geoscience (www.unipd.it). From a structural point of view, the study focused on the qualitative assessment of masonry structures by using NDTs (particularly sonic pulse velocity tests and tomography, video endoscope, infrared thermography and ambient vibration tests (Valluzzi et al. 2019)).

Against that background, further information for the structural evaluation of archaeological structures at Pompeii (and similar contexts) is still required. In particular, multiscale approaches to the mechanical characterization from the scale of the single building materials to the scale of the structures; combined approaches involving NDTs and DTs and relatives correlations; formulations for a simplified primary assessment of typical archaeological structures; information on the structural compatibility of suitable repair materials are still lacking.

Research objectives and organization

The present work aimed at providing fundamental mechanical information, which was still lacking in the literature, and suitable diagnostic methodologies. Multiscale approaches were developed, mainly based on non-destructive techniques and correlations with destructive test outcomes, to support structural assessment and conservation. The investigations mainly focused on two typical constructive elements of ancient Pompeian architecture, among those most representative and vulnerable of the site: rubble stone masonry structures, traditionally known as *opus incertum*; and free-standing multridrum tuff columns. The study was based on scientific cooperation between the Department of Structures for Engineering and Architecture (DiSt), University of Naples Federico II, and the Archaeological Park of Pompeii (PAP). In particular, this involved the three-year agreement n. 22 of 19/03/2018, whose coordinators were Prof. Eng. Andrea Prota for DiSt and Prof. Massimo Osanna for PAP, and the scientific representatives were Prof. Eng. Andrea Prota for DiSt and Dr. Alberta Martellone and Arch. Bruno De Nigris for PAP, and the implementing agreement of 13/11/2019 whose scientific representative was Arch. Annamaria Mauro for PAP. Furthermore, a specific research programme was developed for the design and characterization of a suitable mortar for structural interventions on archaeological structures, to provide a useful and reliable tool to approach the process of restoration at the Pompeii site or similar contexts. This part of the research was developed within a research visit at the University of Minho (Guimaraes, Portugal), Institute for Sustainability and Innovation in Structural Engineering (ISISE) to cooperate in the field of ancient masonry mortars. The mission was coordinated and supervised by Prof. Eng. Miguel Azenha and Prof. Eng. Paulo B. Lourenco for ISISE.

The thesis is organized into six chapters. The first presents a brief overview of the historical background of Pompeii, focusing on the history of the ancient city, the post-excavation history of the archaeological site and the historical evolution in recent years, particularly concerning the Great Pompeii Project and the new excavations started in 2018 at *Regio V*.

The second chapter focuses on the characterization of original building materials collected throughout the excavations at the *Regio V*. They were rock units and pieces of mortar from newly excavated *opus incertum* masonry structures. The characterization involved the execution of NDTs and DTs on the rock units and DTs and the mortar.

The third chapter focuses on the non-destructive characterization of archaeological *opus incertum* masonries, involving newly emerged walls at *Regio V* and formerly emerged walls that already were restored in the past after excavations carried out in the 19th and 20th centuries at *Regio V* and at Villa of Diomedes (located in the North-West corner of the site). The chapter describes the adopted investigation protocol and detailed analysis and discussion of the experimental outcomes. Comparisons with available literature data concerning different masonry typologies at the Pompeii site are also presented.

The fourth chapter focuses on the characterization of Pompeii-like rubble stone masonry panels through NDTs and DTs. Indeed, given the impossibility of performing DTs or MDTs on archaeological structures for conservation reasons, this experimental programme involved the realization and characterization of new rubble stone masonry panels compliant with the ancient building technique *opus incertum.* The panels were produced following the ancient technique with the use of original rock units and new mortar compliant with the ancient one. This latter was produced with precious volcanic sand coming from the same volcanic region where the ancient builders collected their *pulvis puteolanus*, i.e. the Phlegrean area, next to the Bay of Naples. The characterization involved extensive sonic tests, three diagonal compression tests conducted at the Pompeii site and axial compression tests conducted in the laboratory. The chapter also presents comparisons of the results of NDTs and DTs carried out on the Pompeii-like masonry panels and available from the literature, to derive useful correlations for the assessment of ancient structures.

The fifth chapter concerns the study of free-standing multidrum tuff columns. This involved columns in four areas of the site representative of typical column-types (*Casa del Fauno* at *Regio VI* and *Quadriportico dei Teatri*, *Foro Triangolare* and *Palestra Sannitica* at *Regio VIII*), presenting nowadays cracks and detachments which may affect their safety and aesthetics. The study involved an extensive campaign survey for the definition of the mean geometrical properties affecting the dynamic behavior of the columns and the recognition of the most common forms of degradation. A critical analysis of past interventions performed on the columns, specifically focusing on the most degraded ones, is reported. Moreover, a numerical analysis based on the Finite Element Method of the seismic behavior of columns from the *Casa del Fauno* was performed, to assess the seismic capacity of these elements.

The sixth chapter focused on the definition and comprehensive characterization of the repair mortar made with lime putty and pozzolan sand from the Phlegrean region. This involved the definition and preparation of the mortar compliant with traditional techniques typically encountered in the ancient Pompeii and Vesuvius surrounding area. Therefore, the evolution of the main mechanical and physical properties of the mixture was monitored for up to 200 days, based on standard procedures. Moreover, the hardening process was monitored through Differential Thermal Analysis up to 90 days, considering different depths from the external surface of the mortar.

Finally, final remarks and possible future research actives are discussed in the conclusions.

1. THE ARCHAEOLOGICAL SITE OF POMPEII

The archaeological site of Pompeii is one of the most popular ones in Italy and the world with more than three and a half million visitors a year (www.pompeisites.org). It is located inside the modern city of Pompei in the province of Naples, Italy, and covers an area of 85ha (to which are added about 1ha of Villa of the Mysteries). For the preciousness of its tangible and intangible heritage, the ancient city of Pompeii is recognized as UNESCO's World Heritage site since 1997, together with the archaeological areas of Herculaneum and Torre Annunziata (Figure 1).

The site is nowadays managed by the Archaeological Park of Pompeii (*Parco Archeologico di Pompei*, PAP), which is a regional agency of the Italian Ministry of Cultural Heritage and Activities and Tourism (*Ministero per i beni e le attività culturali e per il turismo*, MiBACT) aimed at the preservation and promotion of public use of the archaeological site.

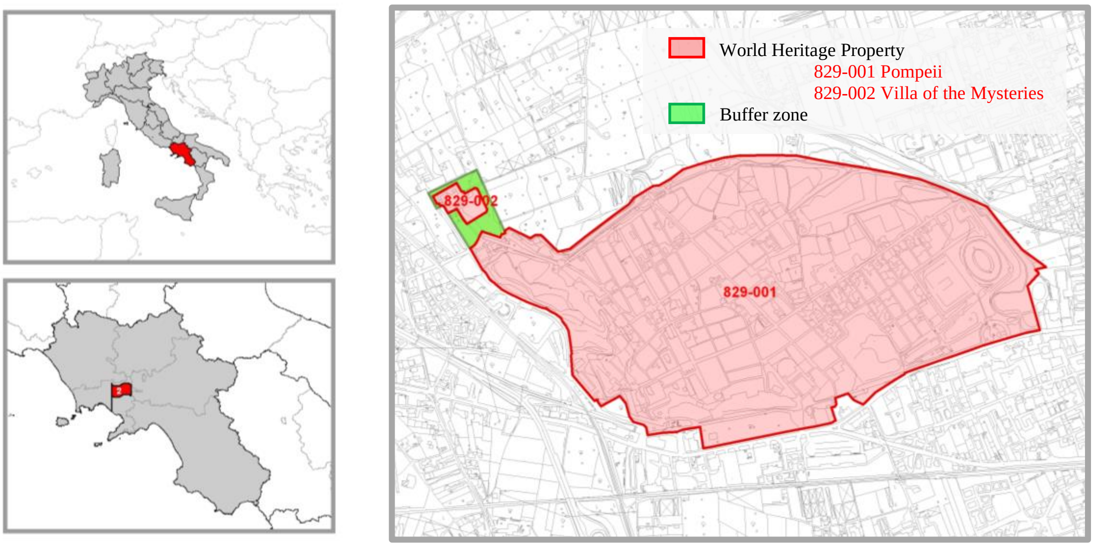

Figure 1. Localization in the province of Naples, Italy, and delimitation of the archaeological area of Pompeii (ancient city and Villa of the Mysteries) with its buffer zone [drawn from www.whc.unesco.org].

1.1. Historical background of the ancient city

The origins of the ancient city of Pompeii can be dated back to between the final phase of the Bronze Age and the beginning of the Iron Age (XI-VIII century BC) when small and sparse settlements in the Sarno Valley had a period of prosperity, related to commercial links with Greek and Etruscan settlements in Campania (Capasso 2002; Pesando 2012; Pesando and Guidobaldi 2006). However, the first urban settlement was founded by the Oscan, an italic people, in the Archaic period (i.e. around VI century BC). The ancient city was situated on a lavic plateau at a height of about 30-40 meters above sea level, close to the mouth of the river Sarno, the sea, and Mount Vesuvius. At the time this latter had a conical shape, different from the current crater-like shape which resulted from the eruptions of 79 AC, 1609 and 1944 (Pesando 2012). After being subjected to the Greek and Etruscan influences, at the end of the V century BC, the ancient city was occupied by the Samnites (i.e. another italic people) and returned to use the Oscan language (Capasso 2002).

In the IV century BC, particularly with the Second Sannitic War, the city went under the domination of the Romans. During the II century BC, under Roman domination, the ancient Pompeii lived the so-called “golden century”. In that period Pompeii was an important port city, where few powerful and rich families invested their wealth in agriculture (especially wine-producing) and artisanship (particularly the productions of ceramics and clay tiles). Works of public interest and embellishing the city were carried out in that age, improving the conditions of the entire city (Pesando and Guidobaldi 2006). In the I century BC the city, alongside other peoples allied of Rome, Pompeii revolted against the Romans to claim full citizenship rights, but it was sorely defeated by the dictator Lucius Cornelius Silla in 80 BC. Thus the city became a Roman colony and the lands of the old noble families were transferred to the veterans of Silla’s army. In the following decades between the late Republican Age and the early Imperial Age, the city experienced important changes in authorities, laws and customs, and finally integrating into the Empire.

In 62 AC, according to the chronology given by Tacitus (*Annales*, XV, 22; while 63 AC was indicated by Seneca in *Naturales Quaestiones*, VI, 2), a strong earthquake struck Campania and particularly involved the ancient cities of Pompeii and Herculaneum. That earthquake was probably the most intense of a series of seismic events that occurred in the region at that time (Pesando and Guidobaldi 2006). While A. Maiuri (Superintendent at Pompeii between 1924 and 1961) referred to seism as occurred in the year 63 AC (Maiuri 1942), more recent references support the dating of the year (Adam 1986; Dobbins 1994; Guidoboni et al. 2007).

Figure 2. Relief of the lalarium of Lucius Cecilium Iucundus showing the Forum of Pompeii (a); relief showing Porta Vesuvio [Maiuri A., 1942].

A relatively short time after, the eruption of Vesuvius of 79 AC buried the ancient city under a thick layer of volcanic ash and stones, while it probably had not yet fully recovered from the seismic event. The eruption, if on the one hand ended the life of the ancient city of Pompeii, on the other, it allowed preserving its history to the present day. Indeed, despite Emperor Tito delivered aids to the affected areas immediately after the eruption, the ancient Pompeii was not reconstructed and resettled. Apart from some looting aimed to retrieve materials and valuable assets, the ancient city has been buried until the modern-day.

1.2. Post-excavation historical background

The first discovery of the ancient city of Pompeii can be dated back to the construction of the Sarno Channel between 1592 and 1600, under the direction of Domenico Fontana. However, at that time the site was identified with the ancient city of *Stabiae*, and not systematically brought to light. Official excavations of Pompeii started only in the 18th century, by order of the Bourbon King of Naples Carlo II in 1748, after the fortuitous discovery of the ancient theatre of Herculaneum in 1710 (Pesando and Guidobaldi 2006). Those excavations were executed according to the “tunneling” technique and had the main purpose to discover valuable assets for the Royal collection in the Palace of Portici (www.whc.unesco.org, www.pompeisites.org). At the same time, the interest of the aristocracy in the ruins of Pompeii made it a fundamental destination of the *Grand Tour*.

The scientific and systematic approach to the excavation began with the Unification of Italy under the direction of Giuseppe Fiorelli (1860-1875), when the ancient city was organized into districts, *Regiones*, and isolates, *Insulae*. From that phase, the technique of creating plaster casts for the conservation of organic elements during the excavation was used. To provided a realistic representation of the ruins, Fiorelli ordered the creation of a model of the city, which was executed by Felice Padiglione between 1861 and 1879. The model was made with cork and wood and is nowadays conserved in the Archaeological Museum of Naples (Figure 3).

Figure 3. View of the 1:100 model of the ruins of Pompeii created under the direction of Giuseppe Fiorelli in 1860 and preserved in the National Archaeological Museum of Naples [photo by Thomas Crognier].

From 1911, with the direction of Vittorio Spinazzola, the excavation was conducted by using a new technique, proceeding from the top down, and always complementing the work with restoration and reconstruction interventions as the buildings were uncovered. This allowed bringing to light walking routes and multi-level buildings. In particular, Spinazzola transferred the focus of the explorations in Pompeii from the north of the city to the path *via dell'Abbondanza,* particularly in the areas between *via Stabiana* and the amphitheater, which was called the "Nuovi Scavi"(Spinazzola 1953) (Figure 4).

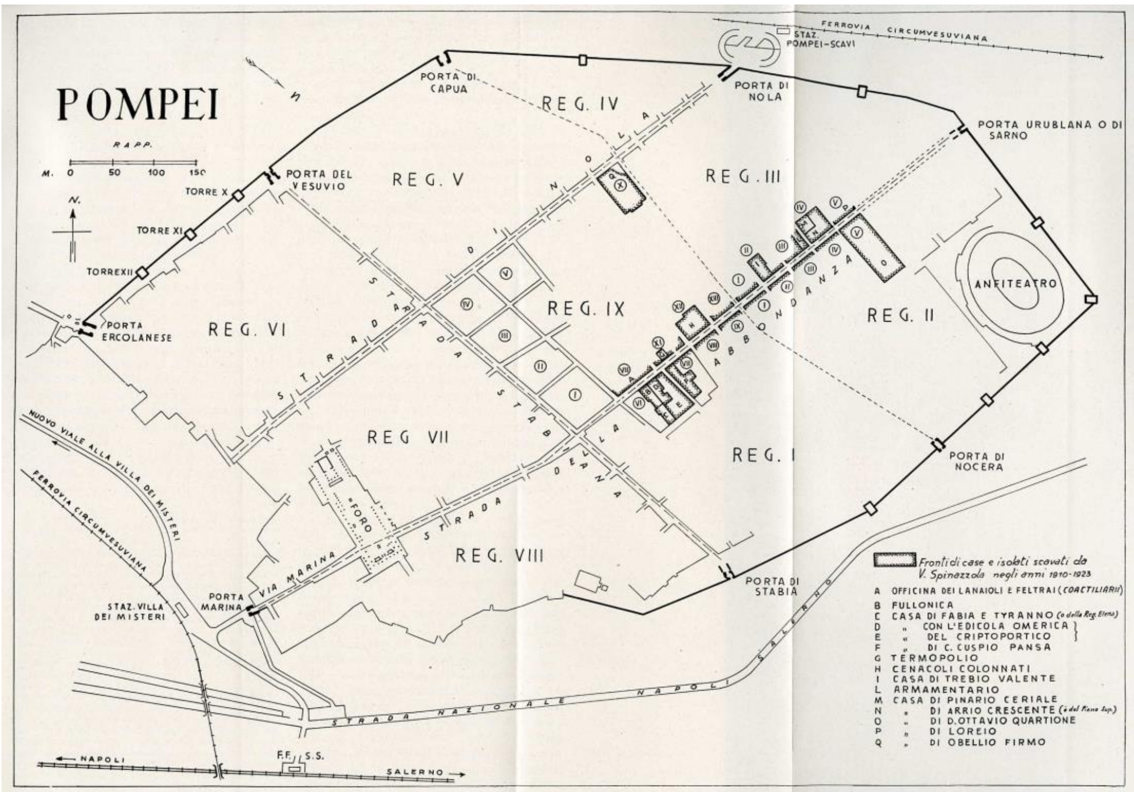

Figure 4. Excavated fronts of buildings and Insulae *under the direction of V. Spinazzola between 1910-1923 [dranw from Spinazzola, 1953].*

In 1923 Spinazzola was relieved from his post of Superintendent of Archeological Works by the fascist regime and followed by Amedeo Maiuri between 1924 and 1961. During his long direction, Maiuri directed systematic explorations in many regions of the sites and the area surrounding the Bay of Naples (www.pompeiiperspectives.org).

In 1943, the site was hit by allied bombing (Figure 5 and Figure 6) antiquities during the Second World War. Maiuri worked to protect the site and its and to reconstruct the structures that had been damaged. In particular, Maiuri implemented six types of actions (Picone 2011): i) covering the damaged spaces for weathering protection; ii) recovery of the archaeological material for restoration and reconstruction interventions; iii) recomposition and relocation in situ of paintings and stucco-works; iv) recovery of the archaeological asset from the Museum, *Antiquarium* and Forum; v) restoration and reconstruction of the *Domus*, with priority for the most significant and visited ones. Among this latter, *Casa del Fauno* was one of the first interventions, started in January 1944, referred to in Chapter 5.

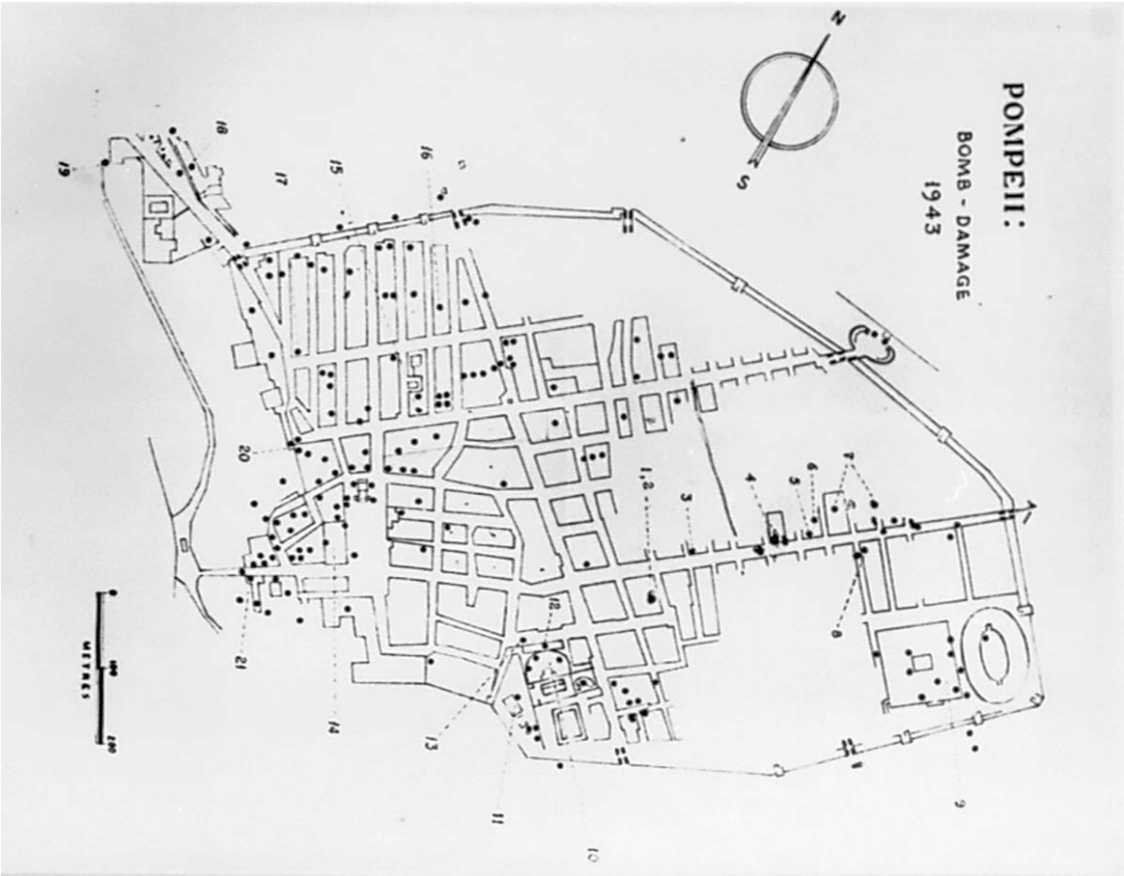

Figure 5. Plan of Pompeii 1943 showing where bombs landed and bomb damage [drawn from www.pompeiiinpictures.com].

(a)

(b)

Figure 6. Historical photos of structures damaged by bombing in 1943 [drawn from Spinazzola, 1953]: Case dei Cenacoli Colonnati *(a);* Casa del Criptoportico *(b).*

On November 23rd, 1980, a devastating earthquake hit the Irpinia region, about 40 kilometers east of Naples with widespread damage in Campania, Basilicata and partially Puglia Italian regions. The event required the implementation of emergency shoring, repairs and reconstructions for many archaeological structures at Pompeii (Figure 7).

(a)

(b)

Figure 7. Historical photos of emergency shoring after the earthquake in 1980 in via dell’Abbondanza *[drawn from www.pompeiiperspectives.org].*

After the earthquake, in 1981 the authority for the management and protection of the site was instituted with the name of “Archaeological Superintendence of Pompeii” (*Sovrintendenza Archeologica di Pompei*), covering other sites in the area surrounding the Vesuvius. Thereby, the management of these areas was detached from the rest of the province of Naples and the National Archaeological Museum, which contained the antiquities from the excavations of Pompeii and Herculaneum, in addition to the Farnese collection, as the behest of the Bourbons (www.pompeiisites.org).

In 1997, together with the archaeological areas of Herculaneum and Torre Annunziata, the site was included the World Heritage List of UNESCO for the preciousness of its tangible and intangible heritage (Figure 8). According to UNESCO, the outstanding universal value of the site lies in three main points: i) the exceptionally good preservation and extent of the ancient city (together with Herculaneum) with no parallels in the world; ii) the preservation of details of the urban, architectural, decorative and daily life aspects of the ancient Roman society from the 1st century BC to the 1st century AD; iii) the preservation of a vivid and comprehensive picture of Roman society at one precise moment: the eruption of Vesuvius in 79 AD (www.whc.unesco.org). In the same year, the Superintendence obtained full scientific, organizational, administrative and financial autonomy. After some successive modifications, the institution obtained its current denomination in 2017, concurrently with the separation of the authority for the archaeological site of Herculaneum, which has become the “Archaeological Park of Herculaneum” (www.pompeisites.org).

Figure 8 shows the plan of Pompeii with the identification of the *Regiones*. Each of them, as well as the *Insulae* and buildings, is distinguished by a progressive number so that every single building is univocally identified and localized in the site by an alphanumeric code, of the type *R.I.B*, where *R* is the number of the *Regio* in Roman numerals (from I to IX), *I* is the number if the Insula and *B* is the number of the building.

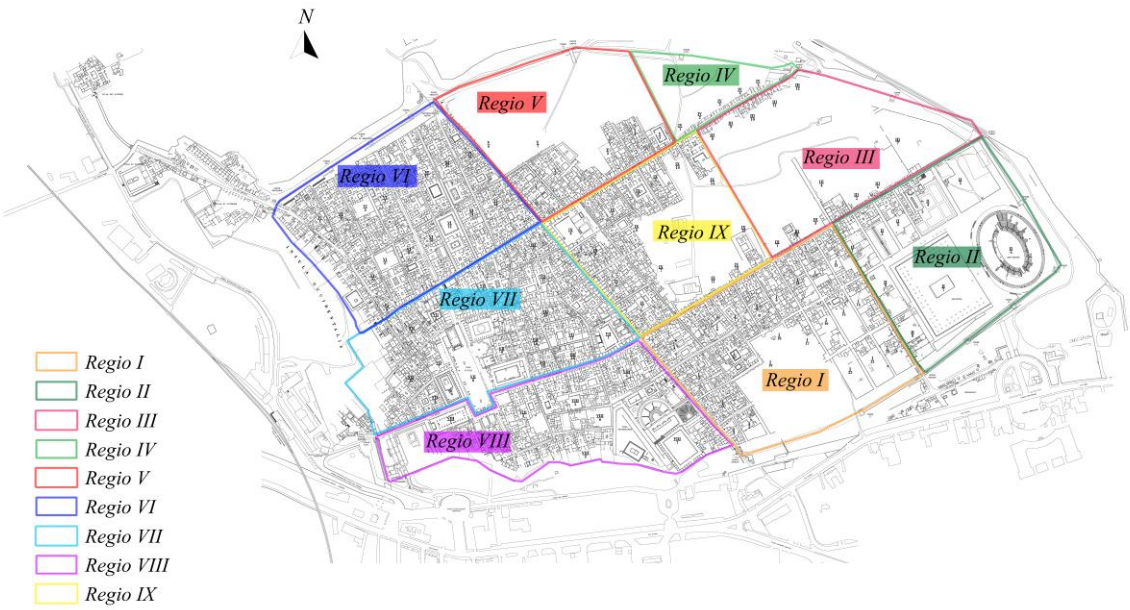

Figure 8. Plan of the archaeological site of Pompeii with the identification of the Regiones.

1.3. The Great Pompeii Project and the excavation in *Regio V*

In 2011 the Italian government (law no. 34/2011, Art. 2) urged the implementation of a specific and urgent programme for the conservation, maintenance, and restoration of the archaeological site of Pompeii. This led to the Great Pompeii Project (GPP), which aimed to promote the effectiveness of conservation action at the site with the establishment of a “planned conservation”, which is based on the definition of a suitable plan for scientific and technical studies aimed at the diagnosis, expansion of scientific knowledge, and providing the direction of the operational choices. The project relied on the Protocol of Legality, signed in 2012, for the Inter-institutional Agreement on Legality and Security between the Italian Ministry of Territorial Cohesion, Ministry of Cultural Heritage and Activities, Ministry of the Interior, Ministry of Education, Universities, and Research, and the President of the Authority for the Supervision of Public Contracts. GPP involved European and national funds and the main areas of the intervention included (www.pompeiisites.org):

- reduction of the hydro-geological risk on the excavation fronts;
- securing the *insulae*;
- consolidation and restoration of masonry;
- consolidation and restoration of decorated surfaces;
- protecting buildings from weather exposure;
- improvement of the video surveillance system.

For its implementation, GPP was divided into 5 operational projects (www.grandepompei.beniculturali.it):

- Plan of knowledge, aimed at defining continuous and progressive actions for the survey, monitoring and assessment of the state of preservation of structures and decorations;
- Plan of work, involving restoration interventions defined based on the advance of the knowledge;
- Plan for the fruition, aimed at the improvement of services for visitors and to enhance communication activities;
- Plan of the safety, involving interventions to strengthen surveillance conditions;
- Plan of strengthening and capacity building SAPES, for the improvement of the technical operational capabilities and the relative endowment of the Superintendence of Pompeii.

The actions under the GPP were concluded in 2019, with a total of 76 executed interventions, shared among the 5 operational plans, 45 restored and secured buildings (www.ponculturaesviluppo.beniculturali.it).

One of the most important and the most popular intervention concluded under the GPP was the new excavation of the so-called “wedge”, *cuneo*, in *Regio V*. The new excavation involved an area of 2000 m^2 and was a part of a larger safety intervention involving more than 2.7 km of excavation faces bordering an unexcavated area of about 22 ha, intended to redress the fronts and protect the archaeological structures that emerged already in the 19^{th} century. The “wedge” consisted of the area located between the *Casa delle Nozze d’Argento* and the *Vicolo di Marco Lucrezio Frontone* (Figure 9).

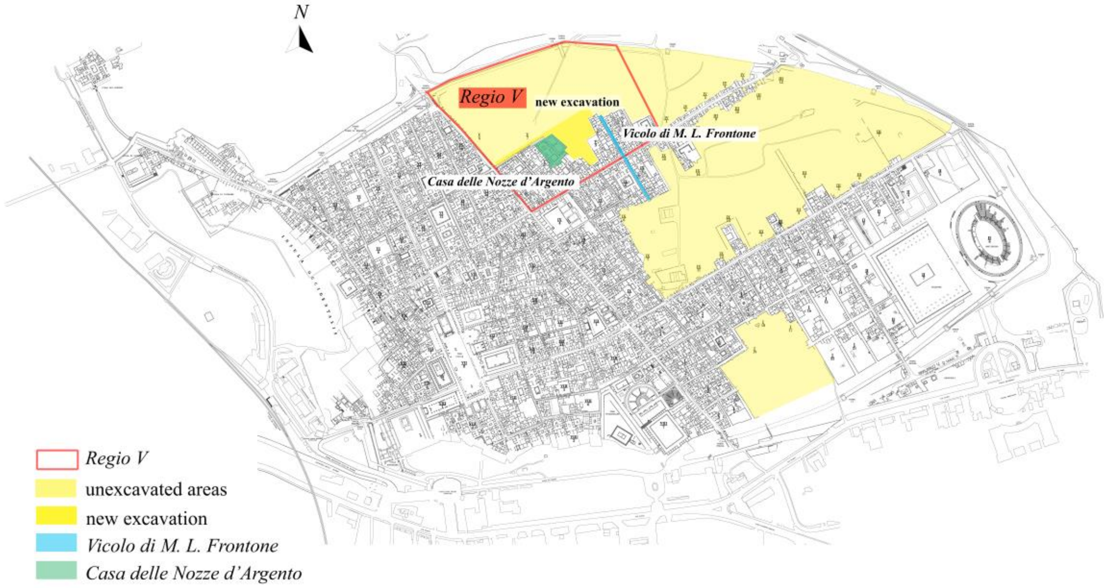

Figure 9. Plan of the archaeological site of Pompeii with the indication of the Regio V *borders, the unexcavated areas,* Casa delle Nozze d’Argento *and* Vicolo di M. L. Frontone.

The new excavation brought to light a part of the city that has never been investigated before, with the recovery of significant data for the knowledge of the ancient city and exceptional discoveries. Throughout the work, 2 entire *domus* emerged, *Casa del Giardino* and *Casa di Orione*, and an alleyway, *Vicolo dei Balconi*, which reconnected the street *Via di Nola*, already opened to visitors and the alleyway *Vicolo delle Nozze d’Argento*, which was previously only partially brought to light. Moreover, the house

Casa di Leda e il Cigno emerged along the street *Via del Vesuvio* (www.ponculturaesviluppo.beniculturali.it).

2. CHARACTERIZATION OF ARCHAEOLOGICAL BUILDING MATERIALS

Different methodologies are available for the investigation of the mechanical properties of existing building materials and structures, involving destructive tests (DTs), minor-destructive tests (MDTs) and non-destructive tests (NDTs). Standard DTs can be performed on portions of single building materials or structures extracted and tested in the laboratory. DTs can also be performed *in situ* on single building materials or properly insulated portions of masonry structures. The most common DTs used for masonry structures are: axial compression test, diagonal compression test and shear-compression test (Borri et al. 2011; Brignola et al. 2009; Chiostrini et al. 2000; Milosevic et al. 2013a; Silva 2012; Valluzzi 2000; Vasconcelos 2005). MDTs are typically performed *in situ* and the most common among them are: single flat-jack test, double flat jack test, shove test and dilatometer test for masonry structures (Binda et al. 2000, 2004); penetration tests applied to mortar joints; pull-out test usually applied to stone or brick elements (Binda 2005; McCann and Forde 2001). NDTs are commonly used for the characterization of single building materials or structures *in situ*, but they can also be performed on specimens in the laboratory. Among the most common NDTs are: sonic/ultrasonic methods (e.g. direct, semi-direct and indirect sonic test; sonic tomography; impact echo; ultrasonic test); endoscopy; infrared thermography; radar scanning; rebound hardness methods (Schmidt hammer or pendulum); ambient vibration test (Binda et al. 2000; Colla et al. 1997; McCann and Forde 2001; RILEM TC 1996, 1998).

However, as regards the cultural heritage, the use of DTs and MDTs is limited for both conservation and technical issues, given that the extraction of undamaged specimens is particularly difficult in historical and archaeological contexts. DTs and MDTs should be performed only when they are indispensable for the structural assessment and definition of interventions. When possible, a limited number of DTs or MDTs is generally allowed, thus the significance of each of their results must be evaluated before their execution, also considering the possibility of obtaining an individual data element. NDTs, on the contrary, are sustainable in terms of i) conservation of the built asset; ii) moderate cost; iii) relatively short implementation. However, NDTs can provide only a qualitative evaluation of the homogeneity of the mechanical parameters of the materials and the structures, or an indirect estimation of the mechanical parameters based on empirical correlations. Moreover, their results depend on the investigated material or structure typology and the test conditions and they should be calibrated on the outcomes of destructive tests.

The new archaeological excavations started in May 2018 at *Regio V* of the Pompeii site (Figure 9) gave the great opportunity to survey and analyze constructive materials and structures that emerged for the first time since the eruption of the Vesuvius in 79 A.D. As regards the characterization of building materials, five pieces of mortars from three different locations of the excavation area and ten stone units of three different rock types (travertine, lava and foam lava) belonging to archaeological masonry structures involved in the eruption were collected and tested according to standard methods. In particular, standard cubic specimens of mortar were tested in uniaxial compression and stone units and standard cubic specimens obtained from them were subjected to ultrasonic pulse velocity tests, UPV, Schmidt hammer rebound tests, SHR, and finally to uniaxial compression tests.

In the following paragraphs, the experimental programs carried out for the investigation of the main mechanical properties of original mortar and stone units are described and the experimental outcomes are reported and discussed. Moreover, as regards the characterization of the stone units, correlations among the results of NDTs and DTs are provided as a tool for the estimation of the main mechanical properties of similar materials.

2.1. Characterization of archaeological mortars

Fundamental mechanical properties of mortar specimens (i.e. flexural and compressive strength) can be obtained through standard tests codified by the European Standard EN 1015-11 (CEN 2007a) for standard-size specimens (i.e. three prismatic specimens 40mm x 40mm x 160mm are subjected to three-point bending test to obtain flexural strength, then the two resulting halves from each prism are subjected to uniaxial compression test to obtain compressive strength). Given the restriction to extract standard size specimens from heritage masonry structures and the technical difficulties to obtain undamaged specimens of mortar, some methodologies to obtain flexural and compressive strength on small specimens were also implemented (Binda 2005; Drdácký et al. 2008). However, it should be considered that: i) standard tests are generally more reproducible; ii) non-standard tests results are not directly comparable with standard tests results; iii) small specimens obtained from mortar joints can be degraded; iv) to obtain undamaged small-size specimens, the sampling of an entire piece of mortar joint is in any case often required (Binda 2005; Drdácký et al. 2008); v) mortar joint can present a different composition and properties compared to the internal core of the structure (Negri 2007).

MDTs for the estimation of the compressive strength of ancient mortar on-site are also available. They involve penetration methods (drilling or percussion) (Binda 2005; Del Monte and Vignoli 2008). However, these kinds of tests are mainly calibrated for contemporary cement concrete so their application to the archaeological asset would require further experimentation. Moreover, these tests can be carried out only on the external part of the mortar joints, rather than on the internal core of the masonry structures.

It should be pointed out that the knowledge of the mechanical behavior of ancient mortars is important for the assessment of the safety level of ancient masonry structures, as well as for the design of repair materials. Indeed, new mortars for restoration interventions must have similar mechanical properties to the ancient ones, as well as the physical, chemical and aesthetic characteristics. Moreover, only a few data are available in the literature as concerns the mechanical properties of historical and archaeological mortars. Baronio and Binda investigated old mortars from the medieval Civic Tower of Pavia, which collapsed in 1989, and found a bulk density ranging between 1862 kg/m^3 and 1914 kg/m^3, compressive strength ranging between 2.92 MPa and 13.37 MPa, and elastic modulus ranging between 268 MPa and 1583 MPa (Baronio and Binda 1991). Baronio et al. report the values of tensile and compressive strength of samples of mortar from the Cathedral of Noto, Italy, constructed in 1693, ranging between 0.42-0.45 MPa and 0.20-0.31 MPa, respectively (Baronio et al. 2003). Valek and Veiga investigated non-standard mortar specimens from medieval Pišece Castle, Slovenia, and found a compressive strength ranging between 0.53 MPa and 2.34 MPa (Válek and Veiga 2005). Moropoulou et al. gave a summary of the main results of wide researches on ancient mortars from different structures in the Mediterranean basin, of different ages (i.e. Greek, Hellenistic, Roman, Byzantine and later historic mortars) and showing bulk density from 1500 kg/m^3 to 2100 kg/m^3, and tensile strength from values lower than 0.35 MPa up to values greater than 0.60 MPa (Moropoulou et al. 2005a). Ozkaya and Boke report the value of density, compressive strength and elastic modulus of mortars from the Roman Serapis Temple from the acropolis of Pergamon, in Turkey, equal to 1500 kg/m3, 6.6 MPa and 631 MPa (Özkaya and Böke 2009). Papayanni et al. report the value of compressive strength of mortar samples taken from the Roman Odeion of the archaeological site of Dion, Greek, ranging between 4.5 MPa and 4.8 MPa (Papayianni et al. 2013). However, to the knowledge of the author, despite different studies investigated the composition of archaeological mortars from Pompeii, (De Luca et al. 2015; Miriello et al. 2010, 2018a) no information is available on their mechanical parameters.

2.1.1. Experimental programme

Five original specimens of ancient mortars were collected as a part of the new excavations from three different locations of *Regio V*: two from *Via del Vesuvio*; one from *Vicolo delle Nozze d'Argento;* two from *Vicolo dei Balconi* (Figure 10).

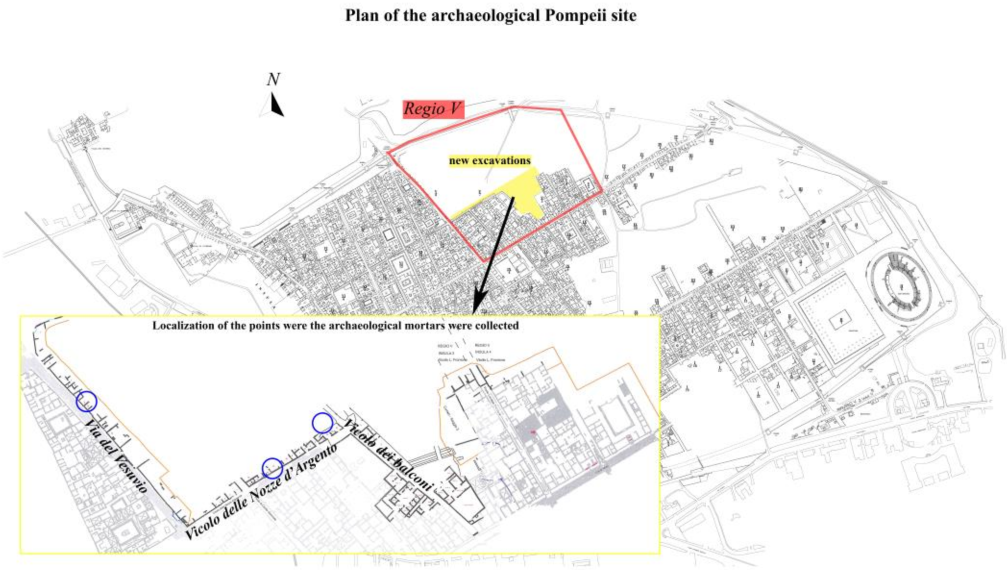

Figure 10. Localization of ancient specimens in the new archaeological excavations area in Regio V.

Each specimen was named by an alphanumeric code made by the initials of the name of the street where they were found (i.e. *Via del Vesuvio*, V, *Vicolo delle Nozze d'Argento*, ND, and *Vicolo dei Balconi*, B) and a serial number. Figure 11 shows the mortar specimens along with their denominations.

V1 **V2** **ND**

(a) (b)

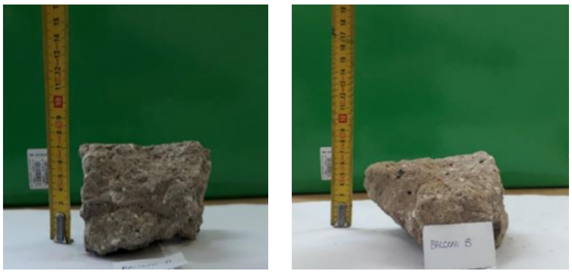

B1 **B2**

(c)

Figure 11. Ancient mortars specimens from archaeological Pompeii site: two from Via del Vesuvio, V1 *and* V2 *(a); one from* Vicolo delle Nozze d'Argento, ND *(b); two from* Vicolo dei Balconi, B1 *and* B2 *(c)*

The specimens represented a unique opportunity to carry out standard DTs to characterize the mechanical properties of ancient mortars. Based on their size, it was possible to assume that they belonged to the core of masonry structures rather than from the external part of the mortar joints. Given the impossibility to obtain standard-size specimens for the flexural test, standard cubic specimens 40 mm x 40 mm x 40 mm were realized, according to (CEN 2007a). Eleven cubic specimens were obtained (four specimens from the piece V1 - V1-1, V1-2, V1-3 and V1-4 - one from V2 - V2-1 - three from ND - ND-1, ND-2 and ND-3 - one from B1 - B1-1 – and two from B2 - B2-1 and B2-2). To prevent damage to the original specimens, the cubes were made in dry conditions. Figure 12 shows the eleven ancient mortar cubic specimens.

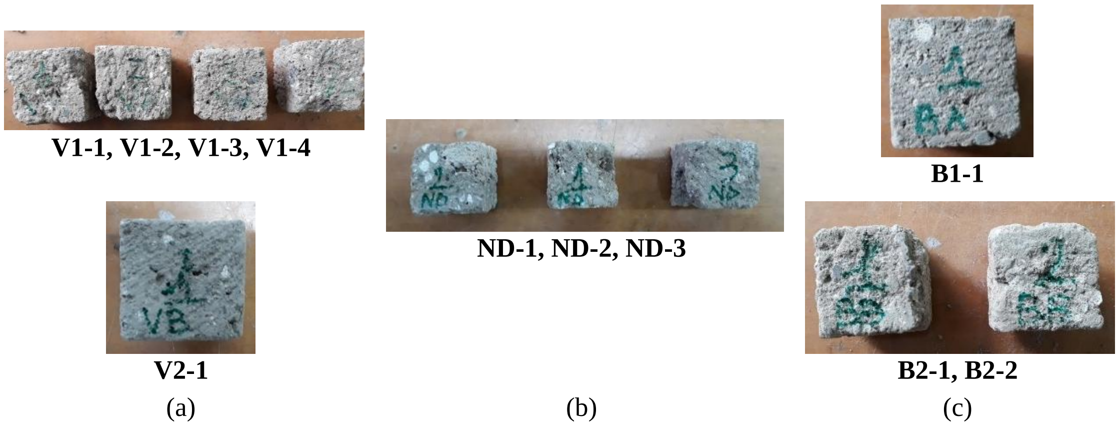

Figure 12. Eleven ancient mortar cubic specimens: V1-1, V1-2, V1-3, V1-4 *and* V2-1 *(a);* ND-1, ND-2 *and* ND-3 *(b);* B1-1 *and* B2-1 *and* B2-2 *(c).*

2.1.1.1. Uniaxial compression tests

Uniaxial compression tests were performed according to the European Standard EN 1015-11 (CEN 2007a), by applying a compression load under displacement control at a constant rate of 0.01 mm/s (

Figure 13). Three vertical Linear Variable Displacement Transducers, LVDTs, were applied to each specimen to control the measurement of the vertical displacement during the test.

Figure 13. Compressive test set up on an archaeological mortar specimen with LVDTs.

The tests allowed obtaining the compressive stress of the mortar, σ, as the ratio between the applied load, P, and cross-sectional area of the specimens, A, as in Eq. (2.1), the compressive strength, evaluated in correspondence with the maximum achieved load, σ_{max}, and the axial strain, ε, as the ratio between the change in measured axial length, ΔL, and the original undeformed axial gage length, L_0, as in Eq. (2.2). The conventional failure was set as a strength degradation of 20% from the achievement of the maximum stress. Moreover, the tangent elastic modulus in correspondence of 30% and 50% of the maximum stress, $E_{t,30\%}$ and $E_{t,50\%}$, were calculated as in Eq. (2.3) (ASTM 1970). The bulk density of each specimen, ρ, was also determined as the ratio between the mass, M, and the volume of the cubic specimens, W, as in Eq. (2.4).

$$\sigma = \frac{P}{A} \tag{2.1}$$

$$\varepsilon = \frac{\Delta L}{L_0} \tag{2.2}$$

$$E_t = \frac{\Delta\sigma}{\Delta\varepsilon} \tag{2.3}$$

$$\rho = \frac{M}{W} \tag{2.4}$$

2.1.2. Discussion of the experimental results

Table 1 summarizes the results obtained for the investigated archaeological mortars in terms of: bulk density, ρ; maximum achieved load, P_{max}; compressive strength, σ_{max}; axial strain in correspondence if the maximum load achieved, ε_{max}; ultimate vertical strain, ε_u; tangent elastic modulus evaluated on the compressive stress-vertical strain curve in correspondence of the 30% of the maximum stress, $E_{t,30\%}$; tangent elastic modulus evaluated on the compressive stress-vertical strain curve in correspondence of the 50% of the maximum stress, $E_{t,50\%}$. Mean values and coefficients of variation, CoV, are also reported for the cubic specimens obtained from the same piece of mortar. Moreover, Figure 14 reports the experimental axial stress-axial strain relationships for each specimen of mortar. This latter showed for all the specimens a first linear upward trend up to the maximum stress followed by a second decreasing branch "softening"; once the maximum load was achieved, a gradual formation of cracks in the mortar was observed. A point representing the failure, conventionally assumed at 80% of the maximum stress, is also reported in Figure 14.

Table 1. Main results of uniaxial compression tests performed on archaeological mortars.

Specimen	**ρ [kg/m3]**	**P_{max} [kg]**	**σ_{max} [MPa]**	**ε_{max} [-]**	**ε_u [-]**	**$E_{t,30\%}$ [MPa]**	**$E_{t,50\%}$ [MPa]**
V1-1	984	0.063	0.48	2.53%	3.71%	56.00	63.99
V1-2	984	0.063	0.41	2.79%	3.47%	26.66	26.68
V1-3	969	0.062	0.42	2.47%	3.64%	32.01	39.99
V1-4	1047	0.067	0.40	2.38%	3.97%	36.00	32.00
mean	996	0.064	0.43	2.54%	3.51%	37.67	40.67
CoV	3%	3%	8%	7%	6%	34%	41%
V2-1	1188	0.076	1.24	2.13%	1.23%	106.59	79.96
ND-1	1094	0.070	0.48	3.66%	3.21%	40.00	37.34
ND-2	1094	0.070	0.45	2.81%	3.49%	48.02	44.00
ND-3	1078	0.069	0.35	1.98%	3.00%	20.00	40.00
mean	1089	0.070	0.43	2.81%	3.23%	36.01	40.45
CoV	1%	1%	16%	30%	8%	40%	8%
B1-1	1188	0.076	1.61	2.27%	2.51%	112.00	170.61
B2-1	1016	0.065	0.32	2.85%	3.19%	12.00	26.67
B2-2	984	0.063	0.36	3.03%	3.96%	24.00	26.67
mean	1000	0.064	0.34	2.94%	3.58%	18.00	26.67
CoV	-	-	-	-	-	-	-

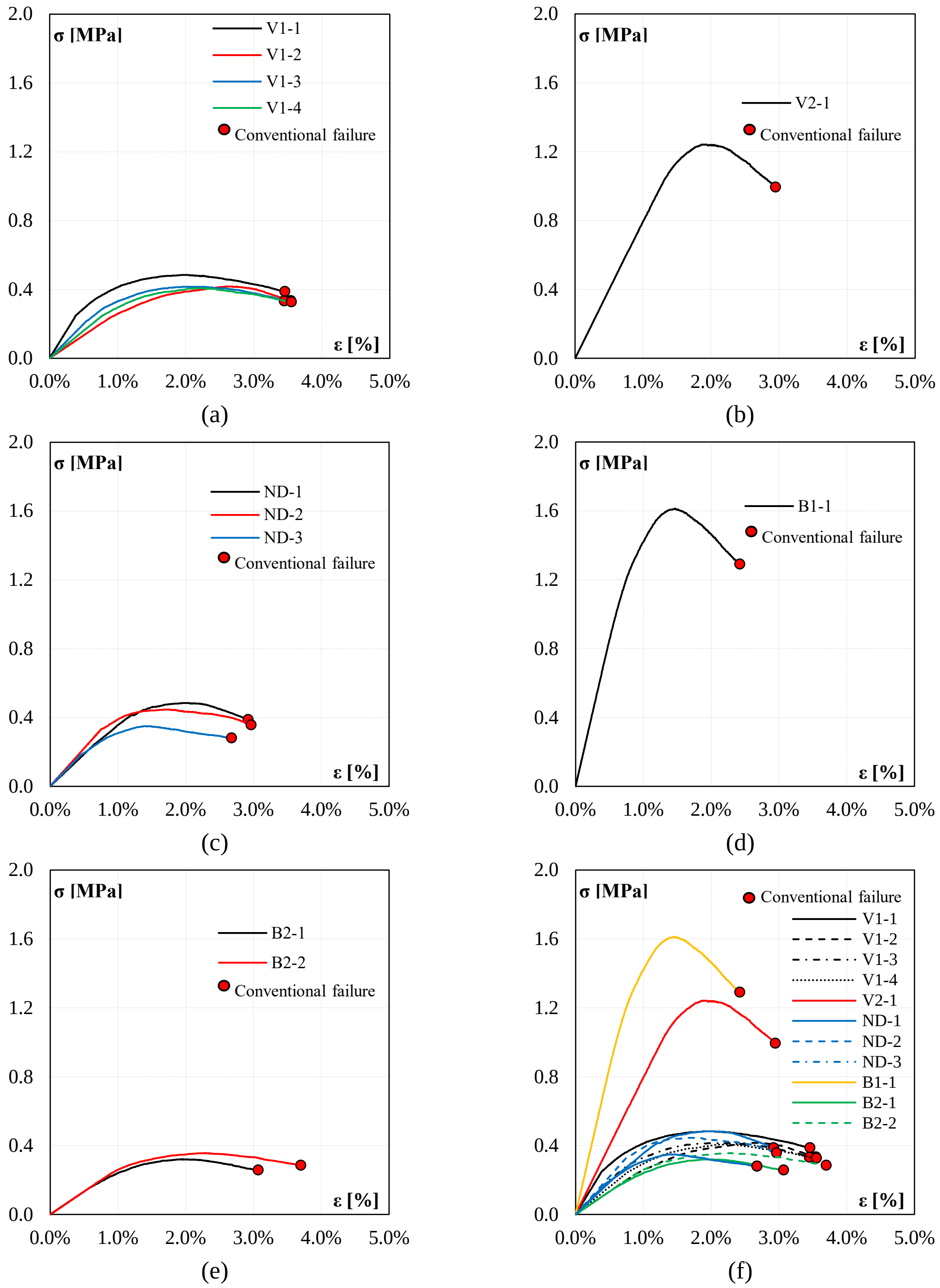

Figure 14. Axial stress-axial strain relationships: V1-1, V1-2, V1-3, VA-4 *(a);* V2-1 *(b);* ND-1, ND-2, ND-3 *(c);* B1-1 *(d);* B2-1, B2-2 *(e); all the specimens (f).*

Nine out of eleven specimens showed almost the same behavior with similar values of compressive strength, with a mean value of 0.41 MPa (CoV 14%). The other two specimens, V2-1 and B1-1 showed higher values of compressive strengths (respectively 1.24 MPa and 1.61 MPa). The calculated values of elastic modulus should be taken as qualitative data, being their values very low and their dispersion large. However, they were consistent with the values found for the compressive strength, with the higher elastic modulus showed by V2-1 and B1-1. The bulk densities of the specimens were consistent with these values, indeed, the nine specimens with the lower strength showed also similar and lower density (i.e. mean value of 1028 kg/m^3, CoV 5%) compared to the two others (both showing a density of 1188 kg/m^3, 16% greater than the mean value). The highest density along with the highest compressive strength could be related to further different properties in their original condition or a different level of chemical, physical and mechanical deterioration from the 79 A.D. Vesuvius eruption until today.

2.2. Characterization of stone units

Standard methods for the investigation of the main mechanical properties of stone units involve DTs, among which: (CEN 2003) for the determination of the compressive strength; (UNI EN 14580:2005 2003) for the determination of the static elastic modulus; (UNI EN 12372:2001 2003) for the determination of the flexural strength. As regards the NDTs, the most common methods for the characterization of rock materials from existing structures are the ultrasonic pulse velocity test, UPV, and the Schmidt hammer rebound test, SHR (Christaras 1996; Moradian and Behnia 2009; Vasanelli et al. 2015, 2016; Vasconcelos 2005; Yasar and Erdogan 2004).

In UPV, the velocity of propagation of ultrasonic wave pulses through the specimen is evaluated. The pulse is generated by an electro-acoustical transducer and received by a second transducer (Figure 15). The propagation time of the pulse, t, is electronically recorded, and the path length equal to the distance between the centers of the transducer faces, d, is measured, thus, the pulse velocity V is calculated as (2.5):

$$V = \frac{d}{t} \tag{2.5}$$

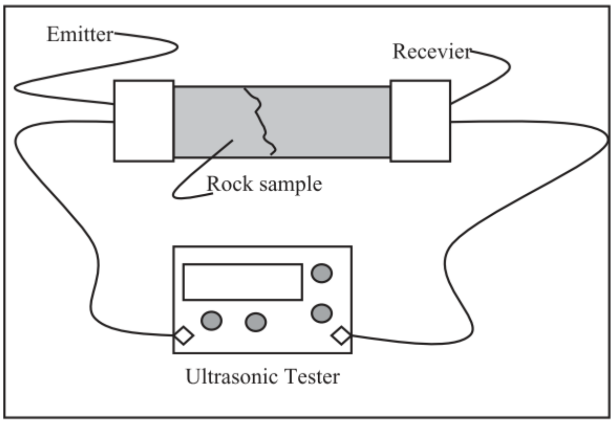

Figure 15. Schematic illustration of UPV measuring equipment (Yasar and Erdogan 2004).

UPV can be used to assess the uniformity of the specimen and the presence of defects or anomalies, other than to estimate the strength and the elastic properties of the tested material (CEN 2005a). UPV can be carried out by direct, semi-direct or indirect transmission according to the relative position of the transmitter and the receiver transducers and allow obtaining the pulse velocity of three types of waves respectively: longitudinal or P-waves, shear or S-waves, surface or R-waves (Figure 16). Since the longitudinal waves are the ones with the maximum energy of the pulse, direct transmission is considered to be the most accurate compared to the other typologies and the most common method applied (Vasanelli et al. 2015; Vasconcelos 2005; Yasar and Erdogan 2004).

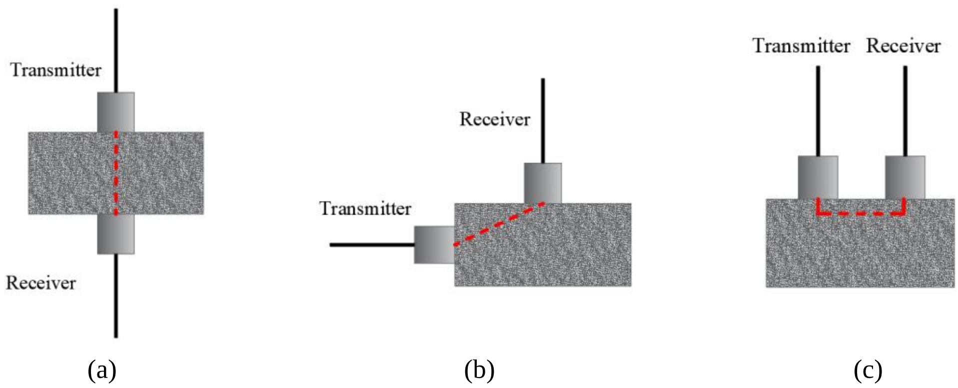

Figure 16. Possible typologies of ultrasonic pulse velocity measurements: direct transmission (a); semi-direct transmission (b); indirect transmission (c).

SHR measures the rebound of a spring-loaded piston that strikes a hammer in contact with the surface of the specimen. The test equipment records the rebound distance in terms of a rebound number, H_r, which depends on the hardness of the tested material. For the characterization of rocks, type “L” hammer, with an impact energy of 0.74 Nm, is used. From the rebound number, it is possible to obtain a rapid classification of the tested material and an indirect estimation of its strength using conversion charts (Figure 17) (Atkinson et al. 1978; CEN 2012a; RILEM TC 1998).

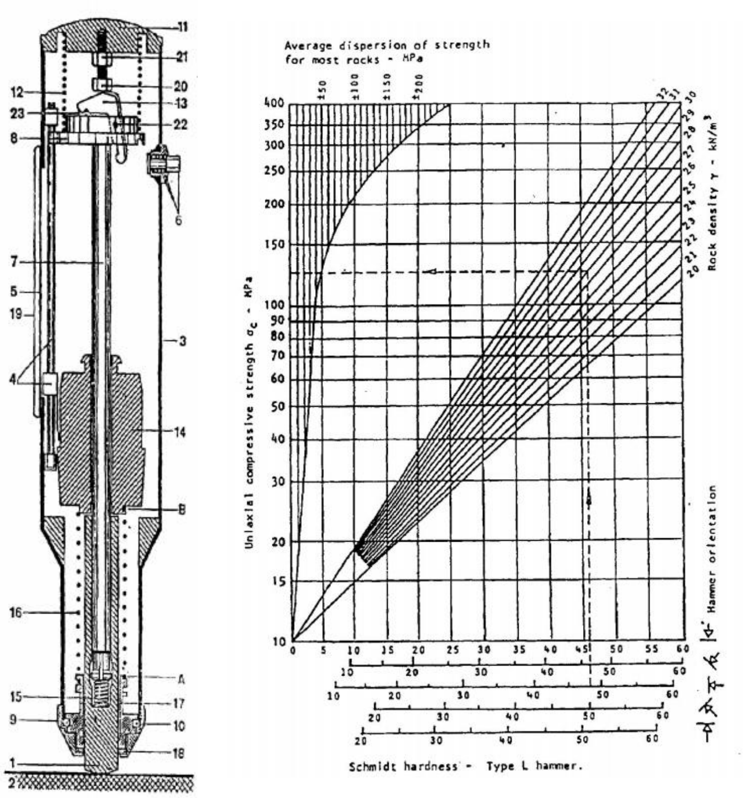

Figure 17. Schmidt hammer “L” type and example of a charter (Falcioni et al. 1995)

Both UPV and SHR were firstly developed for the assessment of concrete structures (ACI 2003; CEN 2005b, 2012a), then they were calibrated and standardized for rock specimens (ASTM 1981, 2017; CEN 2005a). Other methods were developed based on the combined use of UPV and SHR, to obtain a more reliable estimation of the material strength (ACI 2003; CEN 2012a). Technical literature presents many empirical correlations of UPV and SHR results with mechanical and physical properties of rock specimens (i.e. compressive strength, σ, Young’s modulus, E, dynamic modulus of elasticity, E_d, dynamic Poisson ratio, ν_d, density, ρ) (Christaras 1996; Moradian and Behnia 2009; Vasanelli et al. 2015, 2016; Vasconcelos 2005; Yasar and Erdogan 2004).

However, specific experimentation on the traditional rock types used in the ancient building techniques in the Pompeii site is still needed.

2.2.1. Experimental programme

Ten rock units of three different rock types were collected within the archaeological excavations at *Regio V*: three travertine units, five lava units and two foam lava units. Each specimen was identified by an alphanumeric code made by the initials of the traditional name of the rock type (i.e. *calcare del Sarno*, CS, *lava*, L, and *cruma*, CR) and a serial number: CS1, CS2, CS3, L1, L2, L3, L4, L5, CR1 and CR2 (Figure 18). The units were subjected to UPV and SHR.

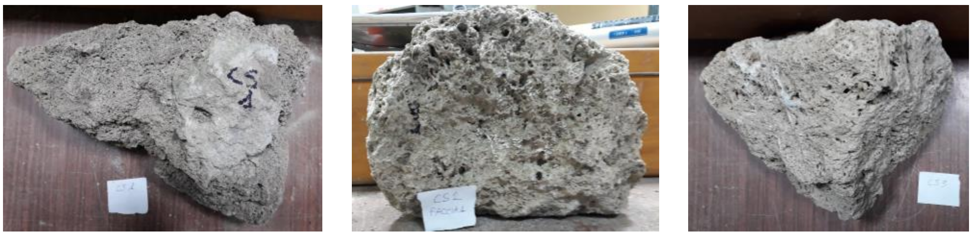

CS1 **CS2** **CS3**

(a)

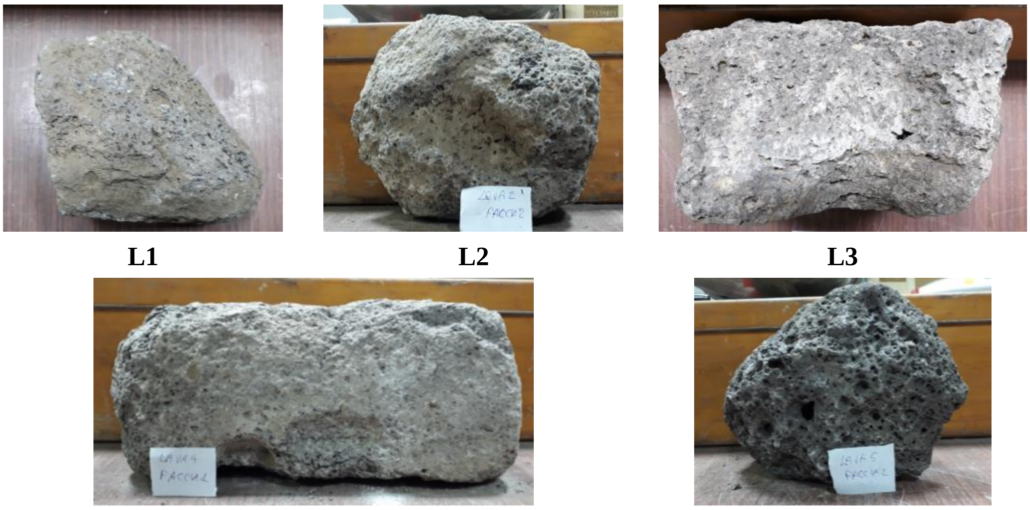

L1 **L2** **L3**

L4 **L5**

(b)

CR1 **CR2**

(c)

Figure 18. Archaeological stone unit from the Pompeii: travertine units, CS1, CS2, CS3 (a); lava units, L1, L2, L3, L4, L5 (b); foam lava units, CR1, CR2 (c).

After that, standard cubic specimens 70 mm x 70 mm x 70 mm were realized from the units, according to (CEN 2003). 51 specimens were obtained: 4 specimens from CS1; 5 specimens from CS2; 4 specimens from CS3; 2 specimens from L1; 2 specimens from L2; 5 specimens from L3; 4 specimens from L4; 1 specimen from L5; 4 specimens from CR1; 20 specimens from CR2. Each cubic specimen was named by adding a further serial number to the name of the unit of origin (i.e. CS1-1, CS1-2, CS1-3, and CS1-4) (Figure 19). UPV was carried out on 51 cubic specimens obtained from the units at ordinary moisture content and after drying. Finally, uniaxial compression tests were carried out on 32 cubic specimens.

CS1-1, CS1-1, CS1-3, CS1-4

CS2-1, CS2-2, CS2-3, CS2-4, CS2-5

CS3-1, CS3-2, CS3-3, CS3-4

(a)

L11, L1-2 **L2-1, L2-2**

L3-1, L3-2, L3-3, L3-4, L3-5

L4-1, L4-2, L4-3, L4-4 **L5-1**

(b)

CR1-1, CR1-2, CR1-3, CR1-4

CR2-1,…, CR2-20

(c)

Figure 19. The cubic specimen obtained from each unit: travertine specimens obtained from CS1, CS2 and CS3 (a); lava specimens obtained from L1, L2, L3, L4 and L5 (b); foam lava specimens obtained from CR1 and CR2 (c).

2.2.1.1. Ultrasonic pulse velocity

Ultrasonic pulse velocity tests, UPV, were carried out using the “MAE I-SONIC” apparatus. It allowed obtaining the propagation time and the transmission velocity of longitudinal compression wave pulses through the specimen and visualizing the acquired data on a graphic display. Transducers of the natural resonance frequency of 53 kHz were used. Compression wave velocities, V, were obtained through direct transmission. Coupling material was used between the specimen and each transducer to guarantee an adequate acoustical coupling. UPV was carried out on the units at ordinary moisture content first, thus, after the cut of the units, UPV was carried out on the cubic specimens at ordinary moisture content and after drying. Figure 20 shows the test equipment.

(a) (b)

Figure 20. UPV equipment: UPV with a stone units (a); UPV with a cubic specimen (b).

As concerns UPV on the units, compression wave velocities were evaluated as the mean of three measurements obtained along a single direction. The transducers were fit to the irregular shape of each unit to ensure their alignment for the direct transmission and avoid local defects or fractures. For each unit, the distance between the transducers was recorded for the computation of the compression wave velocity. Note that it was not possible to collect data for two units, L2 and L4, probably due to the presence of cracks or voids inside the tested materials. As concerns UPV on the cubic specimens both at ordinary moisture content and after drying, compression wave velocities were evaluated in two orthogonal directions, each of them calculated as the mean of three measurements. UPV on the cubic specimens was carried out at ordinary moisture content first, then UPV was repeated on the specimens after drying at a temperature of 70±5 °C to constant mass according to the standard EN 14579 (CEN 2005a).

2.2.1.2. Schmidt hammer tests

Schmidt hammer tests, SHR, were carried out on the units using a low-impact energy hammer, L-type (RILEM TC 1998). For the execution of SHR, each unit was stuck in a clamp and the hammer was positioned horizontally. Figure 21 shows the hammer used in the present experimentation.

Figure 21. SHR equipment.

The rebound distance of the piston was visualized on a linear scale on the instrument and recorded to the nearest whole number. According to the standard ASTM D 5873 - 00 (ASTM 1981), ten values of the rebound number were recorded for each unit in different locations on the specimen surface, placed at a distance equal at least to the diameter of the piston. Thus, acquisitions differing more than seven units from the mean of the ten recorded values were rejected and H_r was evaluated as the mean of the remaining values. Note that data were not recorded for the unit CS1, as local rupture on the surface of this specimen occurred during the rebound testing, so the test was rejected.

2.2.1.3. Uniaxial compression tests

Uniaxial compression tests were carried out on the cubic specimens according to the standard EN 1926 (CEN 2003). To correlate the uniaxial compressive strength with the ultrasonic pulse velocity, UPV was repeated on the cubic specimens before the execution of DTs along the direction of the compression load, z, and V_z was evaluated as the mean of three records. Uniaxial compression tests were carried out under displacement control with a constant rate of 0.01 mm/s. During the tests, the vertical shortening was measured employing LVDTs (Linear Variable Displacement Transducers) (Figure 22).

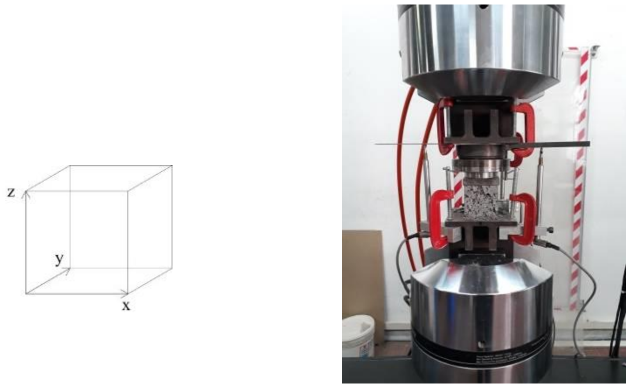

(a) (b)

Figure 22. Reference system for cubic specimens (a) and compression test set up (b).

The test programme involved 32 specimens: 11 travertine specimens, 8 lava specimens and 13 foam lava specimens. The tests allowed obtaining the compressive stress, σ (2.1), and the axial strain, ε (2.2), for each test, and the mean compressive strength for each rock type, from the values calculated in correspondence with the maximum achieved loads, σ_{max}. The conventional failure was set, as for the mortars, as a strength degradation of 20% from the achievement of the maximum stress. Moreover, the secant elastic modulus between 30% and 50% of the maximum stress, $E_{(30\%-50\%)}$, was calculated (2.5) (ASTM 1970). Finally, the bulk density of each specimen, ρ, and the mean value for each rock type, were also determined as in Eq. (2.4).

$$E_{(30\%\text{-}50\%)} = \frac{\sigma_{50\%}\text{-}\sigma_{30\%}}{\varepsilon_{50\%}\text{-}\varepsilon_{30\%}} \tag{2.5}$$

2.2.2. Discussion of the experimental results

2.2.2.1. UPV and SHR

The results of NDTs on the units are summarized in Figure 23 and Table 2 in terms of mass, M_{unit}, ultrasonic pulse velocity, V_{unit}, and rebound number, H_r, for each unit with their respective CoV. As regards the UPV, it resulted that the maximum velocity values were recorded on travertine units, showing a mean velocity of 2350 m/s. Lava units showed a mean velocity of 1616 m/s while foam lava units showed a mean velocity of 1320 m/s. Note that it was not possible to collect data for two units, L2 and L4, probably due to the presence of cracks or voids inside the tested materials. From the SHR, the maximum mean rebound number equal to 29 was found for lava units, while foam lava units and travertine units had mean rebound number 15 and of 17, respectively. Note that data were not recorded for units CS1 and L4, as local rupture occurred on the surface of the specimens during the rebound testing, so the tests were rejected.

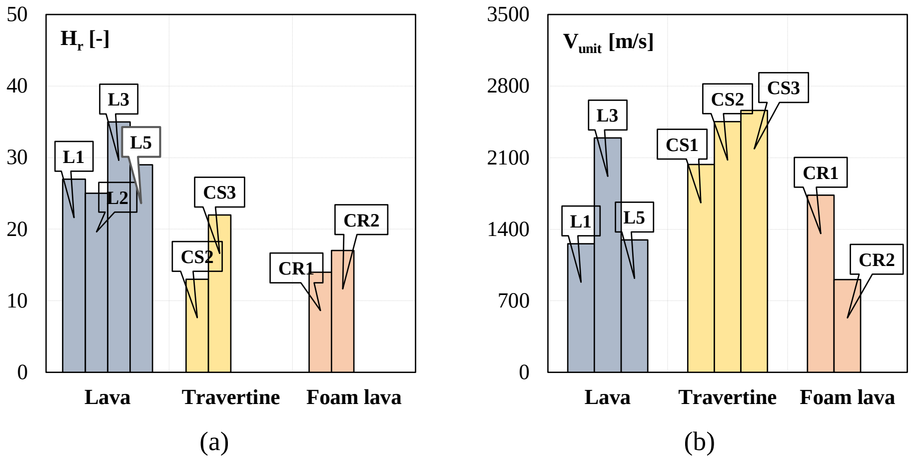

Figure 23. NDTs results on the stone units: mean ultrasonic pulse velocity (a) and mean Schmidt rebound number (b).

Table 2. Mass, mean ultrasonic pulse velocity and mean Schmidt rebound number and coefficients of variation for each unit.

Unit [-]	**M_{unit}** [kg]	**V_{unit}** [m/s]	**CoV** [-]	**H_r** [m/s]	**CoV** [-]
CS1	4.8	2034	12%	-	-
CS2	6.7	2453	2%	13	4%
CS3	6.0	2563	17%	22	21%
L1	5.3	1258	13%	27	17%
L2	4.6	-	-	25	13%
L3	12.6	2294	15%	35	12%
L4	12.7	-	-	-	9%
L5	5.6	1296	45%	29	15%
CR1	6.7	1733	3%	14	18%
CR2	13.0	908	16%	17	23%

After that, UPV was carried out on 51 cubic specimens, 70 mm side, obtained from the units at ordinary moisture content and after drying to evaluate the effect of the drying process on the ultrasonic velocities. Table 3 reports for each set of cubic specimens obtained from each unit the number of specimens, n_s, the mean bulk density and the ultrasonic velocity at ordinary moisture content, ρ and V, and the mean bulk density and the ultrasonic velocity after drying, ρ_d and V_d. The bulk densities were calculated for each cubic specimen as the ratio between its mass, at ordinary moisture content and at after drying respectively, and its volume. The ultrasonic velocities obtained by UPV on the cubic specimens at ordinary moisture content and after drying are also reported in Figure 23 (a) and (b), respectively. A higher scatter of results was found among cubic specimens from different lava units. However, despite the percentage differences of the velocity at ordinary moisture conditions concerning the one after drying, ΔV, were different among the specimens the trend of the velocities among the different rock types was the same between the two conditions. Moreover, except for 8 specimens, these percentage differences did not exceed ±20%. These values of variation were considered as acceptable as compared with the own variation showed in every single set of tests.

Table 3. The number of cubic specimens obtained from each unit and corresponding mean bulk density and ultrasonic velocity at ordinary moisture content and the mean bulk density and the ultrasonic velocity after drying with their coefficients of variation.

Unit	Cubic specimen	ρ [kg/m^3]	V [m/s]	ρ_d [kg/m^3]	V_d [m/s]	ΔV [%]
L1	**L1.1**	2280	1115	2245	1044	-7%
	L1.2	2329	2275	2327	2114	-8%
	mean	2305	1695	2286	1579	-7%
	CoV	-	-	-	-	-
L2	**L2.1**	2190	837	2175	956	12%
	L2.2	2131	797	2117	913	13%
	mean	2160	817	2146	935	13%
	CoV	-	-	-	-	-
L3	**L3.1**	2341	2844	2332	2696	-5%
	L3.2	2367	2626	2362	2547	-3%
	L3.3	2359	2768	2356	2644	-5%
	L3.4	2350	1857	2350	1462	-27%
	L3.5	2318	2764	2324	2457	-13%
	mean	2347	2572	2345	2361	-9%
	CoV	1%	16%	1%	22%	-
L4	**L4.1**	2286	959	2277	772	-24%
	L4.2	2280	886	2280	677	-31%
	L4.3	2184	701	2181	610	-15%
	L4.4	2259	713	2251	626	-14%
	mean	2252	815	2247	671	-21%
	CoV	2%	16%	2%	11%	-

L5	**L5.1**	2096	1078	2061	1178	8%
	CS1.1	1242	2521	1117	2858	12%
	CS1.2	1210	1302	1085	2113	38%
	CS1.3	1312	2186	1195	2555	14%
CS1	**CS1.4**	1184	1994	1117	2205	10%
	mean	1237	2001	1128	2433	18%
	CoV	4%	26%	4%	14%	-
	CS2.1	1440	2383	1434	2731	13%
	CS2.2	1399	2251	1391	2842	21%
	CS2.3	1376	2278	1367	2716	16%
CS2	**CS2.4**	1356	2247	1350	2712	17%
	CS2.5	1402	2165	1394	2948	27%
	mean	1395	2265	1387	2790	19%
	CoV	2%	3%	2%	4%	-
	CS3.1	1644	2903	1542	3028	4%
	CS3.2	1749	3045	1668	3166	4%
	CS3.3	1761	3239	1671	3237	0%
CS3	**CS3.4**	1513	3003	1344	2939	-2%
	mean	1667	3048	1556	3093	1%
	CoV	7%	5%	10%	4%	-
	CR1.1	971	1631	959	1776	8%
	CR1.2	1076	1807	1064	1972	8%
	CR1.3	997	1910	988	2111	10%
CR1	**CR1.4**	883	1233	848	1869	34%
	mean	982	1645	965	1932	15%
	CoV	8%	18%	9%	7%	-143%
	CR2.1	980	1170	901	1530	24%
	CR2.2	866	1895	840	1662	-14%
	CR2.3	930	1726	880	1644	-5%
	CR2.4	1026	1884	983	1633	-15%
	CR2.5	974	1835	921	1651	-11%
	CR2.6	910	1718	863	1786	4%
	CR2.7	985	1585	930	1878	16%
	CR2.8	962	1424	895	1499	5%
	CR2.9	895	2226	872	1812	-23%
CR2	**CR2.10**	1099	1525	1047	1977	23%
	CR2.11	1047	1937	1035	2178	11%
	CR2.12	1012	2130	991	2124	0%
	CR2.13	1023	2190	1015	1928	-14%
	CR2.14	863	1554	872	1802	14%
	CR2.15	1020	1936	997	1897	-2%
	CR2.16	895	1571	880	1855	15%
	CR2.17	977	1722	971	1799	4%
	CR2.18	886	1766	869	1781	1%
	CR2.19	1052	2180	1050	2001	-9%

CR2.20	860	1936	845	1844	-5%
mean	963	1795	933	1814	1%
CoV	7%	15%	8%	10%	-

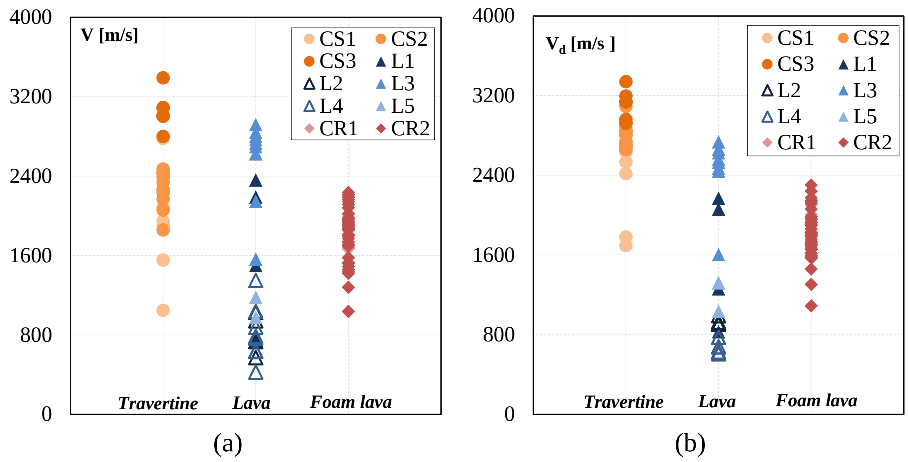

Figure 24. UPV results on the cubic specimens obtained from each unit at the ordinary moisture content (a) after drying (b).

Before the execution of DTs, UPV was repeated on the 32 cubic specimens in three orthogonal directions (each one involving three recordings). From these measurements, the degree of anisotropy was calculated as in Eq. (2.6) (Vasanelli et al. 2015):

$$Anisotropy(\%) = \frac{V_{max}\text{-}V_{min}}{V_{max}} \quad (2.6)$$

The results of the latter UPV are reported in Table 4. The degree of anisotropy ragìnged between 7% and 33%. The maximum value was shown by the specimens from CS1, while the other travertine specimens showed the lowest anisotropy.

Finally, uniaxial compression tests were performed in the direction z corresponding to the maximum acquired ultrasonic velocity, except for the specimens which presented imperfections on the loaded surfaces in that direction.

Table 4. Bulk density, ultrasonic velocities in the three orthogonal directions and degree of anisotropy for 32 specimens subsequently subjected to uniaxial compression tests.

Specimen [-]	**ρ** [kg/m^3]	**V_z** [m/s]	**V_y** [m/s]	**V_x** [m/s]	**Anisotropy** [%]
L1.1	2243	1528	1014	1237	34%
L1.2	2325	2202	2096	2187	5%
mean	2284	1865	1555	1712	19%
-	-	-	-	-	-
L2.2	2115	950	774	nd	19%
L3.1	2332	2335	2383	2244	6%
L3.2	2360	2274	2161	2368	9%
L3.3	2356	2414	2397	2334	3%
L3.4	2353	1926	1212	938	51%
L3.5	2318	2264	2166	2401	10%
mean	2344	2243	2064	2057	16%
CoV	1%	8%	24%	31%	127%
CS1.2	1080	1658	1612	1038	37%
CS1.3	1192	2000	1597	1978	20%
CS1.4	1112	2108	1237	2108	41%
mean	1080	1658	1612	1038	33%
CoV	5%	12%	14%	34%	34%
CS2.1	1433	2414	2365	2430	3%
CS2.2	1392	2245	2518	2465	11%
CS2.3	1369	2307	2276	2259	2%
CS2.4	1350	2018	1984	2017	2%
CS2.5	1392	2191	2040	1757	20%
mean	1387	2235	2237	2186	7%
CoV	2%	7%	10%	14%	106%
CS3.1	1542	2555	2448	2398	6%
CS3.2	1671	2632	2555	2397	9%
CS3.3	1671	3338	3136	nd	6%
mean	1628	2842	2713	2398	7%
CoV	5%	15%	14%	0%	23%
CR1.1	958	1650	1351	1535	18%
CR1.2	1063	2024	1635	1528	25%
CR1.3	990	1627	1446	1569	11%
CR1.4	872	1324	1317	933	30%
mean	970	1656	1437	1391	21%
CoV	8%	17%	10%	22%	38%
CR2.1	899	1357	1220	1529	20%
CR2.2	840	1576	1617	1440	11%
CR2.3	879	1535	1429	1606	11%
CR2.4	983	1541	1535	1362	12%
CR2.5	921	1643	1627	1282	22%

CR2.6	860	1422	1301	1330	9%
CR2.7	927	1423	1406	1296	9%
CR2.8	894	1190	1086	1129	9%
CR2.9	669	1598	1174	1576	27%
mean	875	1476	1377	1394	14%
CoV	10%	10%	14%	11%	47%

2.2.2.2. Uniaxial compression tests

Table 5 summarizes the results obtained for the investigated archaeological mortars in terms of: maximum achieved compressive load, $P_{max,z}$; compressive strength, $\sigma_{max,z}$; axial strain in correspondence if the maximum load achieved; $\varepsilon_{max,z}$, ultimate vertical strain, $\varepsilon_{u,z}$; secant elastic modulus between 30% and 50% of the maximum stress, $E_{(30\%\text{-}50\%)}$. Mean values and coefficients of variation, CoV, are also reported for the cubic specimens obtained from the same stone unit. The experimental axial stress-axial strain relationships for each rock type are reported in Figure 25. After the achievement of the maximum compressive stress, each curve showed a decreasing “softening” branch. The failure of each specimen, conventionally assumed at 80% of the maximum stress, is also reported.

Table 5. Main results of uniaxial compression tests performed on archaeological stone units.

Specimen	$P_{max,z}$ [kN]	$\sigma_{max,z}$ [MPa]	$\varepsilon_{z,max}$ [-]	$\varepsilon_{z,u}$ [-]	$E_{(30\text{-}50\%)}$ [MPa]
L1.1	128	26.2	0.5%	0.8%	2924
L1.2	225	45.8	0.8%	1.1%	5172
mean	176	36.0	0.7%	1.0%	4048
CoV	-	-	-	-	-
L2.2	77	15.8	1.5%	1.9%	1190
L3.1	251	51.2	1.3%	1.7%	7691
L3.2	215	43.8	1.0%	3.2%	5864
L3.3	308	62.8	1.0%	2.4%	9093
L3.4	166	33.8	1.0%	1.1%	4639
L3.5	138	28.1	1.2%	1.5%	4046
mean	215	43.9	1.1%	2.0%	6267
CoV	31%	31%	14%	41%	34%
CS1.2	9	1.8	0.4%	0.5%	507
CS1.3	15	3.2	0.6%	0.8%	670
CS1.4	8	1.7	1.3%	1.5%	422

mean	11	2.2	0.8%	0.9%	533
CoV	36%	36%	60%	52%	24%
CS2.1	21	4.2	1.0%	1.2%	574
CS2.2	18	3.6	0.2%	0.4%	2688
CS2.3	28	5.7	0.3%	0.5%	3147
CS2.4	18	3.7	0.5%	0.9%	863
CS2.5	31	6.4	0.3%	0.5%	2656
mean	23	4.7	0.5%	0.7%	1986
CoV	26%	26%	76%	51%	59%
CS3.1	36	7.3	0.4%	0.7%	1739
CS3.2	50	10.2	1.0%	1.2%	1621
CS3.3	82	16.7	1.7%	1.8%	1947
mean	56	11.4	1.0%	1.2%	1769
CoV	42%	42%	66%	47%	9%
CR1.1	21	4.4	0.8%	1.0%	588
CR1.2	27	5.4	0.8%	1.0%	696
CR1.3	21	4.4	0.7%	0.9%	691
CR1.4	9	1.8	0.9%	0.8%	236
mean	20	4.0	0.8%	0.9%	553
CoV	39%	39%	8%	10%	39%
CR2.1	10	2.0	5.2%	5.4%	426
CR2.2	18	3.7	1.0%	1.1%	578
CR2.3	26	5.2	0.5%	1.0%	1174
CR2.4	27	5.5	0.8%	1.3%	750
CR2.5	19	3.9	0.7%	0.9%	606
CR2.6	18	3.7	0.9%	2.1%	655
CR2.7	27	5.6	0.7%	0.9%	946
CR2.8	11	2.2	3.0%	4.9%	168
CR2.9	14	2.8	0.6%	0.7%	635
mean	19	3.9	1.5%	2.0%	660
CoV	35%	35%	107%	89%	44%

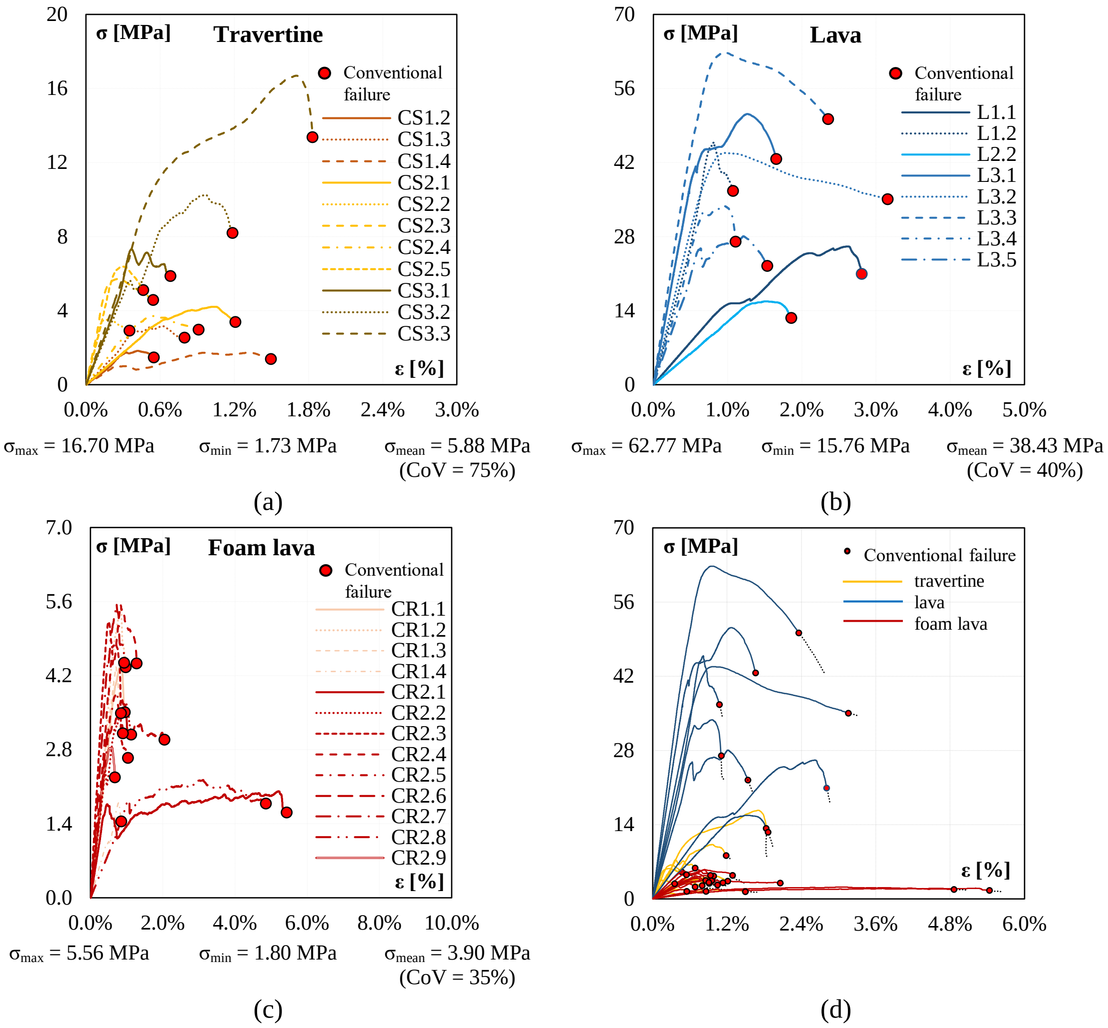

Figure 25. Axial stress-axial strain relationship for travertine cubic specimen (a); lava cubic specimens; foam lava cubic specimen (c); all the specimens (d).

A high scatter of results was found for each of the three rock types, due to the proper heterogeneity and mechanical and physical decay of each unit. Lava specimens showed the maximum compressive strength ranging between 15.8 MPa and 62.8 MPa, with a mean value of 38.4 MPa (CoV = 40%) and the maximum elastic modulus ranging between 1190 MPa and 9093 MPa, with a mean value of 5077 MPa (CoV = 50%). Foam lava showed the minimum strength ranging between 1.8 MPa and 5.6 MPa, with a mean value of 3.9 MPa (CoV = 35%) and the minimum elastic modulus ranging between 168 MPa and 1174 MPa, with a mean value of 627 MPa (CoV = 42%). Finally, travertine showed more significant variability of the results, with the strength ranging between 1.8

MPa and 16.7 MPa, with a mean value of 5.9 MPa (CoV = 75%) and the elastic modulus ranging between 422 MPa and 3147 MPa, with a mean value of 1530 MPa (CoV = 65%).

2.2.2.3. Correlations between NDTs and DTs results

The results showed high variability among the different rock materials and also a high scatter of the results in each test. This is related to the natural heterogeneity of the selected rock typologies (e.g. orientation of crystals, grains, cracks and pores, stratification, and lamination structures) and the different mechanical and physical decay of each unit. Table 6 reports the main outcomes of the tests performed on the rock units and cubic specimens.

Table 6. Main results of tests performed on the stone specimens.

Rock type	n_{units}	H_r [-]	n_{cubes}	ρ [kg/m^3]	V_z [m/s]	$\sigma_{max,z}$ [MPa]	$E_{(30\text{-}50\%)}$ [MPa]
Travertine	3	17	11	1382 (CoV = 14%)	2315 (CoV=19%)	5.88 (CoV = 75%)	1530 (CoV = 65%)
Lava	5	29	8	2300 (CoV = 4%)	1987 (CoV=26%)	38.43 (CoV = 40%)	5077 (CoV = 40%)
Foam lava	2	15	13	904 (CoV = 10%)	1532 (CoV=13%)	3.90 (CoV = 35%)	627 (CoV = 42%)

The obtained results confirmed the relationship between the compressive strength of the material and the value of the rebound number, being this latter higher when the first is higher. Indeed, a linear relationship between these two parameters was found to match the obtained experimental results as showed in Figure 26 (a) (R^2 = 0.80). Moreover, analytical expression was also found to correlate with a good matching of the uniaxial compressive strength with the parameter $V_z \cdot \rho$ (R^2 = 0.75), as shown in Figure 26 (b).

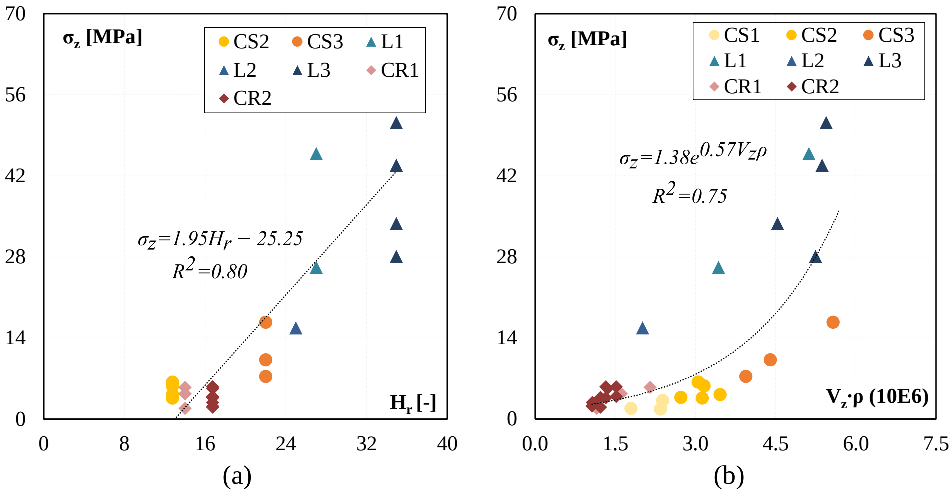

Figure 26. Correlations between the DTs and NDTs outcomes: the non-linear relationship between the uniaxial compressive strength evaluated along the direction z, σ_z, and the parameter $V_z{\cdot}\rho$ (a) and linear relationship between the uniaxial compressive strength evaluated along the direction z, σ_z, and the Schmidt hammer rebound on the units, H_r (b).

3. CHARACTERIZATION OF ARCHAEOLOGICAL MASONRIES

The achievement of deep knowledge of the mechanical behavior of ancient masonry structures is a critical issue for the preservation of the built heritage, especially in the archaeological field (De Nigris and Previti 2017). However, as for the single building materials, the need to preserve the built heritage set restrictions to the collection of standard specimens for the execution of laboratory tests masonry assemblages or to the execution of destructive and minor-destructive tests *in situ*. Thus, the development of new methodologies and investigation protocols for the knowledge of the built heritage is required and should include: i) the contribution of different disciplines to achieve a comprehensive knowledge and to limit the number of tests needed; ii) the application of non-destructive methodologies, to ensure the preservation of the heritage (ICOMOS 2003; Italian Ministry of Cultural Heritage and Activities 2010).

Of the available NDTs for masonry structures, the sonic pulse velocity test (ST) is widely used to diagnose heritage structures, as it can provide valuable information on the compactness, homogeneity, inner condition and the general state of preservation of historical masonry structures (Binda et al. 2001; Cantini 2016; Cescatti et al. 2019; Dessales et al. 2016; Miranda et al. 2013, 2012; RILEM TC 1996; Valluzzi et al. 2018, 2019). In the sonic pulse velocity test on masonry structures, the velocity of a low-frequency mechanical pulse generated on the surface of the masonry specimen is evaluated through the measurement of its first travel time (Figure 27).

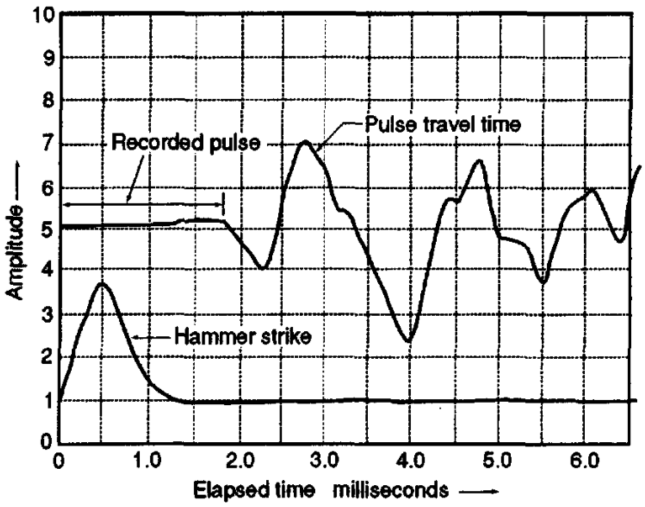

Figure 27. Recorded waveforms, showing both the input hammer pulse and the received pulse (RILEM TC 1996).

The test equipment includes an instrumented hammer for the mechanical generation of the pulse, an accelerometer for receiving the transmitted pulse and an acquisition system for the acquisition, monitoring and storage of the data (

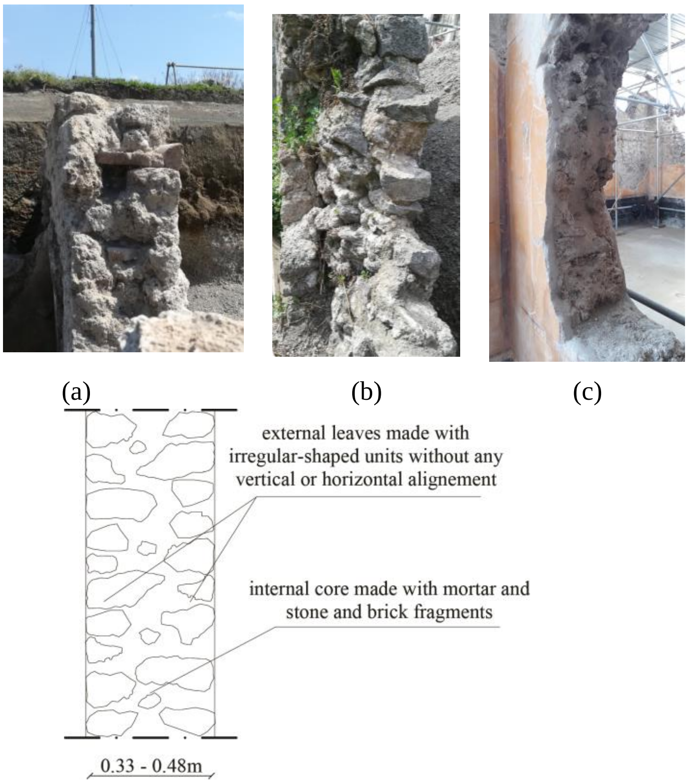

(a) (b) (c)

(d)

Figure 32).

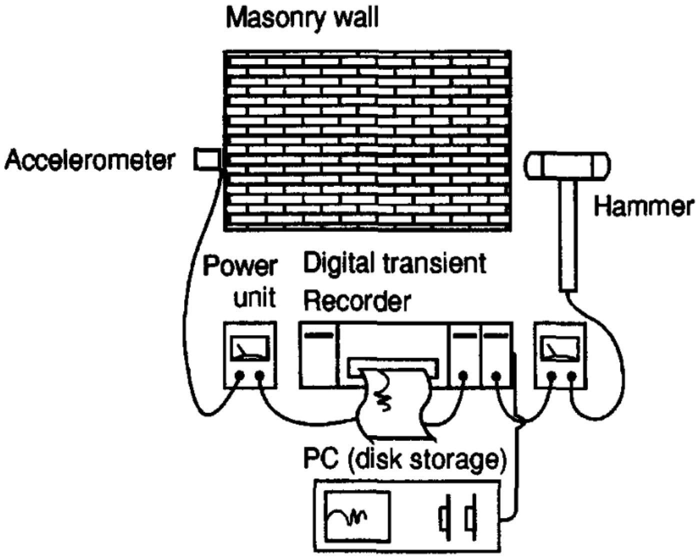

Figure 28. Sonic test equipment (RILEM TC 1996).

According to the relative position of the hammer and the receiver, the test can be performed in three configurations: direct path (i.e. with the hammer and the receiver located in line on opposite sides of the specimen); semi-direct path (i.e. with the hammer and the receiver located on orthogonal sides), indirect path (i.e. with the hammer and the receiver located on the same side) (Figure 29). Indeed, the travel time of three types of waves can be measured: longitudinal or P-waves, shear or S-waves, surface or R-waves.

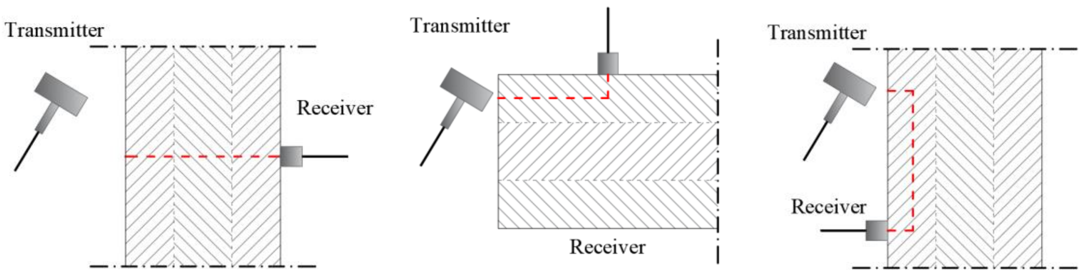

(a) (b) (c)

Figure 29. Three configurations to perform the sonic test: direct transmission (a); semi-direct transmission (b); indirect transmission (c)(RILEM TC 1996)(RILEM 1996).

In the application to masonry structures, the sonic test is generally performed by direct transmission (i.e. by transparency) and the velocity of longitudinal waves is calculated from a conventional path length equal to the mean wall thickness divided by the measured travel time.

The outcomes of the test are very useful for: the qualitative assessment of a masonry structure; the detection of weaker parts in a masonry specimen; the comparison among the conditions of different masonries; the evaluation of the effectiveness of interventions (Binda et al. 2001; Cantini 2016; Miranda et al. 2013, 2012; RILEM TC 1996; Valluzzi et al. 2018, 2019). Indeed, the longitudinal wave velocities are sensitive to the variation of density in the specimen. Thus, by collecting the pulse velocity in different points of a masonry specimen, a direct sonic test can be an effective tool to evaluate its homogeneity and to detect the presence of internal voids or discontinuity. Moreover, the estimation of the mean pulse velocity of an investigated structure is useful for comparisons with similar masonry constructions. In the technical literature, mean velocity ranges have been associated with the quality of existing masonry structures (Forde et al. 1985; Valluzzi et al. 2019). For stone masonries, a mean sonic pulse velocity exceeding 2500 m/s is associated with good-quality masonry; a mean velocity in the range of 1500–2500 m/s is linked with medium-quality masonry; and a mean velocity below 1500 m/s is associated with poor-quality masonry (Forde et al. 1985; Valluzzi et al. 2019) (Table 7).

Table 7. Relationship between masonry state of preservation and average velocity of wave propagation.

Masonry state of preservation	**Average velocity [m/s]** (Forde et al. 1985; Valluzzi et al. 2019)	
	Stone masonry	Brick masonry
Good	>2500	>2000
Medium	1500-2500	1000-2000
Low	<1500	<1000

Another test for masonry structures based on the evaluation of the velocity of low-frequency mechanical pulses is sonic tomography. Sonic tomography was implemented in many studies for the assessment of the hidden conditions and morphology of old masonry structures as well (Binda et al. 2003; Cescatti et al. 2019; Dessales et al. 2016; Valluzzi et al. 2018, 2019). The test is based on the evaluation of the velocity of the longitudinal waves of a low-frequency mechanical pulse through the masonry specimen as well with the equipment including one transmitter and multiple receivers. The transmitter and the receivers can be placed on adjacent or opposite wall surfaces and all the measurements are processed in a velocity distribution map on a cross-section plane in the horizontal, vertical, or sloping direction. Figure 30 reports a scheme of the execution of a tomographic test in the vertical direction. Sonic tomography could provide very accurate results, but it generally needs more time of execution due to a greater number of acquisitions compared to the sonic test.

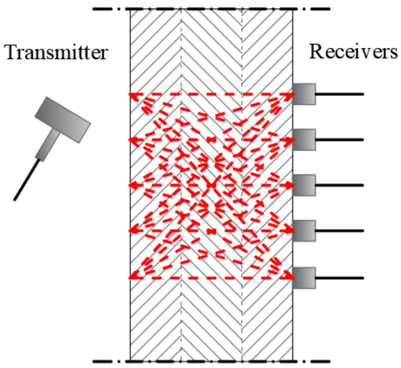

Figure 30. Scheme of execution of a tomographic test in the vertical direction.

Since masonry is not a homogeneous material, a direct estimation of physical and mechanical properties through the sonic pulse velocity is not possible (Binda et al. 2001; Valluzzi et al. 2018). Anyway, the use of the well-known equations defined for solid, elastic, isotropic and homogeneous materials, valid for concrete, Eq. (3.1) (ASTM 2003), was considered for a rough estimation of certain mechanical properties of as masonry specimen (i.e. density, dynamic modulus and Poisson ratio) as well (Miranda et al. 2013, 2012).

$$V = \sqrt{\frac{E_d\,(1 - \nu_d)}{\rho\,(1 + \nu_d)\,(1 - 2\,\nu_d)}} \tag{3.1}$$

Where:

- V is the sonic pulse velocity of the longitudinal stress waves;
- E_d is the dynamic modulus of elasticity;
- ν_d is the dynamic Poisson ratio;

- ρ is the density.

The implementation of an appropriate database of the results of STs on heritage masonry structures could provide a useful tool for their qualitative assessment, based on appropriate comparisons and analogies. However, despite ST being widely considered as an effective tool for the qualitative structural assessment of historical masonries, limited literature is available on STs in archaeological contexts. Few studies presented the application of sonic or tomographic tests at the Pompeii site (Dessales et al. 2020; Masini et al. 2017; Valluzzi et al. 2019) and certain other studies presented the application of sonic tests on new masonry panels reproducing traditional historical masonry typologies that are partially comparable to the Pompeian ones (Valluzzi et al. 2018).

In this chapter, a wide non-destructive investigation programme based on STs on archaeological masonry structures at the Pompeii site is presented. The investigation focused on one of the most common ancient masonry typologies, the rubble stone masonry, i.e. the ancient *opus incertum*. This part of the research aimed to provide valuable information on the qualitative structural assessment of the archaeological masonry structures, taking into account the impossibility of performing minor destructive tests or destructive tests.

3.1. Experimental programme

The non-destructive investigation programme involved geometric and material surveys, visual inspections and an extensive programme of STs. Archaeological masonry structures of different ages, state of preservation and types of modern interventions were involved. Eleven masonry portions were involved, with a total of 1965 acquired velocities. They belonged to newly emerged walls from the excavations started in May 2018 at *Regio V* and formerly emerged walls that already were restored in the past after excavations carried out in the 19^{th} and 20^{th} centuries at *Regio V* and at Villa of Diomedes (located in the North-West corner of the site). Based on the obtained outcomes, a detailed analysis of typical factors affecting the mean sonic pulse velocities, which should be considered in similar historical and archaeological contexts. A comparative analysis of the results of sonic tests obtained by the authors and available literature data for different masonry typologies at the Pompeii site is also presented. This was done to evaluate how the outcomes of STs could be affected by different building materials and techniques, state of preservation and age of the investigated masonry and to provide a useful tool for a primary assessment of similar masonry structures based on appropriate analogies.

3.1.1. Tests location

The wall portions to be investigated were selected taking into account: i) the masonry typology under investigation; ii) accessibility for operators and instrumentation; iii) the possibility to acquire correct and sufficient data. The accessibility of the specimens concerns different issues, especially in historical and archaeological sites. Indeed, it was necessary to ensure that the masonry wall portion was safely accessible by operators and available on both sides at the same quote for direct transmission. Furthermore, sufficient space was required to safely use and install the instrumentation. According to such criteria, Figure 31 shows the masonry structures selected for the execution of tests at the *Regio V* and at Villa of Diomedes; the tested masonry portions were labeled as STi, with i representing a progressive number assigned to the investigated portions (i.e. from 1 to 11).

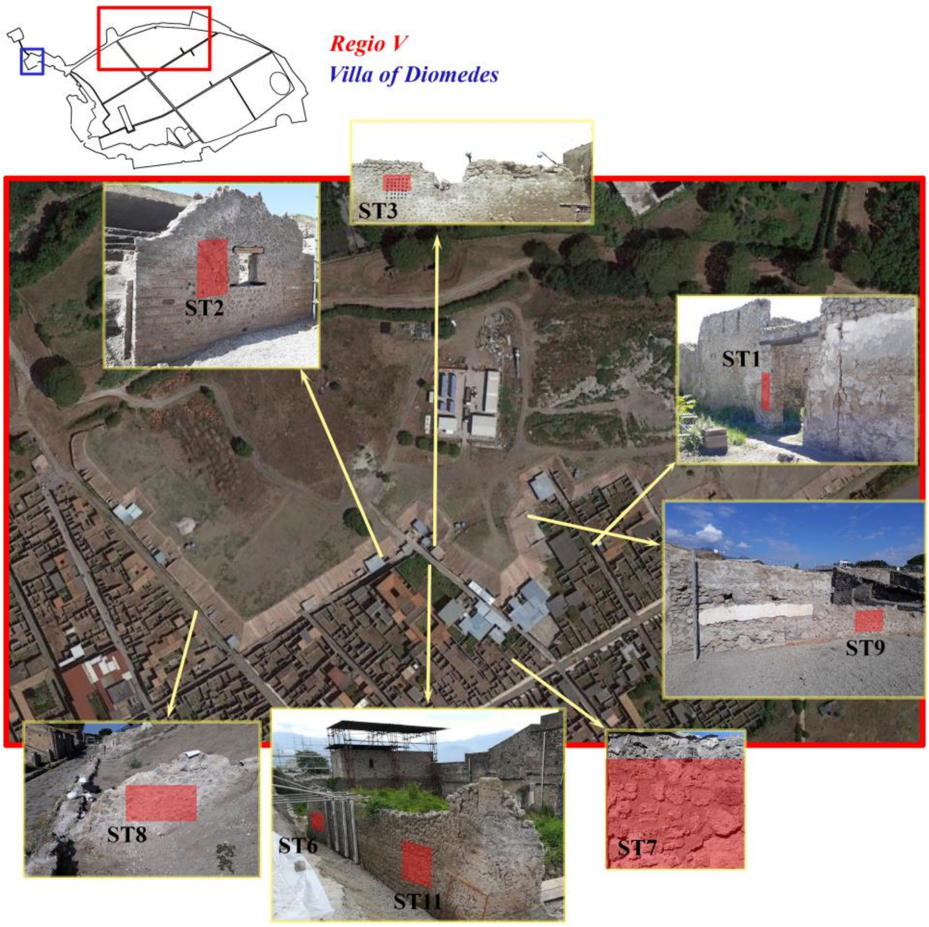

(a)

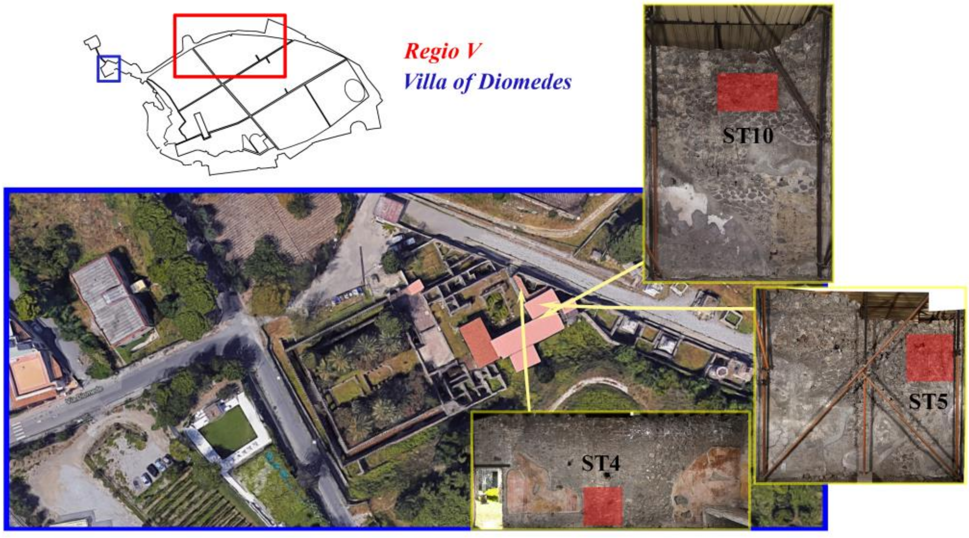

(b)

Figure 31. Localization of investigated opus incertum *masonries at* Regio V *(a) and Villa of Diomedes (b).*

3.1.2. Survey of *opus incertum*

The rubble stone is the most common masonry building type at the Pompeii archaeological site and it is traditionally known as *opus incertum*. *Opus incertum* was typically made of two external leaves with an internal core. The external leaves had an irregular arrangement, being the irregular-shaped units embedded in the mortar without any vertical or horizontal alignment and typically without any transverse connecting elements (i.e. diatones). The different shaped and sized units were arranged so that the smallest ones filled the gaps between the largest. The internal core was made of mortar and any rock or clay fragments (Giuliani 2007; Maiuri 1942). According to surveys carried out at *Regio V* and Villa of Diomedes, it was possible to collect data on the characteristics of masonry walls. It emerged that transverse connecting elements between the leaves were generally missing, except for sporadic elements. Wall thickness data collected on masonry walls at the site ranged between 0.33 m to 0.48 m. Figure 32 shows pictures of the cross-section of newly emerged rubble stone masonries at the *Regio V*.

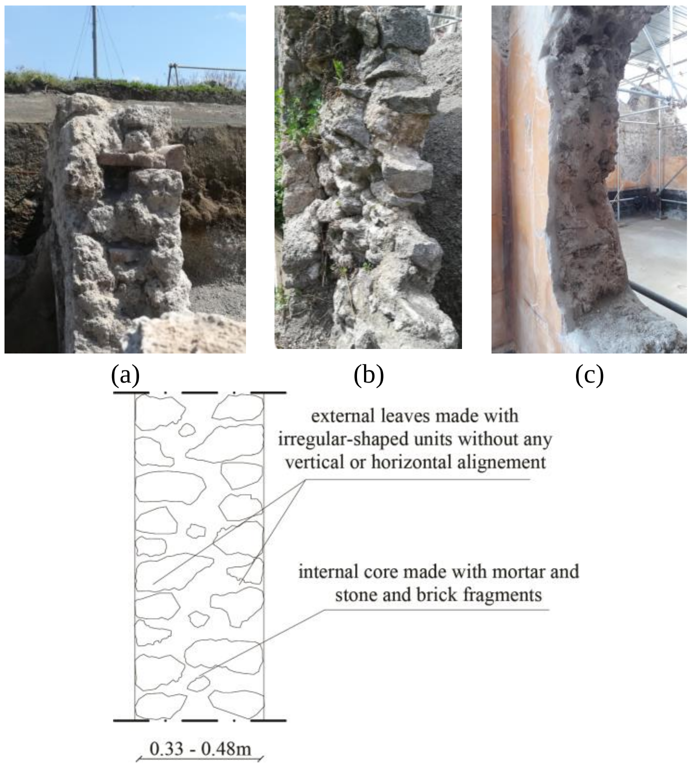

(d)

Figure 32. Views of the cross-section of rubble stone masonry structures at the Regio V of the Pompeii archaeological site (a), (b), (c) and a schematic representation of the typical cross-section (d).

Opus incertum masonries at the Pompeii site were mostly made by traditional rock types (i.e. travertine, lava, foam lava and tuff) including, in several cases, the re-use of architectural fragments (clay and marble elements) (Maiuri 1942) and abundant mortar. To define the relative proportions of the different materials composing the external leaves of a typical *opus incertum* masonry structure within the area of study, a 1.00 m x 1.00 m area of an original *opus incertum* wall surface was chosen within the excavation area at *Regio V* and examined in detail. The selection was made based on the following requirements: i) it had emerged for the first time during the excavation work (no restoration intervention was carried out on the analyzed surface); ii) the surface was easily observable (no plaster or decorative or foreign elements hindered the survey); iii) it was entirely constructed using the *opus incertum* technique; iv) it belonged to the central part of the masonry wall, and was thus considered to be representative of the typical masonry building technique; and v) it was possible to observe the transverse cross-section of the wall. The chosen ancient wall surface corresponds to the investigated masonry portion that is named ST6 in what follows. In this, the stone units were mainly lava and travertine with minor foam lava and some fragments of clay tiles or marble elements. Figure 33 describes the geometrical and material survey carried out over a 1.00 m x 1.00 m area of the original *opus incertum* wall surface.

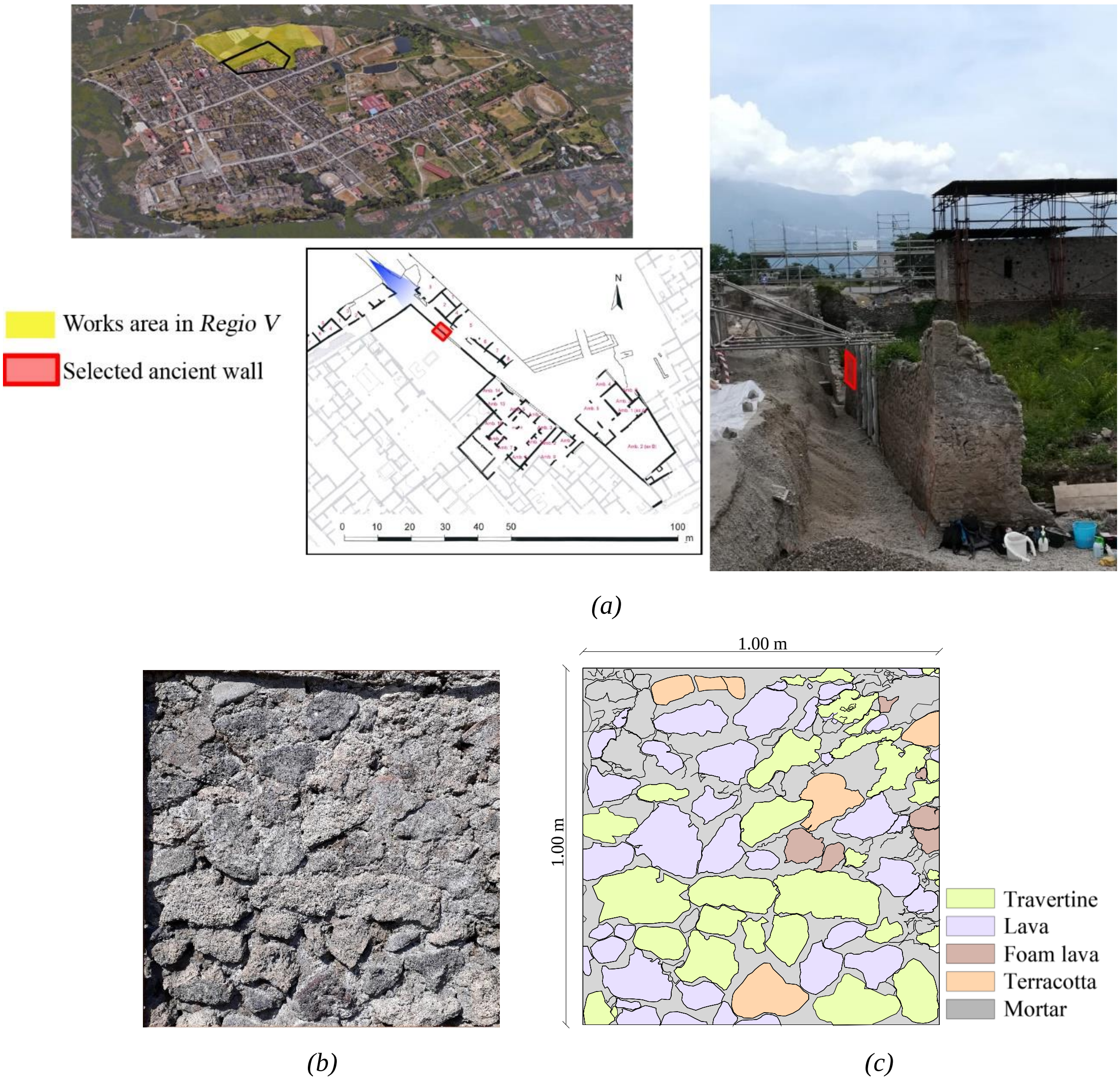

Figure 33. Ancient opus incertum *at the archaeological excavation work at* Regio V*: localization of the selected ancient wall (a); original wall surface 1.00 m x 1.00 m (b); geometrical and material survey (c).*

Based on the geometrical and material survey, it was possible to define: i) the mean size of the units; ii) the proportions between the different rock types, and iii) the proportions between the rock units and the mortar. In particular, the proportion between the different rock types within each leaf of the panels was arranged based on the following percentage values: lava units – 32%; travertine units – 30%; foam lava units – 4%; and fragments – 4%. Mortar, therefore, occupied about 30% of the wall surface. Furthermore, it was detected that: the lava units had a mean size of 151 x 91 mm, with a mean ratio between the maximum and minimum dimensions of 3:5; the travertine units had a mean size of 178 x 99 mm and a ratio of 5:9; and the foam lava units had a mean size of 117 x 78 mm and a ratio of 2:3. Obviously, for the own nature of such masonry type, the specific amount of mortar and relevant proportions among the different rocks may strongly differ in each single masonry wall.

Table 8 summarizes a description of all the tested masonry structures with the specification of the typology of composing stone units, the state of preservation of the structure and the presence of any modern intervention.

Table 8. Details of the tested rubble stone masonry structures.

ID	Description	State of preservation and deterioration	Time of excavation	Modern interventions
ST11	The masonry was prevalently made of irregular travertine and lava units, with few foam lava units and mortar.	The masonry surfaces were partially disintegrated, due to weathering. The mortar and the travertine units were friable and tendency to powder.	20^{th} century.	The masonry portion was rebuilt after the excavation with modern mortar and original stones.
ST10	The masonry was made of irregular lava units and mortar.	The masonry surfaces were in a discrete state of preservation.	19^{th} century.	Superficial repointing interventions with modern mortars were possibly carried out after the excavation.
ST9	The masonry was prevalently made of irregular travertine and lava units, with few foam lava units and mortar.	The masonry surfaces were partially disintegrated, due to weathering. The mortar and the travertine units were friable and tendency to powder.	Newly emerged.	None.
ST8	The masonry was prevalently made of irregular travertine and lava units, with few foam lava units and mortar.	The masonry surfaces were partially disintegrated, due to weathering. The mortar and the travertine units were friable and tendency to powder.	Newly emerged.	None.
ST7	The masonry was prevalently made of irregular travertine units, with few pieces of lava, foam lava units and terracotta fragments, and mortar.	The masonry surfaces were partially disintegrated, due to weathering. The mortar and the travertine units	20^{th} century.	Superficial repointing interventions with modern mortars were carried out after the excavation.

		were friable and tendency to powder.		
ST6	The masonry was prevalently made of irregular travertine and lava units, with few foam lava units and mortar.	The masonry surfaces were partially disintegrated, due to weathering. The mortar and the travertine units were friable and tendency to powder.	Newly emerged.	None.
ST5	The masonry was made of irregular lava units and mortar.	The masonry surfaces were partially disintegrated, due to weathering. The mortar was friable and tendency to powder.	19^{th} century.	Superficial repointing interventions with modern mortars were possibly carried out after the excavation.
ST4	The masonry was prevalently made of lava units, with few pieces of travertine, foam lava units, terracotta fragments, and mortar.	The masonry surfaces were in a discrete state of preservation.	19^{th} century.	Superficial repointing interventions with modern mortars were possibly carried out after the excavation.
ST3	The masonry was prevalently made of irregular travertine units and mortar.	The masonry surfaces were partially disintegrated, due to weathering. The mortar and the travertine units were friable and tendency to powder.	Newly emerged.	None.
ST2	The masonry was prevalently made of irregular travertine and foam lava units associated with horizontal courses of travertine ashlars alternated with terracotta tiles (*opus mixtum*) and squared pieces of travertine and foam lava diagonally aligned (*opus reticulatum*) and mortar. The tested masonry portion was located between a window and a wall intersection.	The masonry surfaces were partially disintegrated, due to weathering. The mortar and the travertine units were friable and tendency to powder. Widespread cracks are also evident	Newly emerged.	None.
ST1	The masonry was prevalently made of irregular travertine units, with few foam lava units and terracotta fragments, and mortar. The tested masonry portion was located between a door and a wall intersection.	The masonry surfaces were partially disintegrated, due to weathering. The mortar and the travertine units were friable and tendency to powder.	20^{th} century.	Superficial repointing interventions with modern mortars were carried out after the excavation.

3.1.3. Sonic tests investigation protocol

The ST protocol for the assessment of the archaeological masonry structures at the Pompeii site involved tests performed by transparency. A modular mesh defining a set of acquisition points was marked on both the surfaces of the investigated walls. The travel time of the longitudinal compression waves generated through the masonry wall was measured and the acquired signals were in turn displayed on a monitor to check its quality. A piezoelectric hammer transducer and a cylindrical piezoelectric broadband receiver (55 KHz resonance frequency, internally pre-amplified 20 dB), were used for each test. A coupling material was interposed between the receiver and the masonry surface to ensure a good acquisition of the received signal. Figure 34 reports a flowchart of the protocol adopted in the present study.

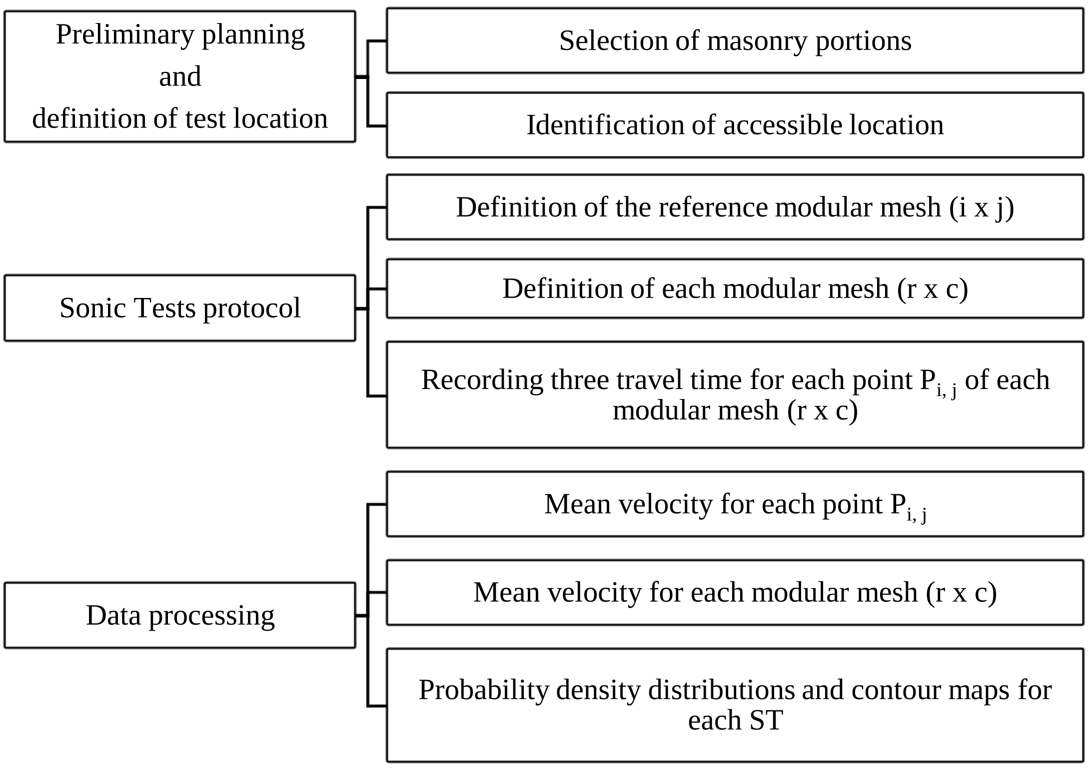

Figure 34. The protocol was adopted for the execution of sonic pulse velocity tests.

3.1.3.1. Testing procedure

The masonry portion to be investigated and the number of the points of acquisition (i.e. the size of the mesh and the spacing) were defined based on the accuracy desired in the evaluation and on the expected variability of the test results (RILEM TC 1996). A reference modular mesh 1.00 m x 1.00 m, 0.10 m spaced, involving 121 acquisition points was defined for the present experimental protocol. Nonetheless, to comply with the need for accuracy with the accessibility issues and the specific features of the single masonries, the size and spacing of the mesh were modified in many cases due to: i) a smaller available masonry portion; ii) the presence of evident voids or cracks, iii) the presence of a plaster. Figure 35 shows examples of different mesh sizes due to the specific features of the single specimens; the figure also shows the content and location of different rock units and grey color indicates mortar presence. A progressive numbering was given to the rows and the columns of the meshes on the hammer side, thus each point on the hammer side was identified by double subscript i, j (i.e. Pi, j with i = 1,… r and j = 1,… c and r = number or rows ≤11, c = number of column ≤11). For each point $P_{i,\,j}$ three recordings of travel time were collected, and the path length was conventionally assumed as the mean wall thickness. Furthermore, for each masonry portion, the reason for selecting a proper mesh size is reported in the figure legend.

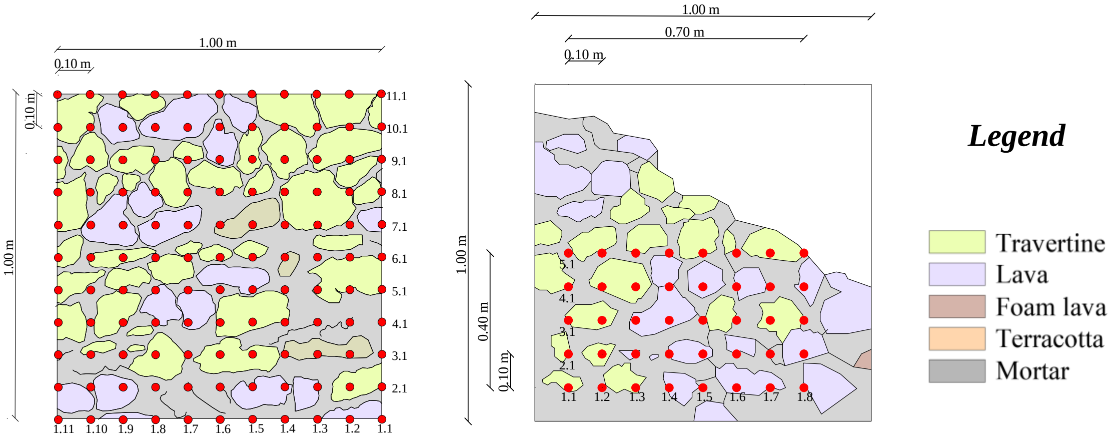

ST11: masonry portion suitable for a reference modular mesh.

(a)

ST8: masonry portion with partially available reference modular mesh due to partial collapse.

(b)

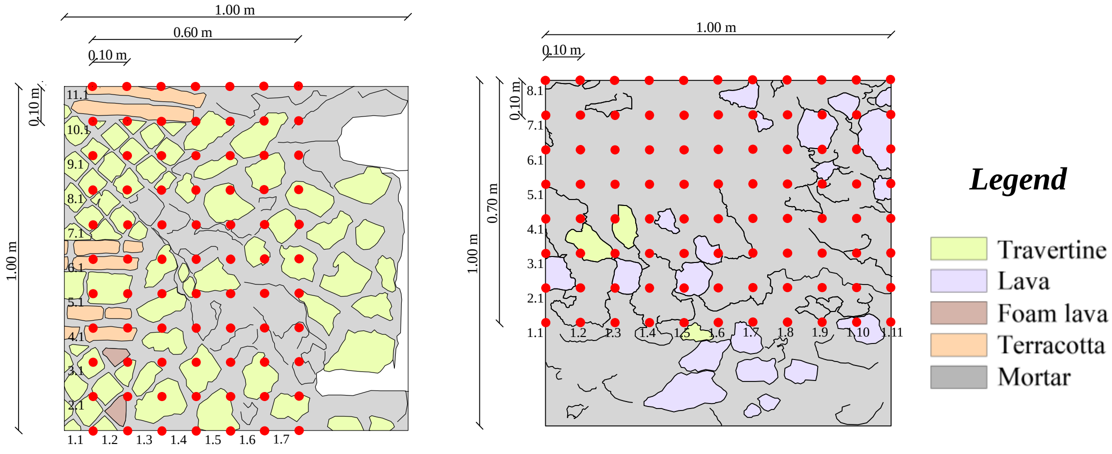

ST2: masonry portion with partially available reference modular mesh due to the presence of a window and a wall intersection.

(c)

ST6: masonry portion with partially available reference modular mesh due to severely deteriorated surface.

(d)

Figure 35. Examples of different meshes sizes on: ST11 [1.00 m x 1.00 m] (a); ST8 [0.70 m x 0.40 m] (b); ST2 [0.60 m x 1.00 m] (c); ST6 [1.00 m x 0.70 m] (d).

3.1.3.2. Data processing

For each point $P_{i,j}$ three velocities (i.e. $V_{i,j,1}$, $V_{i,j,2}$, $V_{i,j,3}$) were calculated as the ratio between each recorded travel time, t_1, t_2 and t_3, and the path length, d, Eq. (3.2):

$$V_{i,j,n} = \frac{d}{t_n} \qquad (3.2)$$

Where n =1, 2, 3 indicates the number of the recording.

The sonic pulse velocity for each point of acquisition, $V_{i,j}$, was evaluated as the mean of the three calculated velocities, Eq. (3.3):

$$V_{i,j} = \frac{V_{i,j,1} + V_{i,j,2} + V_{i,j,3}}{3} \qquad (3.3)$$

Then, the mean velocity of the masonry specimen was calculated as the mean of the velocities of all the points of acquisition Eq. (3.4):

$$V = \frac{\sum_{i=1}^{r} \sum_{j=1}^{c} V_{i,j}}{n} \tag{3.4}$$

Where V is the mean velocity of the masonry portion, $V_{i,j}$ is the velocity at generic point $P_{i,j}$ of the mesh, r is the number of the rows of the mesh, c is the number of the columns of the mesh and n is the number of the points of acquisition. After that, the frequency distribution and the probability density function were defined for each test. Finally, the outcomes of the sonic tests were also processed in terms of velocity distribution contour maps. The velocity distribution maps are an effective tool for the evaluation of the homogeneity of a masonry specimen (i.e. the presence of cracks or voids; variations in density; variations in unit and mortar strength) through the visualization of the areas with different velocities (Miranda et al. 2013; RILEM TC 1996).

3.2. Discussion of the results of sonic tests

The STs showed mean velocities in a range from 390 m/s to 1560 m/s and a CoV ranging between 22% and 65%. A summary of the outcomes of STs is reported in Table 9 in terms of mean velocity and CoV calculated for each masonry portion. The masonry data and location are also reported.

One test showed a mean velocity exceeding 1500 m/s, which is conventionally taken as a threshold for medium-quality stone masonry structures (Forde et al. 1985; Valluzzi et al. 2018) (i.e. ST11, the masonry portion that emerged since 20th century at *Regio V* and was rebuilt after the excavation with original units and new mortar). All the other investigated masonry portions, including newly and formerly emerged structures, showed mean velocity below this limit and they did not exceed 808 m/s.

Table 9. Outcomes of STs on archaeological rubble stone masonry structures.

ID	localization	mesh area [m]	number of points	wall thickness [m]	V [m/s]	CoV [%]
ST11	*Vicolo dei Balconi*	1.00x1.00	121	0.41	1560	22
ST10	*Villa of Diomedes*	1.00x0.60	24	0.40	808	33
ST9	*Regio V, Insula 3*	1.00x0.50	66	0.36	747	35
ST8	*Via del Vesuvio*	0.70x0.40	40	0.46	742	34
ST7	*Regio V, Insula 2*	1.00x0.80	99	0.39	669	65
ST6	*Vicolo dei Balconi*	1.00x0.70	88	0.44	591	28

ST5	*Villa of Diomedes*	1.00x1.00	36	0.40	558	37
ST4	*Villa of Diomedes*	1.00x1.00	36	0.48	539	25
ST3	*Vicolo dei Balconi*	0.50x0.30	24	0.33	518	37
ST2	*Via delle Nozze d'Argento*	0.60x1.00	77	0.48	413	24
ST1	*Vico di M. L. Frontone*	0.30x1.00	44	0.42	390	48

3.3.Factors affecting STs results

Different factors typically encountered in archaeological and historical contexts may affect the results of STs. For instance, the presence of large internal voids, cracks, or detachments may lead to an underestimation of the calculated sonic velocity. Indeed, the velocity is calculated as the conventional path length divided for the measured travel time, while the real path followed by the sound wave can be altered by these elements. In the following, an analysis of typical factors affecting the results of STs on ancient masonry structures is reported. Before that, the outcomes obtained for ST11, which showed a better condition compared to the other investigated masonry structures, are reported for the sake of comparison (Figure 36). Indeed, different regions of the specimen showed velocity equal to or greater than 2500 m/s with the maximum detected value of 2855 m/s and the lowest value equal to 774 m/s. With the same rock units composing that masonry portion, this result is probably related to the homogeneity and consistency of the new mortar used for its reconstruction.

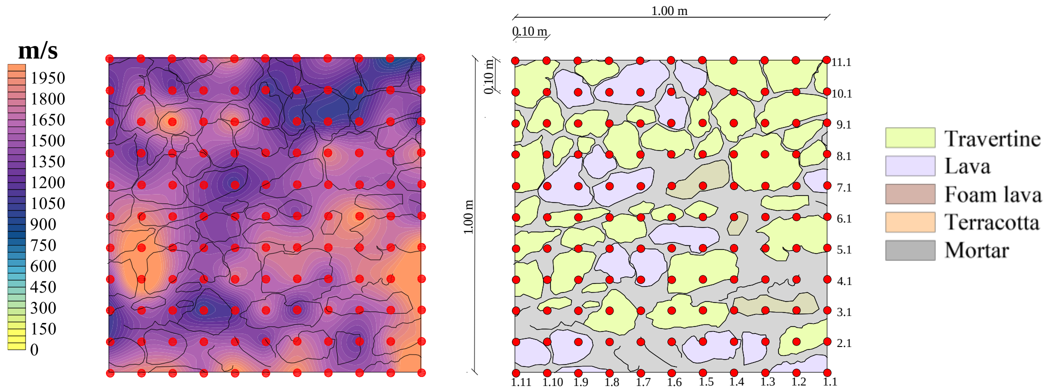

(a) (b)

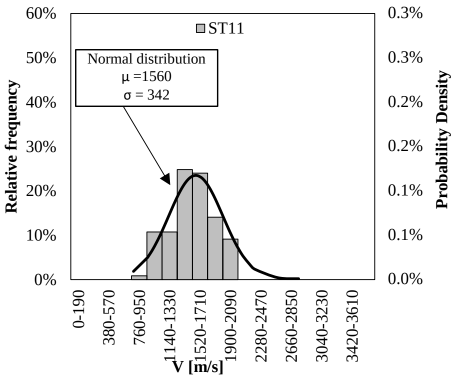

V_{mean} = 1560 m/s (CoV = 22%)
(c)


(d)


(e)

Figure 36. Example of a masonry portion with relatively good compactness and homogeneity: velocity distribution map (a); the material survey of the hammer side (b); histogram of the recorded velocities and probability density distribution (c); a picture of the hammer side (d); a picture of the receiver side (e).

3.3.1. Modern repointings

The presence of superficial modern interventions, such as mortar infills and repointing, did not provide a relevant improvement of the sonic velocity. Indeed, a meaningful improvement of compactness and homogeneity may be achieved through interventions involving the internal core of the masonry structure, such as grout injections or partial reconstructions with new mortars. Furthermore, superficial modern interventions carried out decades ago probably involved low compatible mortars that are nowadays likewise deteriorated or even detached.

For instance, Figure 37 reports the outcomes obtained on the masonry portion ST7, emerged over the 20th century at *Regio V* and repaired with modern mortar infills, that showed mean velocity comparable with the other investigated masonry structures (i.e. 669 m/s), with certain areas showing a good condition (V_{max}= 2583 m/s) and certain others showing a very poor condition, probably related to the presence of internal voids and cracks, resulting in the highest coefficient of variation (i.e. 65%).

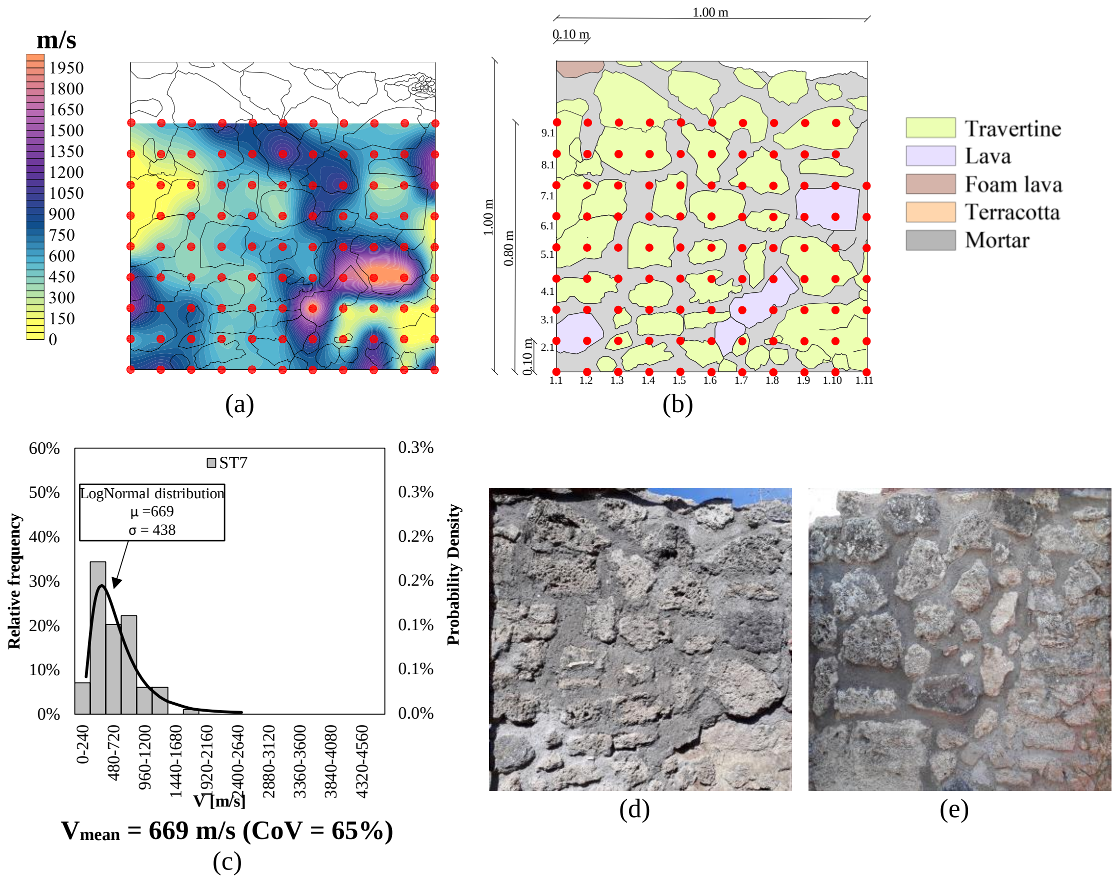

Figure 37. *Example of a masonry portion with superficial repointing: velocity distribution map (a); the material survey of the hammer side (b); histogram of the recorded velocities and probability density distribution (c); a picture of the hammer side (d); a picture of the receiver side (e).*

3.3.2. Severely deteriorated surfaces

Archaeological and historical masonry structures are generally characterized by rough surfaces due to the absence of plasters, heterogeneity and material deterioration. When the masonry surface is excessively deteriorated and brittle, the use of coupling material between the receiver and the masonry surface can be not sufficient for a perfectly correct acquisition of the sonic signal. For instance, the lower part of the masonry portion ST6 was particularly decayed and the surface was much more irregular than the upper part (Figure 38**Errore. L'origine riferimento non è stata trovata.**). A reduction of the velocity in the lower part was detected (i.e. with mean velocities equal to 637 m/s and 545 m/s for the upper and lower part, respectively). Indeed, in the present investigation, it was found that masonry portions with excessively irregular surfaces had a mean decrease of velocity of 24% compared to more regular parts.

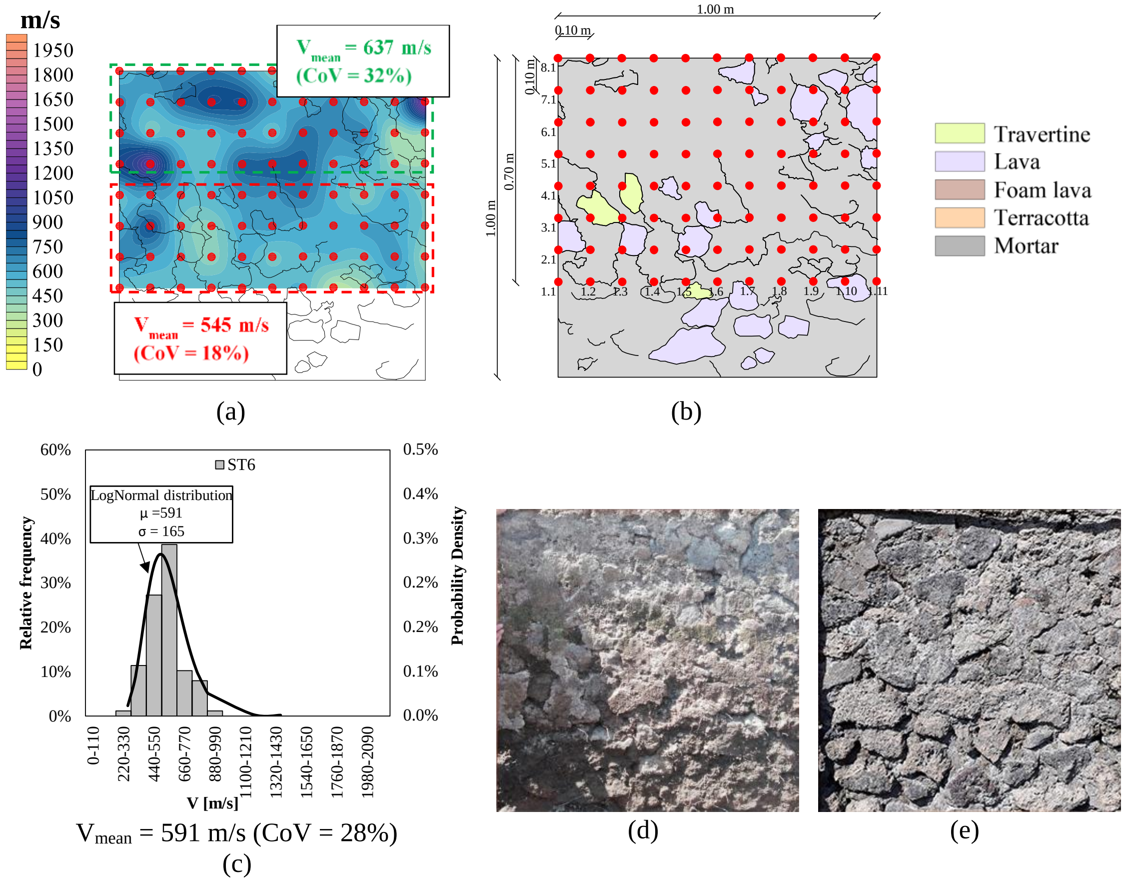

Figure 38. Example of a masonry portion with deteriorated and brittle mortar in the lower part: velocity distribution map (a); the material survey of the hammer side (b); histogram of the recorded velocities and probability density distribution (c); a picture of the hammer side (d); a picture of the receiver side (e).

3.3.3. Presence of openings and wall intersections

In correspondence of wall intersection and frames of the openings more regular masonry typologies were typically associated with the *opus incertum*. The presence of different materials and arrangements could provide different velocities. Moreover, the presence of openings leads to a reduction of the velocity due to the dispersion of the waves. For instance, ST2 was located within a window and a wall intersection, thus portions of *opus reticulatum* and *opus mixtum* were present on both sides of the wall and both the surfaces. The state of preservation resulted quite poor for the entire masonry portion, with a mean velocity equal to 413 m/s. However, a decrease of velocity from the wall intersection to the opening was detected, with the portion within a distance to the edge of the window equal to the wall thickness showing a mean velocity about 25% lower compared to the innermost part of the wall (Figure 39).

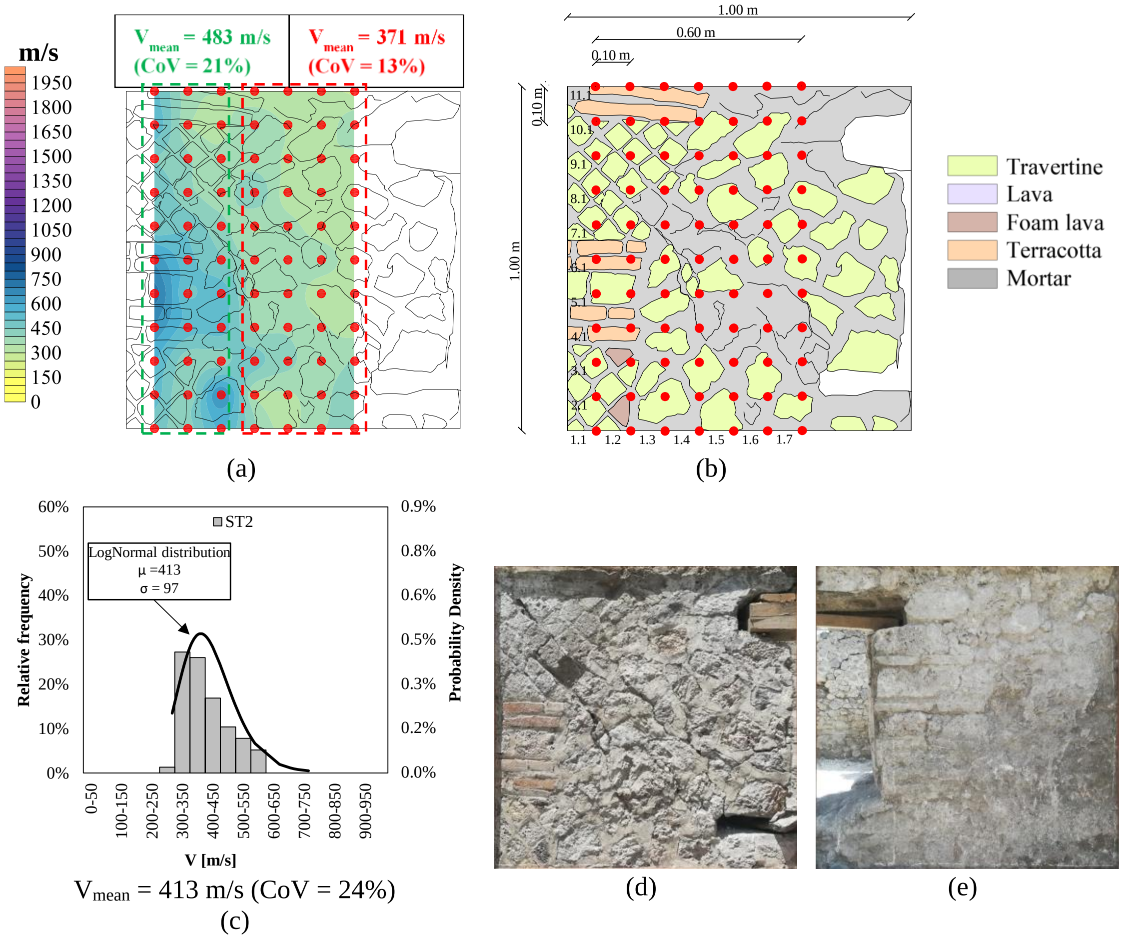

Figure 39. Example of a masonry portion between a window and a wall intersection part: velocity distribution map (a); the material survey of the hammer side (b); histogram of the recorded velocities and probability density distribution (c); a picture of the hammer side (d); a picture of the receiver side (e).

Moreover, most of the archaeological masonry walls are partially preserved in height. In these cases, masonry portions very close to the top edge exhibit a lower velocity compared to the innermost part of the wall. In the present investigation, the mean velocity of masonry portions within a distance equal to the wall thickness was estimated to be 25% lower (643 m/s) than the innermost part (862 m/s). As an example, Figure 40 reports the results obtained for ST8, and the different velocities recorded in the closer part to the edge and the inner part are highlighted (i.e. with mean velocities equal to 643 m/s and 862 m/s, respectively).

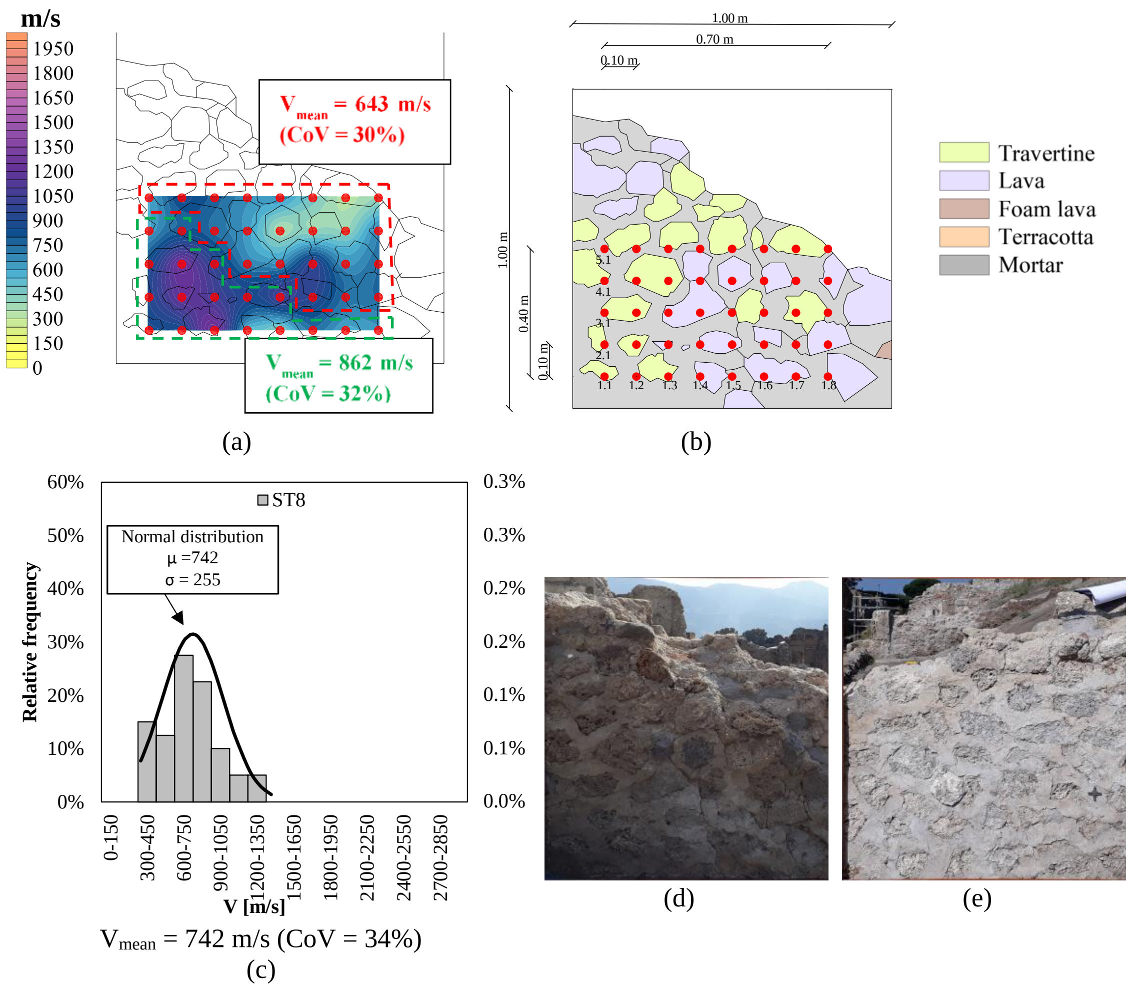

Figure 40. Example of a masonry portion close to the upper part of the wall: velocity distribution map (a); the material survey of the hammer side (b); histogram of the recorded velocities and probability density distribution (c); a picture of the hammer side (d); a picture of the receiver side (e).

3.3.4. Deterioration and detachment of a plaster

The detachment of layers covering the wall surfaces, such as plasters or waterproof layers made of *cocciopesto*, or the natural weathering of these parts can lead to low velocities. Moreover, the pulse generated on a layer made of mortar or plaster can be less energic compared to hammering directly on the masonry surface, due to the risk of damaging the mortar/plaster.

3.4. Comparison with available data of sonic tests

The implementation of a wide database of STs involving ancient masonries differing in building materials and techniques, ages and state of preservation may be a useful tool supporting the knowledge of such structures. To extend the available dataset of STs results of ancient masonry structures, the results of the present experimental programme are herein associated with available data from the present study and the literature on direct STs performed on different masonry typologies at the Pompeii site (Dessales et al. 2020; Valluzzi et al. 2019). Moreover, the review was extended with available data on the new Pompeii-like masonry panels, as reported in the following chapter. This is useful for the comparison between the archaeological and new masonry structures reported in the following. The available data are summarized in Figure 41.

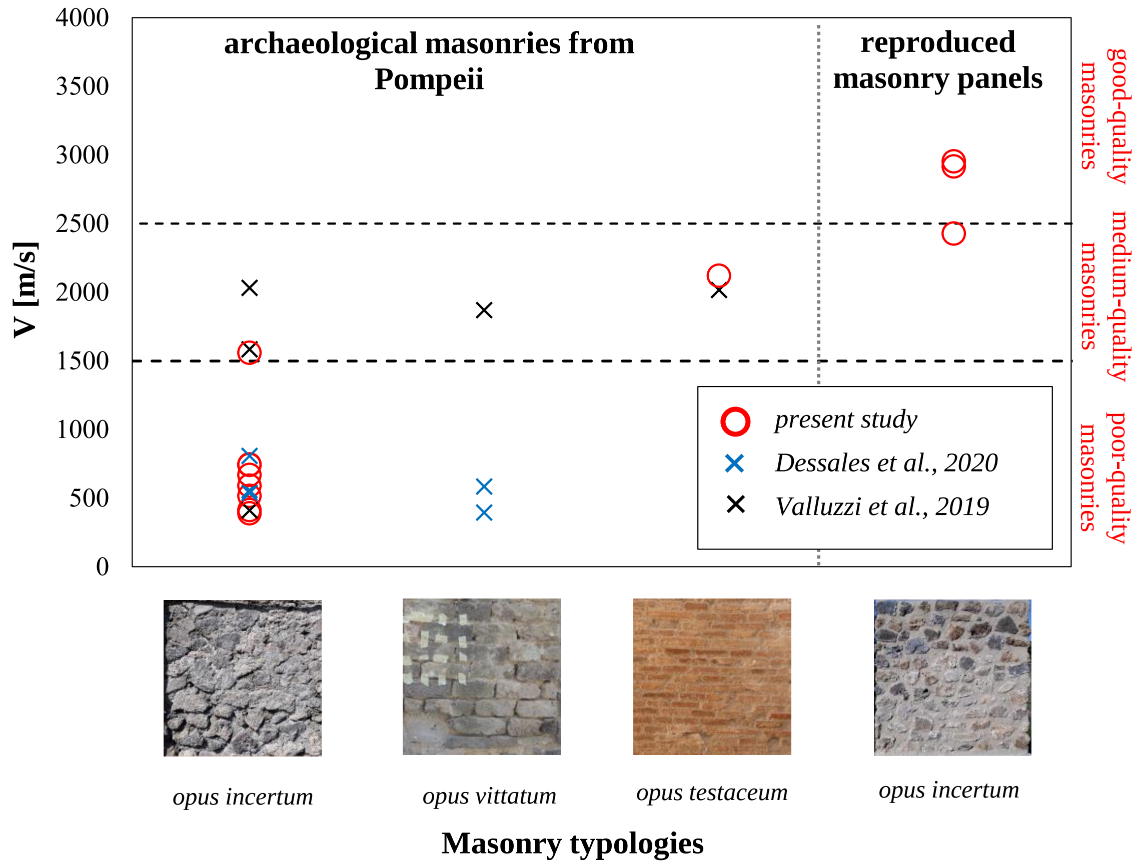

Figure 41. STs results obtained by authors and available literature for different masonry typologies at the Pompeii site and on reproduced masonry panels.

As regards the archaeological masonry structures, mean velocities ranged from very low values up to values not exceeding 2500 m/s, corresponding to the conventional poor-quality and medium-quality categories (Forde et al. 1985; Valluzzi et al. 2018). The higher sonic pulse velocities showed by the panels compared to the archaeological masonry are related to their higher compactness, particularly attributable to the new mortar.

All the involved masonry typologies (*opus incertum*, *opus vittatum* and *opus testaceum*) traditionally consist of two external leaves with an internal core made of mortar and fragments. Besides the specific conditions of each tested masonry, the type of constituent building materials and their arrangement may affect the sonic velocity. Indeed, the large amount of mortar in the external leaves and the irregular shape of the stone units may lead to low velocities in the *opus incertum*. In the *opus vittatum*, despite a lower amount of mortar on the surfaces and a more regular arrangement of the units compared to the *opus incertum*, low velocities can be related to the high porosity and weathering of the tuff elements. Finally, the limited amount of mortar in the external leaves and the compactness of the terracotta tiles may lead to higher velocities in the *opus testaceum*, compared to the other typologies.

4. CHARACTERIZATION OF POMPEII-LIKE MASONRY PANELS

Due to the impossibility to perform destructive tests, DTs, or minor-destructive tests, MDTs, on heritage structures as well as to collect large-size specimens, after the characterization of the ancient rubble stone masonry structures through the sonic pulse velocity tests, STs, the next phase of the experimental programme involved the realization of masonry panels reproducing the ancient technique *opus incertum* for the execution of both STs and standard DTs (i.e. diagonal compression tests and axial compression tests).

The execution of standard DTs is fundamental for a direct estimation of the main mechanical properties of masonry assemblages. Axial compression test and diagonal compression test are among the most common standard DTs used for the characterization of stone masonry structures.

The axial compression test allows obtaining important information on the mechanical properties of masonry specimens in the vertical direction: the ultimate compressive strength; the deformation capacity; the elasticity properties (i. e. modulus of elasticity and Poisson ratio) (CEN 1999a). The axial compression test consists of applying monotonically or cyclically a uniform compression load to the masonry specimen. To obtain the compressive strength of the masonry and investigate the deformation capacity in compression, the load must be applied to the specimen up to the failure and the maximum load achieved and the vertical displacement must be recorded. If the modulus of elasticity, E, is to be determined, specific measuring devices must be applied to the specimen for measuring the vertical shortening. Moreover, for the definition of the modulus of elasticity, the compressive load should be applied by several loading cycles until a load stage is estimated to be in the elastic range compared to the maximum load expected. The European Standard EN 1052-1 (CEN 1999a) specifies the testing method for the determination of the masonry compressive strength (and modulus of elasticity) concerning a one-leaf masonry specimen made with regular bricks and mortar, and it is also commonly adapted to experimentations with three-leaves rubble stone masonry specimens (Magenes et al. 2010; Milosevic et al. 2013a; Silva 2012; Valluzzi 2000) (Figure 42).

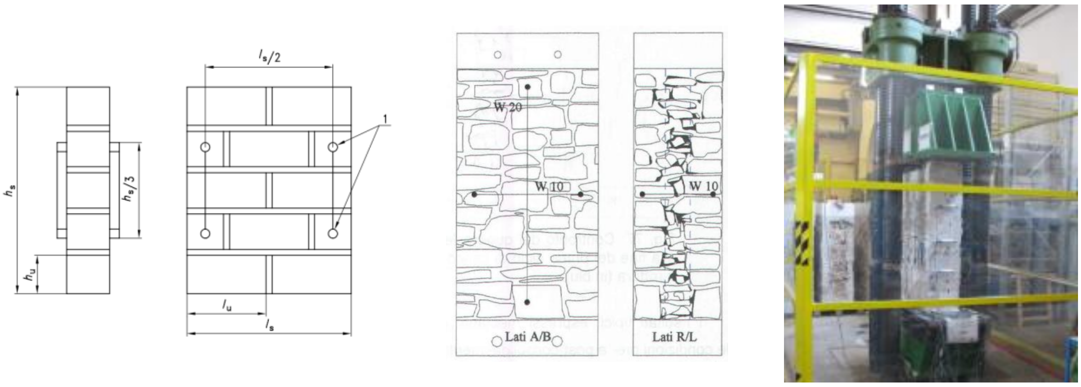

(a) (b) (c)

Figure 42. Test specimen and positioning of the measuring devices indicated by the Standard EN 1052-1 (CEN 1999a) *(a) and adopted for three-leaves rubble stone masonry specimens from* (Valluzzi 2000) *(b) and test equipment reported in* (Silva 2012) *(c).*

The diagonal compression test is one of the most common methods used to investigate the shear behavior of masonry structures: the shear strength, the secant shear modulus, the shear deformability. Studies in the literature report on different investigations and numerical analyses that use diagonal compression tests to examine the shear behavior of ancient rubble stone masonry walls (Borri et al. 2011; Brignola et al. 2009; Chiostrini et al. 2000; Milosevic et al. 2013a; b). Such experiments were carried out on existing *in situ* masonry walls (Borri et al. 2011; Brignola et al. 2009; Chiostrini et al. 2000), or on reproduced masonry panels in the laboratory (Milosevic et al. 2013a; b). The test consists of applying a compressive load on one of the diagonals of a square masonry panel, through a hydraulic jack placed on the upper edge of the panel. When the test is performed in the laboratory, the masonry panel is positioned with its diagonals parallel to the vertical and horizontal directions, while when the test is performed on-site on existing masonry structures, the masonry panel is isolated from the wall through cuts carried out by a diamond wire along its perimeter, except for a section on the lower side. In both cases, the values of the diagonal displacements are measured by two Linear Variable Displacement Transducers (LVDT) on each side of the specimen (Figure 43).

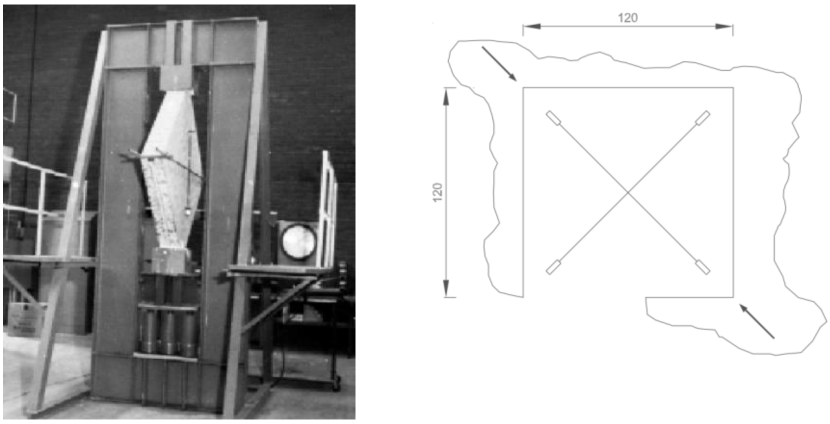

(a) (b)

Figure 43. Test specimen and positioning of the measuring devices indicated by the Standard ASTM E-519-02 (ASTM 2002) *for a test performed in the laboratory (a) and schematic representation of the set-up of the in-situ diagonal compression test by* (Borri et al. 2011) *(b).*

Two main methodologies are used for the interpretation of the diagonal compression test outcomes: the one proposed by ASTM Standard E-519-02 (ASTM 2002) and the one proposed by RILEM Standard LUM B6 (RILEM TC 1994). The two interpretations mainly differ in the definition of the stress field inside the masonry specimen when subjected to diagonal compression. According to the ASTM standard, the diagonal compression test produces uniform shear stress in the specimen, while according to the RILEM formulation the stress field is not uniform; thus the two interpretations lead to different values of the tensile strength of the masonry (Brignola et al. 2009).

However, very few studies concerning DTs on archaeological masonry structures are available. Indeed, using such tests on original *in situ* masonry walls requires large volume specimens, meaning that, for conservation purposes, the application of these tests in heritage contexts is strictly limited. A possible approach for the investigation of mechanical properties of traditional masonry typologies through standard DTs is the construction of new masonry panels that comply with the ancient structures, based on a detailed knowledge of the specific masonry techniques used in antiquity and the properties of the materials, rather than the use of skilled workmanship.

In this chapter, a wide experimental programme involving the construction and characterization through NDTs and DTs of rubble stone masonry panels compliant with the ancient building technique *opus incertum* is presented. The panels were constructed with archaeological stone units and compatible mortar, by carefully following the ancient technique *opus incertum* found at Pompeii. The programme involved the execution of sonic tests, with the same setup and methodology adopted for the archaeological walls, diagonal compression tests conducted at the Pompeii site and axial compression tests conducted in the laboratory.

4.1. Experimental programme

Three panels 1.20m x 1.20m x 0.45m were specifically designed based on an in-depth survey of the archaeological *opus incertum* structures at the site. Indeed, original stone units from the ruins emerged in the excavations at *Regio V* and lime and pozzolana based mortars compliant with the traditional typologies were selected to build the panels. A campaign of sonic tests was performed on the panels as a preliminary phase to the execution of DTs at different ages to: i) evaluate the evolution of the hardening process of the panels; ii) compare the results with the ones of the DTs to be performed; iii) provide useful data to set up a comparison with similar archaeological structures at the site. Afterward, the first phase of the experimental programme of DTs involved the execution of three in-situ diagonal compression tests to derive the masonry shear strength and relevant correlation with sonic velocities. Diagonal compression tests were performed according to (ASTM 2002), with a specific set-up designed for the execution of outdoor tests. Finally, after the diagonal compression tests, five masonry specimens were extracted from the undamaged portion of the panels to perform laboratory axial compression tests.

The following sections describe in detail: the creation of the panels; the results of the sonic tests; the crack patterns, failure mode and shear capacity of the panels subjected to diagonal compression tests; the results in terms of axial compression strength and elastic modulus as well as the analysis of the crack pattern and failure mode as regards the specimens subjected to the axial compression test; the correlation between the results of the NDTs and DTs.

4.1.1. Design of the masonry wall panels

4.1.1.1. Wall assemblage

The definition of the shape, size, nature and arrangement of the rock units for the construction of the Pompeii-like masonry panels was based on detailed surveys of original structures, particularly focusing in the area of the *Regio V* at the site, while the definition of the mortar was mainly based on the traditional composition and materials knowledge. Masonry panels were therefore produced based on geometric and material surveys, following the original building technique. The leaves were made up of irregular-shaped rock units embedded in the core without transverse connecting elements. The wall fabric had no vertical alignments or horizontal levelling-elements; the different shaped and sized units were arranged so that the smallest ones filled the gaps between the largest. The rock units were mainly lava and travertine with minor foam lava, tuff and some fragments of clay tiles or marble elements with approximatively the following proportions: lava units – 30%; travertine units – 30%; foam lava units, tuff units and fragments – 10%. Mortar therefore occupied about 30% of the wall surfaces. The thickness of the panels was established according to in situ surveys on eleven similar rubble stone masonry panels in the area under investigation at the site. The collected thickness values ranged between 0.33 m to 0.48 m. To be fully representative of existing full-scale masonry panels a thickness of 0.45 m was selected for the tests.

4.1.1.2. Building materials

The stone units used for the realization of the panels were collected within the archaeological excavations at the *Regio V* and belonged to original *opus incertum* masonry structures partially collapsed over the eruption of the Vesuvius in 79 A.C. The main rock types used were travertine, lava and foam lava (i.e. "*calcare del Sarno*", "*lava*" and "*cruma*"). The characterization of these rock typologies is described in chapter 2.

As regards the mortar, the mixture was defined to be as compatible as possible with the mortars traditionally produced by the Ancient Roman builders in this area: a mixture based on the traditional techniques in terms of binder/aggregate ratio (i.e. 1:3, according to the Vitruvius provisions) and the constituent materials (i.e. putty lime as binder and pozzolana as aggregate) was selected (Adam 2014; Giuliani 2007). In particular, the precious and limitedly available natural pozzolan used for the mortar came from the Phlegrean Fields in Campania, Italy, the same volcanic area where the ancient builders in Roman time collected their aggregate and called it *pulvis puteolanus*. For the mechanical characterization of such mortar six prismatic specimens 40mm x 40mm x 160mm were realized, then flexural and compression tests were performed according to (CEN 2007a). The flexural tests allowed obtaining the flexural strength of the mortar, f, according to Eq. (4.1), and the compression tests performed on the two halves obtained from each prismatic specimen after the flexural test allowed obtaining the compressive strength, f_c, equal to the maximum attained compressive stress for each specimen, σ_{max}.

$$f = 1.5\frac{F\,l}{b\,d^2} \tag{4.1}$$

Where F is the maximum load attained by the prismatic specimen trough three-point bending test, b is the width of the specimen (40mm) and d is the distance between the supports of the specimen in the three-point bending test (100mm).

This mortar was produced and cured in a proper area at the Pompeii site, which was specifically organized for the realization of the masonry wall panels and for the execution of the diagonal compression tests. Moreover, to evaluate the strength evolution, a set of three specimens was tested at one month and another set of three specimens was tested at two months from casting. Figure 44 shows the realization of the mixture and the specimens *in situ*.

(a) (b) (c)

Figure 44. Realization of the mortar in situ*: raw materials (a); hand mixing (b) and preparation of the prismatic specimens (c).*

The main mean outcomes obtained on each set of specimens are summarized in Table 10. In detail Table 10 reports: the age at which the tests were performed; the number of prismatic specimens, n_{prisms}; the mean bulk density evaluated on the prismatic specimens, ρ; the mean flexural strength evaluated on the prismatic specimens, f; the number of cubic specimens, n_{cubes}; the mean compressive strength evaluated on the cubic specimens, f_c. The results showed an increase of +21% of the compressive strength moving from one month to two months of curing time.

Table 10 Main mean results of tests performed on the mortar specimens.

Age	n_{prisms}	**ρ [kg/m³]**	**f [MPa]**	n_{cubes}	f_c **[MPa]**
1 month	3	1181 (CoV = 3%)	0.77 (CoV = 6%)	6	2.39 (CoV = 3%)
2 month	3	1105 (CoV = 2%)	0.55 (CoV = 9%)	6	2.87 (CoV = 5%)

4.1.1.3. Specimens construction

Three double-leaf masonry panels with the dimensions 1.20 m × 1.20 m × 0.45 m were produced using the ASTM standard E 519-02 (ASTM 2002) and named S1, S2 and S3 in what follows. The panels were built and cured in a proper area at the Pompeii site, which was specifically organized for the execution of our tests. The diagonal compression tests were carried out after five months of curing. The four sides of each panel were named as follows: “A” for the E-oriented wall surface; “B” for the W-oriented wall surface; “C” for the N-oriented transverse surface; and “D” for the S-oriented transverse surface.

The realization of the panels was carried out by specialist manual workers following the technique *opus incertum*. The laying of the rock units and the mortar was monitored to obtain masonry panels as similar as possible to the selected masonry wall. Basic criteria were therefore guaranteed: i) the width of the mortar joint between the overlapped units had to be no larger than about 4 cm; ii) the rock units had to be arranged to combine those with a polyhedral shape and those with an elongated shape; and iii) the rock units had to be arranged to combine units of different sizes. The transverse cross-section of the panels, with a thickness of 45 cm, was filled in its internal part with fragments of units of the different rock types. Figure 45 shows the execution stages for the masonry wall panels and the labels used for the four sides of each panel.

(a)

(b)

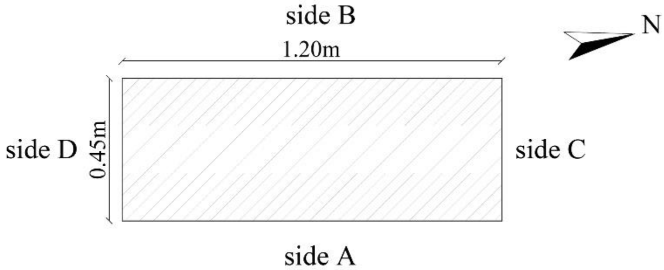

(c)

Figure 45. Construction of the masonry panels: laying of a rock unit on a wall surface (a); first half of a panel (b); labels for the four sides of each panel (c).

After the realization of the panels, the effective areas occupied by the mortar and rock units for the two sides of each panel were measured based on the geometric survey and are set out in Table 11. Figure 46 shows the three complete panels.

Figure 46. Complete masonry panels: from the right S1, S2 and S3.

Table 11. The areas occupied by mortar and stone units for the two surfaces of each panel.

	S1				S2				S3			
	side A		**side B**		**side A**		**side B**		**side A**		**side B**	
	[m²]	**[%]**	**[m²]**	**[%]**	**[m²]**	**[%]**	**[m²]**	**[%]**	**[m²]**	**[%]**	**[m²]**	**[%]**
Mortar	0.69	48%	0.61	42%	0.62	43%	0.60	42%	0.64	44%	0.57	40%
Units	0.75	52%	0.83	58%	0.82	57%	0.84	58%	0.80	56%	0.87	60%
Total area	1.44	100%	1.44	100%	1.44	100%	1.44	100%	1.44	100%	1.44	100%

4.1.2. Sonic tests investigation protocol

To investigate the evolution of the consistency of the masonry panels with the hardening process, three sonic tests were carried out on each panel at 12, 44 and 148 days from the time of the construction. The last sonic test was carried out five days before the execution of the diagonal compression test (153 days). This was done to correlate the results of the NDTs with the results of the DTs. The adopted procedure and data processing are described in the following. They were compliant with the test protocol defined for the archaeological masonries, as described in chapter 3.

4.1.2.1. Testing procedure

The sonic test equipment consisted of: i) an instrumented hammer for generating the input pulse; ii) an accelerometer to receive the transmitted pulse; and iii) an acquisition unit coupled with a computer to acquire, monitor, store and process the data. The tests were carried out by direct transmission, i.e. placing the hammer and the accelerometers in line on the opposite wall surfaces of each panel. The hammer side corresponded to side A of each panel.

Given the substantial heterogeneity of the masonry type, a significant number of acquisitions were collected along the entire surface of each panel. To this end, a modular mesh (100 mm spaced) was designed on the two wall surfaces of each panel, meaning that 121 acquisition points were defined for each one. The rows and columns of the mesh were specified concerning the hammer side by a progressive number from left to right and from bottom to top. Each point was specified by a double subscript indicating the row and column, respectively ($P_{i,j}$, where i = 1, …11 and j = 1, …11) (Figure 47). This was consistent with the reference mesh defined for the archaeological walls.

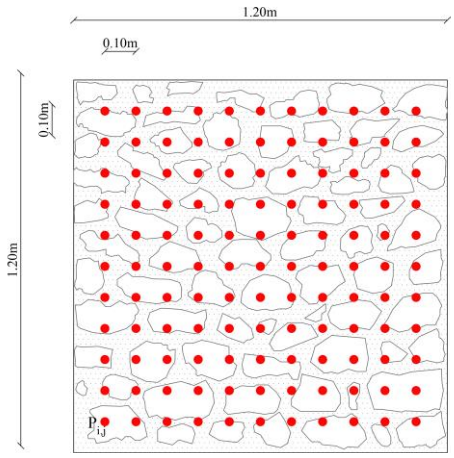

Figure 47. Mesh and acquisition points on the hammer side of the panel S1.

4.1.2.2. Data processing

For each sonic test performed at time t, where t = 12, 44 and 148 days, the velocity in a single point of the mesh, $V_{i,j}$, was evaluated as the mean of three recordings (for a total of 363 recordings on each panel), according to Eq. (3.2) where the path length, d, was equal to 0.45m, and Eq. (3.3). Consequently, a reference velocity for each panel at each age, V_t, was defined as the mean of the velocities of the single points, according to Eq. (4.2).

$$V_t = \frac{\sum_{i=1}^{11} \sum_{j=1}^{11} V_{i,j}}{121} \tag{4.2}$$

Similarly to what was done for the archaeological masonry structures, the outcomes of the sonic tests were also processed in terms of the frequency distribution, the probability density functions and distribution contour maps for each test.

4.1.3. Diagonal compression tests

The experimental outcomes were processed according to the ASTM standard E 519-02 (ASTM 2002). In this formulation, the shear stress, τ, is evaluated as reported in Eq. (4.3):

$$\tau = \frac{0.707 \cdot P}{A_n} \tag{4.3}$$

concerning net area of the panel, calculated as reported in Eq. (4.4):

$$A_n = \frac{t \cdot (w + h)}{2} \tag{4.4}$$

where w, h and t are the width, height and thickness of the panel, respectively. The shear strength of each panel was evaluated as the shear stress corresponding to the maximum applied load, τ_{max}. In the ASTM formulation this is equal to the tensile strength of the masonry, f_t. The mean strains on the compressed and tensile diagonals, ε^- and ε^+, were computed as the mean displacements on the two sides over the gauge length. The shear strain, γ, was evaluated as the mean shear strain on the sides of the panel. This was calculated for each side as the sum of the compressive and tensile strain related to the LVDT recordings, Eq. (4.5):

$$\gamma = \varepsilon^- + \varepsilon^+ \tag{4.5}$$

The secant shear modulus, $G_{30\%}$, was evaluated as the ratio between the shear stress and the shear strain in the elastic field at a strength level corresponding to 30% of the peak force, as also reported in (Chiostrini et al. 2000; Milosevic et al. 2013a; b), Eq. (4.6):

$$G_{30\%} = \frac{\tau_{30\%}}{\gamma_{30\%}} \tag{4.6}$$

The conventional failure was defined in correspondence with a strength degradation of 20% of the peak force, while the shear deformability ratio, μ_γ, was computed as the ratio between the mean shear strain at the conventional failure, γ_u, and at the peak force, $\gamma_{\tau max}$, Eq. (4.7):

$$\mu_\gamma = \frac{\gamma_u}{\gamma_{max}} \tag{4.7}$$

Energy dissipation, ED, during the test was also computed by calculating the area below the stress-strain curves.

4.1.3.1. Set-up of the in-situ tests

The diagonal compression tests were carried out with a specifically designed set-up for the *in-situ* tests. Two “L”-shaped steel shoes were used to apply the diagonal compression load to two opposite corners of the panels. A layer of 40/50 mm-thick shrinkage-free and quick-setting mortar was applied to the two corners of each panel to prevent local brittle failures at the interface between the steel shoes and the panel. The steel shoes were connected by two steel-threaded rods linked by spherical hinges to absorb potential out-of-plane displacements during the tests. A set of adjustment screws on the top steel shoe helped with the correct fitting of the shoes to the panels. The placement of the steel shoes was carried out to minimize the eccentricity between the application axis of the diagonal compression load and the geometric axis of each panel. One side of the base of each panel was removed to realize the mortar layer and the placement of the lower steel shoe. The upper part of the base on the opposite side of each panel was also removed to allow free strain on the panels during the tests. Tests were carried out on the displacement control to enable the monitoring of the post-peak response with a 0.02 mm/s rate. The displacement was applied using a servo-hydraulic jack operated by an electrical pump connected to the lower steel shoe. During the tests, the in-plane displacements along the principal directions were measured using four LVDTs (Linear Variable Displacement Transducers) and two S-LVDTs (Stringer Linear Variable Displacement Transducers) for each panel. Two LVDTs were placed on both diagonals of each side of the panels, over a gauge length of 400 mm, while the S-LVDTs were placed on the two diagonals subjected to tensile activity. The set-up for the diagonal compression tests and the instrumentation for measuring the displacements are shown in Figure 48.

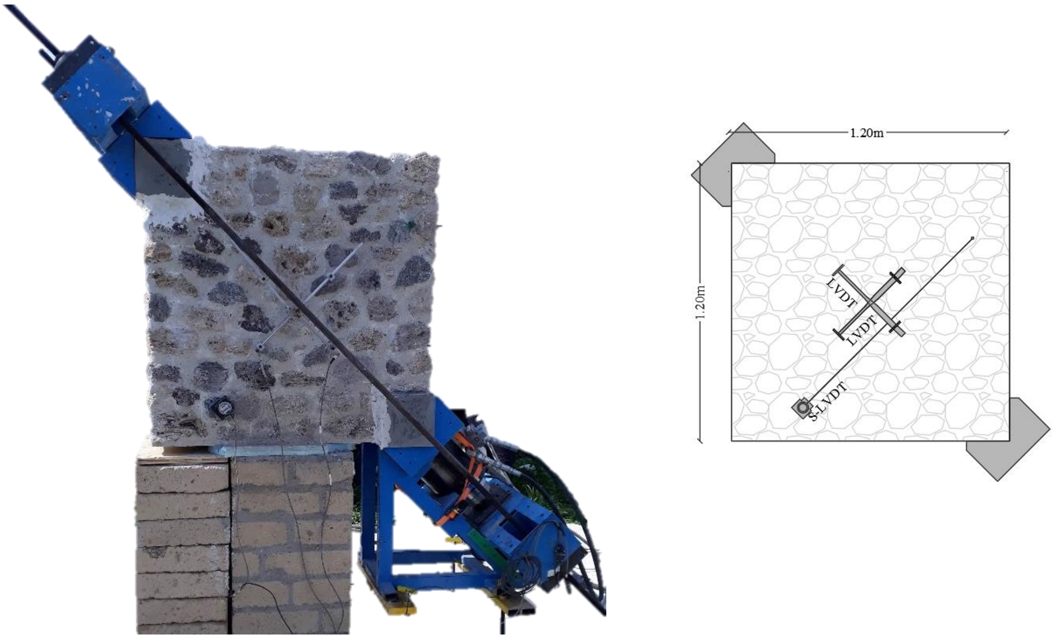

(a) (b)

Figure 48. Test set-up for diagonal compression tests (a); location of LVDTs and S-LVDTs on each side of the panels (b).

4.1.4. Axial compression tests

After the execution of the diagonal compression tests, five masonry specimens were extracted from the undamaged portion of the panels to perform laboratory axial compression tests (Figure 49).

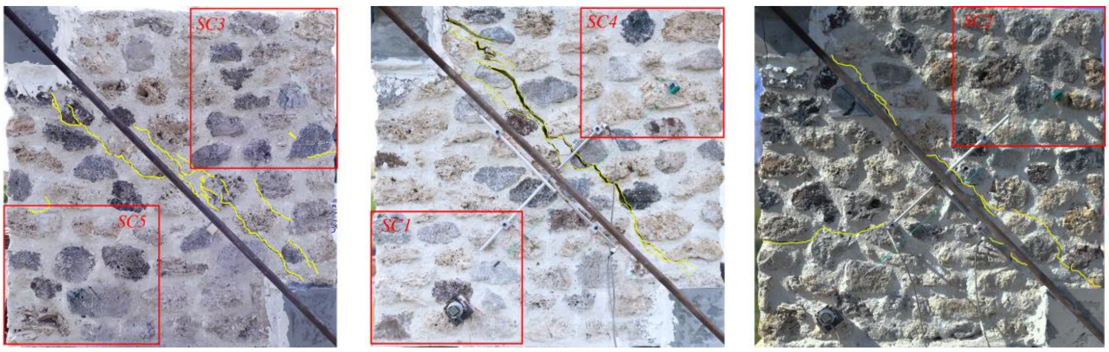

(a) (b) (c)

Figure 49. Masonry panel 1.20m x 1.20m x 0.45m (a); scheme indicating the portion of one of the panels extracted for the execution of the axial compression tests; one of the extracted specimens (c).

The extracted specimens were labeled as: SC1, SC2, SC3, SC4 and SC5. For each test, the axial compressive strength, f_{ci}, was evaluated as the maximum load recorded, $F_{max,i}$, divided by the area of the loaded cross-section, A_i, according to Eq. (4.8):

$$f_{c,i} = \frac{F_{max,i}}{A_i} \tag{4.8}$$

The first test performed on SC1 involved a single loading ramp in order to define the maximum attained force, $F_{max,1}$. The following tests involved cyclic testing protocols set between the 10% and the 50% of $F_{max,1}$, in order to investigate the elastic behavior of the specimen (CEN 1999a). To that end, the loading ramps of the cycles, except for the first, were considered. Note that two cycles after the first were performed for SC2 and three cycles were performed for SC3, SC4 and SC5.

The vertical, horizontal and transverse deformation, $\varepsilon_{v,i}$, $\varepsilon_{h,i}$, $\varepsilon_{t,i}$, were computed as the mean of the displacements measured from the corresponding devices over their initial lengths (being the horizontal direction parallel to the external leaves and the transversal direction parallel to the thickness of the panels), according to Eq. (4.9), (4.10), (4.11), (4.12):

$$\varepsilon_i = \frac{\Delta l_i}{l_{0,i}} \tag{4.9}$$

$$\varepsilon_{v,i} = \frac{\sum_{k=1}^{4} \varepsilon_{v,k,i}}{4} \tag{4.10}$$

$$\varepsilon_{h,i} = \frac{\sum_{k=1}^{2} \varepsilon_{h,k,i}}{2} \tag{4.11}$$

$$\varepsilon_{t,i} = \frac{\sum_{k=1}^{2} \varepsilon_{t,k,i}}{2} \tag{4.12}$$

Therefore, two values of elastic modulus were calculated (ASTM 1970). The first is the secant elastic modulus evaluated from zero stress to one-third of the compressive strength, $E_{1/3,i}$, in line with what reported in the European Standard EN 1052-1 (CEN 1999a), Eq. (4.13):

$$E_{1/3,i} = \frac{f_{c,i}}{3 \cdot \varepsilon_{v,i}(1/3)} \tag{4.13}$$

where $\varepsilon_{v,i}(1/3)$ is the vertical strain corresponding to one-third of the compressive strength, calculated as the mean of the values recorded on the selected loading ramps of the loading/unloading cycles.

The second is the mean elastic modulus of the loading/unloading cycles: i.e. evaluated by making a linear least-squares fit the loading ramp of the cycle in the stress-strain curves and calculating the mean of the slopes of the three obtained lines, $E_{m,i}$, according to Eq. (4.14), as shown in Figure 50.

$$E_{m,i} = \frac{slope_{1,i} + slope_{1,i} + slope_{1,i}}{3} \tag{4.14}$$

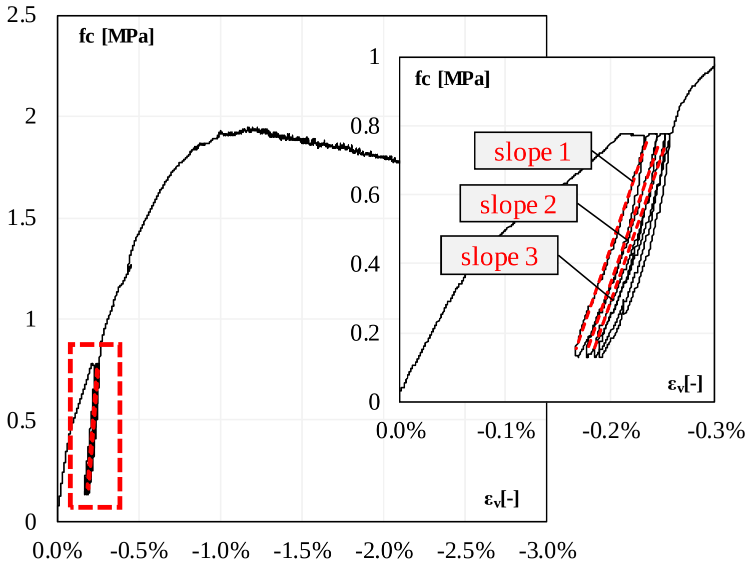

Figure 50. Scheme of determination of the mean elastic modulus of the three loading/unloading cycles of each test.

Considering the anisotropy of masonry specimens, two different Poisson ratios were also calculated for each specimen: one in the horizontal, $\nu_{h,i}$, and one in the transverse, $\nu_{t,i}$, direction, Eq. (4.15) and (4.16):

$$\nu_{h,i} = \frac{\varepsilon_{h,i}(1/3)}{\varepsilon_{v,i}(1/3)} \tag{4.15}$$

$$\nu_{t,i} = \frac{\varepsilon_{t,i}(1/3)}{\varepsilon_{v,i}(1/3)} \tag{4.16}$$

where $\varepsilon_{v,i}$(1/3), $\varepsilon_{h,i}$(1/3) and $\varepsilon_{t,i}$(1/3) represent the vertical, horizontal and transversal strain corresponding to the to one third of the compressive strength, being each of them calculated as the mean of the values recorded on the selected loading ramps of the loading/unloading cycles.

Given the modulus of elasticity and the Poisson ratio, two values of shear modulus, $G_{1/3,i}$ and $G_{m,i}$ were also calculated as Eq. (4.17) and (4.18):

$$G_{1/3,i}= \frac{E_{1/3,i}}{2(1+\nu_{h,i})} \tag{4.17}$$

$$G_{m,i}= \frac{E_{m,i}}{2(1+\nu_{h,i})} \tag{4.18}$$

Being the conventional failure defined in correspondence of a strength degradation of 20% of the peak force, the vertical deformability ratio, $\mu_{\varepsilon,i}$, was computed as the ratio between the mean vertical strain at the conventional failure, $\varepsilon_{v,u,i}$, and at the peak force, $\varepsilon_{v,max,I}$, Eq. (4.19):

$$\mu_{\varepsilon,i} = \frac{\varepsilon_{v,u,i}}{\varepsilon_{v,max,i}} \tag{4.19}$$

Finally, the energy dissipation, ED_i, during the test was also computed by calculating the area below the stress-strain curves. In the following, the set-up and the results of the axial compression tests are reported for each masonry specimen.

4.1.4.1. Set-up of the tests

Layers of about 30 mm-thick shrinkage-free and quick-setting mortar were applied at the top and bottom surfaces of each specimen to ensure that the load distribution faces of the specimens were flat, parallel between them and perpendicular to the direction of application of the load and also to prevent local brittle damages. Between the specimens and the hydraulic cylinder of the testing apparatus, a steel beam, a steel plate was placed on the top surface of the specimens to ensure a uniform loading. For specimens SC3, SC4 and SC5 a load-cell with a hinge was also inserted.

All the tests were performed under displacement control with a rate of 0.02 mm/s. As above mentioned, the first test involved a single loading ramp up to the failure, the following tests involved cyclic testing protocols set between 10% and 50% of the maximum attained load in the first test. This was done to investigate the elastic behavior of the specimens by using the recordings on the loading ramps of the cycles, discarding the first loading ramp. Two cycles after the first were performed for SC2 and three cycles were performed for SC3, SC4 and SC5. Figure 51 reports the time-load curve obtained from the test on SC4 and the adjacent table reports all the ramps identified by a progressive number with the specification of the initial load, F_1, and the ending load, F_2. Note that at the end of each loading and unloading ramp of the cycles, a constant ramp of 60 seconds was set, to stabilize the state of stress in the specimen. All the test protocol was defined so that the entire test lasted about 30 minutes.

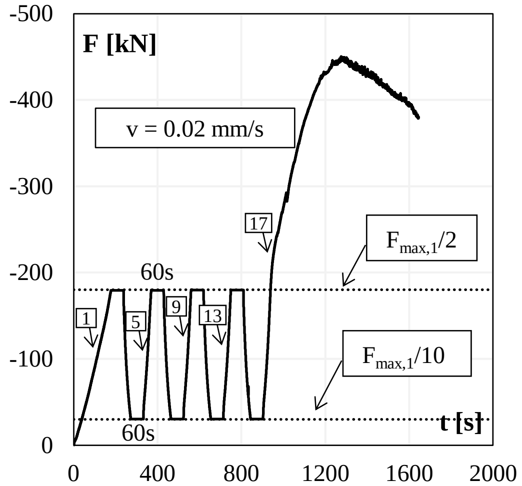

Ramp	F1 [kN]	F2 [kN]
1	0	-180
2	-180	-180
3	-180	-30
4	-30	-30
5	-30	-180
6	-180	-180
7	-180	-30
8	-30	-30
9	-30	-180
10	-180	-180
11	-180	-30
12	-30	-30
13	-30	-180
14	-180	-180
15	-180	-30
16	-30	-30
17	-30	failure

Figure 51. The time-load curve obtained from the test on SC4 and identification of all the ramps by a progressive number with the specification of the initial load, F_1, and the ending load, F_2.

Several measuring devices, i.e. linear variable displacement transducers, LVDTs, were applied to the specimens. Given a reference system with the axes x parallel to the leaves of the masonry specimen (i.e. horizontal direction), the axes y parallel to the cross-section (i.e. transverse direction) and the axes z in the vertical direction, the measuring devices were positioned for each specimen as follows: i) two horizontal LVDTs (i.e. positioned along the direction x and fixed to external support; ii) two transverse LVDTs (i.e. positioned along the direction y and fixed to external support); iii) four vertical LVDTs (i.e. positioned along the direction z and directly fixed to the specimen); iv) three vertical LVDTs placed on the top of the steel platen recording any rotation of it. Figure 52 shows the preparation of the specimens, the test set up and the location of the measuring devices.

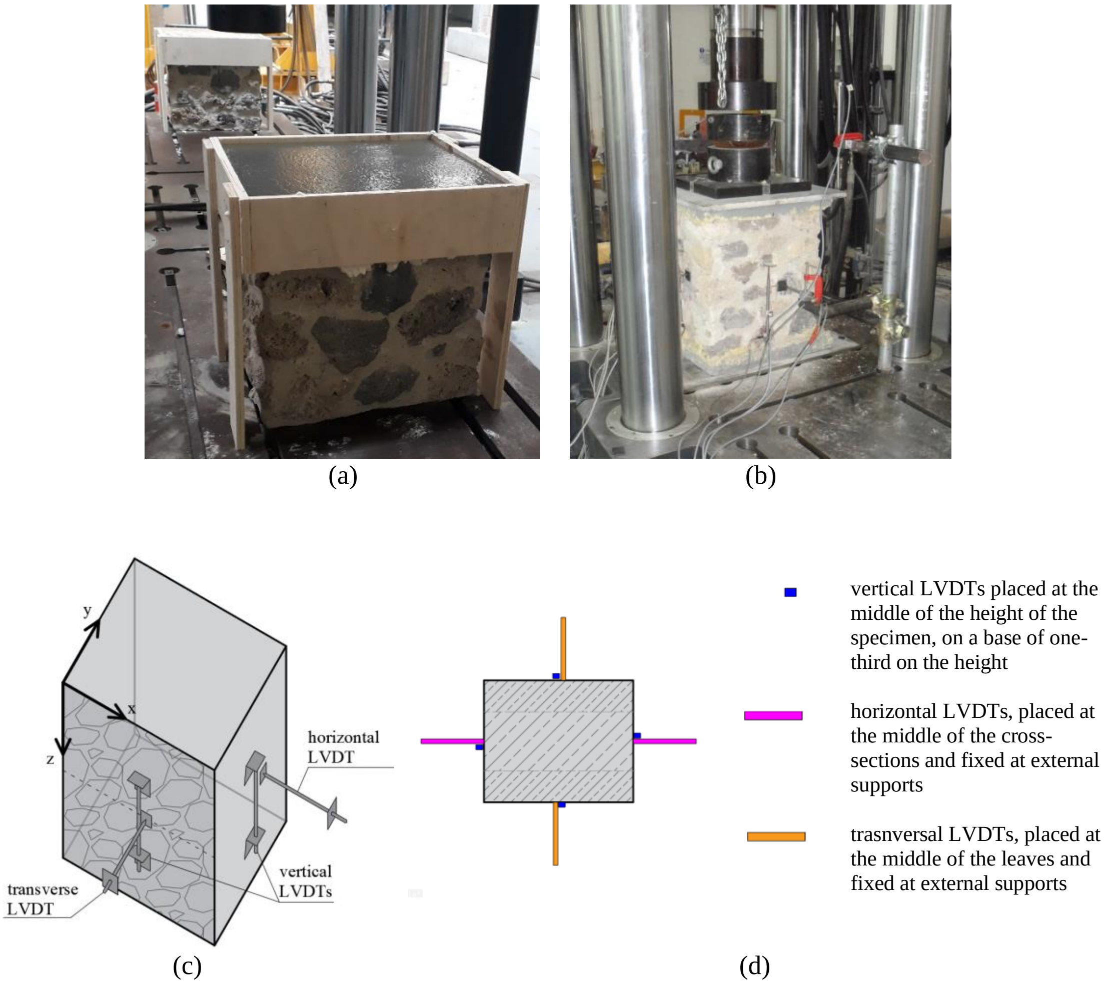

Figure 52: Compensating layer on the up and bottom surfaces of the specimens (a); test set up (b); view of the location of the measuring devices on each panel (c); scheme of the location of the measuring devices on the four sides of the specimens (d).

4.2. Discussion of the experimental results

4.2.1. Sonic tests

The outcomes of the STs are summarized in Table 12 in terms of: mean velocity calculated for each panel at each age, $V_{t=12}$, $V_{t=44}$, $V_{t=148}$, along with their coefficients of variation, CoV, and overall mean values and coefficient of variations. Moreover, the percentage variations of the velocities between the different ages, $\Delta V_{44\text{-}12}$, $\Delta V_{148\text{-}44}$ and $\Delta V_{148\text{-}12}$, are reported. These latter were computed as Eq. (4.20):

$$\Delta V_{t''\text{-}t'} = \frac{(V_{t''} - V_{t'})}{V_{t'}} \tag{4.20}$$

Table 12. Outcomes of the sonic tests.

Specimen	$V_{t=12}$ [m/s]	CoV	$V_{t=44}$ [m/s]	CoV	$V_{t=148}$ [m/s]	CoV	$\Delta V_{44\text{-}12}$ [m/s]	$\Delta V_{148\text{-}44}$ [m/s]	$\Delta V_{148\text{-}12}$ [m/s]
S1	1673	19%	2297	20%	2428	25%	37%	6%	45%
S2	1919	23%	2163	19%	2923	23%	13%	35%	52%
S3	2070	23%	2381	16%	2918	23%	15%	23%	41%
Mean	1890		2280		2767		21%	22%	46%
CoV	11%		5%		11%		63%	72%	15%

The mean velocities ranged between 1673 and 2070 m/s at 12 days (with CoV ranging between 19% and 23%), 2163 and 2381 m/s at 44 days (with CoV ranging between 16% and 20%) and 2428 and 2923 m/s (with CoV ranging between 23% and 25%). In detail, at t = 12 days S1 showed the lowest mean velocity and S3 showed the highest mean velocity (i.e. the mean velocities were equal to 1673 m/s, 1919 m/s and 1890 m/s for S1, S2 and S3 respectively). At t = 44 days S2 showed the lowest mean velocity and S3 showed the highest mean velocity (i.e. the mean velocities were equal to 2297 m/s, 2163 m/s and 2381 m/s for S1, S2 and S3 respectively). Finally, at t = 148 days S1 showed the lowest mean velocity and S2 showed the highest mean velocity (i.e. the mean velocities were equal to 2428 m/s, 2923 m/s and 2918 m/s for S1, S2 and S3 respectively). Details of the evolution of the velocities for each panel at each age are reported in the following section.

4.2.1.1. Evolution of the velocities with the time

Figure 53, Figure 54 and Figure 55 report the histograms of the velocity distributions at the different ages (i.e. t =12, 48 and 148 days) for S1, S2 and S3, respectively. The figure also sets out the lognormal probability density functions, which were evaluated from each experimental velocity distribution. Moreover, Figure 56 summarizes the probability density distribution at all the ages for each panel and evolution of the value of mean velocity for each panel with the time.

As expected, for all the panels the mean velocity increased over time, related to the evolution of the hardening process of the mortar (RILEM TC 1996). Indeed, it is known that mortars made with aerial lime show a low development of their hardening properties and achieve their mechanical properties within few months up to some years (Baronio et al. 1999; Moropoulou et al. 2005b). It can be noted that the panel S1 had the most significant increase in velocity between the first and second sonic tests, with ΔV_{44-12} = 37% (Table 12). At t = 44, S1 achieved a velocity closer to the final value, ΔV_{148-44} = 6%. Panels S2 and S3 had slower and more uniform velocity increases. The percentage velocity variations between the first and second sonic tests were ΔV_{44-12} = 13% and ΔV_{44-12} = 15% for S2 and S3, respectively, while the percentage velocity variations between the second and third sonic tests were ΔV_{148-44} = 35% and ΔV_{148-44} = 23% for S2 and S3, respectively.

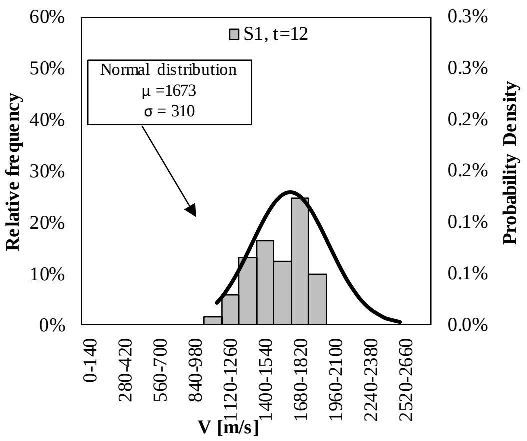

(a)

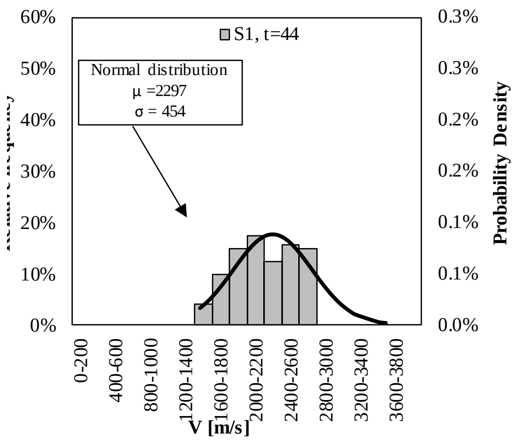

(b)

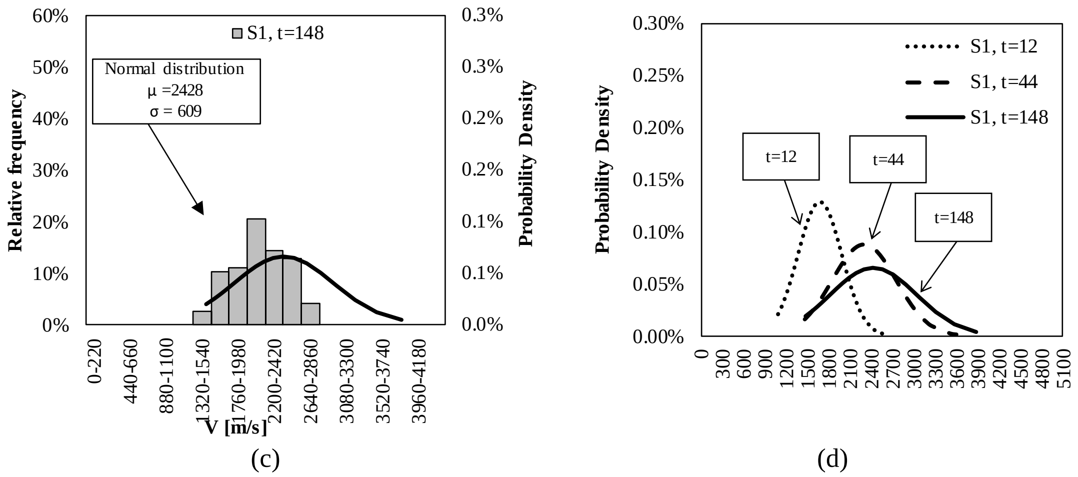

Figure 53. Histograms of the velocity distributions and their respective probability density distributions at t = 12 days (a), t = 44 days (b), and t = 148 days (c) and probability density distributions at all the ages (d) for S1.

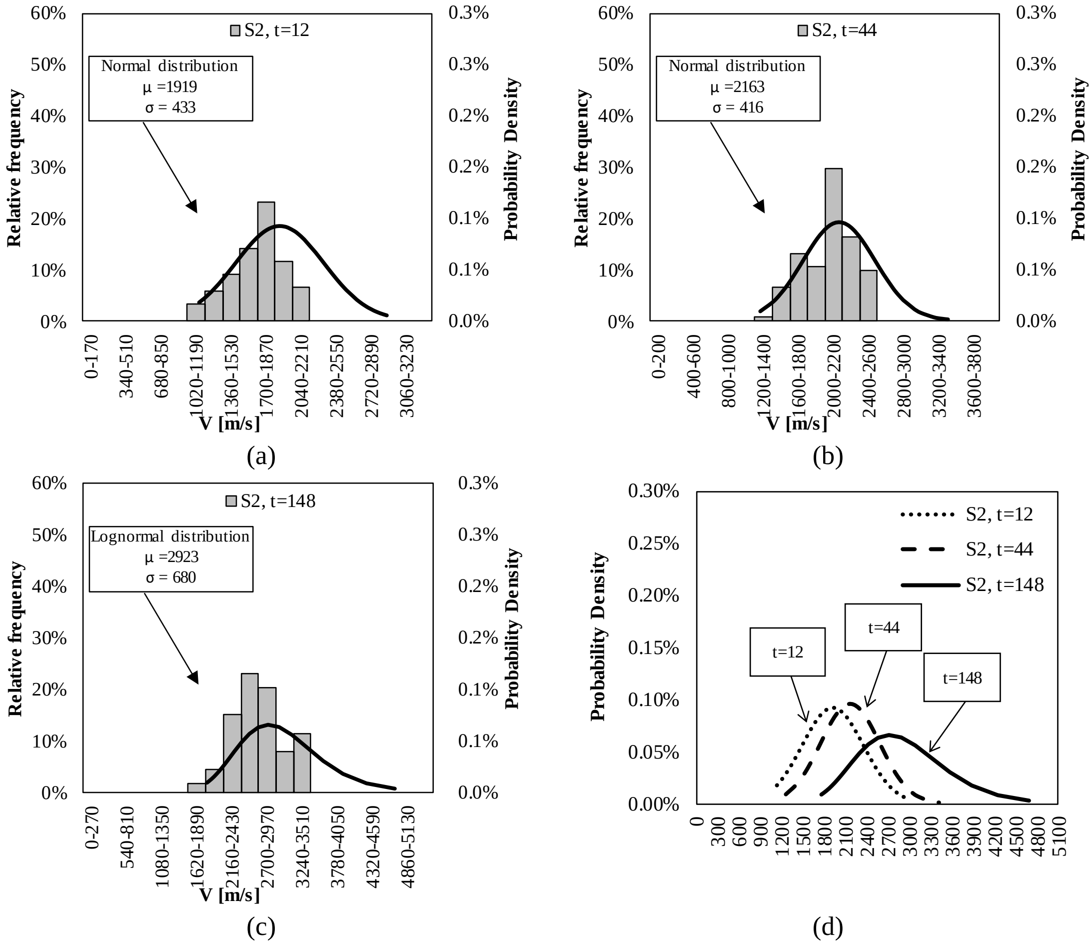

Figure 54. Histograms of the velocity distributions and their respective probability density distributions at t = 12 days (a), t = 44 days (b), and t = 148 days (c) and probability density distributions at all the ages (d) for S2.

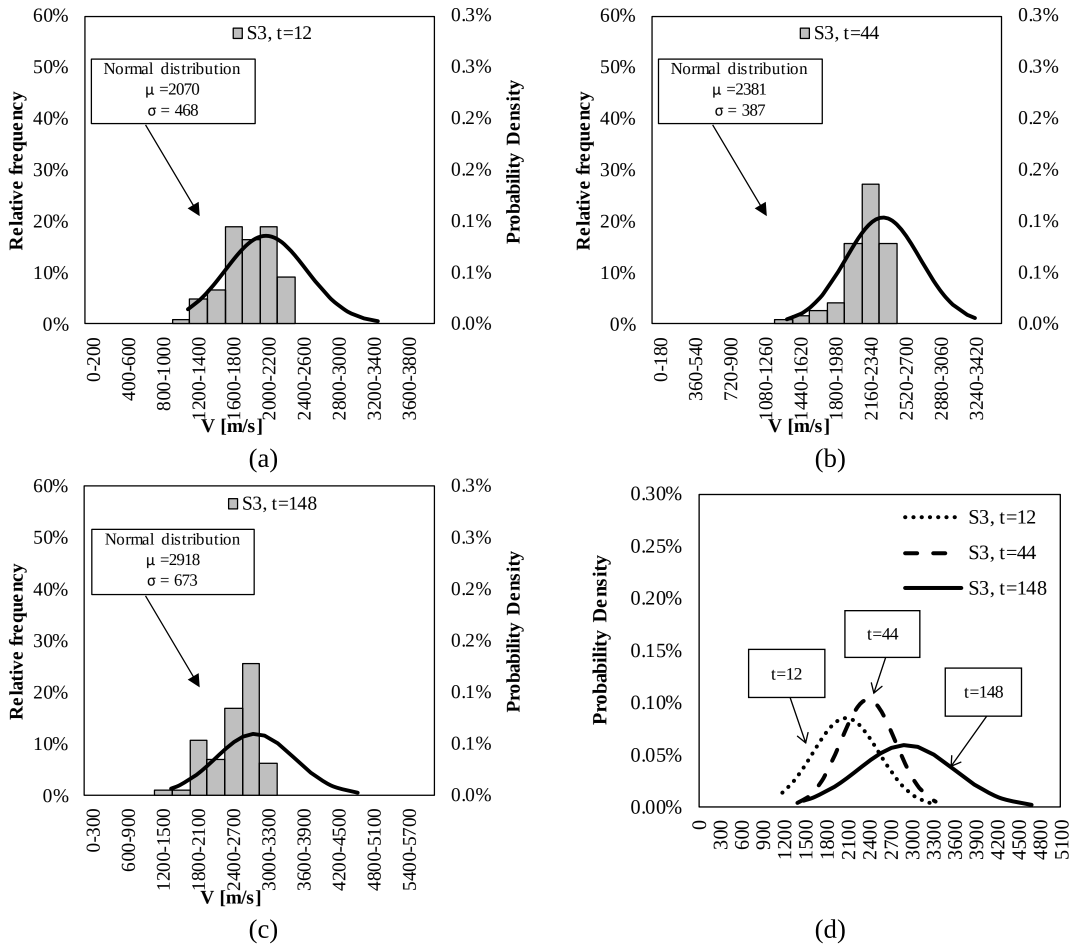

Figure 55. Histograms of the velocity distributions and their respective probability density distributions at t = 12 days (a), t = 44 days (b), and t = 148 days (c) and probability density distributions at all the ages (d) for S3.

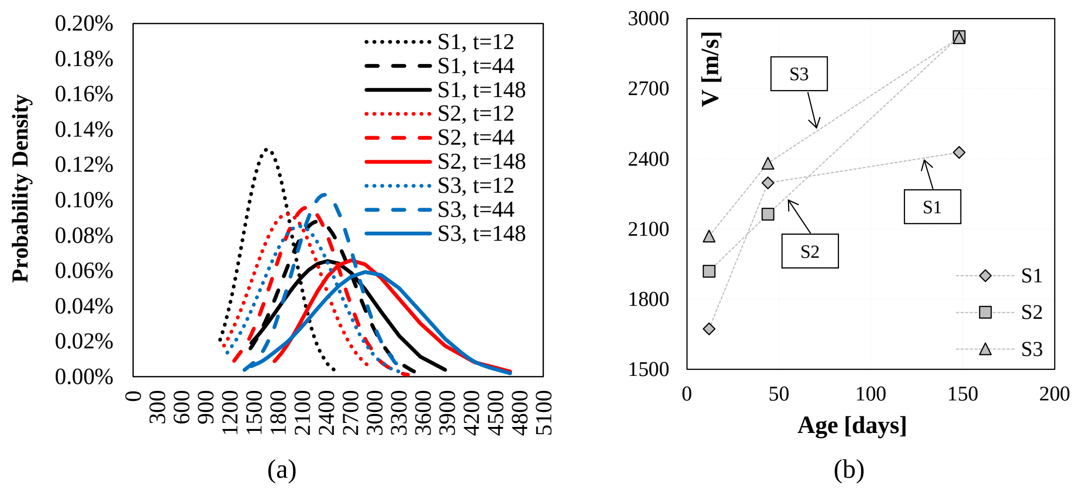

Figure 56. Probability density distribution at all the ages for each panel (a) and evolution of the value of mean velocity for each panel with the time (b).

4.2.1.2. Velocity distribution maps

The outcomes of the sonic tests were also processed by mapping software to obtain contour maps of the velocity distributions relating to the hammer side of each panel. Figure 57 shows the velocity distribution maps at t = 12, t = 44 and t = 148 days and the material survey of the A and B sides of each panel. Note that, concerning t = 44 and t = 148, certain velocities were not recorded at the corners, due to the constraints related to the set-up of the diagonal compression tests.

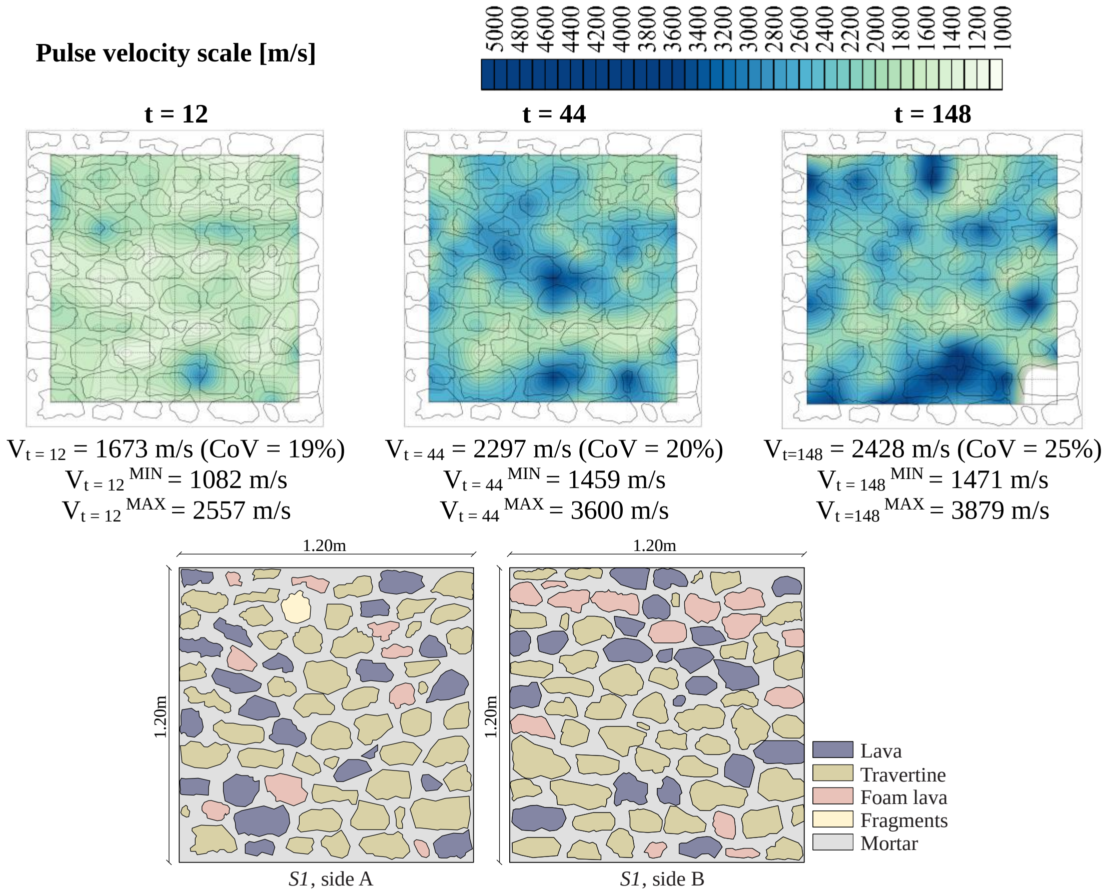

(a)

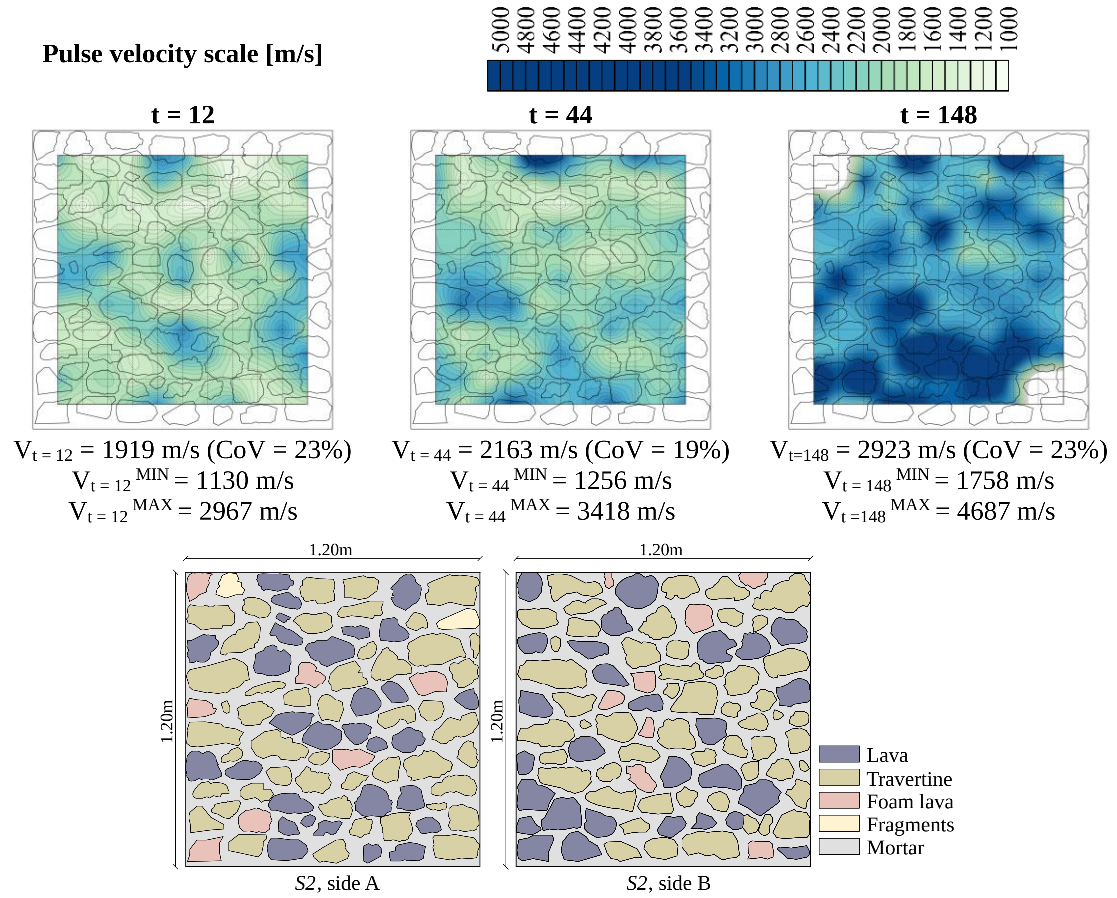
Pulse velocity scale [m/s]
5000 4800 4600 4400 4200 4000 3800 3600 3400 3200 3000 2800 2600 2400 2200 2000 1800 1600 1400 1200 1000
t = 12
t = 44
t = 148
$V_{t=12}$ = 1919 m/s (CoV = 23%)
$V_{t=12}^{MIN}$ = 1130 m/s
$V_{t=12}^{MAX}$ = 2967 m/s
$V_{t=44}$ = 2163 m/s (CoV = 19%)
$V_{t=44}^{MIN}$ = 1256 m/s
$V_{t=44}^{MAX}$ = 3418 m/s
$V_{t=148}$ = 2923 m/s (CoV = 23%)
$V_{t=148}^{MIN}$ = 1758 m/s
$V_{t=148}^{MAX}$ = 4687 m/s
1.20m
1.20m
1.20m
1.20m
S2, side A
S2, side B
Lava
Travertine
Foam lava
Fragments
Mortar

(b)

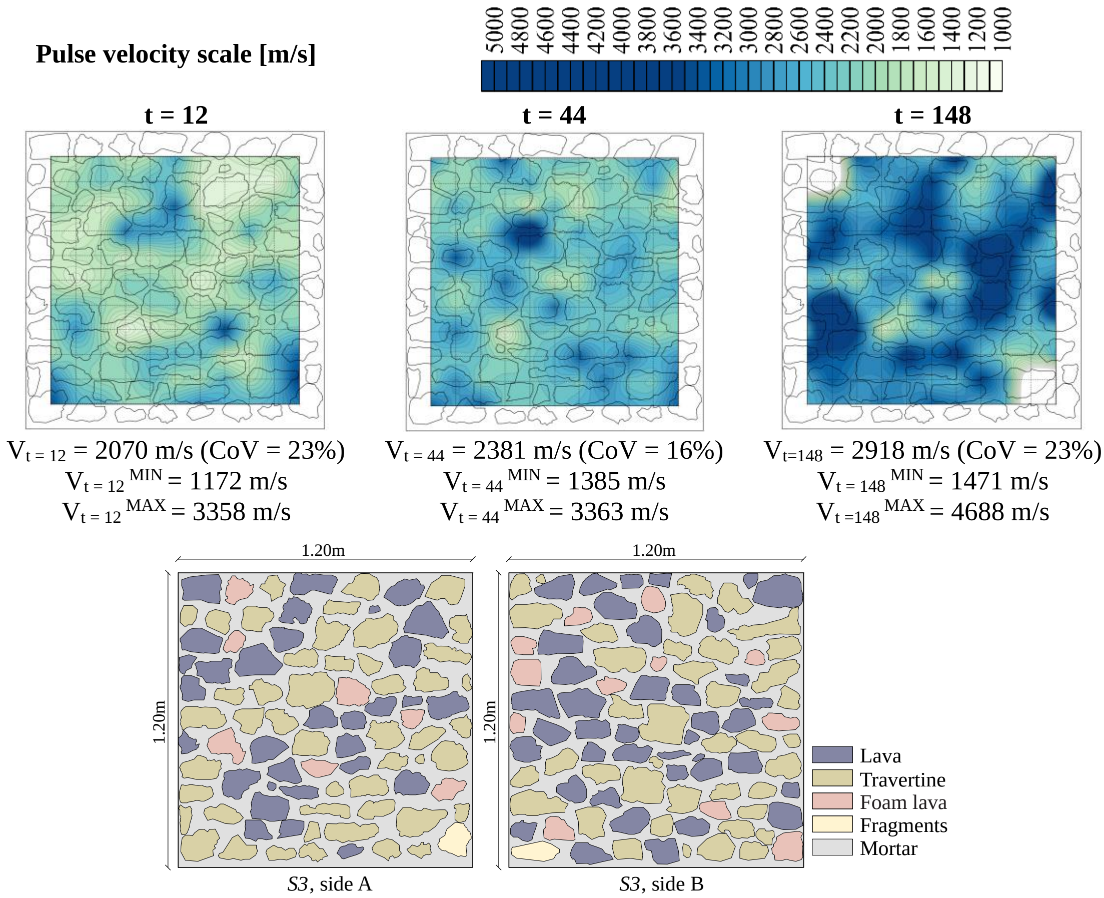

(c)

Figure 57. Velocity distribution maps for the first, second and third tests: t *= 12 days,* t *= 44 days, and* t *= 148 days and material survey for* S1 *(a),* S2 *(b) and* S3 *(c).*

The velocity distribution maps provided a graphic representation of the variability of the outcomes within each panel in the single test. They also provided a graphic representation of the velocity increasing over time for each panel. The variabilities of the outcomes within each panel in the single tests were almost similar, ranging between CoV = 16% and CoV = 25%. S1 had an increase of variability at t = 12, t = 44 and t = 148 days of CoV = 19%, 20% and 25%, respectively. Panels S2 and S3 showed similar behaviour with CoV = 23%, 19% and 23%, and CoV = 23%, 16% and 23% at t = 12, t = 44 and t = 148 days, respectively. In S1, the contour maps of the velocity distributions showed that there were higher velocities mainly in the lower part of the panel and in limited perimetrical areas; for panels S2 and S3, the higher velocity areas were more uniformly distributed. These results are probably due to: i) the larger area occupied (in percentage terms) by mortar in S1; and ii) the more uniform distribution of the different rock types within S2 and S3.

4.2.2. Diagonal compression tests

Table 13 summarize the main outcomes of the diagonal compression tests in terms of: maximum load attained, P_{max}; shear strength evaluated according to the ASTM formulation, τ_{max}; shear strain corresponding to the maximum shear stress, γ_{max}; shear strain during the conventional failure, γ_u; secant shear modulus, $G_{30\%}$; shear deformability ratio, μ; and energy dissipation during the test, E.

The local recordings made by the LVDTs were continuous and accurate, including the initial stage (i.e. elastic field), while the S-LVDTs recordings started in proximity to the maximum load and were discontinuous. The analysis reported herein is therefore mainly based on the outcomes produced by the former. The comparison between the LVDTs recordings on the diagonal tension side of the two wall surfaces for each panel revealed similar curves. A certain variability was detected among the shear capacity of the panels. The peak loads and the shear strength attained on each panel were 146 kN and 0.19 MPa, 204 kN and and 0.27 MPa, 187 kN and 0.25 MPa, for S1, S2 and S3 respectively. Indeed, given the same masonry type, rock types and mortar defined to build the panels, the experimental performances of the specimens were certainly affected by several factors: i) the irregular shape and the specific arrangement of the units resulted in each panel, ii) the specific distribution of the units of different nature within each panel, iii) the exact amount of mortar resulted in each panel. In particular, the lower performances of S1 compared to the other two specimens were probably related to: i) the greater amount of mortar detected in S1 compared to S2 and S3; ii) the greater number of soft rocks, namely travertine, in the center of the panel.

No significant differences were detected in terms of γ_{max} in the specimens; there was also a significant ductility factor greater than five in each specimen, with a maximum value of μ =12.77. Very similar shear modulus values, G, were derived on S1 and S2, with G about 521 MPa, while it was not possible to evaluate the shear modulus on S3, due to inaccurate local recordings detected on the panel.

Table 13. Main experimental outcomes of the diagonal compression tests.

Specimen	P_{max} [kN]	τ_{max} [MPa]	$\gamma_{\tau max}$ [-]	γ_u [-]	$G_{30\%}$ [MPa]	μ_γ [-]	ED [J]
S1	146	0.19	0.16%	0.90%	522	5.69	602
S2	204	0.27	0.17%	2.13%	520	12.77	2369
S3	187	0.25	0.16%	1.24%	-	7.86	1130
mean	179	0.23	0.16%	1.42%	521	8.77	1367
CoV	16%	16%	3%	44%	-	41%	66%

4.2.2.1. Local recordings

Figure 58 reports the shear stress-diagonal strain relationships on sides A and B for each masonry panel. The curves refer to local recordings obtained from the different devices. Note that, due to the detachment of LVDTs from the panel surface, the shortening recordings on S3 ended in correspondence with the maximum load. Specimens S2 and S3 showed a first softening branch after the peak load, followed by a slight increase in load. This was not showed by S1. For S2 and S3, the second peak load was 91% and 92% of the first peak load, respectively.

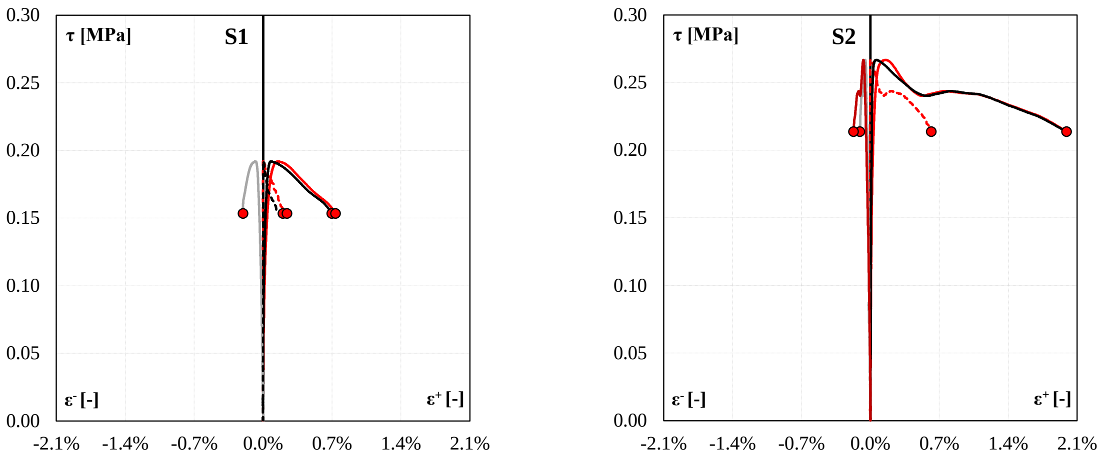

(a) (b)

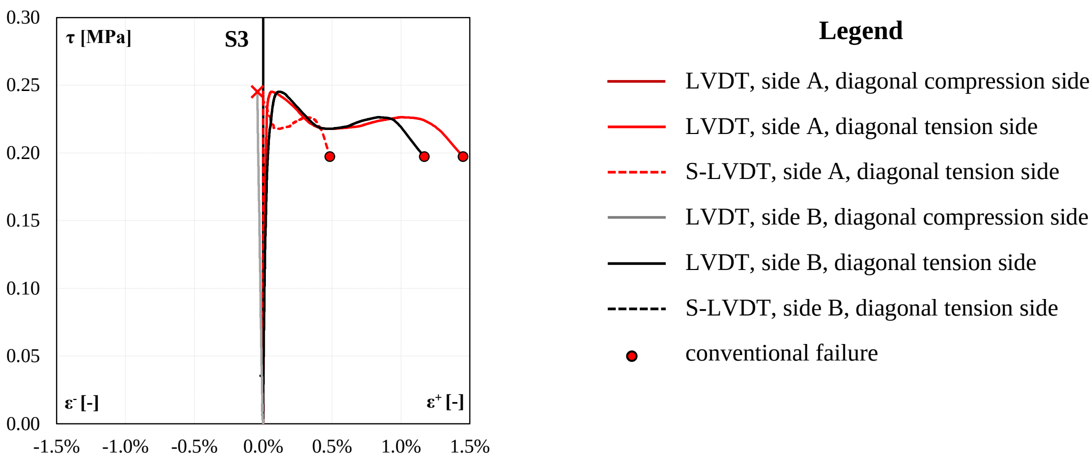

(c)

Figure 58. Shear stress - diagonal strain relationships: S1 (a); S2 (b); and S3 (c). Note that recordings related to devices detached since the first phase of the tests were discarded, while the recordings related to LVDT on the diagonal compression side on the side B of S3 was stopped in correspondence with the maximum load.

4.2.2.2.Shear stress-strain relationships and failure mode

Figure 59, Figure 60 and Figure 61 summarize the shear stress-strain relationships and the failure mode for each panel. The figures also show the failure mode, the cracks at the conventional failure for side A and the crack pattern at the end of the test on the four sides of each panel. Moreover, Figure 62 reports the comparisons of the compressive stress- vertical strain curves recorded on each specimen.

The final crack pattern mainly consisted of the main crack extended along the compressed diagonal. Each panel was divided by such a crack into two almost symmetrical parts, depending on the arrangement of the units. The cracks mainly developed inside the mortar matrix, but several rock units were also intercepted. Cracks in the units mainly interested travertine and foam lava, whose investigated compressive strength were closer to that of the mortar than to the one of the lava (5.88 MPa, 3.90 MPa and 2.87 MPa for travertine, foam lava and mortar respectively, compared to 38.43 MPa for lava). Consequently, the shear strength of each panel was greatly affected by the arrangement of the rock units, as well as the mortar strength. Note that i) the large voids in the cavernous fabric of the travertine and the air-bubble voids in the foam lava and certain other lavas could determine the preferred fracture plane, and ii) certain lava units presented pre-existing cracks. The upper part of the panels tended to rotate around the bottom corner. This rocking mechanism was especially visible for S2. Sub-horizontal cracks were visible on the transverse wall surfaces, C and D, of each panel. These developed at an intermediate height or in proximity to the steel shoes. S3 had much more marked cracks on the transverse wall surfaces. A sub-horizontal crack crossed the entire thickness of the panel on side C and was also visible on sides A and B for about one-third of the panel length. Indeed, the lower part of the panel displayed horizontal separation and the activation of a second rocking mechanism. No out-of-plane mechanisms were detected in the panels.

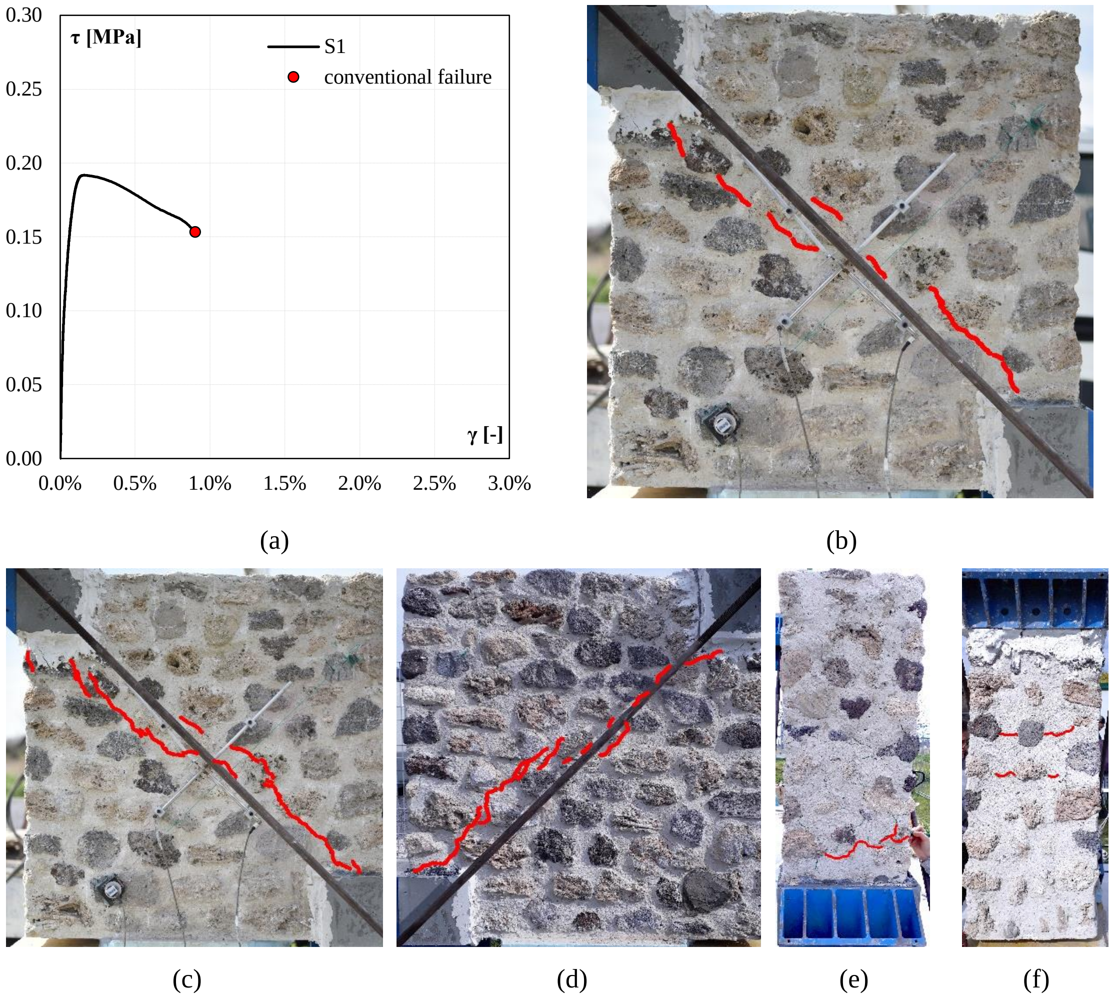

Figure 59. Shear stress-strain relationship (a) and failure mode for panel S1: crack pattern survey related to the conventional failure for side A (b); final crack pattern survey on side A (c), side B (d), side C (e) and side D (f).

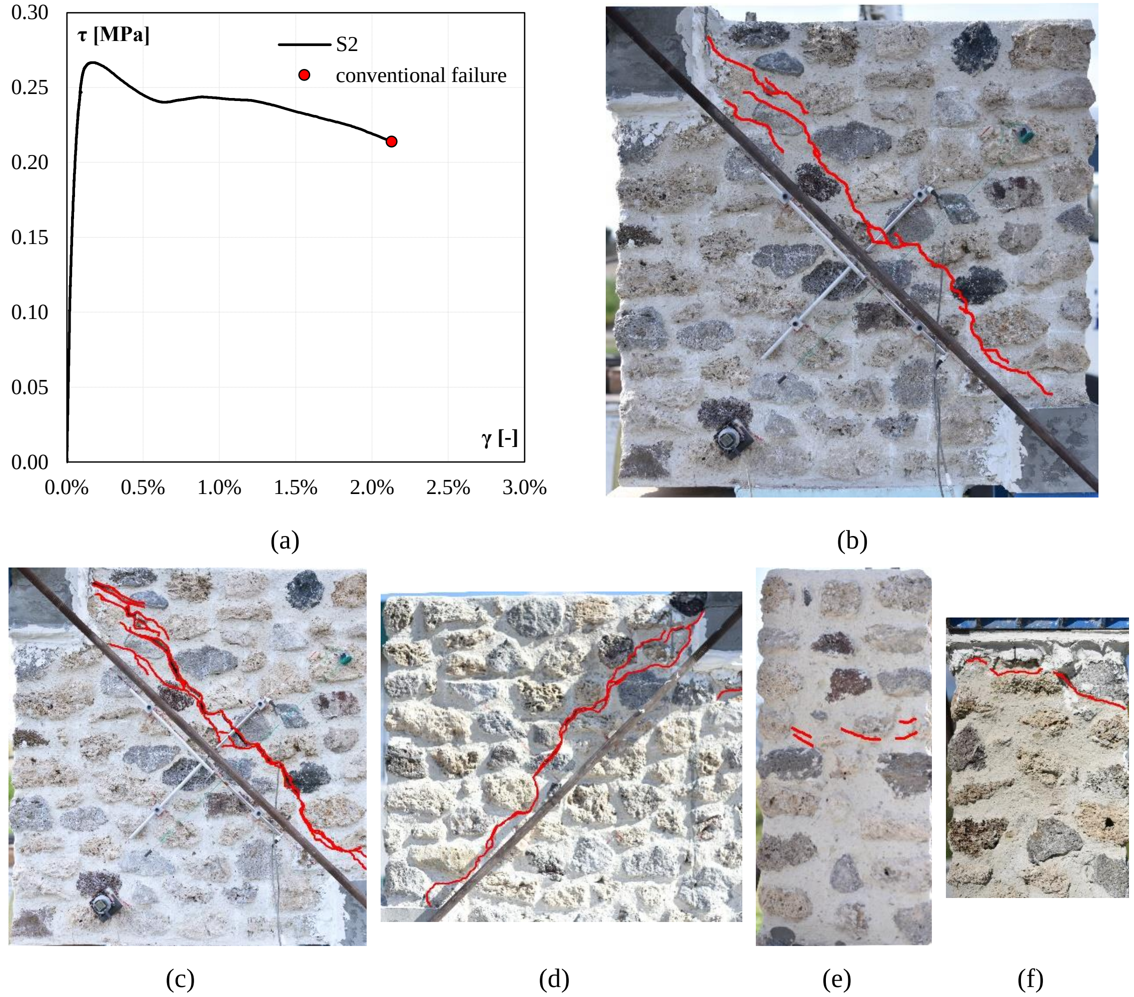

Figure 60. Shear stress-strain relationship (a) and failure mode for panel S2: crack pattern survey related to the conventional failure for the side A (b); final crack pattern survey on side A (c), side B (d), side C (e) and side D (f).

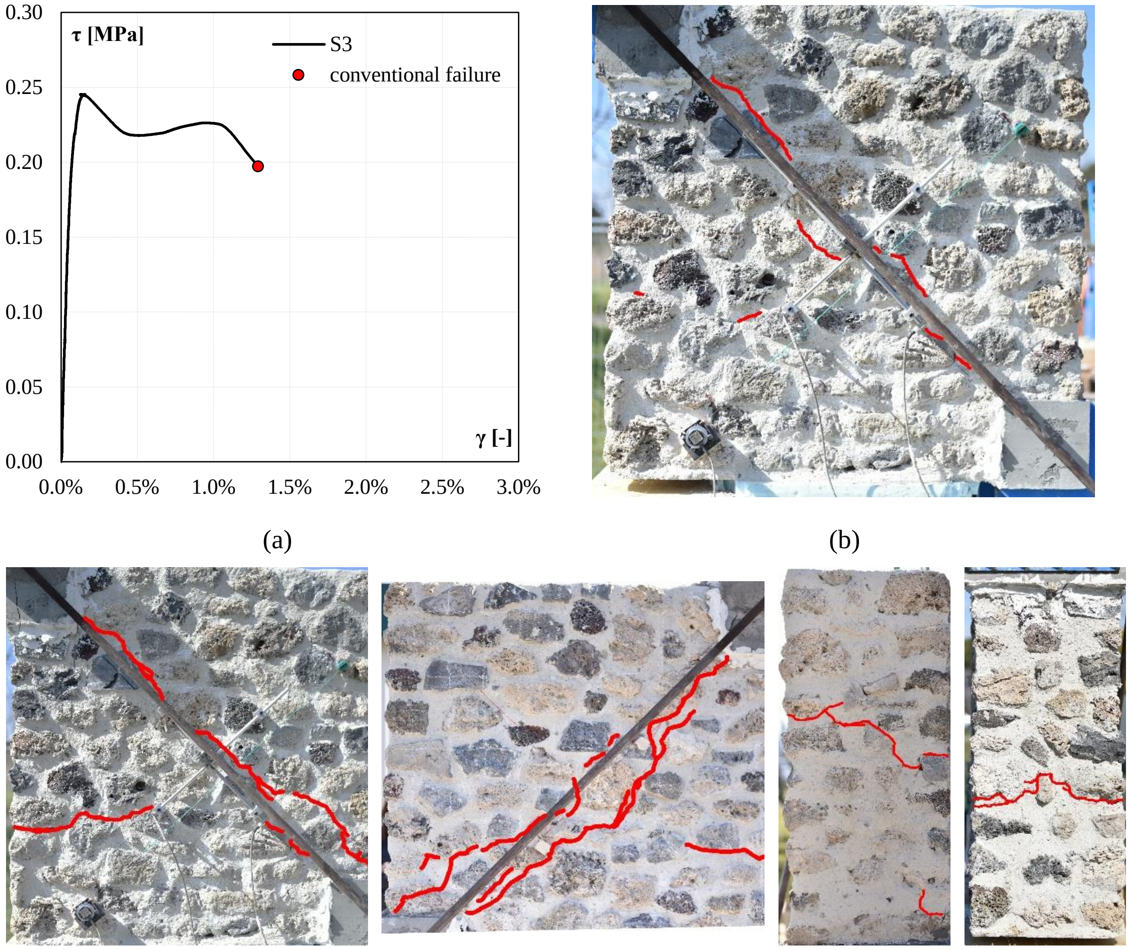

(a) (b)

(c) (d) (e) (f)

Figure 61. Shear stress-strain relationship (a) and failure mode for panel S3: crack pattern survey related to the conventional failure for the side A (b); final crack pattern survey on side A (c), side B (d), side C (e) and side D (f).

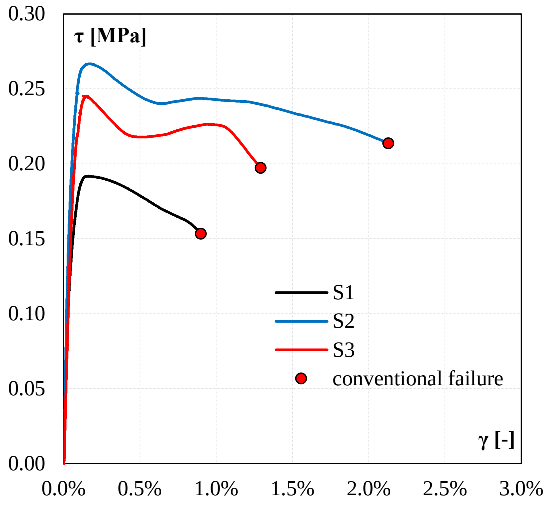

Figure 62. Shear stress-strain curves.

4.2.3. Axial compression tests

Errore. L'origine riferimento non è stata trovata. summarize the main o utcomes of the axial compression tests in terms of: the compressive strength, f_c; the secant elastic modulus evaluated from zero stress to one-third of the compressive strength, $E_{1/3}$; the elastic modulus evaluated as the mean of the slopes of the three obtained lines, E_m; the Poisson ratio in the horizontal direction, ν_h; the Poisson ratio in the transverse direction, $\nu_{t,}$; the shear modulus calculated from the secant elastic modulus and the Poisson ratio in the horizontal direction $G_{1/3}$; the shear modulus calculated from the elastic modulus obtained from the slopes and the Poisson ratio in the horizontal direction G_m; the vertical strain corresponding to the maximum stress, $\varepsilon_{v,max}$; the vertical strain corresponding to the conventional failure, $\varepsilon_{v,u}$; the vertical deformability ratio, μ_ε; the horizontal strain corresponding to the maximum stress, $\varepsilon_{h,max}$; the transverse strain corresponding to the maximum stress, $\varepsilon_{t,max}$; the energy dissipation, ED. SC3 showed the lowest compressive strength (f_c = 0.99 MPa) and SC4 showed the highest compressive strength (f_c = 1.95 MPa), while the other specimens showed similar values (1.52 MPa, 1.49 MPa and 1.46 MPa, for SC1, SC2 and SC5, respectively. However, the overall dispersion was considered acceptable considering the proper inhomogeneity of the masonry typology and what is already found from the sonic tests and diagonal compression tests. The mean elastic modulus calculated from the slopes of the loading ramps was found to be higher than the one calculated in correspondence of one-third of the maximum stress with mean values equal to 1003 MPa, CoV =19% and 307 MPa, CoV = 48 %, for E_m and $E_{1/3}$, respectively. As regards the horizontal and transversal strain, fewer correct recordings were obtained. Indeed, no information in the horizontal plane was obtained for SC3 and SC5. The mean Poisson ratio in the horizontal direction (i.e. 0.13) was found to be higher than the one in the transversal direction (i.e. 0.05). Finally, the mean shear modulus calculated from the mean elastic modulus (G_m = 499 MPa) was comparable with the one obtained from the diagonal compression tests (G = 521 MPa).

Table 14. Main experimental outcomes of the axial compression tests.

Sp.	**f_c [MPa]**	**$E_{1/3}$ [MPa]**	**E_m [MPa]**	**ν_h [-]**	**ν_t [-]**	**$G_{1/3}$ [MPa]**	**G_m [MPa]**	**$\varepsilon_{v,max}$ [-]**	**$\varepsilon_{v,u}$ [-]**	**μ_ε [-]**	**$\varepsilon_{h,max}$ [-]**	**$\varepsilon_{t,max}$ [-]**	**ED [J]**
SC1	1.52	565	-	0.08	-	261	-	-0.6%	-	-	0.2%	-	2052
SC2	1.49	278	1253	0.24	0.03	112	504	0.5%	-	-	0.5%	0.2%	1690
SC3	0.96	205	843	-	-	-	-	-0.4%	-	-	-	-	428
SC4	1.95	270	1053	0.07	0.08	127	494	-1.2%	-2.8%	2.37	0.5%	0.5%	1843
SC5	1.46	219	862	-	-	-	-	-0.9%	-2.4%	2.68	-	-	1093
mean	1.48	307	1003	0.13	0.05	166	499	-0.5%	-2.6%	2.52	0.4%	0.4%	1421
CoV	24%	48%	19%	75%	-	49%	-	-128%	-	-	49%	-	46%

4.2.3.1. Local recordings

Figure 63 reports the compression stress-strain relationships related to the local recordings obtained from the different devices for each specimen. Missing or partial curves are related to a low quality of acquisitions or measuring devices detached before the achievement of conventional failure.

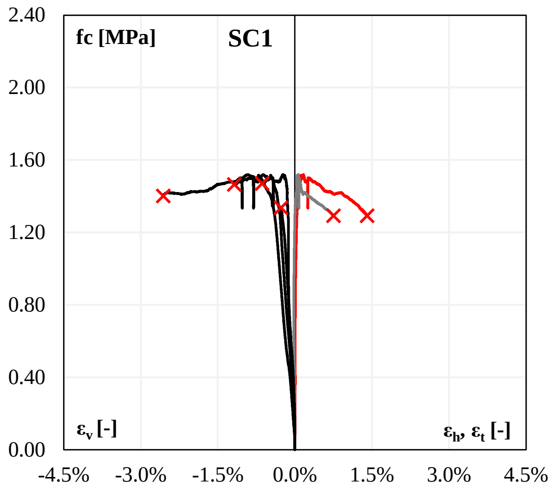

(a)

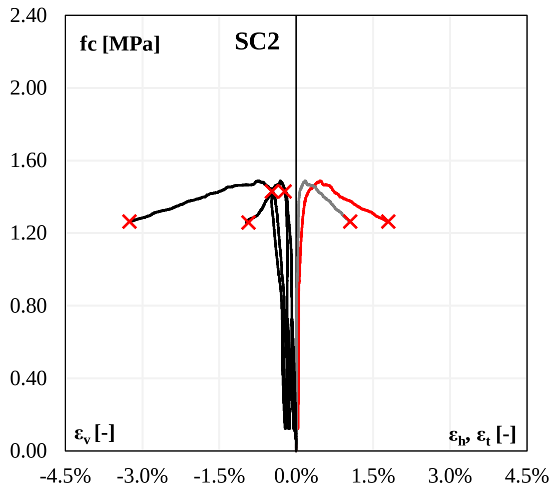

(b)

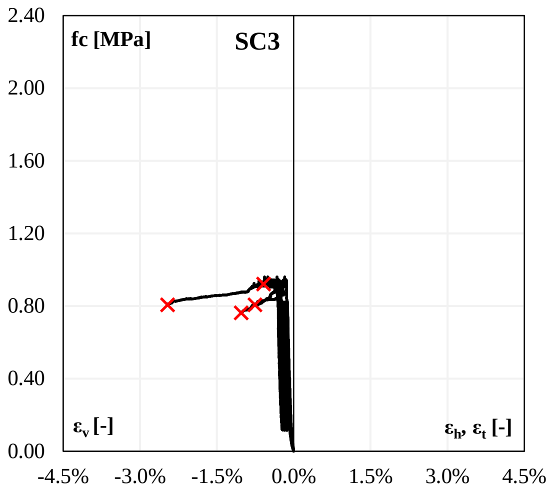

(c)

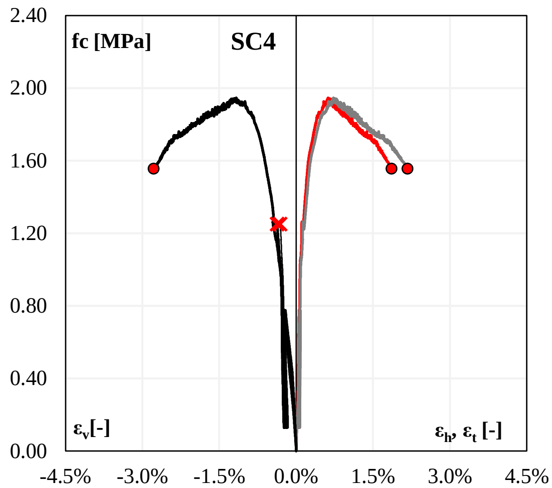

(d)

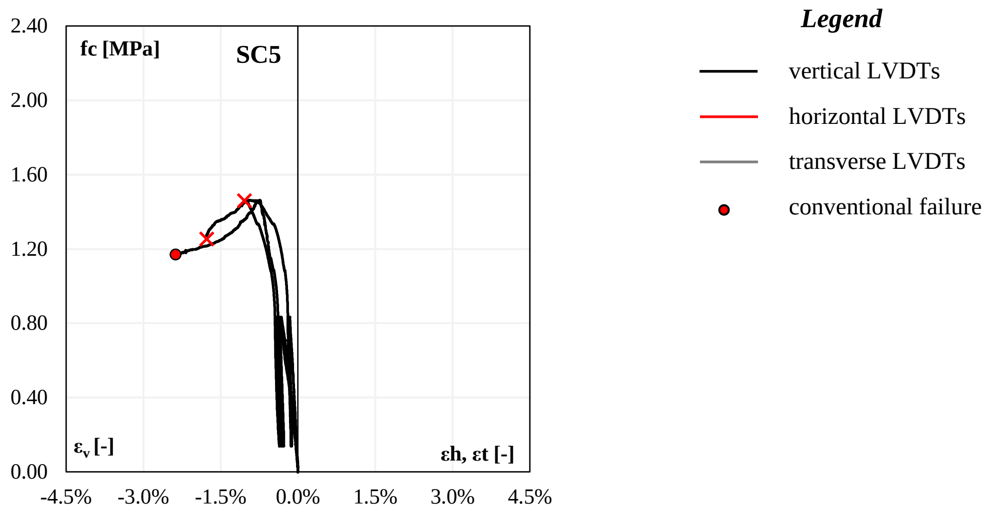

(e)

Figure 63. Compression stress-strain relationships: SC1 (a); SC2 (b); SC3 (c); SC4 (d) and SC5 (e). Note that inconsistent recordings were interrupted or totally discarded.

The local records here presented confirmed the variability detected with the diagonal compression tests. As concerns the compressive strength, an exceptionally low value was found for SC3 (i.e. f_c = 0.99 MPa), while the other specimens showed a mean compressive strength of 1.58 MPa and CoV =16 %, that is the same dispersion detected for the shear strength. Only three recordings for SC4 and on recording for SC5 were correctly acquired until the conventional failure. This was related to the early detachment of the other measuring devices, related to the formation of cracks and the expulsion of material outward. No horizontal and no transverse recordings were correctly obtained for SC4 and SC5.

4.2.3.2. Compressive stress-vertical strain relationships and failure mode

Figure 64, Figure 65, Figure 66, Figure 67 and Figure 68 summarize the compressive stress- vertical strain relationships and the failure mode for each masonry specimen (note that the curves were obtained by considering the mean of the recordings of the vertical LVDTs). The figures also show the failure mode with a view of the collapsed specimen and the crack pattern at the end of the test on the four sides of each specimen. Moreover, Figure 69 reports the comparisons of the compressive stress-vertical strain curves recorded on each specimen.

The curves were correctly registered up to the conventional failure only for SC4 and SC5, while for the other specimens the curves were interrupted shortly before. SC4 and SC5 showed the highest value of vertical strain corresponding to the maximum stress (i.e. -1.2% and 0.9% for SC4 and SC5, respectively). They resulted in a vertical deformability ratio of 2.37 and 2.68, for SC4 and SC5, respectively. However, the shape of the curves was similar for all the specimens, showing a softening branch after the attainment of the maximum stress.

For all the specimens, vertical thin cracks developed in the mortar matrix at first, then the crushing of certain units and the expulsion of material outward also occurred in the proximity of the failure. The units that were mainly involved in the cracks were travertine, foam lava and clay fragments, consistently with what was found in the diagonal compression tests. In many cases, the first cracks developed in the central part of the C and D sides, i.e. corresponding to the internal core. SC3 showed the formation of notable vertical cracks on the C and D sides at very low values of stress (i.e. since the first loading ramp). This was probably related to the particular poor condition of these specimens that resulted in the exceptionally low compressive strength. For all the specimens, clear detachments of the external leaves from the internal core were not detected on the final crack pattern but rather cracks distributed over the entire cross-section of the wall. Indeed, due to the irregular arrangement of the masonry assemblage along with its thickness, the separation between the core and the leaves is no sharply defined.

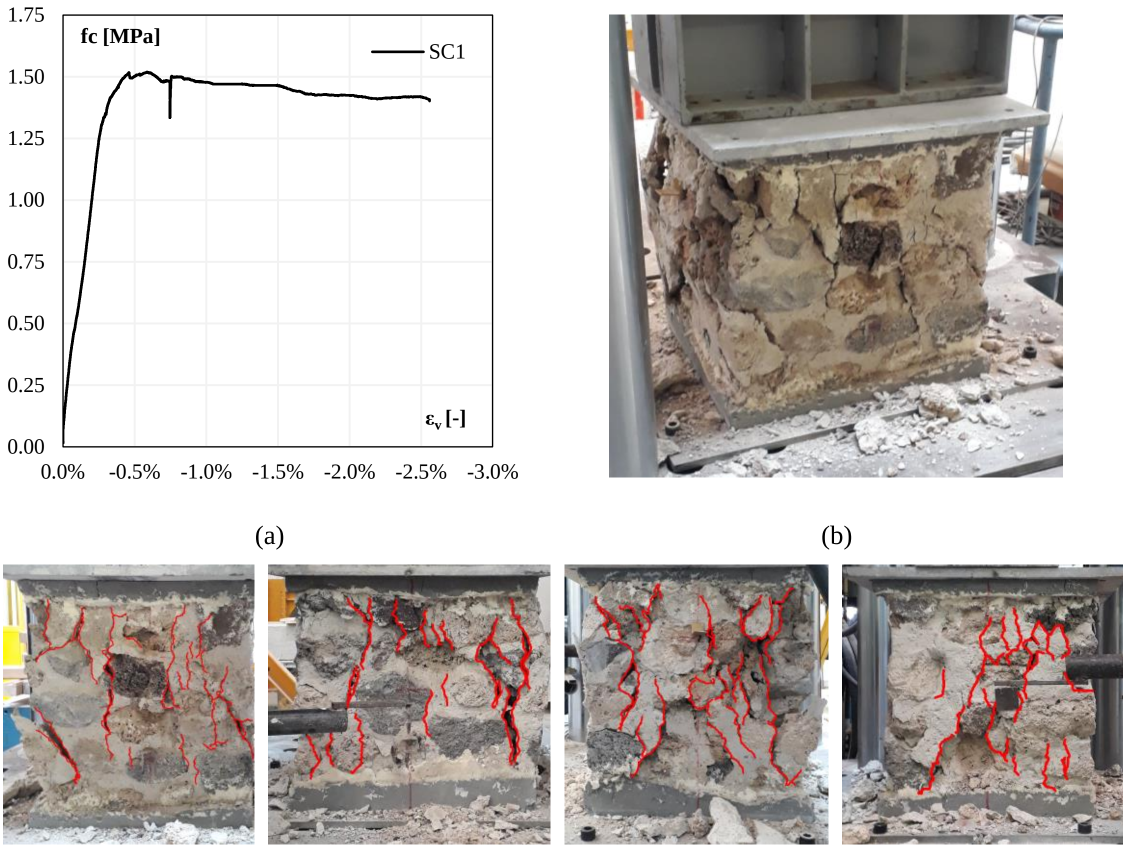

(a) (b)

(c) (d) (e) (f)

Figure 64. Compressive stress-vertical strain relationship (a) and failure mode for panel SC1: view of the collapsed specimen (b); final crack pattern survey on side A (c), side B (d), side C (e) and side D (f).

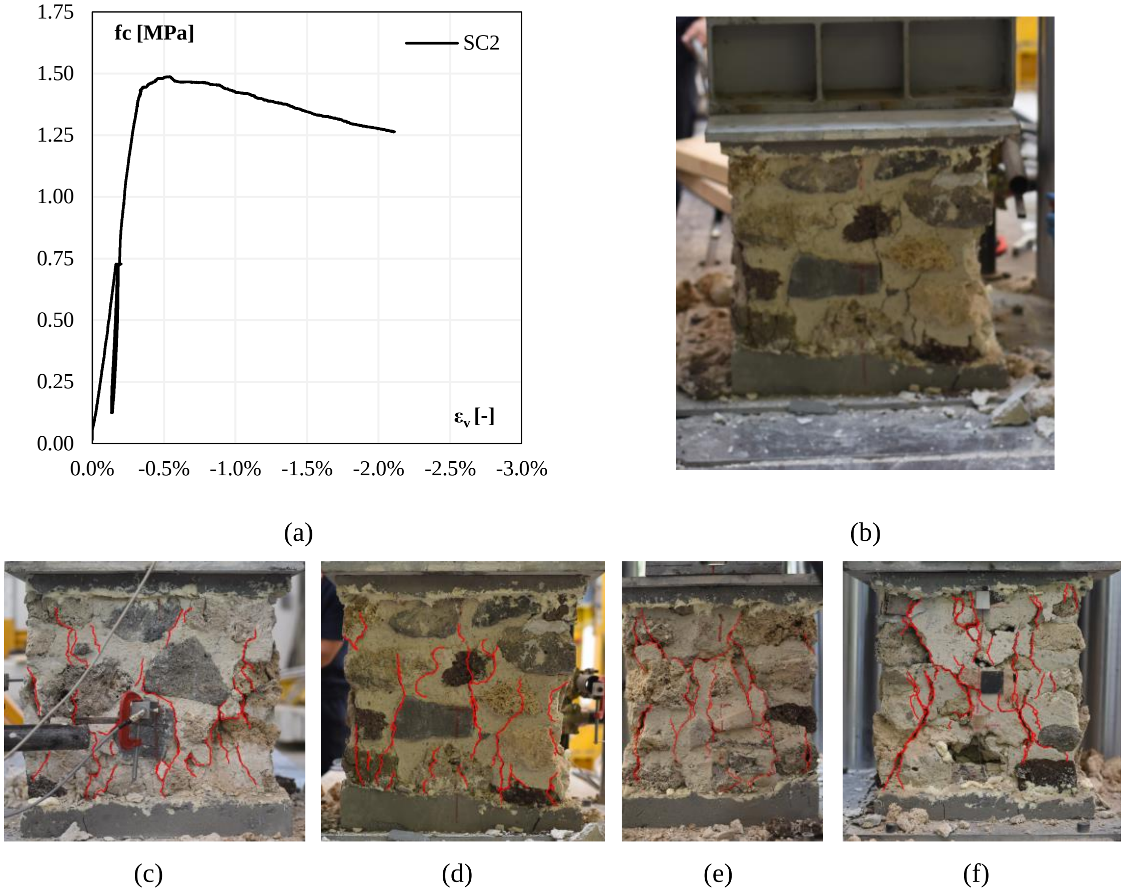

Figure 65. Compressive stress-vertical strain relationship (a) and failure mode for panel SC2: view of the collapsed specimen (b); final crack pattern survey on side A (c), side B (d), side C (e) and side D (f).

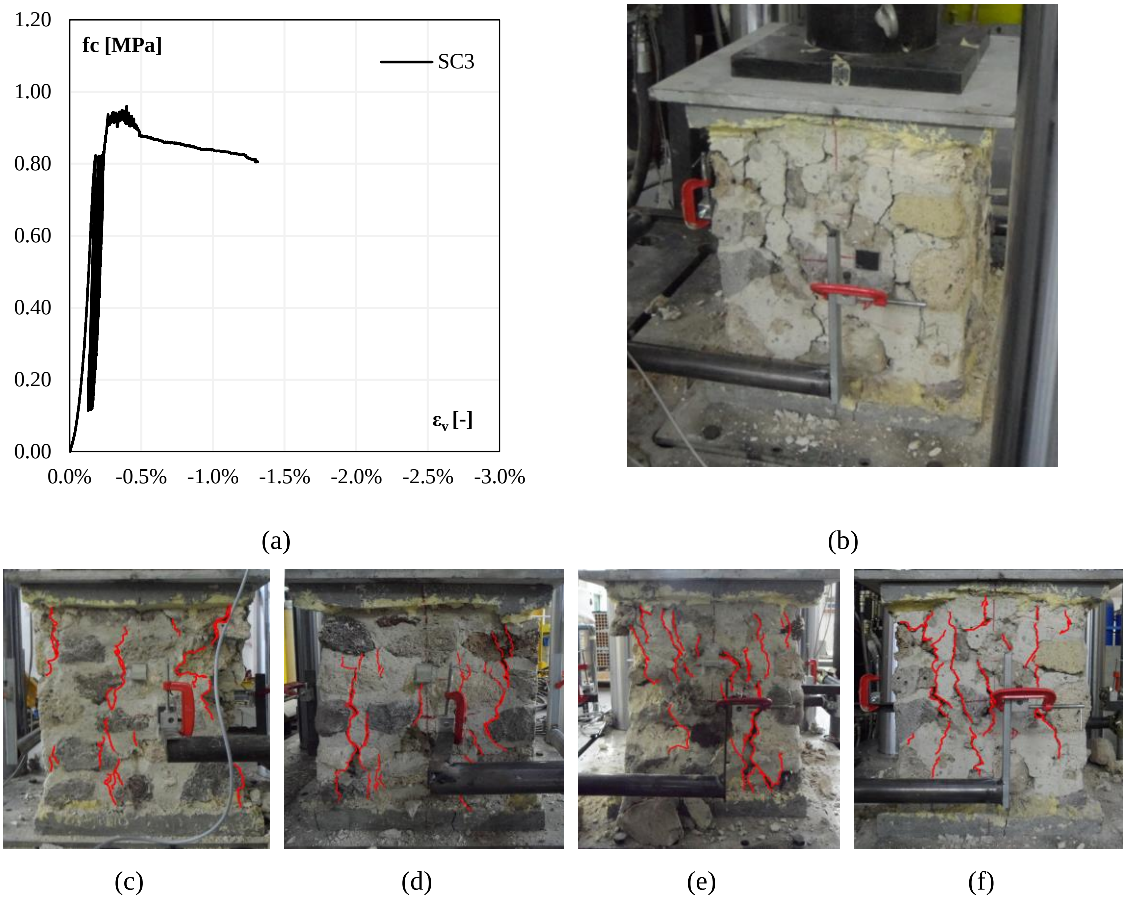

Figure 66. Compressive stress-vertical strain relationship (a) and failure mode for panel SC3: view of the collapsed specimen (b); final crack pattern survey on side A (c), side B (d), side C (e) and side D (f).

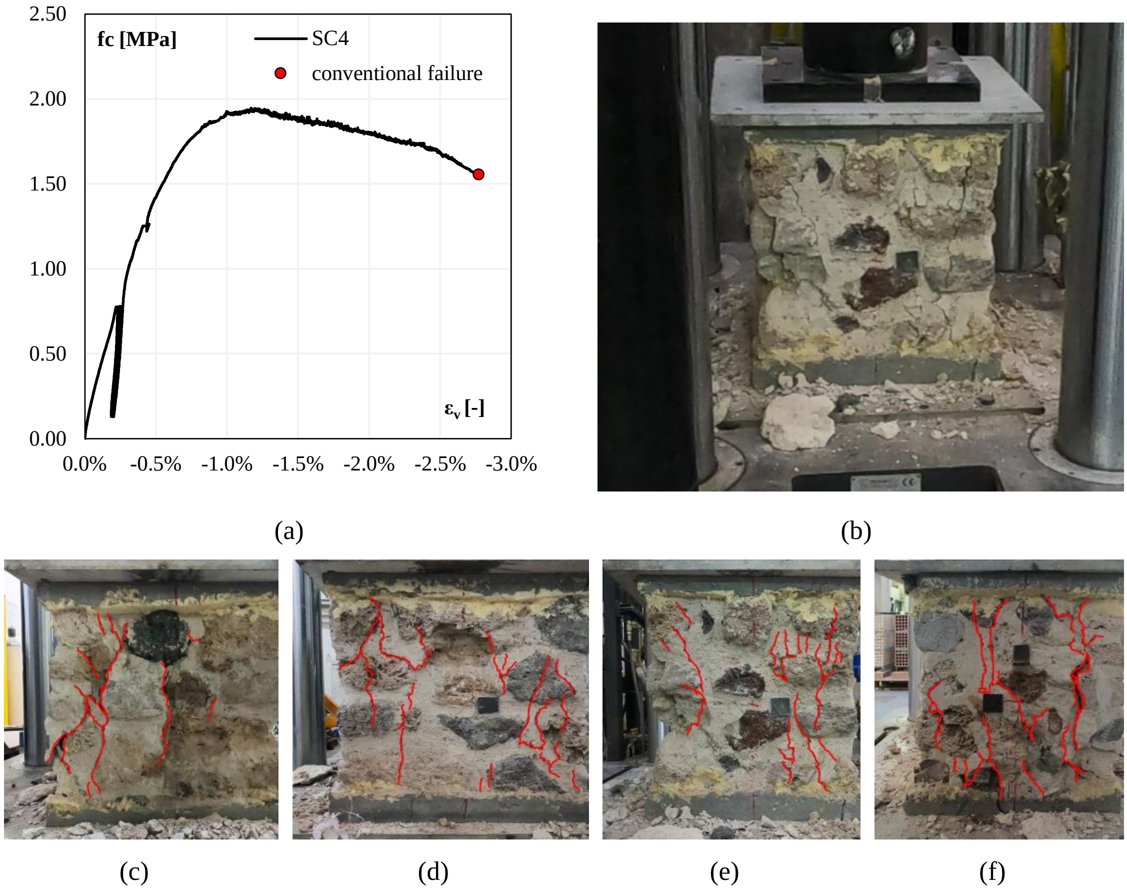

Figure 67. Compressive stress-vertical strain relationship (a) and failure mode for panel SC4: view of the collapsed specimen (b); final crack pattern survey on side A (c), side B (d), side C (e) and side D (f).

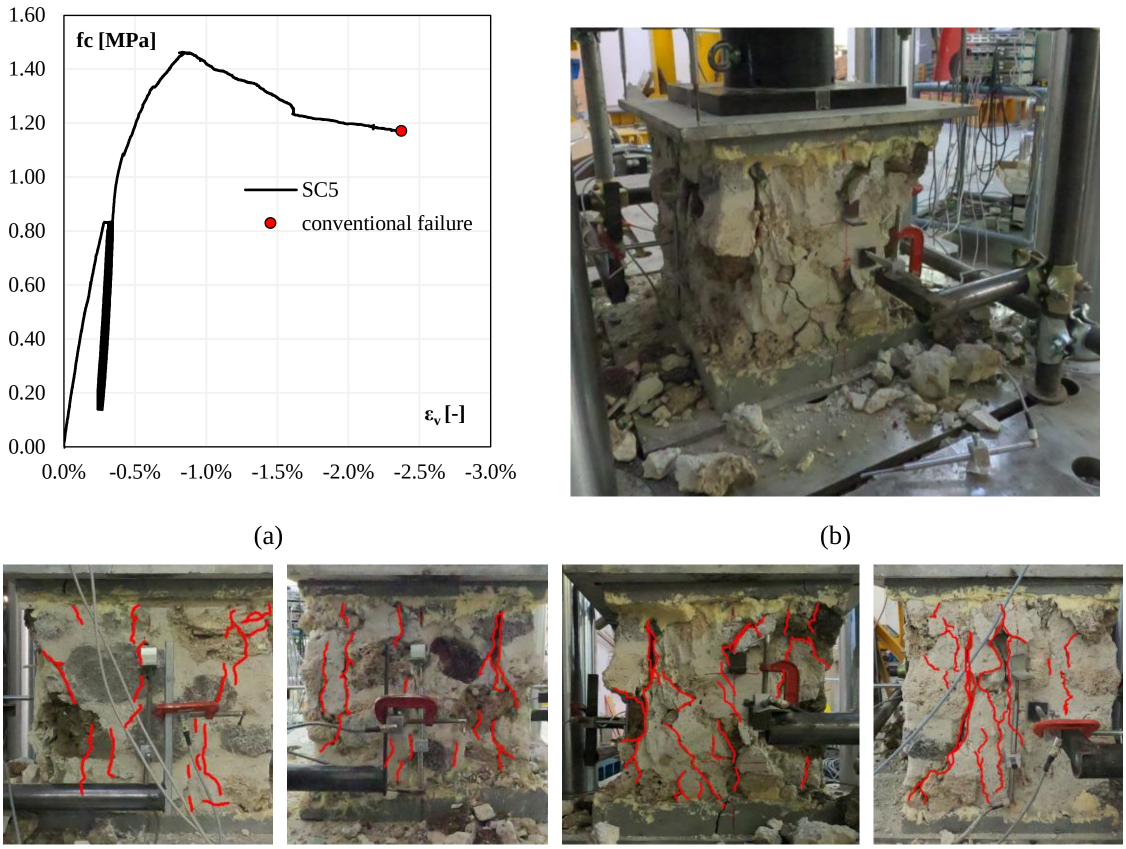

Figure 68. Compressive stress-vertical strain relationship (a) and failure mode for panel SC5: view of the collapsed specimen (b); final crack pattern survey on side A (c), side B (d), side C (e) and side D (f).

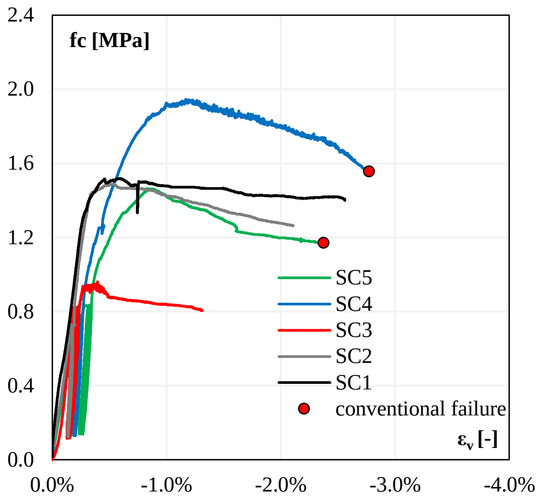

Figure 69. Compressive stress-strain curves.

4.3. Comparative analysis of the non-destructive and destructive characterization of *opus incertum* masonry

The following sections focus on a comparative analysis of the non-destructive and destructive characterization of opus incertum masonry. In particular, at first, the results of sonic tests carried out on the Pompeii-like masonry panels are compared with the results of diagonal compression tests and axial compression tests performed on the same specimens, then the results of sonic tests carried out on the Pompeii-like masonry panels are compared with the results of the sonic test on archaeological structures.

4.3.1. Comparison between NDTs and DTs outcomes of the Pompeii-like masonry panels

The comparison between the outcomes of the sonic and diagonal compression tests exhibited good agreement. Indeed, the higher the mean velocity in the last sonic test, the higher was the shear capacity (τ_{max} = 0.27 MPa and $V_{t=148}$ = 2923 m/s for S2; τ_{max} = 0.25 MPa and $V_{t=148}$ = 2918 m/s for S3; and τ_{max} = 0.19 MPa and $V_{t=148}$ = 2428 m/s for S1). The final crack patterns complied with the velocity distribution map of each panel since the development of cracks avoided areas where maximum velocity ranges were detected. In particular, diagonal shear cracks mainly developed through the mortar joints, on the unit-mortar interfaces along the diagonal compression side for each panel, and only intercepted certain rock units, as shown in Figure 70 for S1, S2 and S3.

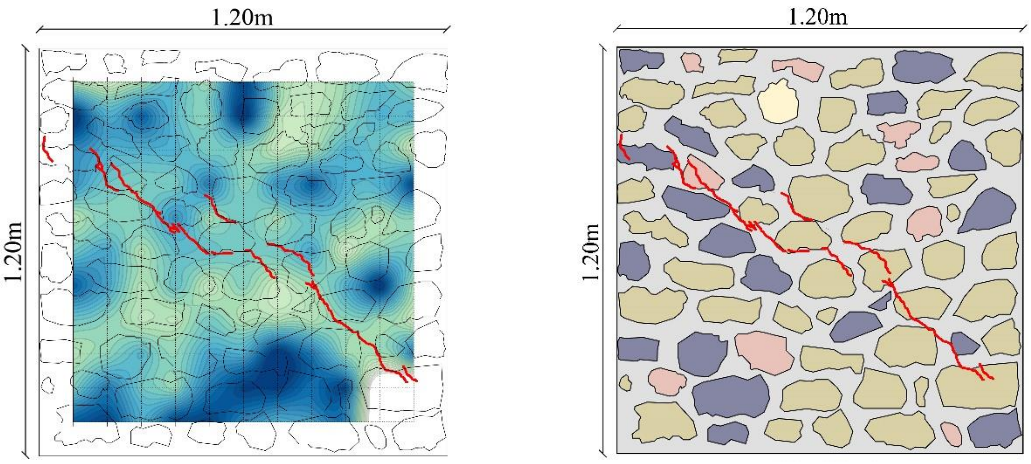

(a)

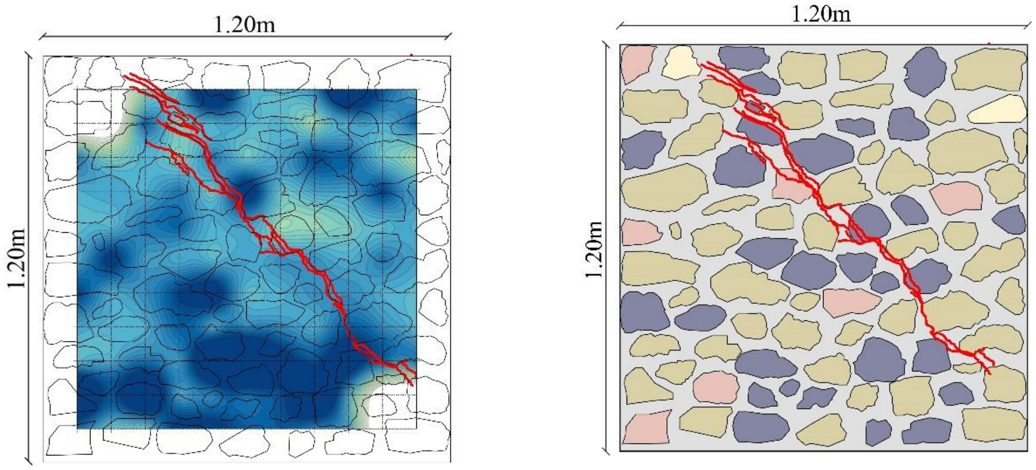

(b)

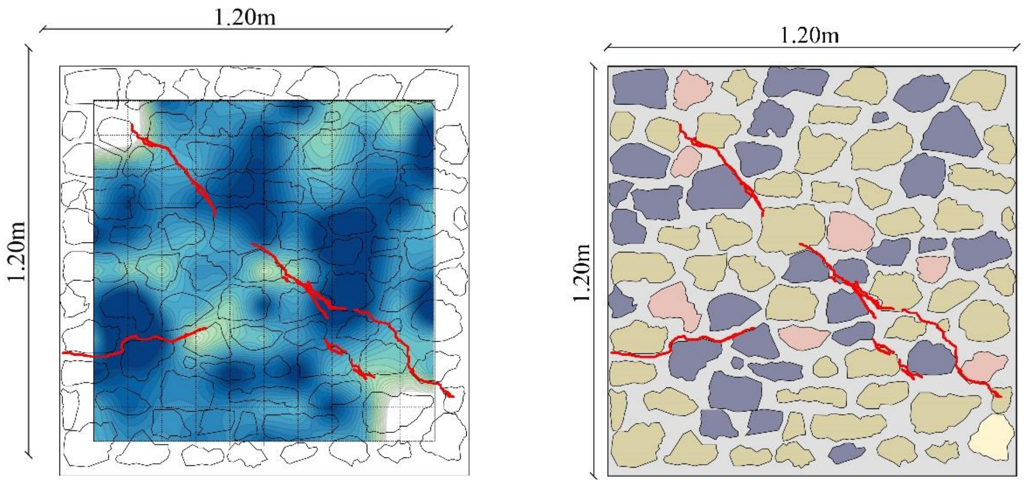

(c)

Figure 70. Final crack pattern on the velocity distribution map at t =148 and final crack pattern on the material survey for panels S1 (a), S2 (b) and S3 (c).

As regards the axial compression tests, a comparison between the elastic modulus computed through the sonic pulse velocity test and the elastic modulus experimentally obtained was performed. This comparison was based on the relationship defined for concrete (Eq. 3.1)(ASTM 2003), which is defined on the assumption of solid, elastic, isotropic and homogeneous material. Despite masonry is not a homogeneous material, certain studies have taken into account this equation for a primary estimation of the mechanical properties of a masonry specimen from the results of a sonic pulse velocity test (Miranda et al. 2013, 2012). Thus, to assess a comparison between compression tests and sonic pulse velocity tests results, the dynamic modulus of elasticity E_d was calculated, as, Eq. (4.21):

$$E_d=V^2\frac{\rho(1\text{-}2\nu)(1+\nu)}{(1\text{-}\nu)} \tag{4.21}$$

Where the sonic velocity was assumed to equal the mean sonic pulse velocity of the specimens at 148 days, V = 2767 m/s. The Poisson ratio was assumed as the mean value obtained from the axial compression tests in the horizontal direction, ν = 0.13. The density was evaluated according to a simplified homogenization procedure based on the bulk density of the single components. To do that, the masonry assemblage was assumed as composed of three adjacent layers of the same thickness. The external leaves were considered as composed of 30% of lava, 30% of travertine, 10% of foam lava and 30% of mortar, resulting in a bulk density ρ_{leaves} = 1527 kg/m^3. For the internal core, the same composition was considered with the density of the rock units reduced to 60%, according to what was reported in (Giuliani 2007) and resulting in a bulk density ρ_{core} = 1049 kg/m^3. The bulk density of the masonry was therefore evaluated as ρ = 1406 kg/m^3. This procedure led to a dynamic modulus of elasticity equal to 10058 MPa, i.e. about 10 times greater than the static modulus of elasticity evaluated as the mean of the slopes of the three obtained lines, $E_{m.}$ This confirmed the need to establish specific experimental relationships for the estimation of mechanical parameters from the sonic test results, based on the specific masonry typology.

4.3.2. Comparison between Pompeii-like masonry panels and archaeological structures

Despite STs provide qualitative results, the combination of STs results with the results of other tests obtained on the same typology of structure, particularly DTs, is very important to define indicative evaluations of fundamental mechanical properties. Therefore, the results obtained from STs and the archaeological structures (see chapter 3) are herein associated with the outcomes of the characterization of the Pompeii-like masonry panels. Moreover, obtained data were extended with other available information from the literature concerning experimental programmes involving both STs and DTs performed on rubble stone masonry structures. In particular, Figure 71 shows the correlations between the direct sonic velocities and compressive strength and modulus of elasticity obtained from the same masonry specimens, namely the Pompeii-like masonry panels presented in this chapter, reproduced rubble stone masonry panels by Valluzzi (2000), Silva (2012) and Mazzon (2010) (Mazzon 2010; Silva et al. 2014; Silva 2012; Valluzzi 2000) and existing rubble stone masonry structures by Riva et al. (1997) (Riva et al. 1997). A similar correlation was already suggested by (Silva et al. 2014). Besides, the figure reports the ranges of mean sonic velocities found for archaeological *opus incertum* and the Pompeii-like masonry panels found in this study and by Valluzzi et al. (2019) (Valluzzi et al. 2019). Despite available data are still not sufficient to establish reliable analytical correlations, the collected information can be useful to indicatively estimate the possible ranges of mechanical properties for the ancient structures.

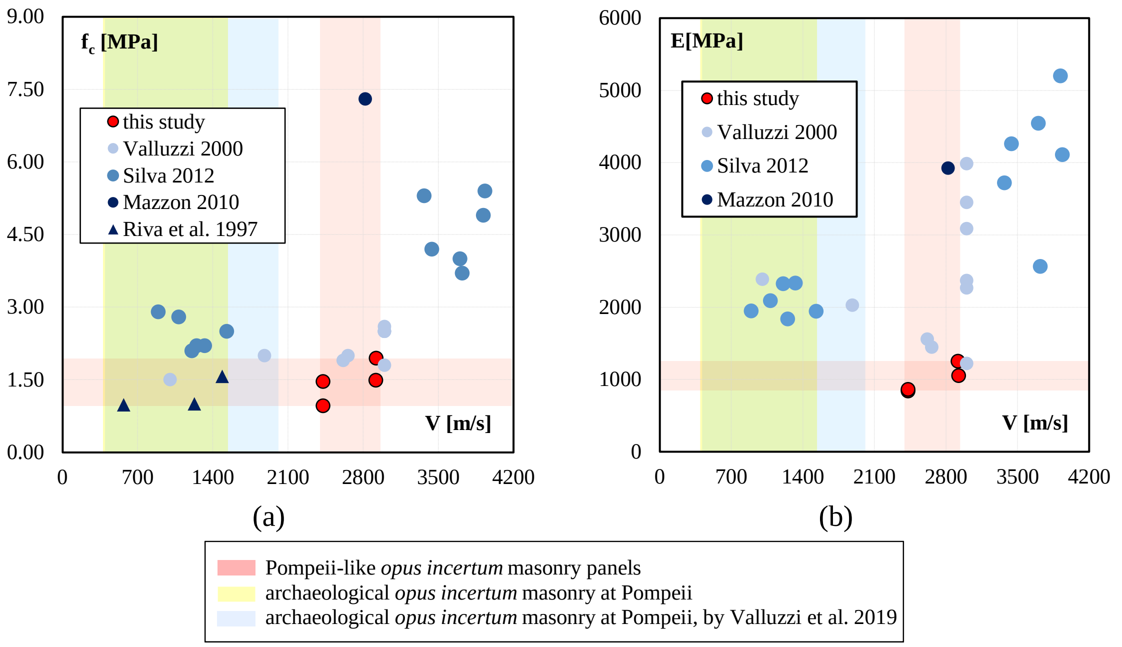

Figure 71. Comparison between available data from this study and the literature of direct STs results and DTs results on stone masonry structures: the relation between mean sonic velocity and compressive strength (a); the relation between mean sonic velocity and elastic modulus (b). The ranges of mean velocities found for archaeological opus incertum *at Pompeii in this study and by Valluzzi et al. (2019) and for Pompeii-like masonry panels in this study are also highlighted.*

5. ASSESSMENT OF THE SEISMIC RELIABILITY OF ARCHAEOLOGICAL COLUMNS

Columns are typical constructive elements of Greek and Roman architecture, present in many archaeological sites in all the Mediterranean area. The study of the seismic behavior of ancient Greek and Roman columns is of particular interest due to the significant seismic activity of the Eastern Mediterranean area (Papadopoulos et al. 2019).

Columns had both a structural function and an architectural meaning, according to their role and position in a private or public building. Besides the different architectural orders, building materials, size and proportions, related to the place and time of construction, ancient columns are vertical elements composed of a shaft and a capital. They could be placed on a base, with or without a pedestal, or a stylobate and could support an entablature and a sloped roof. Ancient columns could be monolithic or composed of overlapped natural stone pieces, the drums. In multidrum columns, the drums were dry overlapped, sometimes connected through metallic or wooden elements (Adam 2014), that, however, did not significantly affect their seismic response, particularly as concerns the rocking motion (Pitilakis and Tavouktsi 2010; Psycharis 1990, 2018). Nowadays, many ancient columns are free-standing elements with low or zero axial load, due to missing entablature and roofs. Moreover, material decay, due to the time and natural or anthropic phenomena, foundation failures, presence of cracks, missing or misplaced parts, compromise their stability and seismic capacity.

The dynamic behavior of a multidrum free-standing column is controlled by rocking, sliding, or a combination of the two mechanisms of the single drums or groups of them. When subjected to seismic excitation, such multi-block systems show many patterns of the rocking motion, whose number increase with the number of constituent blocks, and they continuously move from one of them to another. Thus natural modes of vibration in the classical meaning cannot be defined. Therefore, dynamic analysis and seismic assessment of these elements are particularly difficult to approach, since their response is highly complex, non-linear and sensitive to even trivial changes of the parameters of the model and the seismic input (Papadopoulos et al. 2019; Pitilakis and

Tavouktsi 2010; Psycharis 2018). Several studies focused on this topic, based on three main approaches: i) analytical (DeJong and Dimitrakopoulos 2014; Housner 1963; Minafò et al. 2016; Psycharis 1990; Spanos et al. 2001), ii) numerical, based on the Discrete Element Method, DEM, or Finite Element Method, FEM (Komodromos et al. 2008; Konstantinidis and Makris 2005; Lignola et al. 2014; de Martino et al. 2012; Papadopoulos et al. 2019; Papadopoulos and Vintzileou 2014; Pappas et al. 2014, 2016; Pitilakis and Tavouktsi 2010; Psycharis et al. 2003, 2000; Sarhosis et al. 2016; Toumbakari and Psycharis 2010), or iii) experimental (Drosos and Anastasopoulos 2014; Mouzakis et al. 2002).

Since the seismic response of classical multidrum columns is dominated by rocking, it partially follows the dynamics of rocking rigid blocks (Psycharis 2018). The first systematic and landmark study on the analysis of the rocking response of a single rigid block was presented by G. W. Housner in 1963 (Housner 1963) and it was an important reference for this type of investigation. The study concerned the rocking motion of an inverted pendulum type structure considered as a monolithic rigid block, standing on a rigid and horizontal base, with the assumption of infinite compressive strength of the block and no sliding between the block and the base (Figure 72).

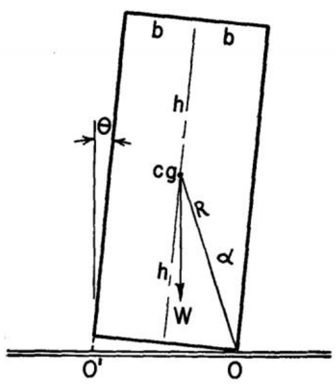

Figure 72. Rocking block by (Housner 1963).

Housner found that the dynamic response of a slender rigid rocking block depended on its size and slenderness as well as the characteristics of the applied excitation. Indeed, Housner's analysis and later studies proved that the dynamic response of a single rocking block and other dynamically equivalent systems subjected to a horizontal ground motion (on the assumption that sliding and bouncing do not occur) can be solely expressed through four dimensionless terms (DeJong and Dimitrakopoulos 2014; Psycharis 2018): i) ω_g/p; ii) $a_g/(g\tan\alpha)$; iii) α; iv) ε; where ω_g is the frequency of the excitation; $p = \sqrt{mgR/I_0}$ is the characteristic rocking frequency parameter of the structure; m is its mass; R is the distance from the center of mass of the structure to the base perimeter; I_o is the mass moment of inertia around the point O; α=b/h is the slenderness angle (see Figure 72) and ε is the coefficient of restitution. The first term increases with the frequency of the excitation and with the size of the structure computed through R; the second term measures the strength of the excitation (a_g) compared to the acceleration required for the overturning of the block ($g\tan\alpha$). Giving ε as known and constant, it was found that for a given excitation and slenderness of the block (ω_g, a_g and α) larger blocks are more stable than smaller ones. This was defined as an "unexpected size effect" by Housner and it was explained by the fact that the seismic action is not scaled with the dimensions of the block (Housner 1963). For a given block (α and p) long-period excitation are more dangerous than high-frequency ones, namely the normalized amplitude of the excitation required for the overturning of the block ($a_g/(g\tan\alpha)$) is smaller for excitation with a higher predominant period (Psycharis 2018).

Recent numerical studies on multidrum columns confirmed these conclusions defined for rocking rigid blocks. Pappas et al., based on DEM simulations, defined a preliminary seismic assessment form with the definition of influence factors taking into account all the parameters affecting the seismic response of ancient free-standing multidrum columns (i.e. slenderness, height, number of drums, structural conditions and soil type) (Pappas et al. 2016). It was found that by keeping constant the other factors when increasing the slenderness, the probability of collapse increased, conversely when the size of the column was increased, the probability decreased. Papadopoulos et al., from FEM analysis, derived criteria for the seismic stability of ancient free-standing multidrum columns in which, for a given seismic input, larger columns were more stable than smaller ones with the same aspect ratio (Papadopoulos et al. 2019).

Concerning the influence of other geometrical characteristics of multidrum columns investigated with numerical approaches, the number of drums was found to be another important parameter affecting the seismic response of a column in terms of sliding and energy dissipation due to friction (Papadopoulos et al. 2019; Papadopoulos and

Vintzileou 2014). The influence of this parameter depends on the frequency of the seismic action (Pappas et al. 2014). Literature studies (Papadopoulos et al. 2019; Papadopoulos and Vintzileou 2014; Pappas et al. 2016) found that columns with a higher number of drums were less vulnerable compared to columns with few drums and the monolithic ones, when they are on hard soils, while such effect was less noticeable on soft soils due to the lower frequencies produced. The configuration of the base of the columns could affect their seismic response also (Papadopoulos et al. 2019). Indeed, it was found that a column placed on several layers of stone blocks showed higher seismic stability compared to a column placed on a single block, probably due to the higher dissipation of energy through the relative displacement of those additional stone blocks. Papadopoulos et al. investigated the effect of the presence of entasis at the shaft of the columns and found that it did not affect the results of the numerical analyses (Papadopoulos et al. 2019; Papadopoulos and Vintzileou 2014). Finally, Konstantinidis and Makris found that the presence of wooden connecting elements between the drums did not affect significantly the dynamic response of the multidrum columns while stiff metallic connections could have an unfavorable impact on their seismic stability (Konstantinidis and Makris 2005).

As concerns the material properties, in numerical approaches the deformability of the drums was considered according to the selected modeling approach, while the coefficient of friction was generally a fundamental parameter (along with the geometry and the density of the material). Relevant numerical studies based on FEM, considered the drums as isotropic and elastic elements, taking into account the modulus of elasticity and Poisson ratio of the material (Papadopoulos et al. 2019; Pitilakis and Tavouktsi 2010). In particular, Pitilakis and Tavouktsi investigated the effect of degradation of the elastic properties of the material related to aging (accounted with a reduction of the elastic modulus) and found that it could lead to a higher probability of collapse, related to higher in-plane and out of plane displacements (Pitilakis and Tavouktsi 2010). However, other approaches based on DEM considered the deformability of the drums as negligible compared to the significant displacements produced by strong seismic input and defined them as infinitely rigid elements, in the interest of a lower computational effort (Komodromos et al. 2008; Konstantinidis and Makris 2005; Pappas et al. 2016). On the other hand, both in FEM and DEM-based approaches, the tangential interaction between the drums was modeled based on the Coulomb friction law with zero cohesion (Komodromos et al. 2008; Papadopoulos et al. 2019; Pappas et al. 2016; Pitilakis and Tavouktsi 2010). It was found that for lower values of the coefficient of friction the sliding mode prevails, while for higher values of the coefficient rocking mode prevails (Komodromos et al. 2008; Pitilakis and Tavouktsi 2010). Commonly, a single value of the coefficient of friction was set in the analyses, with the kinetic coefficient equal to the static one (Papadopoulos et al. 2019; Pappas et al. 2016; Pitilakis and Tavouktsi 2010). Indeed, Papadopoulos et al. found that varying the value of the kinetic coefficient of friction did not affect the results of the analysis with a specific trend.

Numerous studies concluded that classical multidrum columns can withstand important seismic actions (Papadopoulos et al. 2019; Pitilakis and Tavouktsi 2010). However, several studies investigated the effect of typical imperfections related to material degradation and structural damages (such as the presence of cracks, lacking parts, tilting due to soil failure, dislocation of the drums, reduced contact surfaces between the drums) and demonstrated that they can significantly reduce di seismic capacity of these elements (Pappas et al. 2016; Psycharis et al. 2003).

Recent studies focused on the static and dynamic assessment of the two-story colonnade at the Civil Forum at the Pompeii site (Lignola et al. 2014; de Martino et al. 2012; Sarhosis et al. 2016). However, these studies specifically concerned that peculiar colonnade, while several ancient columns at the Pompeii archaeological site are free-standing multidrum columns. Therefore, a continuous commitment to consolidate the knowledge of such elements, monitor their state of preservation and design proper restoration interventions, is still needed. Moreover, many of these elements are in an advanced state of degradation due to the material decay and successive tampering related to different restoration and consolidation interventions, requiring urgent safety measures, restoration and reconstruction of materials.

This chapter presents a wide investigation aimed at the knowledge of the state of preservation and assessment of the seismic reliability of free-standing multidrum tuff columns at the Pompeii site. This was the main objective of a scientific collaboration between the Archaeological Pompeii Park (PAP) and the Department of Structures for Engineering and Architecture (DiSt) of the University of Naples Federico II, aimed to support the development of proper programmes of intervention. The study involved a wide number of columns representative of typical column typology at the site were investigated: free-standing multidrum tuff columns.

5.1. Investigation programme

The first part of the study involved extensive *in situ* inspections, surveys and a study of archival sources from the historical and scientific archives of the PAP concerning a wide set of 103 multidrum grey-tuff columns from four different areas at the site, including private and public buildings: *Casa del Fauno* at *Regio VI* and *Quadriportico dei Teatri*, *Palestra Sannitica* and *Foro Triangolare* at *Regio VIII*. This part of the study allowed defining the mean geometrical properties affecting the dynamic behavior of the columns and to recognize the most common forms of degradation. As regards this latter, a critical analysis of past structural interventions performed on several columns at the site was performed.

After that, specific dynamic analyses were developed to assess the seismic vulnerability of such elements. Indeed, four columns representative of the ones under study were selected and their seismic behavior was studied through the FEM approach. seismic records were selected for the analyses, to investigate the influence of different frequencies and amplitudes of the seismic inputs.

5.1.1. Localization of the columns

This part of the investigation involved structures from four different areas of the site: 4 columns from *Casa del Fauno* (*Regio VI*), 54 columns from *Quadriportico dei Teatri*, 19 columns from *Palestra* Sannitica, and 26 columns from *Foro Triangolare* (*Regio VIII*) (Figure 73 and Figure 74). Note that pictures related to the *Tetrastyle atrium* of *Casa del Fauno* predate the recent restoration intervention (January 2021), which allowed removing the lateral supporting props shown in Figure 74 and the following images.

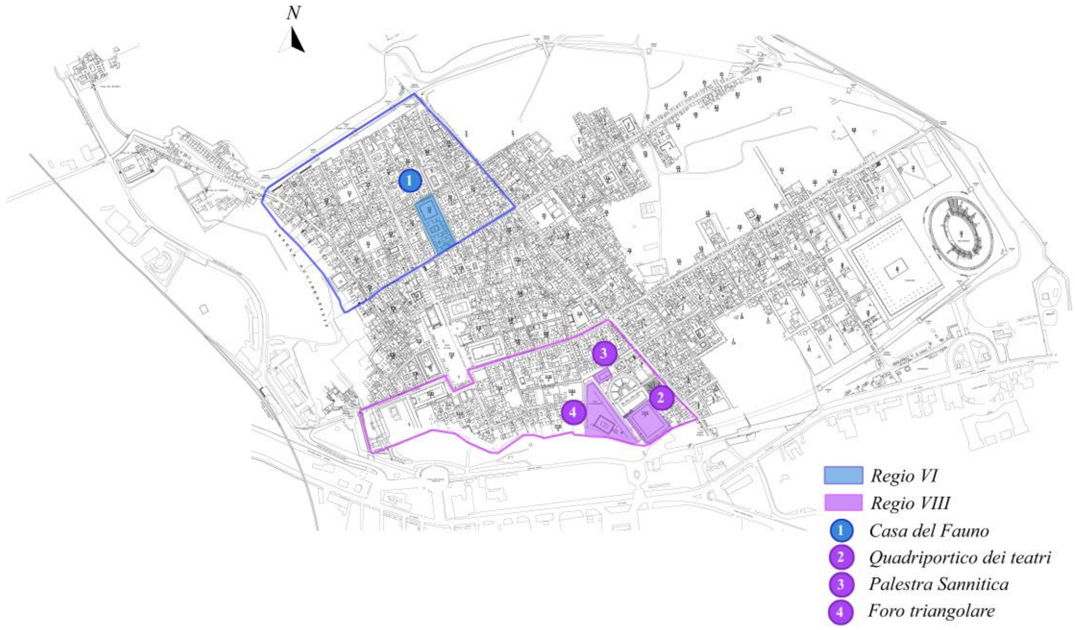

Figure 73. Plan of the archaeological Pompeii site and localization of the research areas: Casa del Fauno at Regio VI and Quadriportico dei Teatri, Foro Triangolare and Palestra Sannitica at Regio VIII.

Tetrastyle atrium, Casa del Fauno, Regio VI, Insula 12.

Quadriportico dei teatri, Regio VIII, Insula 7.

Palestra Sannitica, Regio VIII, Insula 7.

Foro triangolare, Regio VIII, Insula 7.

Figure 74. Research areas.

Casa del Fauno was one of the largest private houses at the ancient Pompeii, dated to the second century B.C., occupying an entire *Insula* at the *Regio VI*. The main excavation of the house is dated between 1829 and 1833. The name of the house came from a statue of a mythological figure, namely *Fauno*, found in the house, whose copy is nowadays in the main atrium. The study focused on 4 Corinthian columns of the tetrastyle atrium at the South-East side of the house, one of which showed significant degradation and needed safety devices.

Quadriportico dei Teatri, *Palestra Sannitica* and *Foro Triangolare* at *Regio VIII* were all public buildings. *Quadriportico dei Teatri* occupied a large part of the "theaters area" of Pompeii in the South-West area of the site. It originally had the function of the foyer for the Large Theatre then, after the earthquake of the 62 A.D., it became a barracks for gladiators. Among the 74 Doric columns composing the building, the 54 free-standing ones were selected and analyzed in the present study, while the remaining 30 columns were not involved in the present study since they bore a sloped roof realized in the last decades. *Palestra Sannitica*, located to the North-West of the *Quadriportico dei Teatri*, was a stadium dated back to pre-Roman times in the second century B.C. All the 19 Doric columns of the three remaining sides of the original colonnade were studied. *Foro Triangolare*, located to the South-West of the *Quadriportico dei Teatri*, took its name from its triangular shape, dating the second century B.C. The 26 grey-tuff columns remaining of the external colonnade that surrounded the area of the Doric Temple were analyzed in the present study. These research areas at *Regio VIII* were mainly brought to light in the second half of the XVIII century.

For each area, a progressive number was assigned at each column, so that they were uniquely identified through an alphanumeric code structured as follows: P_RIA_CX

Where:

- *P* is the initial letter of the site (i.e. Pompeii);
- *R* stands for the number of the *Regio*, in Roman numerals;
- *I* stands for the number of the Insula;
- *A* indicates the name of the research area (i.e. *CF* stands for *Casa del Fauno, QT* stands for *Quadriportico dei Teatri*, *PS* stands for *Palestra Sannitica* and *FT* stands for *Foro Triangolare*);
- *C* is the initial letter of the structural element (i.e. column);
- *X* is the assigned number within each area.

As an example, column 10 at the *Quadriportico dei Teatri* was identified by the code: P_VIII7Q_C10. Figure 75 reports the plan of each research area with the numbers of the studied columns.

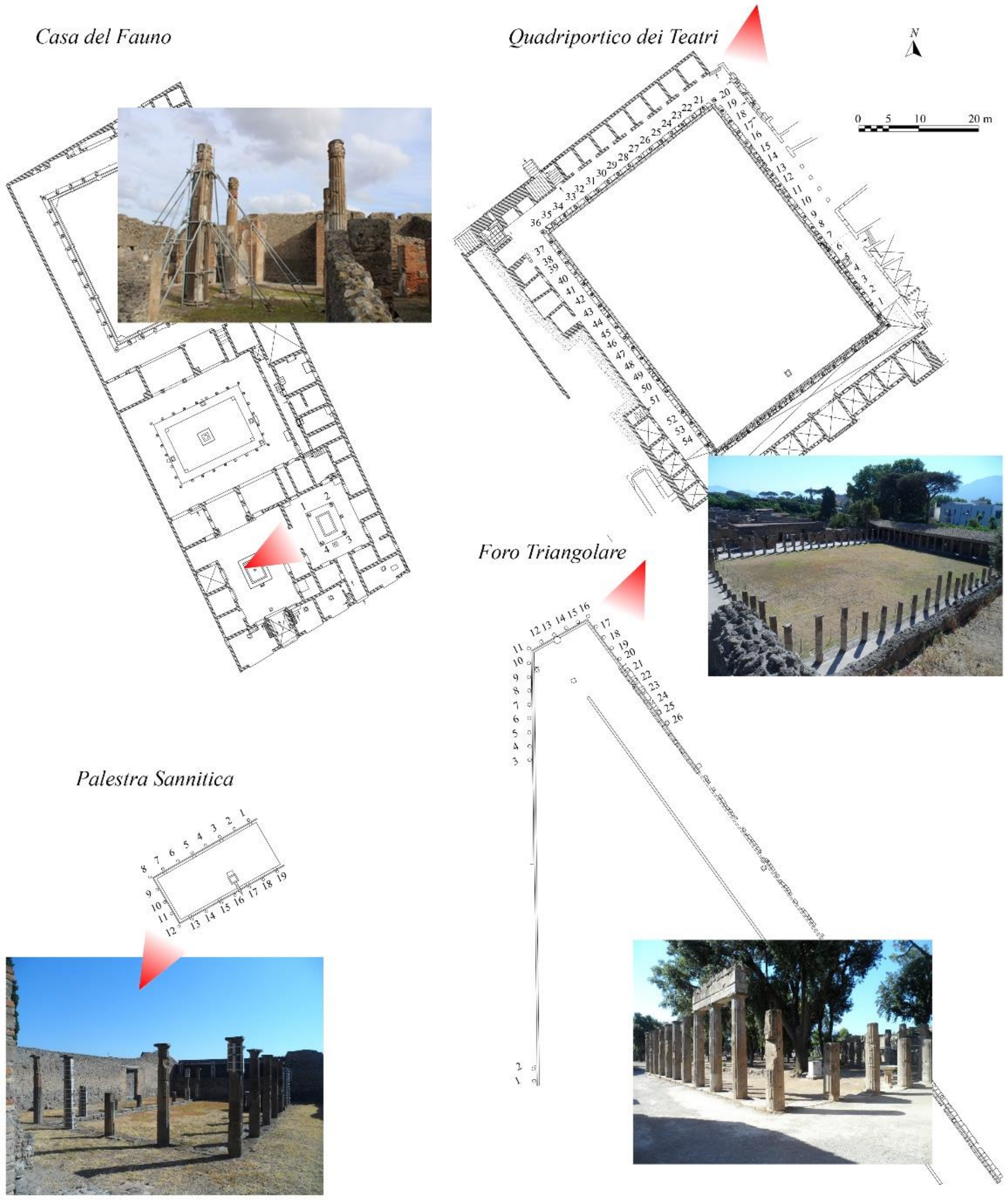

Figure 75. Plan and pictures of the research areas area with the enumeration of the studied columns.

5.2.Geometrical survey

According to what was found in previous numerical studies (Pappas et al. 2016; Pitilakis and Tavouktsi 2010; Psycharis 1990) geometrical properties affect the seismic behavior of multidrum classical columns, thus their definition could be useful for primary evaluation of the seismic vulnerability of such elements. As concerns this study, the following data were collected related to columns and drums: i) the column overall height, H, ii) the diameter of the drum at the base, d, iii) the drum height, h_i, iv) the drum diameter at the bottom, d_{inf}, and v) the drum diameter at the top, d_{sup}. Thus, the aspect ratio H/d and the distance from the center of mass of the column to the circumference at the base, R, were also evaluated (Figure 76).

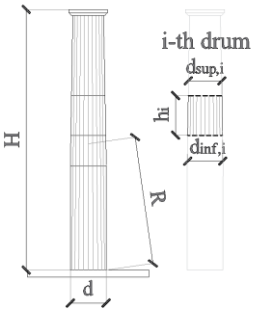

Figure 76. Main overall geometrical parameters affecting the seismic response of the columns.

5.2.1. Complete and incomplete columns

In each one of the four research areas several incomplete columns were found, i.e. columns where one or more drums or the capital are missing. Indeed, as part of the excavation work and/or later restoration intervention, many columns were only partially re-erected, due to missing or damaged drums and capitals. Figure 77 shows examples of completely re-erected columns (i.e. all the parts from the base to the capital are present today) and partially re-erected ones (i.e with missing parts). In the tetrastyle atrium of the *Casa del Fauno*, three out of four columns are complete, while only the capital is missing in the remaining one.

Casa del Fauno (tetrastyle atrium) | Quadriportico dei Teatri | Palestra Sannitica | Foro Triangolare

Complete columns

Incomplete columns

Figure 77. Complete and incomplete columns at Casa del Fauno, Quadriportico dei Teatri, Palestra Sannitica and Foro Triangolare.

Figure 78 shows the percentage of complete and incomplete columns in the investigated areas and Table 15 reports the number of investigated columns and the complete and incomplete columns for each area. *Palestra Sannitica* had the lowest number of incomplete columns, while *Foro Triangolare* had the highest one, with more than half of the total columns being incomplete. The total number of incomplete columns was 48 out of 103.

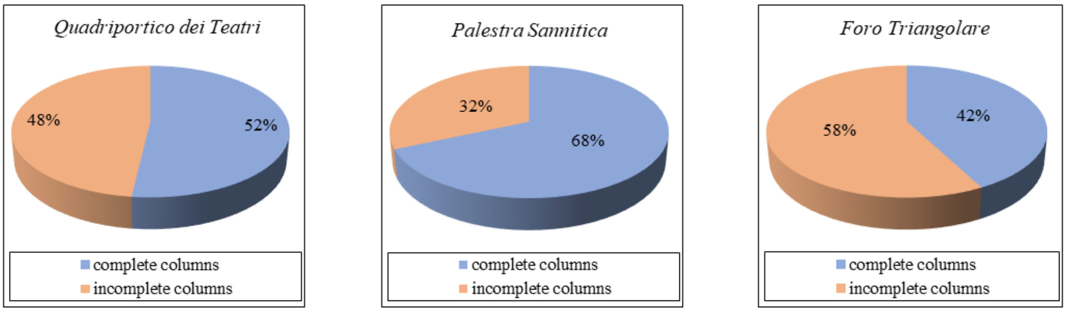

(a) (b) (c)

Figure 78. Percentage of complete and incomplete columns at Quadriportico dei Teatri (a), Palestra Sannitica (b) and Foro Triangolare (c).

Table 15. Number of investigated columns for each area and complete and incomplete elements.

	CF	Q	PS	FT	Total
number of free-standing columns	4	54	19	26	103
number of complete columns	3	28	13	11	55
number of incomplete columns	1	26	6	15	48

5.2.2. Geometrical properties of the columns

Figure 79 shows a schematic representation of one complete column for each area and Table 16 summarizes the mean overall characteristics for complete columns in each area: the total height, H; the diameter at the base, d; the aspect ratio, H/d; the quote of the center of mass, y_{CM}; the distance from the center of mass of the column to the circumference at the base, R; the number of drums; the volume; the mass. Note that the positions of the center of mass and the mass of the columns were evaluated based on the assumption of the columns being homogeneous solid of grey tuff with density ρ= 2600 kg/m^3.

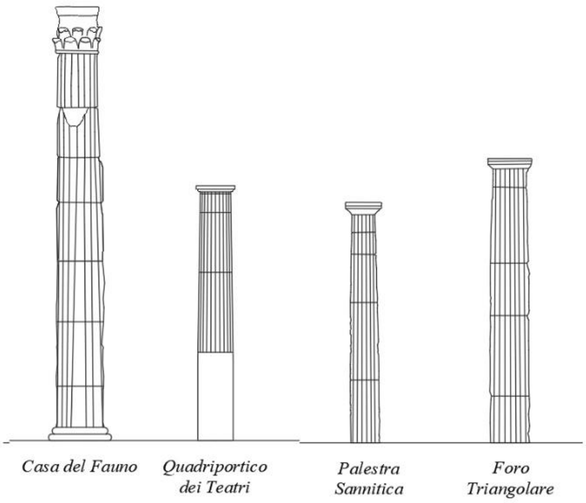

Figure 79. Column-type representative of each investigated area.

Table 16. Main overall characteristics for complete columns in each area.

	CF	Q	PS	FT
Total height, H [m]	5.74	3.56	3.30	3.99
Diameter at the base, d [m]	0.71	0.49	0.39	0.53
Aspect ratio, H/d [-]	8.09	7.27	8.53	7.50
Quote of the center of mass, yCM [m]	2.79	1.70	1.58	1.88
Distance center of mass - base perimeter, R [m]	2.82	1.72	1.59	1.90
Number of drums	6	5	5	5
Volume, V [m3]	1.70	0.63	0.37	0.85
Mass, M [kg]	2058	1634	972	2214

The main geometrical properties that may affect the seismic response of complete columns, namely H, d and R, are also shown in Figure 80 along with the corresponding standard errors. Moreover, Figure 81 plots relationships among these parameters, particularly: column height versus diameter at the base (a), and aspect ratio, H/d, versus R (b). Columns at *Casa del Fauno* had larger dimensions compared to columns at the other areas, probably related to both the different architectural styles and the different functions (i.e. a private Corinthian tetrastyle atrium instead of public Doric colonnades). In the other areas, the mean overall properties were comparable; columns at *Palestra Sannitica* showed the smallest dimensions and columns at *Foro Triangolare* showed the largest ones. The aspect ratio varied between 7.27 for columns at the *Quadriportico dei Teatri* to 8.53 for columns at *Palestra Sannitica* (with a coefficient of variation, CoV = 7%).

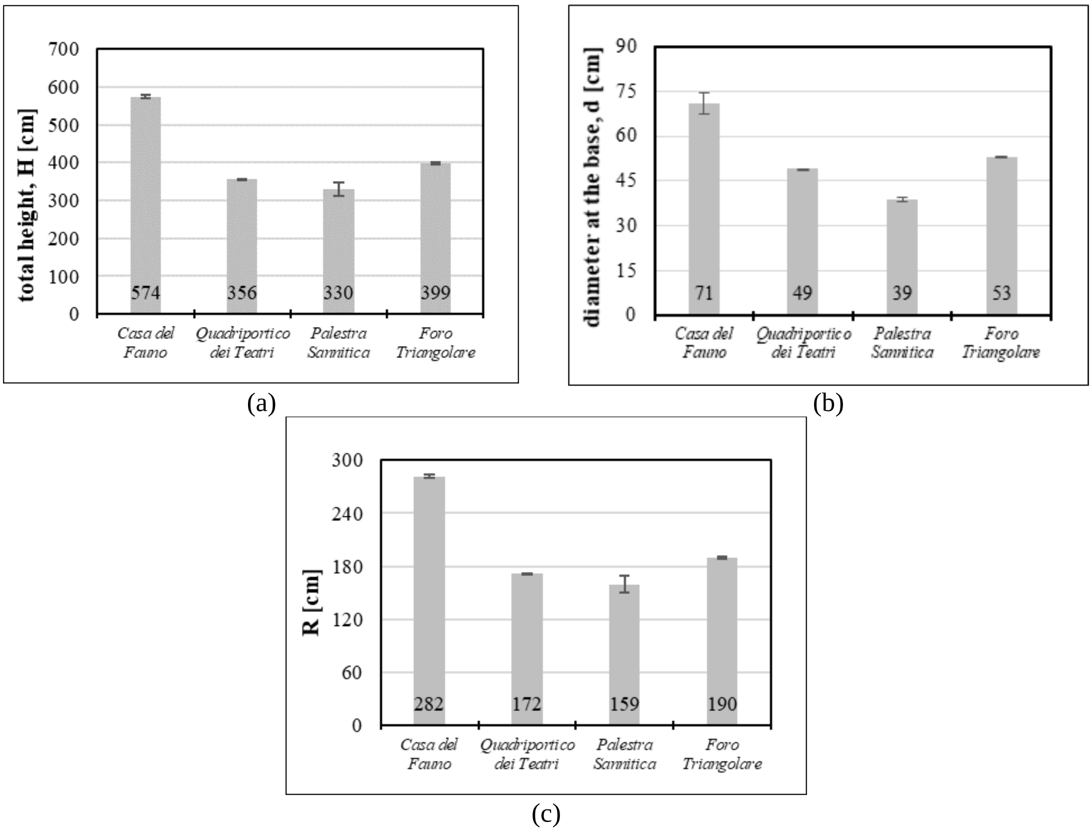

Figure 80. Mean overall geometrical properties of complete columns in each area.

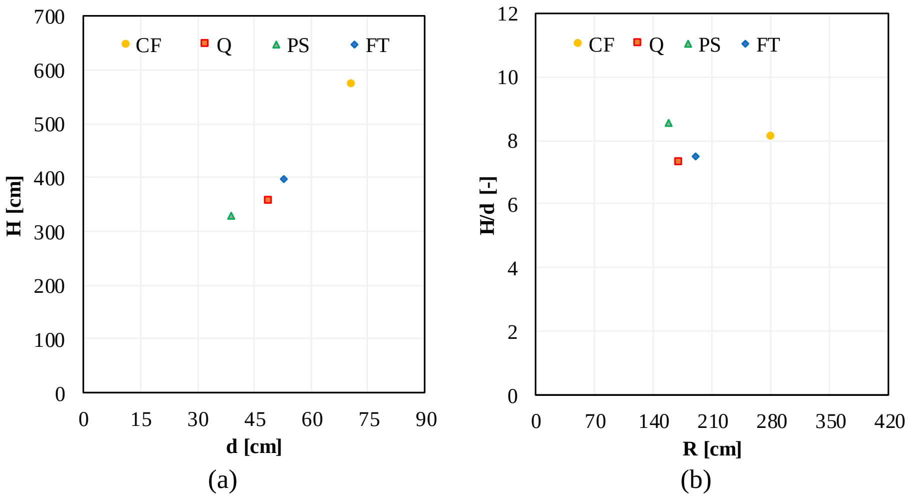

Figure 81. Relationship between geometrical parameters of multidrum complete columns: column height versus diameter at the base (a), and aspect ratio, H/d, versus R (b).

The geometrical properties of incomplete columns were also investigated. Their aspect ratio varied from 1.73 to 6.63 at *Quadriportico dei Teatri*, from 2.26 to 4.45 at *Palestra Sannitica* and from 2.07 to 7.30 at *Foro Triangolare*. Pappas et al. stated that columns with an aspect ratio lower than 4 could be considered relatively stable (Pappas et al. 2016); this happens only for 14 out of 48 incomplete columns herein investigated. Thus, despite they were only partially preserved in height the remaining 34 incomplete columns had a significant aspect ratio (i.e. greater than 4) and would require specific analysis to properly define their seismic capacity as in the case of complete columns. Figure 82 shows the relationship between H and d and between H/d and R for the incomplete columns.

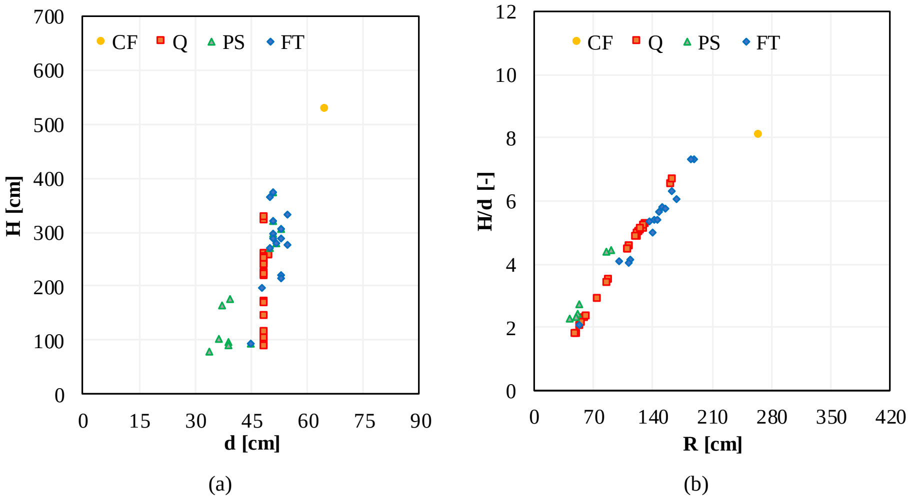

Figure 82. Relationship between geometrical parameters of all the incomplete multidrum columns: overall height versus diameter at the base (a), aspect ratio, H/d, versus R (b).

5.2.3. Number and size of drums

According to (Pappas et al. 2016) the number of drums affects the seismic response of the columns, especially if they are located on soft soils (Pappas et al. 2014, 2016). Therefore, the number and size of drums of a column are important information to investigate its seismic behavior. The investigated columns had different numbers and sizes of the drums, probably related to both their original configuration (depending on the available materials at that time) and post-excavation interventions (re-erection and subsequent alterations of the columns). Concerning complete columns, the ones at the *Casa del Fauno* had six drums, except for column number 4, with seven drums. In the other areas, the number of drums of the complete columns varied from three to seven at *Quadriportico dei Teatri* and between four and five at *Palestra Sannitica* and *Foro Triangolare* (Figure 83).

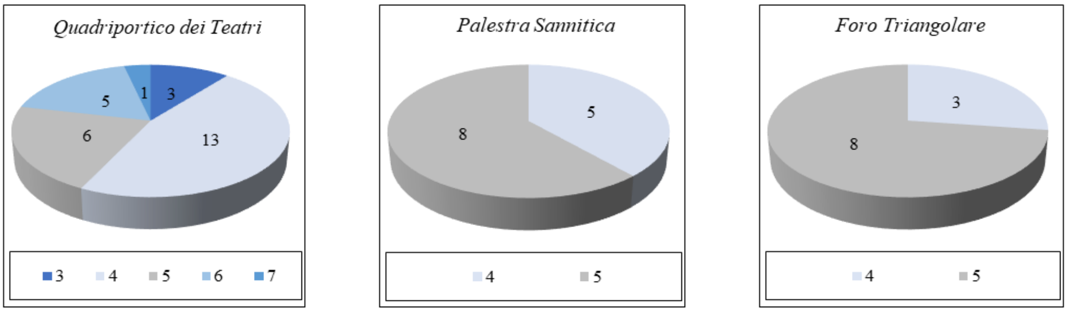

(a) (b) (c)

Figure 83. Distribution of the number of drums of complete columns at Quadriportico dei Teatri (a), Palestra Sannitica (b) and Foro Triangolare (c).

To provide specific indications for the structural modeling of a representative column for each area of study, the mean dimensions of the drums for complete columns with the most frequent number of drums are reported in Table 17: six drums at *Casa del Fauno*; four drums at *Quadriportico dei Teatri* and five drums at *Palestra Sannitica* and *Foro Triangolare*.

Table 17. Mean dimensions of the drums of complete columns with 6 drums at Casa del Fauno; 4 drums at Quadriportico dei Teatri, and 5 drums at Palestra Sannitica and Foro Triangolare.

	CF			**Q**			**PS**			**FT**		
	h [cm]	**d_{inf} [cm]**	**d_{sup} [cm]**	**h [cm]**	**d_{inf} [cm]**	**d_{sup} [cm]**	**h [cm]**	**d_{inf} [cm]**	**d_{sup} [cm]**	**h [cm]**	**d_{inf} [cm]**	**d_{sup} [cm]**
drum 1	104	75	63	137	49	48	94	39	38	82	53	52
drum 2	84	63	62	66	48	46	71	38	37	52	51	105
drum 3	98	62	60	100	46	43	67	37	35	105	51	47
drum 4	79	60	60	39	43	42	59	35	33	73	48	44
drum 5	116	60	59				22	33	32	31	45	45
drum 6	45	51	58									
Capital	68			17			18			11		

5.3.Damage and degradation survey

A correct evaluation of seismic performances of multidrum ancient columns must take into account their state of preservation and the presence of specific forms or degradation or damage (i.e. the presence of cracks, lacking parts, tilting due to soil failure, dislocation of the drums, reduced contact surfaces between the drums).

Certain forms of degradation and damage were frequently detected on the investigated columns. The most common are (Figure 84): i) weathering, cracks and detachment of the building material; ii) irregular shape (initial tilting and partial lack of contact among the drums); iii) presence of corroded metallic devices (i.e. ties to connect drums) and too invasive interventions.

(a) (b) (c) (d)

Figure 84. Critical issues on columns: weathering, cracks and detachment of the building material (a); initial tilting and partial lack of contact among the drums (b); presence of corroded metallic devices and too invasive interventions (c) and (d).

Columns showing significant damages would require more urgent interventions aimed to restore the material integrity and shape (reintegration of lacking parts, reparation of cracks, assessment of foundation failures, reparation or removal of invasive earlier interventions).

5.3.1. Past structural interventions

Throughout their post-excavation history, the investigated columns were involved in anthropic and natural events and subsequent restoration interventions that affected their current state of preservation. In particular, during the Second World War, the allied bombing in 1943 involved *Casa del Fauno*, and a bomb struck the tetrastyle atrium, causing the collapse of three of its four columns. Later, in 1980 a 6.9-magnitude earthquake, with its epicenter in Irpinia (Campania, Italy), has struck the entire Campania region, therefore the Pompeii site. After that, invasive structural interventions aimed to reduce the seismic risk were performed on different columns at *Regio VIII*, particularly columns at *Quadriportico dei Teatri*, *Foro Triangolare* and *Palestra Sannitica*. However, in a short time problems emerged due to the repair materials and techniques used for the interventions, thus further interventions followed from 1991 on the columns at *Quadriportico dei Teatri*.

In the following, a detailed description and critical analysis of such interventions are reported. Note that in the following it will be referred to as “type-A intervention” for the set of interventions carried out from 1981 and “type-B intervention” for the set of interventions carried out from 1991.

5.3.1.1. Interventions after the allied bombing of 1943

The allied bombing of September 1943 caused the collapse of three of the four Corinthian tuff columns of the tetrastyle atrium of *Casa del Fauno*. The column on the North side of the atrium was the one surviving the bombing. The columns were re-erected in 1946 under the supervision of Amedeo Maiuri (Figure 85). According to the principles of restoration reported in the Athens Charter and promoted by Maiuri, particularly distinguishability of the interventions and the use of anastylosis, the columns were reconstructed by recovering the collapsed archaeological material, and by using distinguishable clay bricks for lacking parts (Picone 2011). However, incompatible materials, such as cement-based mortars and iron clips and studs for the reparation of damaged drums, were used as part of the same restoration work, causing deterioration of the archaeological materials over time. Indeed, these types of elements were recently still visible and their utilization by Maiuri in similar contemporary interventions is documented (Picone 2011). Figure 86 shows a historical picture from the technical archives of PAP of the reconstructed columns after the 1943 bombing.

Figure 85. Reconstruction of the columns at the tetrastyle atrium of Casa del Fauno *[drawn from* (Picone 2011)*].*

Figure 86. Reconstructed columns of the tetrastyle atrium of Casa del Fauno *after the 1943 bombing (PAP technical archive).*

After the reconstruction in 1946, also after 1980, columns at the tetrastyle atrium of *Casa del Fauno* were subjected to further interventions that caused further deterioration of the archaeological material over the years. Until very recent times, the columns were in critical condition with one of them that needed the presence of supporting props to ensure its stability (Figure 87). Finally, with the most recent restoration work carried out in January 2021, the integrity of the columns were restored, and incompatible materials were removed.

Figure 87. A recent picture of columns at the tetrastyle atrium of Casa del Fauno *before the last restoration works of January 2021* (Pompeii, 2020).

5.3.1.2. Interventions after the Irpinia earthquake of 1980

Type-A intervention was carried out from 1981 and involved columns at *Quadriportico dei Teatri*, *Foro Triangolare* and *Palestra Sannitica.* It was aimed to connect the drums to allow the columns to behave as a single block. To do that, a steel bar was introduced in the core of each column, after the realization of a hole in the center of each drum. The connection between the columns and the ground was realized by digging the steel bars into the ground for a certain length. As a completion, a metallic nut was placed at the top of the columns to fix the capitals to the steel bars. Based on the research carried out in the technical archives of PAP, a summary of the executive phases and a schematic representation of the type-A intervention is reported in Figure 88, and pictures at the time of the execution of the intervention for the different executive phase are reported in Figure 89.

i. disassembling the drums;
ii. realization of a hole (ϕ80mm) in the core of each drum;
iii. inserting the steel bar (ϕ30mm) into the ground;
iv. stacking the drums on the bar;
v. inserting a metallic pipe (ϕ50mm) into the holes and hammering it in into the ground;
vi. filling the space between the pipe and the drums with siliceous sand;
vii. filling the space between the pipe and the bar with mortar;
viii. placing a locking nut and a plate at the top of the column;
ix. completion at the top of the column with mortar and the tuff portion previously removed

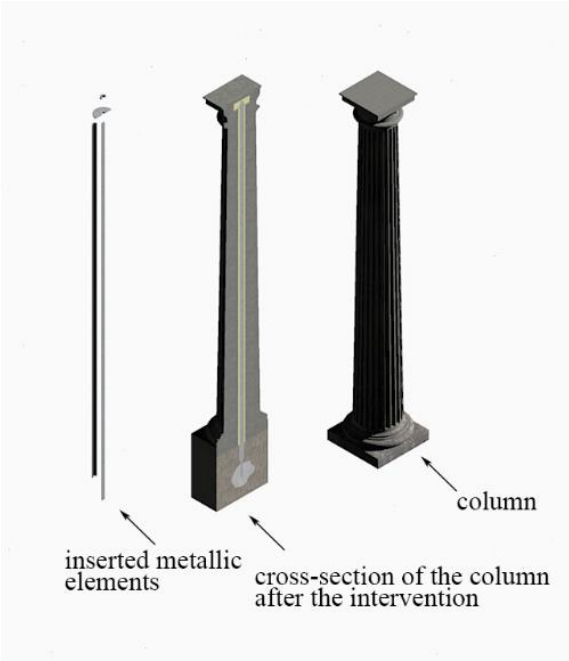

Figure 88. Summary of the executive phases and schematic representation of the type-A intervention.

Builders stacking the drums on the bar (iv)

Builders inserting a metallic pipe (ϕ50) into the holes and hammering it in into the ground (v)

The space between the pipe and the drums is filled with siliceous sand (vi) and the space between the pipe and the bar is filled with mortar (vii)

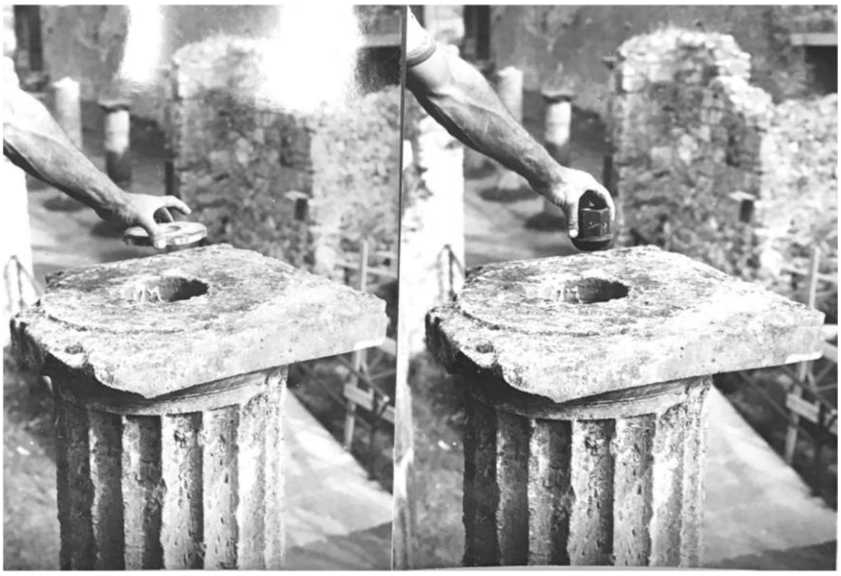

A locking nut and a plate is placed at the top of the column (viii)

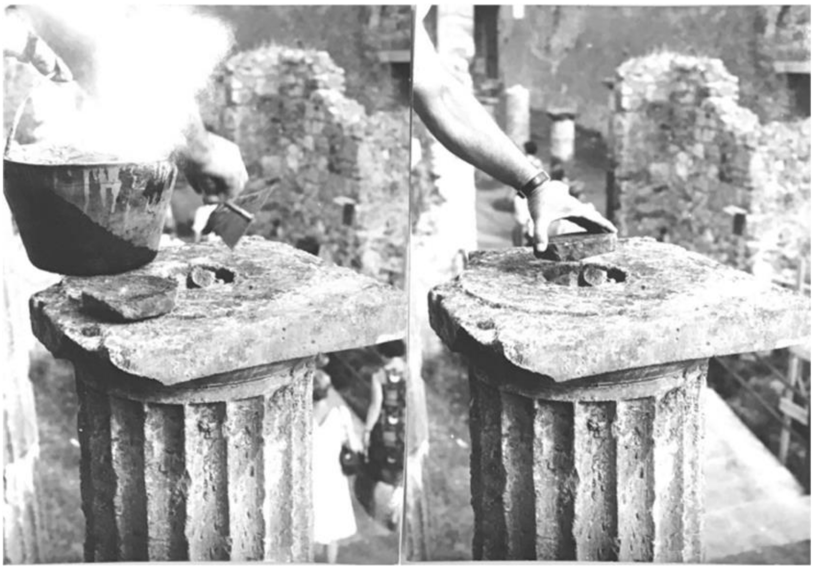

The column is finished with mortar and the tuff portion previously removed (ix)

Figure 89. Pictures at the time of the execution of the intervention for different executive phases from the technical archives of PAP.

5.3.1.3. Interventions carried out in the 90s

The type-B intervention was performed ten years after the type-A one. This was related to the evidence of problems related to the material and techniques used for this first one. The Type-B intervention aimed to replace the metallic elements used in the first one by introducing polymeric material and maintaining the same structural scheme of the column as a monolithic element.

Before carrying out the type-B intervention to replace the type-A one, this was carried out on the columns at *Casa dei Cornelii* (*Regio VIII*), which were not previously restored. After that, despite it was planned to apply the type-B intervention on all the columns subjected to the type-A one, it was performed only on the columns at *Quadriportico dei Teatri*. *In situ* experimentations were performed on two columns at *Casa dei Cornelii* first, then intervention was implemented on columns at *Quadriportico dei Teatri*, and finally, the test was repeated on two columns from this area to verify the effectiveness of the measure. As regards *Casa dei Cornelii*, two columns were tested before and after the intervention (Figure 90a). The test consisted of applying horizontal traction at the top of the columns with increasing intensity. Meanwhile, the displacements in three points of the columns were recorded: 1) next to the base at 0.20 m in elevation; 2) at the middle of the shaft, at 1.80 m and 3) next to the top at 3.40 m (Figure 90b).

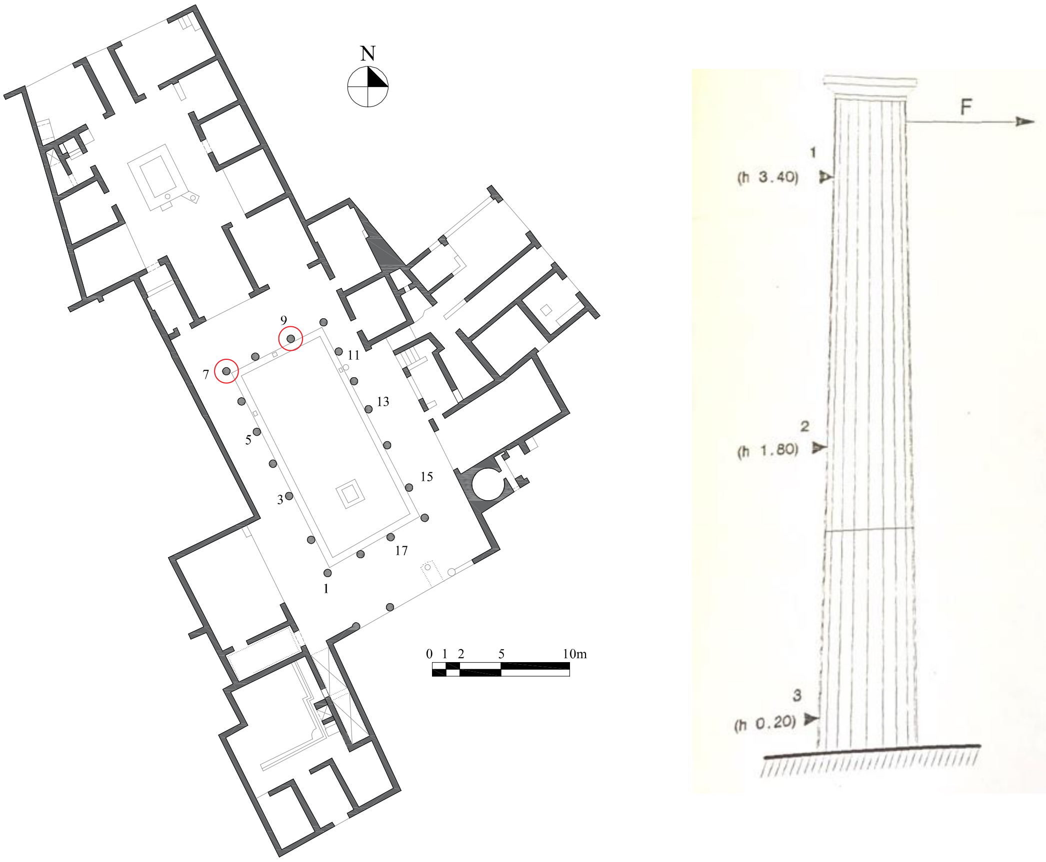

(a) (b)

Figure 90. Plan of Casa dei Cornelii *with the specification of the tested columns (a) and scheme of the applied load and the control point of the displacements (from the technical archive of* PAP*) (b).*

The tests at *Casa dei Cornelii* showed a reduction of the measured displacements for all the reading points after the execution of the type-B intervention for both the investigated columns (Figure 91(a) and (b)).

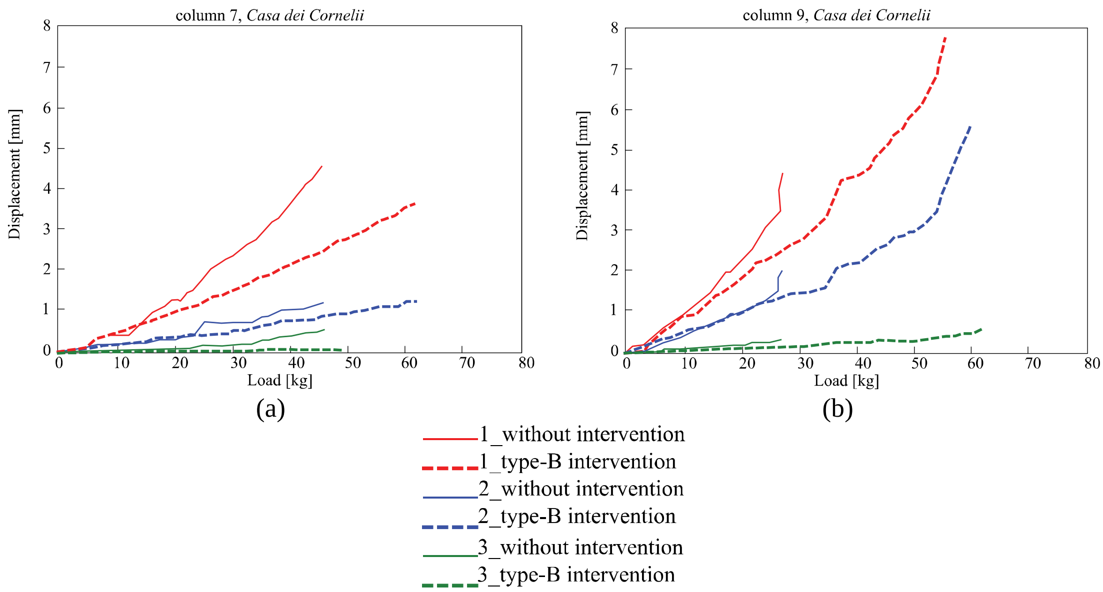

Figure 91. Load-displacement curves from the tests performed on columns 7 (a) and column 9 (b) at Casa dei Cornelii.

After that, the type-B intervention was performed on columns at *Quadriportico dei Teatri*. Based on the research carried out in the technical archives of PAP, it can be summarized that the intervention consisted of two main phases: i) removal of materials related to the type-A intervention; ii) installation of new materials. Removal operations were performed taking into account the state of preservation of every single column, and can be summarized as follows: i) when the drums were well preserved, the columns were disassembled, then the previous repair materials were removed, and finally, the columns were reconstructed; ii) when the drums were notably damaged, at first the drums were repaired with new mortars and polypropylene bars, then the metallic pipes and bars were removed without disassembling the columns by using a diamond core drilling machine. After that, the proper installation of the new measure was performed. The main executive stages of this phase can be summarized as follows: i) insertion of a polypropylene strand (ϕ32mm) into the pre-existing hole; ii) fixing the strand under the basis of the column, through the execution of a transversal injection of mortar at the base of the column; iii) application of a tensile tension of 300kg to the strand; iv) filling the space between the strand and the drums with expanded clay; v) execution of radial injections of mortar over the whole height of the column. Figure 92 reports pictures at the time of the execution of the type-B intervention for different executive phases from the technical archives of PAP.

Removal of metallic pipes and bars from the type-A intervention by using a diamond core drilling machine

Metallic bars, pipes and nuts from the type-A intervention removed from the columns

Insertion of the strand in the pre-existing hole and filling the space between the strand and the drums with expanded clay

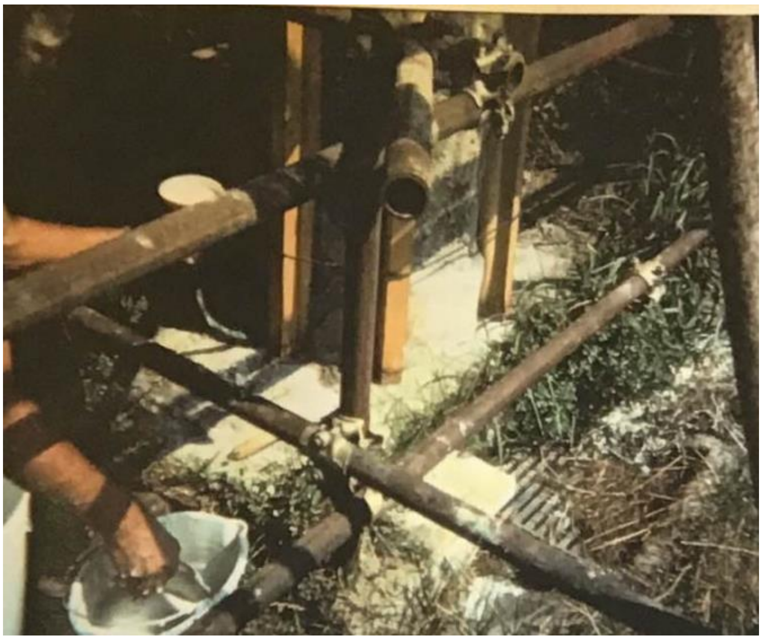

Injections of mortar at the base of the column to fix the strand in the foundation

Radial injections of mortar over the entire height of the column

Figure 92. Pictures at the time of the execution of the type-B intervention for different executive phases from the technical archives of PAP.

The test performed to verify the effectiveness of the type-B intervention at *Quadriportico dei Teatri* involved one column among the ones considered in this study. This column was already subjected to the type-A intervention. Therefore, the test was performed at first on the column with the type-A intervention; then the test was repeated on the column after the removal of the type-A materials; finally, the test was repeated on the column after the implementation of the type-B intervention. The test was performed similarly to what was described for *Casa dei Cornelii*. The test showed lower displacements at all the reading points with both the type-A and the type-B interventions.

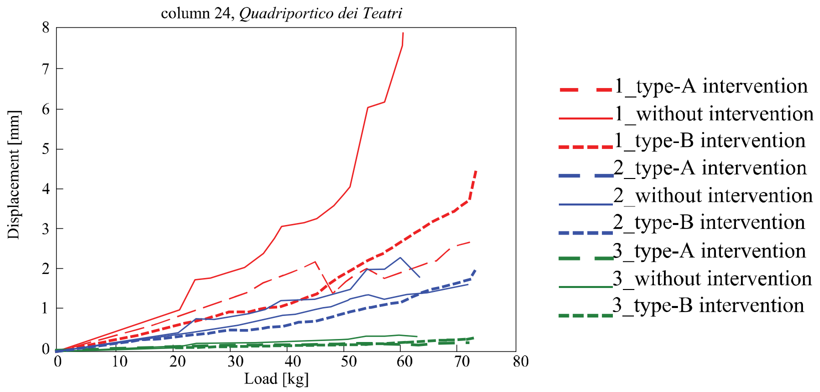

Figure 93. Load-displacement curves from the tests performed on column 24 at Quadriportico dei Teatri.

5.4.Analysis of the seismic response

After detailed surveys, archival researches and visual inspections to define the main geometrical properties of all the investigated columns and the most common forms of degradation and damage, that may affect their seismic behavior, an analysis of the seismic behavior of the four columns at the tetrastyla atrium of *Casa del Fauno* was implemented. Indeed, this is one of the largest and most visited private buildings at the Pompeii site, and when the study started, the columns presented deep degradation and needed specific and urgent attention for its assessment. Note that, since this section is focused exclusively on the four columns of *Casa del Fauno*, these elements are synthetically identified as “column 1”, “column 2”, “column 3”, and “column 4”, in what follows, instead of using the alphanumeric codes P_VI12CF_C1, P_VI12CF_C2, P_VI12CF_C3, and P_VI12CF_C4, respectively.

5.4.1. FEM modeling

The study was carried out based on the Finite Element Method (FEM). Eight seismic records were selected for the analyses, to investigate the influence of different frequencies and amplitudes of the seismic inputs. The modeling phases and the seismic input selected for the analyses are described in the following.

5.4.1.1. Geometry, material, and boundary conditions

The analyses herein presented refer to four columns at the *Casa del Fauno.* The analyses were conducted with finite element modeling (FEM), by using the software Abaqus/CAE. Therefore, the columns were modeled as assemblies of overlapping deformable blocks, the drums. The geometric characteristics used in the model are reported in Table 18.

Table 18. Geometrical parameters used in the model.

Free-standing multidrum columns at the tetrastyle atrium of *Casa del Fauno*												
	Column 1			**Column 2**			**Column 3**			**Column 4**		
	h [m]	**d_{inf} [m]**	**d_{sup} [m]**	**h [m]**	**d_{inf} [m]**	**d_{sup} [m]**	**h [m]**	**d_{inf} [m]**	**d_{sup} [m]**	**h [m]**	**d_{inf} [m]**	**d_{sup} [m]**
drum 1	0.55	0.73	-	1.53	0.76	-	0.54	0.65	-	0.57	0.64	-
drum 2	0.99	-	-	0.69	-	-	1.14	-	-	0.89	-	-
drum 3	0.11	-	-	0.91	-	-	1.07	-	-	0.84	-	-
drum 4	0.76	-	-	0.81	-	-	1.22	-	-	0.81	-	-
drum 5	0.17	-	0.66	0.62	-	-	0.73	-	-	0.63	-	-
drum 6	-	-	-	0.45	-	0.58	0.55	-	0.58	0.69	-	-
drum 7	-	-	-	-	-	-	-	-	-	0.74	-	0.52
capital	0.67	0.66	0.66	0.68	0.58	0.58	-	-	-	0.65	0.52	0.52
entire column	5.72	0.73	0.66	5.69	0.76	0.58	5.25	0.65	0.58	5.82	0.64	0.52

Each drum was modeled as an isotropic and elastic semi-conical solid (Figure 94 (a)) with material properties defined based on information from the technical archive of PAP (Table 19).

Table 19. Material parameters used in the model.

Grey tuff	
Bulk density, ρ [kg/m^3]	1230
Elastic modulus, E [GPa]	4.5
Poisson ratio, ν	0.25
Coefficient of friction, μ	0.5

The discretization of each drum was performed with 8-node hexahedra elements (Figure 94 (c)). Before this, each drum was partitioned into eight portions, to obtain a regular and correct formation of the meshes (Figure 94 (b)).

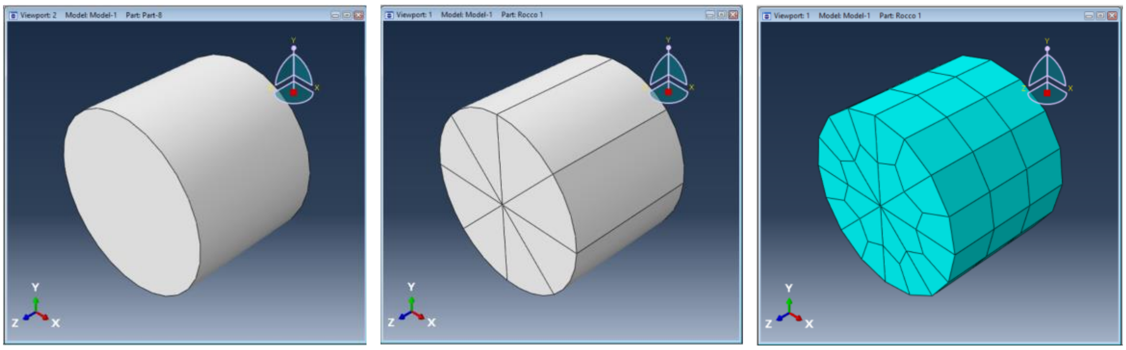

(a) (b) (c)

Figure 94. The geometric model of a drum: semi-conical solid (a), partition in eight parts (b) and mesh configuration (c).

The contact interaction between two consecutive drums was considered as governed by friction. Thus, it was modeled by adopting the Mohr-Coulomb criterion for the tangential stress along the surfaces, with dynamic coefficient friction equal to the static one (i.e. 0.5). This was consistent with the assumption made in other studies which found that the value of the dynamic coefficient friction has not any specific trend on the results of the analyses (Papadopoulos et al. 2019; Pitilakis and Tavouktsi 2010). Moreover, the hard contact behavior was set for the interaction between the drums in the normal direction, with compressive stress developed on the contact surface between two drums and zero stress when the drums are not in contact. Finally, the interactions between consecutive drums and between the first drum and the base of the column were defined by a "master" surface and a "slave" surface. A boundary condition of "encastre" was applied at the base of the columns as well as the input seismic signals. Figure 95 shows the geometric assembly of the entire column 1; the defined interactions between adjacent surfaces; the boundary condition of "encastre" at the base; the application of a seismic input at the base; the final numerical model of the column with the meshes.

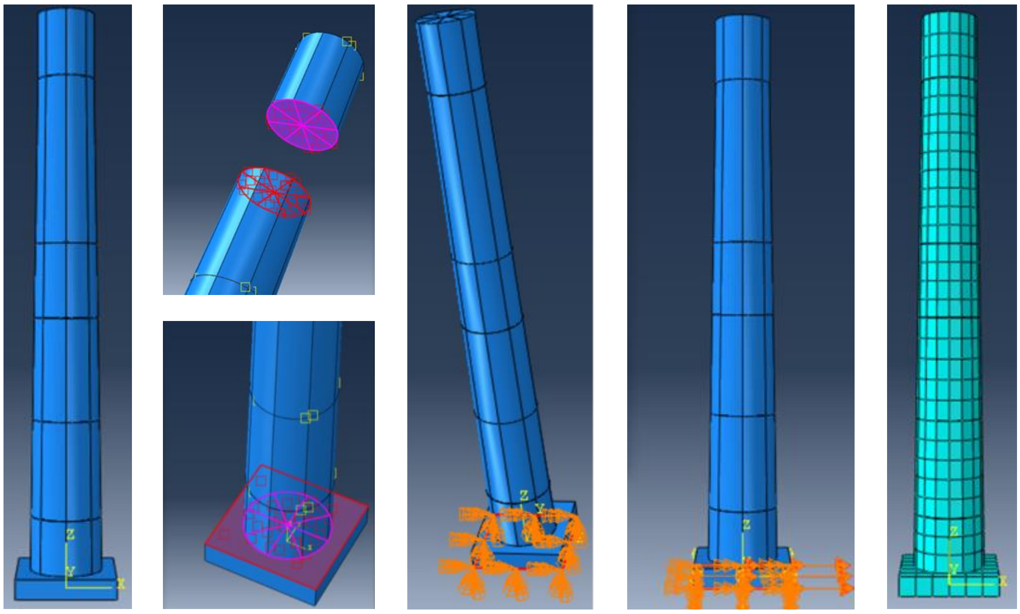

(a) (b) (c) (d) (e)

Figure 95. Phases of the modeling process for column 1: assembling of the single parts constituent the column (a); definition of the interactions between adjacent surfaces (b); definition of the boundary condition at the base (c); application of the seismic input at the base (d); final numerical model of the column with the meshes (e).

Each analysis involved two steps: the first involving the assignment of the geometrical and material properties, interactions and the acceleration of gravity; the second one involving the seismic input signal applied at the base of the columns. The analyses were performed according to the dynamic implicit method, with the time of each step set equal to 0.005s. This latter was equal to the time step of the selected seismic records.

5.4.1.2. Seismic inputs

Eight seismic records with different frequencies and amplitudes were selected for the analyses. These were: i) Irpinia, Italy (1980), recorded at Sturno, close to the epicenter and ii) recorded at Torre del Greco, about 15km from Pompeii; iii); Molise, Italy (2002), recorded at San Severo, about 50 km from the epicenter; iv) L'Aquila, Italy (2009), recorded at v. Aterno – Centro Valle, close to the epicenter; v) Kalamata, Greece (1986), recorded at Kalamata; vi) Edessa, Greece (1990), recorded at Edessa; vii) Aigio (1995), recorded at Aigio; viii) Athens, Greece (1999), recorded at Athens. Table 20 reports the intensity measures and frequency content indicator of the seismic input motions selected for the analysis. In particular, the intensity measures PHA, PHV and PHD represent the maximum vector sums of the accelerations, velocities and displacements, respectively, in the two horizontal directions of the seismic records. The predominant period, T_g, was evaluated as the period corresponding to the maximum ordinate of the 5% damped pseudo-velocity spectrum. Figure 96 plots the seismic records in the two orthogonal directions used in the analyses.

Table 20. Intensity measures and frequency content indicator of the seismic input motions selected for the analysis.

Seismic record	**PGA [g]**	**PGV [cm/s]**	**PGD [cm]**	**PHA* [g]**	**PHV* [cm/s]**	**PHD* [cm]**	**T_g [s]** E-W**	**T_g [s]** N-S**	**T_g [s]** mean**
Irpinia_Str	0.32	70.0	27.8	0.33	72.2	27.8	3.00	3.20	3.10
Irpinia_TdG	0.06	8.1	6.1	0.06	8.8	7.1	6.49	0.67	3.58
L'Aquila	0.66	42.7	6.8	0.77	46.7	6.8	0.67	0.50	0.58
Molise	0.06	2.1	0.3	0.06	2.4	0.3	0.50	0.38	0.44
Kalamata	0.27	31.7	6.5	0.35	38.5	6.7	0.67	0.55	0.61
Edessa	0.10	11.2	1.1	0.11	12.0	1.2	0.67	0.70	0.68
Aigio	0.52	51.3	8.3	0.53	51.3	8.6	0.55	0.55	0.55
Athens	0.31	16.9	2.1	0.38	16.3	2.9	0.65	0.22	0.44

*The maximum vector sum of the two relative components

**Predominant period corresponding to the maximum ordinate of the 5% damped relative velocity spectrum

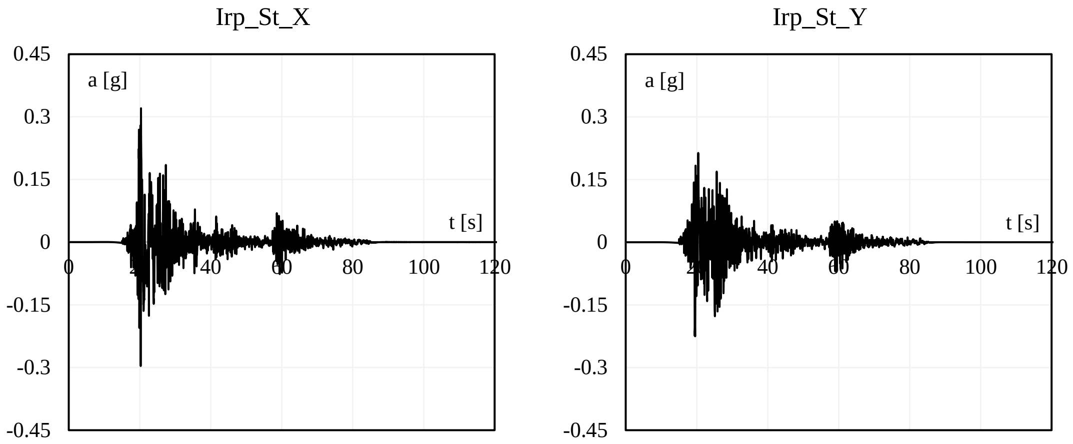

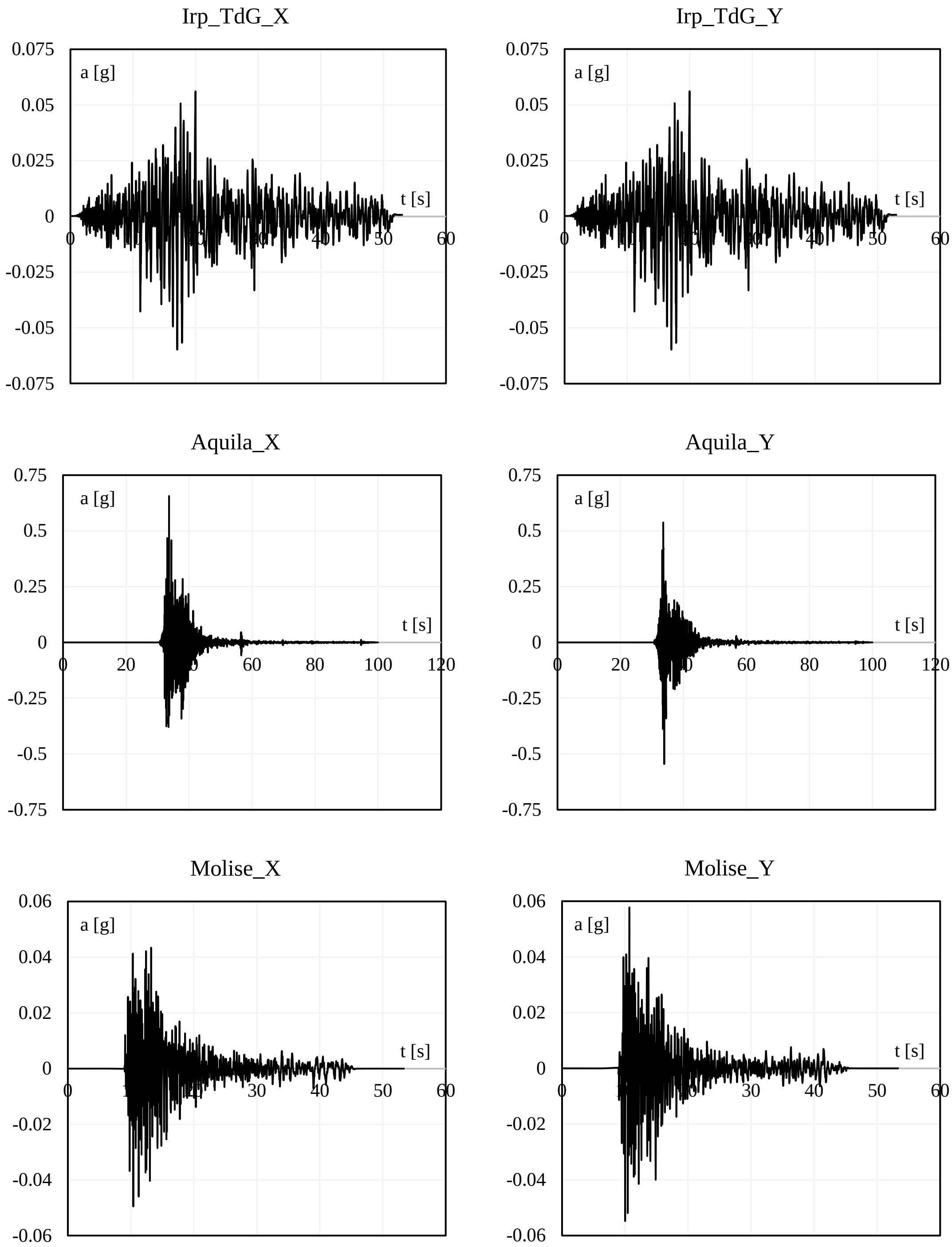
Irp_TdG_X
Irp_TdG_Y
a [g]
t [s]
Aquila_X
Aquila_Y
Molise_X
Molise_Y

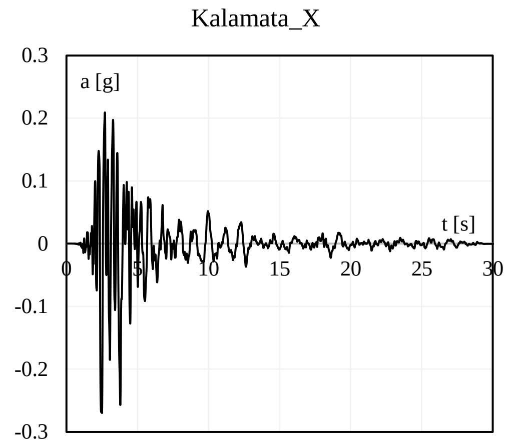
Kalamata_X
a [g]
t [s]
0.3
0.2
0.1
0
-0.1
-0.2
-0.3
0
5
10
15
20
25
30

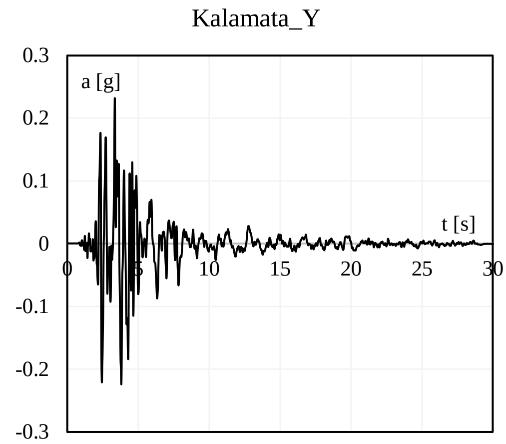
Kalamata_Y
a [g]
t [s]
0.3
0.2
0.1
0
-0.1
-0.2
-0.3
0
5
10
15
20
25
30

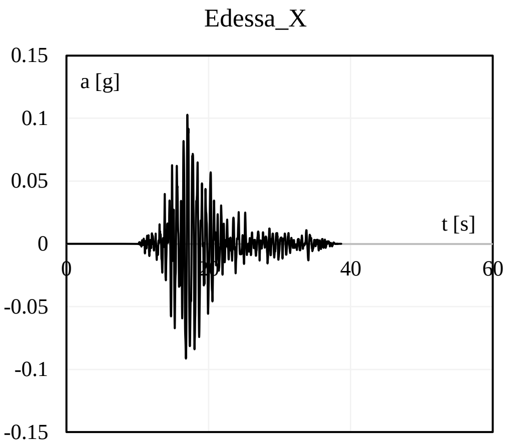
Edessa_X
a [g]
t [s]
0.15
0.1
0.05
0
-0.05
-0.1
-0.15
0
20
40
60

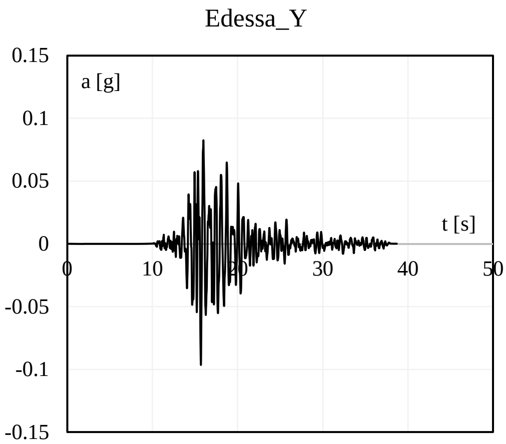
Edessa_Y
a [g]
t [s]
0.15
0.1
0.05
0
-0.05
-0.1
-0.15
0
10
20
30
40
50

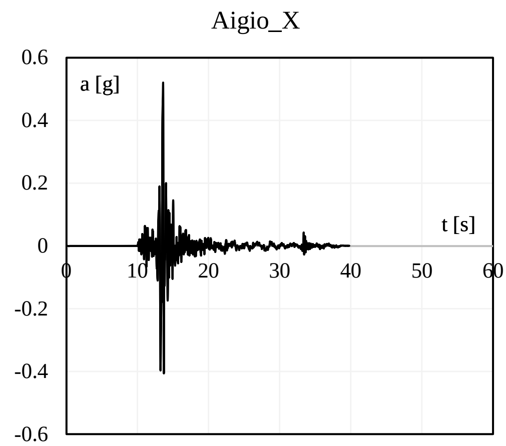
Aigio_X
a [g]
t [s]
0.6
0.4
0.2
0
-0.2
-0.4
-0.6
0
10
20
30
40
50
60

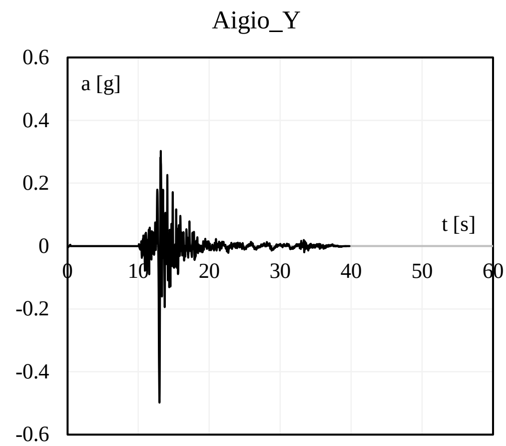
Aigio_Y
a [g]
t [s]
0.6
0.4
0.2
0
-0.2
-0.4
-0.6
0
10
20
30
40
50
60

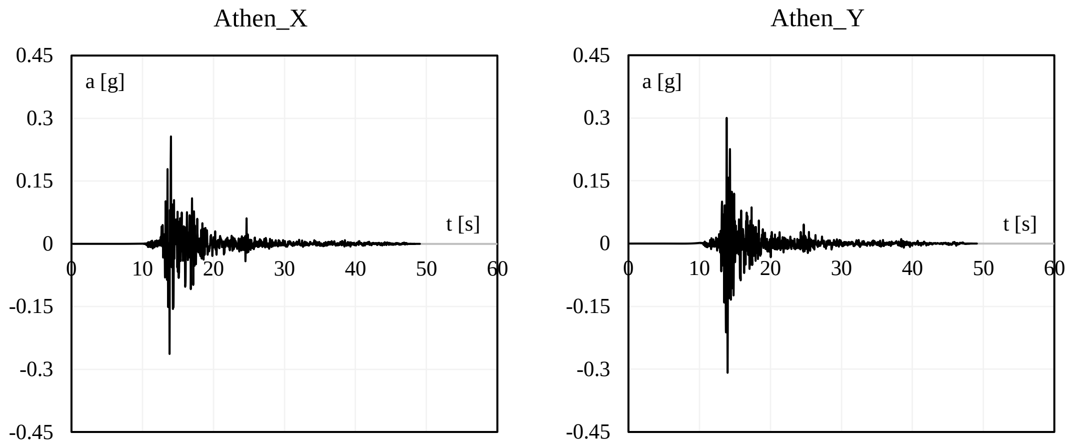

Figure 96. Seismic records in the two orthogonal directions used in the analyses.

5.4.2. Determination of seismic parameters leading to the collapse

To define the maxim ground acceleration, velocity and displacements sustained by the columns for each seismic input without collapsing, a specific parametric analysis was performed by progressively increasing a scale factor applied to the intensities of the seismic records. Indeed, for each seismic input, the minimum value of the scaling factor leading to the collapse of the columns was determined. Table 21 summarizes the outcomes of the analyses in terms of parameters of the seismic input motions leading to the collapse of the columns and the number of collapsed drums beside the capital.

Table 21. Parameters of the seismic input motions leading to the collapse of the columns.

Seismic record	Column	Scaling factor	PHA [g]	PHV [cm/s]	PHD [cm]	Collapsed parts
Irpinia_Str	1	0.50	0.17	36	13.9	Capital and 2 drums
	2	0.65	0.22	47	18.1	Capital and 4 drums
	3	0.45	0.15	33	12.5	6 drums
	4	0.50	0.17	36	13.9	Capital and 6 drums
Irpinia_TdG	1	4.00	0.24	35	28.2	Capital and 4 drums
	2	3.85	0.23	34	27.1	Capital and 3 drums
	3	3.90	0.23	34	27.5	6 drums
	4	3.60	0.22	32	25.4	Capital and 6 drums
L’Aquila	1	1.50	1.16	70	10.2	Capital and 2 drums
	2	0.70	0.54	33	4.8	Capital and 2 drums

	3	1.80	1.39	84	12.2	3 drums
	4	1.70	1.31	79	11.6	Capital and 6 drums
Molise	1	16.80	1.01	41	5.6	Capital and 2 drums
	2	15.35	0.93	37	5.1	Capital and 3 drums
	3	17.80	1.07	43	5.9	5 drums
	4	15.75	0.95	38	5.2	Capital and 4 drums
Kalamata	1	1.10	0.38	42	7.4	Capital and 3 drums
	2	1.05	0.36	40	7.1	Capital and 2 drums
	3	1.00	0.35	39	6.7	5 drums
	4	0.90	0.31	35	6.0	Capital and 5 drums
Edessa	1	3.45	0.38	41	4.2	Capital and 2 drums
	2	2.60	0.29	31	3.1	Capital and 1 drum
	3	3.50	0.39	42	4.2	4 drums
	4	4.30	0.47	51	5.2	Capital and 1 drum
Aigio	1	1.05	0.55	54	9.0	Capital and 2 drums
	2	0.90	0.47	46	7.7	Capital and 2 drums
	3	1.00	0.53	51	8.6	6 drums
	4	0.95	0.50	49	8.2	Capital and 7 drums
Athens	1	3.30	1.24	54	9.5	Capital and 1 drum
	2	2.10	0.79	34	6.0	Capital and 1 drum
	3	2.45	0.92	40	7.0	6 drums
	4	2.50	0.94	41	7.2	Capital and 4 drums

The studied columns showed different dynamic responses for the different input motions. Seismic motions with the higher predominant periods were found to be more dangerous, leading to the collapse with lower values of PHA, and confirming fundamental conclusions found in previous numerical and experimental studies (Psycharis 2018; Psycharis et al. 2003). Indeed, two records of the Irpinia earthquake, characterized by a high value of T_g, led to the collapse with the lowest intensities. Moreover, according to Italian territorial classification (Italian Presidency of the Council of Ministers 2006), the Pompeii site falls in a seismic zone whose acceleration with a probability of exceeding equal to 10% in 50 years ranges between 0.15g and 0.25g. Therefore, considering the maximum vectorial sum, PHA, ranging between 0.21g and 0.35g, the two records of the Irpinia earthquakes for all the columns, Edessa earthquake for column 2, Kalamata earthquake for columns 3 and 4 produced PHA at the collapse falling in this range or below it. Figure 97 plots the value of the PHA that produced the collapse of the columns for each seismic record, represented by the value of its predominant period, and the range of expected PHA derived by Italian seismic classification.

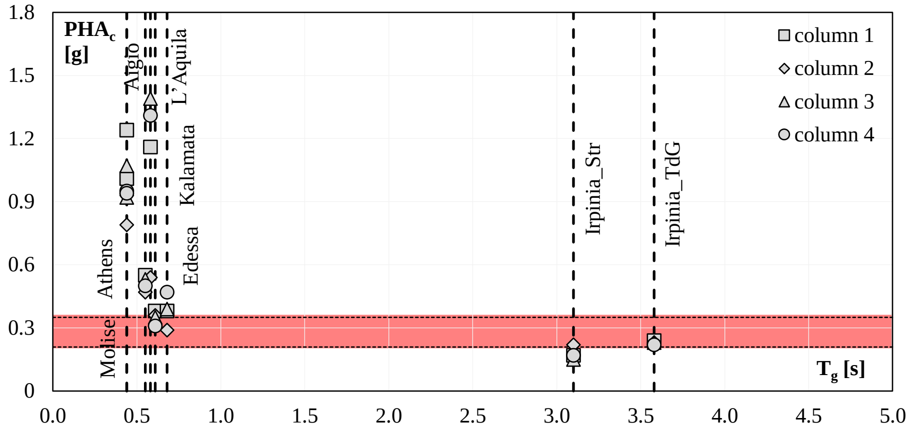

Figure 97. PHA that produced the collapse of the columns for each value of the predominant period corresponding to the different seismic inputs and range of expected PHA derived by Italian seismic classification (red band).

The responses were characterized by different combinations of relative sliding and rocking among the drums. As assessed by previous studies (Psycharis et al. 2003), low-frequency earthquakes led to prevalent rocking, while high-frequency earthquakes led to significant sliding. Indeed, as an example, Figure 98 shows the vectorial sums of displacements and velocities at the capital and base of column 1 under the Iprinia-Sturno and Edessa records.

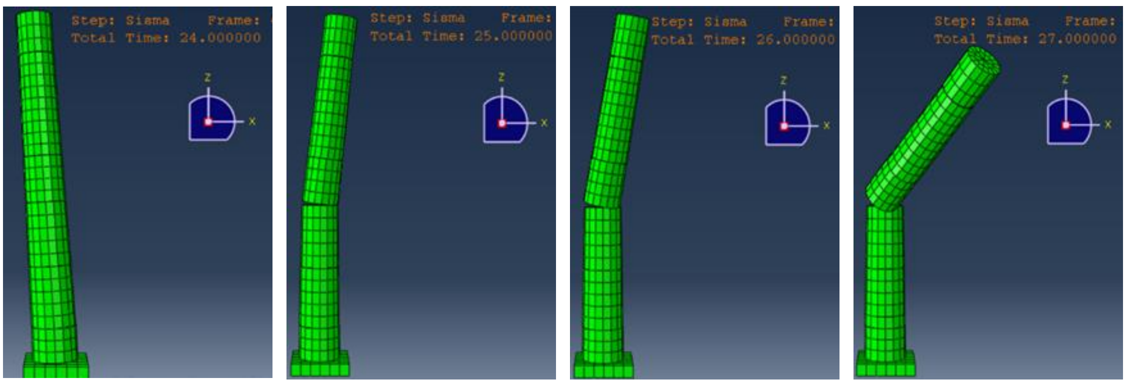

(a)

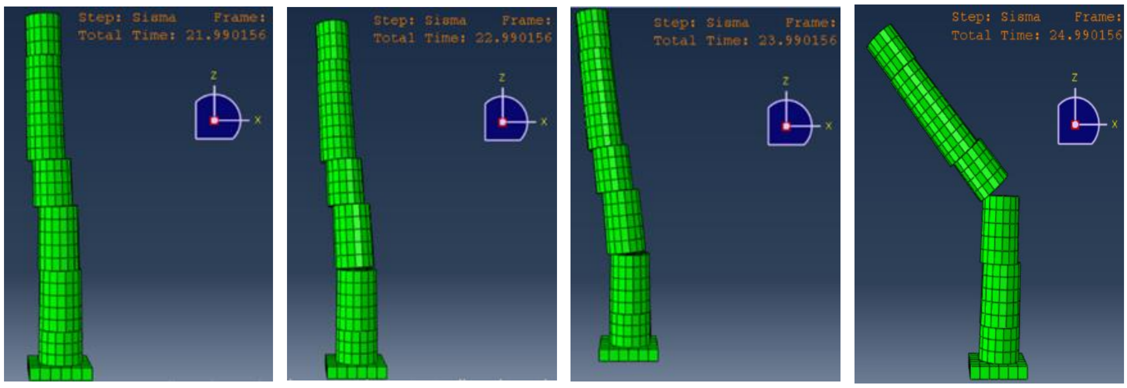

t = 22 s t = 23 s t = 24 s t = 25 s

(b)

Figure 99 shows the failure process of column 1 within the last four seconds until the collapse. Both the records led to the collapse of the capital and two drums of the columns. However, the Irpinia- Sturno record initially induced the rocking of the entire column as a single block, then the failure process involved the rocking of the last two drums and the capital without permanent displacements in the standing part of the column. The second input (i.e. Edessa) induced relative sliding between the drums, other than rocking. Unlike the first case, permanent relative displacements were produced.

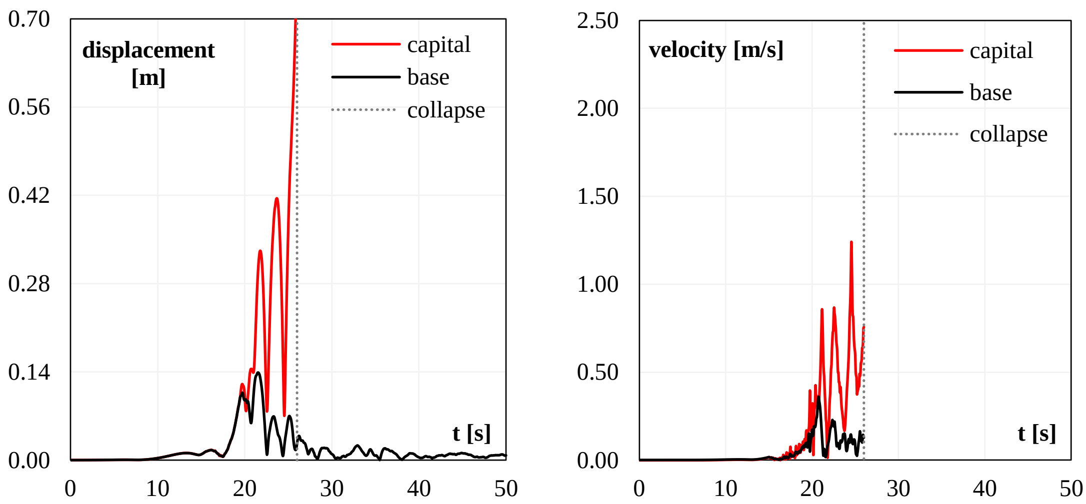

(a)

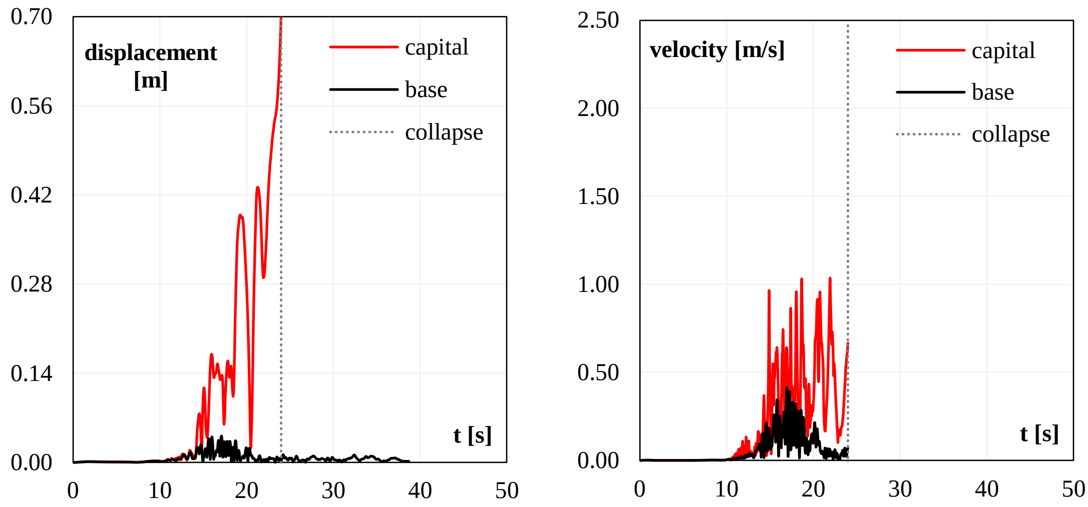

(b)

Figure 98. Vectorial sums of displacements and velocities at the capital and base of column 1 under the Irpinia-Struno (a) and Edessa (b) input motions.

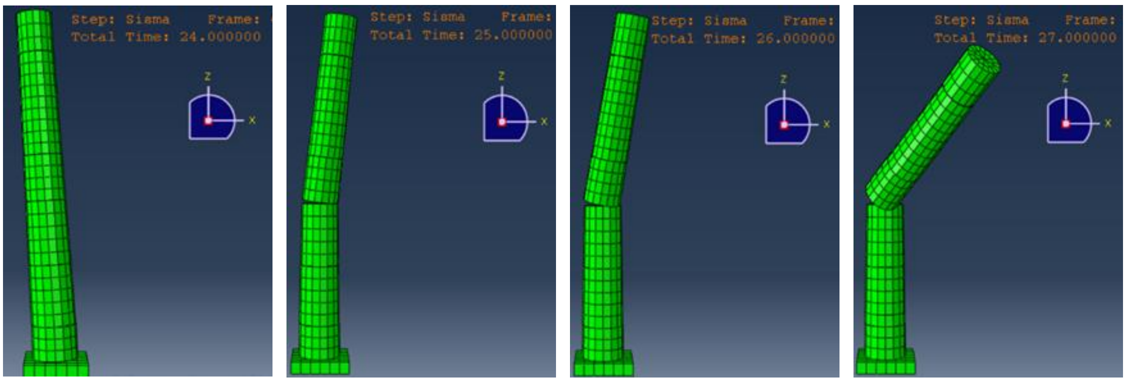

t = 24 s   t = 25 s   t = 26 s   t = 27 s

(a)

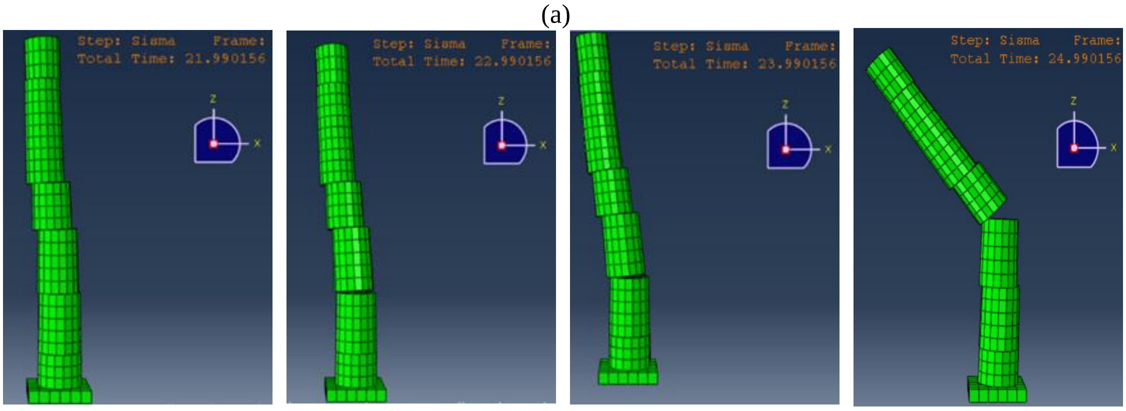

t = 22 s   t = 23 s   t = 24 s   t = 25 s

(b)

Figure 99. Failure process of column 1 under the Irpinia-Struno (a) and Edessa (b) input motions.

Annex 2) reports the diagrams of velocities in two orthogonal directions at the capital and base of the columns under each input motion.

5.4.3. Definition of stability thresholds

A recent study by Papadopoulos et al. derived criteria for the seismic stability of archaeological multidrum stone columns based on main findings by DeJong and Dimitrakopoulos on the rocking response of a single block under harmonic excitation (DeJong and Dimitrakopoulos 2014; Papadopoulos et al. 2019). As abovementioned, this latter found that, for a constant coefficient of restitution, the dynamic behavior of a single rocking block can be solely expressed through the following dimensionless terms (DeJong and Dimitrakopoulos 2014; Psycharis 2018): the ratio between the frequency of the excitation and the frequency parameter of the structure, ω_g/p, the slenderness angle of the block α and the ratio $a_g/(g\tan\alpha)$. This approach defined for a single block is not directly appliable to multidrum columns, because of their spinal construction. However, sound trends were found by Papadopoulos et al. between the frequency/predominant period of the seismic excitations ($\omega_g = 2\pi/T_g$) and intensity measures (PHA, PHV and PHD) required for the collapse of multidrum columns according to numerical predictions, and the aspect ratios and size of the columns (H/d and R, respectively) (Papadopoulos et al. 2019). Following this approach, the values of ω_g and T_g of the ground motions considered in this study were combined with the critical intensity measures obtained from the numerical analyses and the main geometrical properties of the investigated columns. Table 21 and Table 22 summarize the frequency content indicators of the seismic input used in the present analyses and the main geometric and dynamic parameters of the columns, respectively.

Table 22. Frequency content indicator of the seismic input motions used for the analysis: predominant period, T_g, and frequency, ω_g.

Seismic record	T_g [s]	ω_g [rad/s]
Irpinia_Str	3.1	2.0
Irpinia_TdG	3.58	1.8
L'Aquila	0.58	10.8
Molise	0.44	14.3
Kalamata	0.61	10.3
Edessa	0.68	9.2
Aigio	0.55	11.4
Athens	0.44	14.3

Table 23. Main geometric and dynamic parameters of the columns: mass, m, aspect ratio, H/d, size, R, moment of inertia, I_0, and frequency parameter, p.

Column	m [kg]	H/d [-]	R [m]	I_0 [kgm^2]	p [rad/s]
1	2282	7.8	2.6	22062	1.63
2	2043	7.5	2.4	17160	1.67
3	1946	8.1	2.6	17277	1.68
3	1961	9.1	2.8	20666	1.61

In particular, the critical values of PHA derived from the numerical analyses were combined with the frequency parameters, p, and aspect ratio of the columns, H/d, and the frequency of the seismic inputs, ω_g (Figure 100). Moreover, the critical values of PHV were combined with H/d and size, R, of the columns, and the predominant periods of the seismic motions, T_g (Figure 101). Finally, the critical values of PHD were combined with H/d and R (Figure 102). Therefore, the following criteria for an approximate assessment of the seismic stability of archaeological multidrum columns were derived (5.1), (5.2), (5.4):

$$PHA_{crit} \geq 0.15g\frac{d}{H}e^{0.42\frac{\omega_g}{p}} \tag{5.1}$$

$$PHV_{crit} \geq \frac{d}{H}\cdot\left(0.13\frac{R}{T_g}+1.90\right) \tag{5.2}$$

$$PHD_{crit} \geq \frac{d}{H}(0.41\ R\text{-}0.75) \tag{5.3}$$

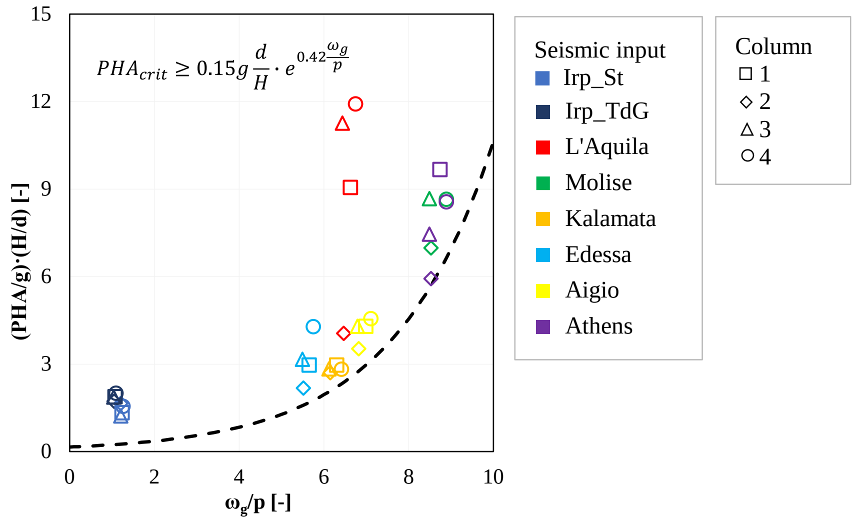

Figure 100. Stability threshold in terms of frequencies of the seismic motions, ω_g, frequency parameters, p, and aspect ratios, H/d, of the investigated columns and critical values of PHA derived from numerical analyses.

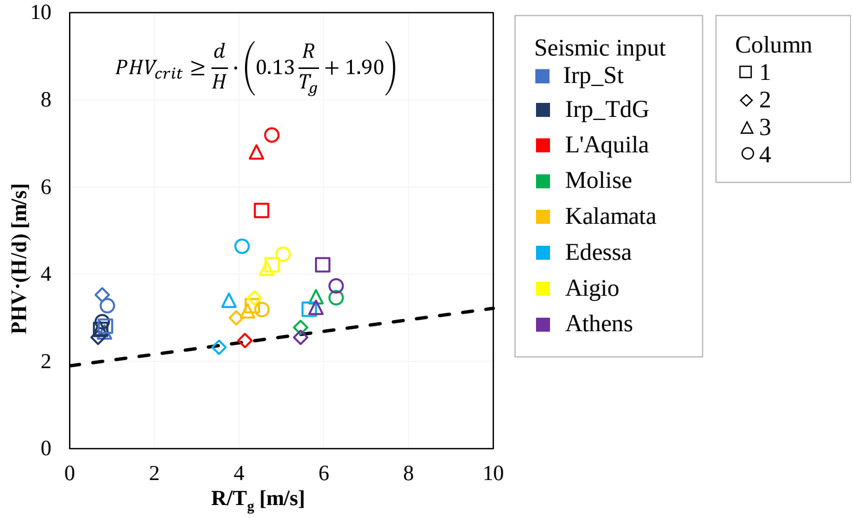

Figure 101. Stability threshold in terms of the predominant period of the seismic motions, T_g, aspect ratios, H/d, and size, R, of the investigated columns and critical values of PHV derived from numerical analyses.

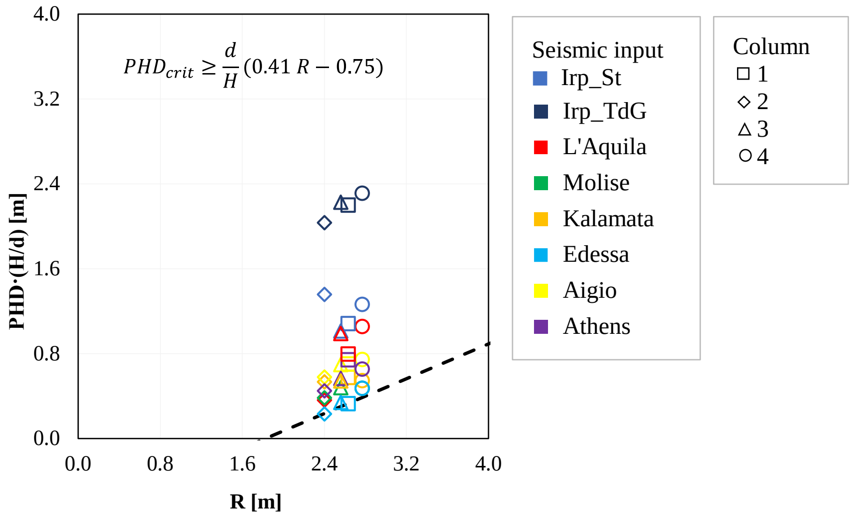

Figure 102. Stability threshold in terms of aspect ratios, H/d, and size, R, of the investigated columns and critical values of PHD derived from numerical analyses.

These criteria could be used for a primary estimation of the stability of multidrum columns towards the seismic risk. These approximate formulations may be used for multidrum columns with geometrical and material properties similar to those of the columns investigated in this study and seismic motions with frequency properties in the range of those herein considered.

It should be noted that such criteria were derived on the assumption that the columns did not have significant damage or forms of degradation affecting their seismic behavior. Papadopoulos et al. suggested the introduction of a reduction factor γ to take into account the presence of minor imperfections, that are not visible to the naked eye, and not computed in the "ideal" numerical model. Based on the comparison between experimental data and numerical analyses, the value γ=0.65 was proposed (Papadopoulos et al. 2019). On the other hand, it should be noted that the proposed criteria were obtained as the lower envelope of the achieved results. Therefore, actual values of seismic intensity measures leading to the collapse of multidrum columns can be rather higher than the ones predicted based on the proposed criteria.

6. DESIGN AND CHARACTERIZATION OF REPAIR MORTARS FOR ARCHAEOLOGICAL STRUCTURES

Restoration interventions of archaeological masonry structures and columns are often based on the use of mortars. As a material for restoration interventions, a mortar should be compatible with the ancient materials, durable and its properties should be well documented (ICOMOS 2003; Ministero della Pubblica Istruzione 1972; Válek et al. 2012). The compatibility with ancient materials of a repair mortar concerns the mechanical properties related to its hardened condition as well as the physical and chemical ones. On the other hand, as a building material mortar should fulfill technical requirements according to its role in the repaired structure (such as adhesion to the substrate, strength, elasticity and weather protection). From a mechanical point of view, a repair mortar should not have too high strength or stiffness compared to the existing materials, since this could cause damage to the old structure due to stress concentration (Lindqvist et al. 2009; Maurenbrecher et al. 2001). The strength and stiffness should be lower than the ones of the existing rock units or bricks and similar or even lower than the ones of the existing mortars (Válek et al. 2012). Indeed, it is normally preferred to repair cracks developed through the mortar joints rather than through the masonry units. Besides, restoration mortars with mechanical properties similar to that of existing ones are easier to be removed and can be replaced without damaging the existing materials (Maurenbrecher et al. 2001). The stiffness of a repair mortar is also crucial regarding the ability of the material to accommodate larger movements without cracking (Maurenbrecher et al. 2001). Nonetheless, a restoration mortar that is too weak would be easily damaged resulting in insufficient durability of the mortar itself and the entire masonry by allowing the ingress of water through cracks (Lindqvist et al. 2009; Válek et al. 2012).

However, the definition of the strength and stiffness of a restoration mortar is not enough itself. Indeed, the compositional and the fresh properties of a mortar (i.e. water content, homogeneity, workability and consistency) strongly affect its hardened properties as well as its durability (Lindqvist et al. 2009). Also, the porosity and the pore size distribution are connected to both the mechanical performance of a mortar and its durability, by affecting the hardening process, final compressive and tensile strength, frost resistance, salt crystallization, capillarity water absorption, hygroscopicity, water vapor permeability and salt crystallization (Lindqvist et al. 2009; Papayianni and Hughes 2019). The definition of a restoration mortar should consider all these aspects and balance the technical requirements with conservation needs (Hughes 2012).

In absence of specific requirements for different or innovative solutions, the use of traditional materials and techniques is generally preferred due to their good compatibility with the substrate material (i.e. free thermal dilation, salt content, stiffness and strength apart from aesthetics and authenticity issues) (Moropoulou et al. 2004b; Papayianni and Hughes 2019; Russlan et al. 2018; Válek et al. 2012). One of the most ancient binders used for the realization of mortars for masonry is lime (Adam 2014; Aggelakopoulou et al. 2019; Giuliani 2007; Lancaster 2005, 2015; Lindqvist et al. 2009; Moropoulou et al. 2005b; Russlan et al. 2018). Aerial lime, i.e. non-hydraulic lime or air lime, is obtained from the calcination at around 900°C of almost pure limestone. Its hardening process takes place through evaporation and carbonation, thus it needs contact with the carbon dioxide in the atmosphere and cannot occur underwater (Lawrence 2006). The carbonation process is gradual and very slow, starting from the outer surface of the joints in the first days after the application until reaching the inner part of the masonry structures from few months up to more than a year depending on the porosity of the mortar and the units, the wall thickness and the environmental conditions, in particular the relative humidity (Maurenbrecher et al. 2001; Oliveira 2015). Since antiquity, the quicklime was slaked and cured in pits for months up to some years and the lime in a form of putty was obtained. As regards the aggregates, since ancient times especially in the Roman period, pozzolanic addictions have been used with the aerial lime for masonry mortars, in the form of natural pozzolanas (volcanic ash or specific kind of earth) or artificial ones (crushed terracotta). Such addictions had the function to react with the lime and the water in the mixture to give it hydraulic properties and to improve the final strength of the mortar (Goldsworthy and Min 2008; Lancaster 2005, 2015; Lindqvist et al. 2009; Moropoulou et al. 2004b; Papayanni et al. 2012; Walker and Pavía 2011). Indeed, the term "pozzolan" comes from the Latin term *pulvis puteolanus* indicating the volcanic ash from the ancient city of *Puteoli* (modern Pozzuoli, close to Naples, Italy). In Roman times volcanic ashes used with this purpose but coming from different places had different denominations (i.e. the *harena fossicia* found around Rome and the Santorini earth). The term “pozzolan” is used in a very general way today, referring to an additive of different nature (i.e. volcanic ashes mixed with lapilli and scoria, crushed clay, or some organic ashes) containing soluble silica able to react with the calcium hydroxide present in the mixture (Lancaster 2015; Walker and Pavía 2011). The addition of pozzolans modifies the hardening process of air lime-based mortars, by introducing the formation of hydration products (calcium silicate hydrates and calcium silicate aluminate hydrates) similar to hydraulic lime or cementitious mortars, but still with a slower process compared to cement pastes (Walker and Pavía 2011).

The production of specifically devised repair mortars by mixing single raw materials *in situ* is advisable in many cases for i) the use of materials available *in situ* or from the surrounding area; ii) the use of specific composition and mixing procedures according to traditional techniques; iii) the achievement of specific mechanical, physical and aesthetical properties. Such mortars should be defined based on an accurate knowledge of the raw materials and the craftsmanship composing the ancient ones. However, the exact definition of the original components often presents economic and technical constraints and when they are known it is often impossible to find the same materials. Several experimental studies on the production of repair mortars based on the known composition of the ancient ones are available in the literature. Some studies focused on aerial lime mortars (i.e. putty lime or hydrated lime) with siliceous or calcareous sand (Aggelakopoulou et al. 2019; Balksten and Steenari 2008; Baronio et al. 1999; Lawrence 2006; Oliveira 2015), while others used natural or artificial pozzolanic additions or hydraulic lime (Goldsworthy and Min 2008; Moropoulou et al. 2004b, 2005b; Ozlem Cizer 2019; Russlan et al. 2018).

At the Pompeii site, the definition of a unique standard repair mortar for structural interventions supported by an experimental study of the physical and mechanical properties is still lacking. Similarly, guidelines to produce repair mortars *in situ*, the laying and the curing of repaired elements in the first days, are still not uniquely defined. As regards the original properties of the mortars, different petrographic, mineralogical and chemical experimental studies were performed on Roman mortars at the Pompeii site and the Vesuvius and bay of Naples areas (i.e. Campania region), while the mechanical properties of such materials nowadays are still poorly studied. It was found that traditional mortar-based materials at the site (bending mortars, plasters and floor mortars) were mainly composed of aerial lime as a binder (i.e. putty lime) and local volcanic aggregates, sometimes with crushed ceramics, limestone sand, or marble powder (Izzo et al. 2016; Leone et al. 2016; De Luca et al. 2015; Miriello et al. 2010, 2018b; Piovesan et al. 2009; La Russa et al. 2015). A study related to the evolution of the compressive strength of mortars made with aerial lime powder, pozzolana from Bacoli (within the Bay of Naples) and water, with the binder/aggregate ratio varying from 1:1 to 1:4 was carried out by (Goldsworthy and Min 2008). However, experimental studies focusing on repair mortars made with putty lime and natural pozzolan from the Naples area, including the investigation of different physical and mechanical properties along the time, are still lacking.

This chapter focuses on the design and characterization of a repair mortar for archaeological structures, with a detailed investigation of the evolution with the time of its mechanical and physical properties and the hardening process. The significance of this experimental programme is related to the distinctiveness of the produced mixture and its similarity with the archaeological mortars, especially regarding the aggregate. Indeed, the natural pozzolan used in the experiments is a precious material whose sourcing and usage is nowadays highly controlled and limited.

6.1.Experimental programme

A repair mortar compatible with the archaeological structures was defined in this study. To this end, the mixture was defined by using: i) raw materials as similar as possible to the ancient ones, ii) a mix design consistent with ancient traditional ones and iii) a mortar consistency suitable for workability. Then, a comprehensive investigation of the mechanical and physical properties was performed to evaluate the suitability of the mortar as a material for repair in masonry structures. The evolution of the flexural and compressive strength, elastic modulus, bulk density, open porosity and ultrasonic pulse velocity were monitored for up to 200 days, according to standard procedures. Moreover, the rate of the hardening process and the evolution of the carbonation front were specifically studied through the Differential Thermal Analysis, DTA. In particular, the tests were performed at different ages up to 90 days and involved samples at different depths from the external surface of cylindrical specimens.

The following sections describe in detail the adopted methodology, raw materials and mix design, test procedures and the obtained outcomes. Finally, a comparative analysis of the obtained results and a comparison with available properties of other types of repair mortars from literature is presented.

6.1.1. Overall methodology

The experimental programme involved 13 batches of mortar, 62 prismatic or cylindrical specimens and different types of destructive and non-destructive tests carried out at different ages from 3 days up to 200 days. A total number of 201 tests were carried out. Figure 103 shows prismatic (40 mm x 40 mm x 160 mm, named “P”) and cylindrical (60 mm x 120 mm, named “Cyl_A” and 60 mm x 60 mm, named “Cyl_B”) specimens used in this work, while Table 24 reports the full experimental programme outline.

P-type 40 mm x 40 mm x 160 mm | Cyl_A-type 60 mm x 120 mm | Cyl_B-type 60 mm x 60 mm

(a) (b) (c)

Figure 103. Types of specimens: prismatic 40 mm x 40 mm x 160 mm, P (a); cylindric 60 mm x 120 mm, CylA (b); cylindric 60 mm x 60 mm, CylB (c).

Table 24. Experimental programme outline.

Test	Outcomes	Type of specimen	Curing condition	Age [days]	Total number of tests
FT	Flow diameter [mm]	FM	-	-	2
BD	Bulk density, ρ [kg/m^3]	P	A	5, 6, 7, 28, 60, 90, 200	57
UPV	Ultrasonic pulse velocity, V [m/s]	P	A	5, 6, 7, 28, 60, 90, 200	57
FC	Flexural and compressive strength, f_f and f_c [MPa]	P	A	7, 28, 60, 90, 200	21
OP	Open porosity [%]	P	A	7, 28, 60, 90, 200	15
C	Compressive strength, f^*_c [Mpa]	Cyl_A	A	7, 28, 60, 90, 200	15
CC	Elastic modulus, E [Mpa]	Cyl_A	A	7, 28, 60, 90	12
DTA	Evaluation of phase transitions	FM and Cyl_B	B	3, 7, 28, 60, 90	22
Total number of tests					201

A = 20±1°C-95±5%RH up to 5 days, 20±1°C-60±5%RH up to testing (CEN 2007a)

B = 20±1°C-95±5%RH up to 2 days, 20±1°C-60±5%RH up to testing

An explanatory nomenclature *B.Ty.C.Te.x.N* was assigned to each test, where:

- B is the number of the batch of provenance (from 1 to 13);
- Ty is the specimen type (fresh mortar, prismatic or cylindrical: FM, P, Cyl_A or Cyl_B);
- C is the curing condition (A or B as a function of humidity and temperature, being A standard conditions and B controlled carbonation conditions, further detailed below);
- Te is the performed test (Flow test, FT, Bulk Density measurement, BD, Ultrasonic Pulse Velocity test, UPV, Flexural and Compression test, FC, Open Porosity test, OP, Compression test, C, Cyclic Compression test, CC, and Differential Thermal analysis, DTA);
- x is the age of testing (3, 5, 6, 7, 28, 60, 90 or 200 days);
- N is the progressive number of the specimen (1, 2, 3) or sample derived from the specimens for DTA (1, 2, 3, 4).

A detailed specification of the performed tests with their relative nomenclature is reported in Table 25.

Table 25. Experimental programme matrix for the characterization of lime putty and pozzolan-based repair mortar.

Batch	Type	Curing	Test	Age [days]	n. of tests	Nomenclature of the test
1	FM	-	FT	-	1	1.FM.FT.1
2	FM	-	FT	-	1	1.FM.FT.2
3	P	A	BD	5	3	3.P.A.BD.5.1/2/3
			BD	6	3	3.P.A.BD.6.1/2/3
			BD	7	3	3.P.A.BD.7.1/2/3
			UPV	5	3	3.P.A.UPV.5.1/2/3
			UPV	6	3	3.P.A.UPV.6.1/2/3
			UPV	7	3	3.P.A.UPV.7.1/2/3
			FC	7	3	3.P.A.FC.7.1/2/3
	P-MC*	A	BD	5	3	3.P-MC.A.BD.5.1/2/3
			BD	6	3	3.P-MC.A.BD.6.1/2/3
			BD	7	3	3.P-MC.A.BD.7.1/2/3
			UPV	5	3	3.P-MC.A.UPV.5.1/2/3
			UPV	6	3	3.P-MC.A.UPV.6.1/2/3
			UPV	7	3	3.P-MC.A.UPV.7.1/2/3
			FC	7	3	3.P-MC.A.FC.7.1/2/3
4	FM	-	DTA	within 2h from t_0	4	4.FM.DTA.1
	P	A	BD	5	3	4.P.A.BD.5.1/2/3
			BD	6	3	4.P.A.BD.6.1/2/3
			BD	7	3	4.P.A.BD.7.1/2/3
			UPV	5	3	4.P.A.UPV.5.1/2/3
			UPV	6	3	4.P.A.UPV.6.1/2/3
			UPV	7	3	4.P.A.UPV.7.1/2/3
			FC	7	3	4.P.A.FC.7.1/2/3
	P	A	OP	7	3	4.P.A.OP.7.1/2/3
5	FM	-	DTA	within 2h from t_0	4	5.FM.DTA.2
	P	A	BD	28	3	5.P.A.BD.28.1/2/3
			UPV	28	3	5.P.A.UPV.28.1/2/3
			FC	28	3	5.P.A.FC.28.1/2/3
	P	A	OP	28	3	5.P.A.OP.28.1/2/3
6	P	A	BD	60	3	6.P.A.BD. 60.1/2/3
			UPV	60	3	6.P.A.UPV. 60.1/2/3
			FC	60	3	6.P.A.FC. 60.1/2/3
	P	A	OP	60	3	6.P.A.OP. 60.1/2/3
7	P	A	BD	90	3	7.P.A.BD.90.1/2/3
			UPV	90	3	7.P.A.UPV.90.1/2/3
			FC	90	3	7.P.A.FC.90.1/2/3
	P	A	OP	90	3	7.P.A.OP.90.1/2/3
8	P	A	BD	5	3	8.P.A.BD.5.1/2/3
			BD	6	3	8.P.A.BD.6.1/2/3
			BD	7	3	8.P.A.BD.7.1/2/3
			BD	28	3	8.P.A.BD.28.1/2/3
			BD	60	3	8.P.A.BD.60.1/2/3
			BD	90	3	8.P.A.BD.90.1/2/3
			BD	200	3	8.P.A.BD.200.1/2/3
			UPV	5	3	8.P.A.UPV.5.1/2/3

			UPV	6	3	8.P.A.UPV.6.1/2/3
			UPV	7	3	8.P.A.UPV.7.1/2/3
			UPV	28	3	8.P.A.UPV.28.1/2/3
			UPV	60	3	8.P.A.UPV.60.1/2/3
			UPV	90	3	8.P.A.UPV.90.1/2/3
			UPV	200	3	8.P.A.UPV.200.1/2/3
			FC	200	3	8.P.A.FC.200.1/2/3
	P	A	OP	200	3	8.P.A.OP.200.1/2/3
9	Cyl$_A$	A	C	7	3	9.CylA.A.C.7.1/2/3
	Cyl$_A$	A	CC	7	3	9.CylA.A.CC.7.1/2/3
10	Cyl$_A$	A	C	28	3	10.CylA.A.C.28.1/2/3
	Cyl$_A$	A	CC	28	3	10.CylA.A.CC.28.1/2/3
			CC	60	3	10.CylA.A.CC.60.1/2/3
			CC	90	3	10.CylA.A.CC.90.1/2/3
11	Cyl$_A$	A	C	60	3	11.CylA.A.C.60.1/2/3
12	Cyl$_A$	A	C	90	3	12.CylA.A.C.90.1/2/3
	Cyl$_A$	A	C	200	3	12.CylA.A.C.200.1/2/3
13	Cyl$_B$	B	DTA	3	4	13.CylB.B.DTA.3.1/2/3/4
	Cyl$_B$	B	DTA	7	4	13.CylB.B.DTA.7.1/2/3/4
	Cyl$_B$	B	DTA	28	4	13.CylB.B.DTA.28.1/2/3/4
	Cyl$_B$	B	DTA	60	4	13.CylB.B.DTA.60.1/2/3/4
	Cyl$_B$	B	DTA	90	4	13.CylB.B.DTA.90.1/2/3/4

*MC indicates that the specimens were mechanically compacted.

Prismatic specimens 40 mm x 40 mm x 160 mm according to the standard EN 1015-11 (CEN 2007a) (Figure 103 (a)), were used for the measurement of the bulk density and the ultrasonic pulse velocity tests at 5, 6, 7, 28, 60, 90 and 200 days, flexural and compression strength tests and open porosity tests at 7, 28, 60, 90 and 200 days. Cylindric specimens 60 mm x 120 mm, Cyl$_A$-type (Figure 103 (b)), were used for compressive strength tests at 7, 28, 60, 90 and 200 days and cyclic compression tests for the evaluation of the elastic modulus at 7, 28, 60 and 90 days; finally, five single cylindric specimens 60 mm x 120 mm, Cyl$_B$-type (Figure 103 (c)), were prepared for the collection of samples to monitor the evolution of carbonation through DTA at 3, 7, 28, 60 and 90 days.

The measurement of the bulk density, ultrasonic test, flexural and compression test, open porosity test, compression and cyclic compression tests for the evaluation of the elastic modulus involved the execution of three tests for each age. The same specimens were used for the measurement of ρ and V at 5, 6 and 7 days and then they were used for flexural and compression tests at 7 days. For each of the following ages (i.e. 28, 60, 90 and 200 days), the same specimens were used for the measurement of ρ and V and finally for the flexural and compression tests. Moreover, the same three specimens were used for the cyclic compression tests at 28, 60 and 90 days.

DTA involved the execution of four tests for each age, according to a specific order for the collection of the samples and testing, to ensure repeatability and effectiveness of the procedure. Moreover, before the execution of DTA on hardened mortar, the test was performed on single raw materials and fresh mortar. To do that, two samples of fresh mortar were collected from two batches of the mortar used for the preparation of the test specimens and tested within 2h from t_0 (Table 25).

6.1.2. Raw materials

The raw materials used in the present work were selected according to compatibility requirement with archaeological materials, following literature information on the production of mortars in Roman times and specific experimental studies on the composition of mortars at the Pompeii site. As regards the binder, it was found that ancient Roman builders used almost pure limestone for the production of the quicklime, then slaked it and cured the slaked lime in the form of putty in specific pits *in situ* (Bonazzi et al. 2007; Goldsworthy and Min 2008; Lancaster 2005). Since the production process of the putty lime was not feasible for economic, logistic, time and safety constraints, commercially available putty lime was used as a binder, i.e. CL90 type, since it ensured the least amount of impurity possible compared to the other commercially available types. In detail, the selected putty was characterized by the following performances certified according to the specification of the standard EN 459-1 (CEN 2015): 98% of the granulometry lower than 0.1mm, CaO + MgO≥ 90%, MgO≤ 5%. CO2 ≤ 4% and SO3≤ 2 %. Considering the difficulty of measuring the exact amount of surplus water contained in each bag of putty lime, all the material contained in every single bag was homogenized by mixing before use. Thus, the bulk density of the putty lime was measured according to the standard for fresh mortar (CEN 2007b) and resulted in 1.23 g/cm^3. As concerns the aggregate, a local volcanoclastic material with variable size from ash to lapillus, collected from the Phlegrean area and called “pozzolan sand” in the following, was used in the mixture. This is a volcanic region next to the Bay of Naples where the ancient Roman builders obtained their pozzolan (traditionally known as *pulvis puteolanus*). The pozzolan sand had a bulk density of 1.49 g/cm^3, measured according to the standard EN 1097-3 (CEN 1999b). Its particle size distribution, showed in Figure 104, was evaluated according to the standard EN 933-1 (CEN 2012b) (Figure 105).

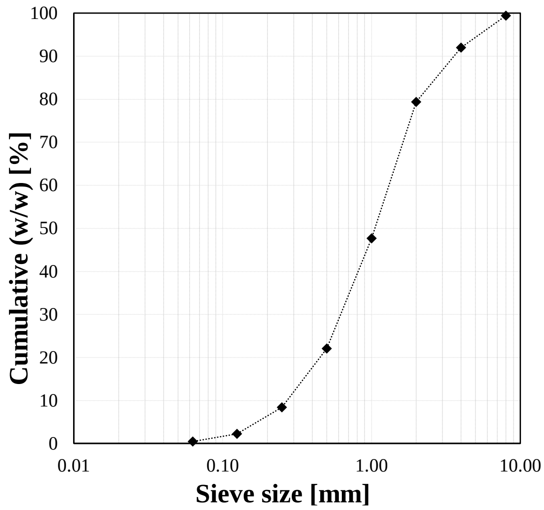

Figure 104. Particle size distribution of the pozzolan sand (0.063-8.0 mm).

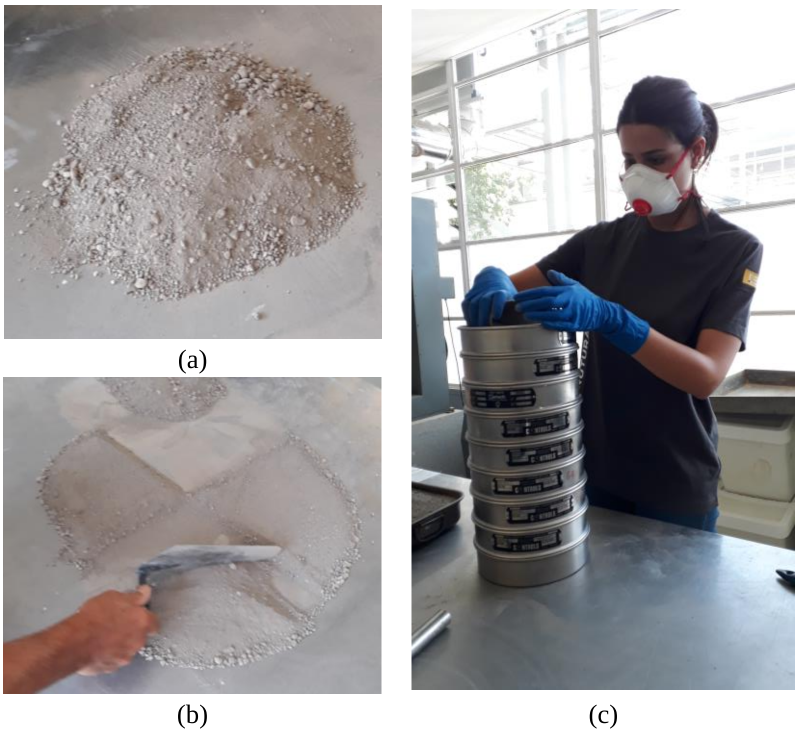

Figure 105. Determination of the particle size distribution of the pozzolan sand by sieving method: pozzolan sand after drying (a); preparation of the sample of sand (b); sieves (c).

DTA on the raw materials was performed according to the same protocol defined for hardened mortar: a single increasing ramp, from 20°C to 1100°C, with a rate of

10°C/min (Garijo et al. 2019; Moropoulou et al. 2004a, 2005b; Oliveira 2015; Scrivener et al. 2018). The heating rate, 10 °C/min value was selected to optimize the duration of every single test as well as the accuracy of the results, according to a common value accepted in the literature (Garijo et al. 2019; Lawrence 2006; Moropoulou et al. 2004a, 2005b; Oliveira 2015; Scrivener et al. 2018). For fresh mortar, two samples were collected directly from the mixing bowl at the end of the mixing processes of batch 4 and batch 5 respectively (as reported in Table 25), using a metallic tip. The samples were immediately wrapped in a plastic film and stored in a controlled environment at 20±1°C and 95±5% relative humidity. Thus, they were tested within two hours from t_0. Figure 106 shows DTA thermograms of lime putty, pozzolan sand and two samples of fresh mortar. The tests confirmed the purity of the lime putty, with two main heat flow peaks related to the presence of free water and calcium hydroxide. The pozzolan sand was tested without any previous oven-drying. After a slight heat flow peak corresponding to the presence of free water, the sand did not show any significant weight loss in the present range of study. The thermograms of the two samples of fresh mortar were consistent with those for the raw materials, showing two main heat flow peaks related to the presence of free water and calcium hydroxide, respectively.

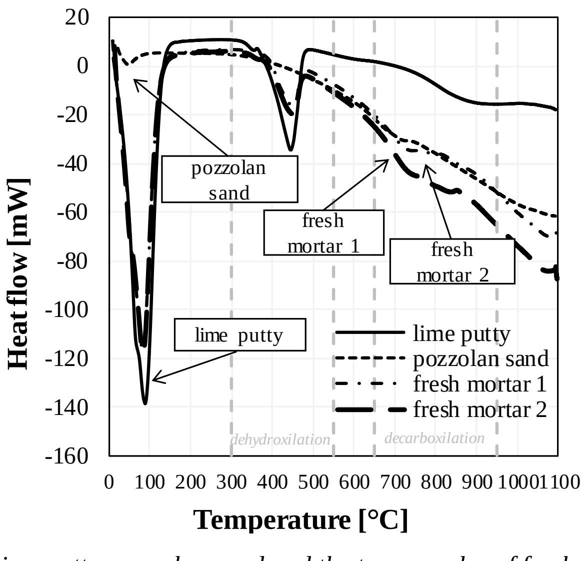

Figure 106. DTA curves of lime putty, pozzolan sand and the two samples of fresh mortar tested within two hours from the start of the mixing protocol.

6.1.3. Mortar composition and mixing procedure

As regards the composition of the mortar, Vitruvius in *De Architectura* recommended mixing one part of lime with three parts of quarry sand or one part of lime with two parts of river/sea sand and one part of crushed terracotta for buildings on land (*Liber II, 5*) and one part of lime with two parts of pozzolana from the bay of Naples for underwater construction (*Liber V, 12*). In *Naturalis Historia* (*Liber XXXVI, 175*) Pliny the Elder recommended mixing one part of lime with four parts of quarry sand or one part of lime with three parts of river/sea sand, preferably with the extra addition of the third part of crushed terracotta (Table 26). Both references confirm that ancient builders were aware of the difference between the aggregates, in particular the effectiveness of using crushed terracotta or natural pozzolana. As regards Vitruvius' recommendation, the reason for a lower amount of pozzolana with the respect to quarry sand was probably related to its higher cost (Goldsworthy and Min 2008; Lancaster 2005).

Table 26. Ancient recommendation for mortar composition

	Vitruvius ***De Architectura*** ***(Liber II, 5*** **and** ***Liber V, 12)*** **15 A.C.**	**Pliny the Elder** ***Naturalis Historia*** **(*Liber XXXVI, 175*)** **77-78 A.C.**
Lime: quarry sand	1:3	1:4
Lime: river/sea sand	1:2	1:3
Lime: river/sea sand: crushed terracotta	1:2:1	1:3:1
Lime: pozzolana from the bay of Naples	1:2	-

Compositional analyses on archaeological mortars from Pompeii found different values of the binder to aggregate ratio, related to different origins of the collected sample, buildings of provenance and age of construction (Bonazzi et al. 2007; Miriello et al. 2010, 2018b). Indeed, ancient builders probably defined the appropriate proportions of a mixture extemporaneously, rather than accurately measuring the relative amounts of binder and aggregate (Bonazzi et al. 2007). In this research, the recommendation provided by Vitruvius in *De Architectura* (*Liber II, 5* and *Liber V, 12*, 15 A.C.) and by Pliny the Elder in *Naturalis Historia* (*Liber XXXVI, 175*, 77-78 A.C.) were taken into account for the definition of the binder to aggregate ratio of 1:3, by volume. This was consistent with proportions found for masonry mortars by Bonazzi et al.

The amount of water was defined after various attempts to obtain a workable mortar, but as stiff as possible. This was consistent with the traditional techniques as indicated in (Goldsworthy and Min 2008; Negri 2007). For each trial a certain amount of water was added to the mixture, then the consistency was defined according to the standard EN 1015-3:1999 (CEN 2004). Finally, the proportion of binder:aggregate:water was defined as 1:3:0.5, by volume, corresponding to a plastic consistency, i.e. a flow diameter of 165 ± 10 mm (Figure 107). Once the desired consistency was achieved, repeatability was checked by repeating the flow test on a different batch of mortar. Then, to simplify the mixing process the composition by volume was converted into weight, based on the density of the raw materials (1000.0: 275.8: 111.7 g).

Figure 107. Fresh mortar after a flow test.

The mortar was prepared by mechanical mixing in a stainless steel bowl, 5l of capacity, with a protocol defined according to (CEN 2010). In particular, the lime was placed at first in the mixer and the mixing procedure was started simultaneously to the addition of the water, at low speed. Time t_0 was defined as the instant at which water came into contact with the binder, which was lime in this case. The pozzolana sand was poured after 30s, in a time interval of 30s, after which mixing continued at high speed for further 30s. Then the mixing was stopped for 90s, of which in the first 30s the mortar adhering to the surfaces of the bowl was removed and placed in the middle, finally mixing was continued for further 60s at high speed, for a total of 210 s. It should be noted that repair mortars are frequently prepared *in situ* using not standardized methods, which can involve hand mixing by using a bucket and trowel or mechanical by using an electric mortar mixer. However, standardized methods and tools were selected for this work to enhance the repeatability of the results.

6.1.4. Preparation of the specimens and curing conditions

All the specimens were hand compacted being the molds filled in two almost equal layers each one compacted by twenty-five strokes of a tamper, as indicated in the standard EN 1915-11 (CEN 2007a) for aerial lime mortars. Hand compaction was consistent with the hand laying of the repair mortar *in situ*, which does not involve vibration. Moreover, such a compaction method was selected in other experimental studies on lime mortars (Garijo et al. 2019; Goldsworthy and Min 2008; Oliveira 2015). Indeed, the method was applied also for the cylindrical specimens since hand compaction was consistent with the hand laying method of the repair mortar *in situ*, which does not involve vibration.

The P-type specimens and the Cyl_A-type ones were stored in a controlled environment at 20±1°C and 95±5% relative humidity up to five days, then they were demolded and cured unsealed for the remaining days up to testing in a controlled environment at 20±1° and 60±5% relative humidity, following the indications of the standard EN 1015-11 (CEN 2007a). This curing method is referred to in the following as "A". For the Cyl_B-type specimens a specific preparation and curing method was adopted, to allow the carbonation process to start as soon as possible and control its progression. Between the cylindrical molds and the mortar, a plastic net was interposed to sustain the mortar and allow to remove the external tube on the first day after casting. Then the specimens were completely sealed with plastic tape at the top and the bottom surfaces and stored at 20±1°C and 95±5%. Since the specimens were too fresh to remove from the cylindrical mold the first day after casting, they were demolded after two days. Thus, to lead the carbonation process to develop only through the lateral surfaces, at the same time of demolding the top and the bottom of the cylinders were completely sealed by putting paraffin layers on them. Then the specimens were cured in a controlled environment at

20±1°C and 60±5% relative humidity. This second curing method is referred to in the following as “B”.

6.1.5. Testing procedures of physical and mechanical properties of the hardened mortar

At each age, the bulk density, ρ, was evaluated for three P-type specimens at first, by calculating the mean of the ratios between the weight of specimen and its volume. After that, ultrasonic tests were performed on the same specimens by positioning the probes in the middle of the specimen along the transversal direction, thus the path length for the calculation of the ultrasonic velocity, V, was equal to 40 mm (Figure 108). Standard ultrasound equipment was used, with probes 25 mm in diameter and an operating frequency of 150 kHz. As abovementioned, The measurement of the bulk density and the ultrasonic test were also performed at each age on the reference specimens.

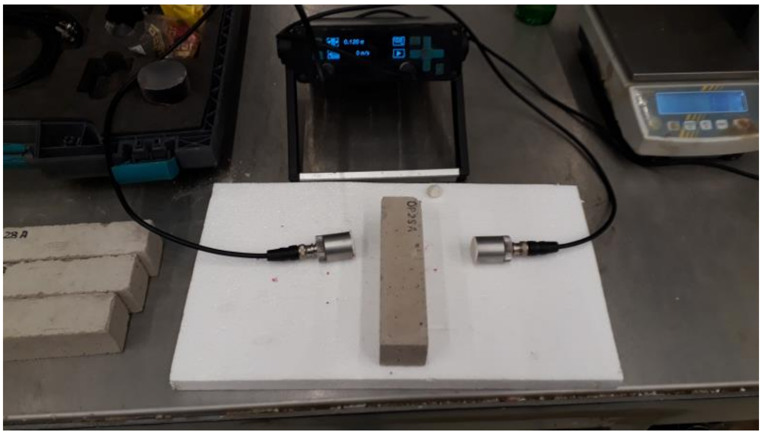

Figure 108. Ultrasonic pulse velocity test equipment.

After that, the evaluation of the flexural and compressive strength was performed according to the standard EN 1015-11 (CEN 2007a). The flexural strength, f_f, was evaluated from three-point bending tests performed in displacement control with a rate of 0.003 mm/s at 7 days and 0.006 mm/s at 28, 60, 90 and 200 days (Figure 109 (a) and (b)), according to Eq. (6.1), where F is the maximum load applied to the specimen, b is the specimen width and d is the specimen length, i.e. the distance between the supports.

$$f_f = 1.5\,\frac{Fl}{bd^2} \tag{6.1}$$

The compressive strength, f_c, was evaluated on the two resulting halves of each prismatic specimen from the flexural test using displacement control with a rate of 0.012 mm/s for all ages (Figure 109 (c) and (d)). It was evaluated as the ratio between the maximum applied load and the nominal area of the specimen. Thus, the compressive strength was evaluated at each age as the mean value obtained from six specimens.

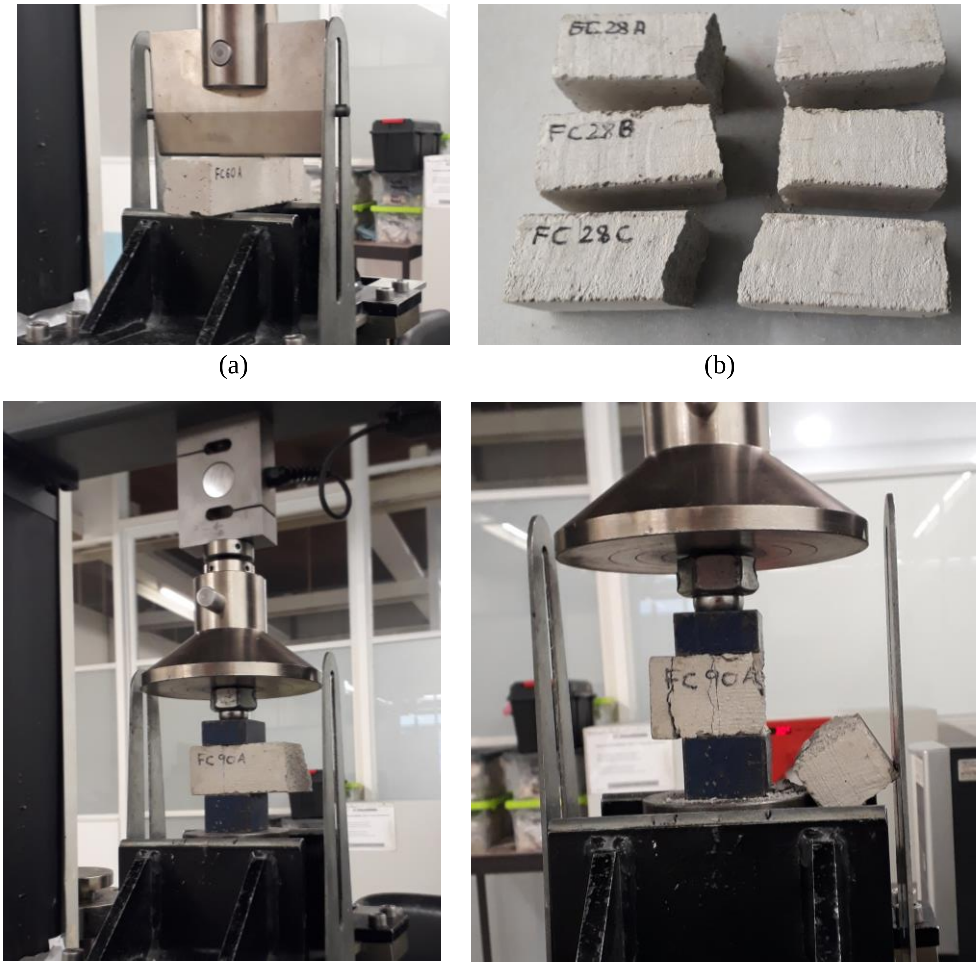

(a) (b) (c) (d)

Figure 109. Set-up for the flexural test (a); two resulting halves of prismatic specimens from the flexural test (b); set-up for compression test (c); specimen after the compression test (d).

For the evaluation of the open porosity, at each age other three P-type specimens were dried, then they were subjected to water saturation in a vacuum pump (Figure 110). The open porosity was evaluated as the mean of the values obtained, calculated, according to Eq. (6.2), where M_1 is the dried weight, M_2 is the immersed weight and M_3 is the saturated weight. This method was applied by adapting the recommendations RILEM TC 25-PEM for stone (RILEM TC 25-PEM 1980), with the time of immersion and vacuum modified to 3h.

$$open\ porosity = \frac{M_3\text{-}M_1}{M_3\text{-}M_2} \times 100 \tag{6.2}$$

Figure 110. Equipment for the evaluation of the open porosity.

The static elastic modulus, E, was evaluated by adapting the method presented in the standard EN 12390-13 (CEN 2013) for concrete. At each age, at first, a simple compression test, C, was performed on three Cyl_A-type specimens (by using displacement control at a rate of 0.012 mm/s), for the evaluation of the mean maximum load and compressive strength. Then other three Cyl_A-type specimens were tested with five loading/unloading cycles up to one-third of the mean maximum load, in force-control with the rate defined so that the ramps lasted about 60s. The elastic modulus of each specimen was evaluated from the measurements of three Linear Variable Differential Transducers (LVDTs), placed at the middle of the height of the specimens, on a base of one-third on the height, being supported by two steel rings and spaced of 120°. Before the execution of compression and cyclic compression tests, each specimen was rectified employing thin layers of epoxy resin applied on the top and the bottom surfaces. Figure

111 shows pictures of CylA-type specimens after demoulding and after the application of layers of epoxy resin on the top and the bottom surfaces, and the set-ups for simple compression test and cyclic compression test.

(a)

(b)

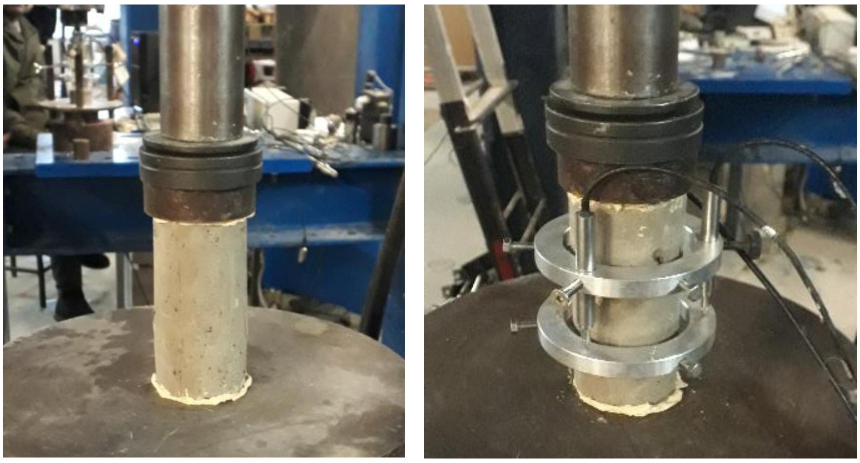

(c) (d)

Figure 111. Cyl_A-type specimens after demoulding (a); specimens with thin layers of epoxy resin applied on the top and the bottom surfaces (b); set-up for simple compression test (c); set-up for cyclic compression test (d).

6.1.6. Assessment of repeatability

Additional tests were performed for the assessment of the repeatability of the results as concerns the mechanical and physical properties. In particular, six extra P-type specimens were prepared from the same batch of mortar (i.e. batch 3 as reported in Table 25) and used to assess the repeatability of results with hand compaction compared to mechanical compaction. For that, three specimens were compacted by hand according to the method indicated above and three specimens were compacted by using a jolting apparatus according to the method indicated in the standards EN 459-2 and EN 196-1 (CEN 2005c, 2010) (i.e. filling the mold in two layers each one compacted for 60s). Therefore, the mean bulk density and ultrasonic pulse velocity at 5, 6 and 7 days and the mean flexural and compressive strength obtained at 7 days of the hand compacted specimens were compared with the ones of the mechanically compacted specimens. Additionally, to check the quality of the specimens and the repeatability of the results of specimens obtained from different batches of the same mix, the measurement of ρ and V was performed on three reference specimens at 5, 6, 7, 28, 60 and 90 days (i.e. on the specimens used for the measurement of ρ and V and the flexural and compression tests at 200 days) and the values obtained were compared with the ones obtained on the specimens tested at every single age.

6.1.7. DTA methodology for the study of the carbonation process

For the execution of DTA, one specimen Cyl_A-type was cut in the middle at each age (at half of the height) and 4 samples were collected at different depths of the cut surface of one of the obtained halves, while the other half was stored in a plastic bag (Figure 112 (a) and (b)). Each sample had a volume of about 12 mm x 12 mm x 12 mm and was extracted using a metallic device with a slender tip. The samples were collected according to a pre-defined order (i.e. the first on the external surface, the second at the middle of the radius, the third at the core and the fourth on the opposite surface) (Figure 112 (c)). After the collection of each sample, a pretreatment was applied to the samples to prevent the evolution of the carbonation. Such procedure was inspired by one of the two methods suggested by Scrivener (Scrivener et al. 2018) regarding cementitious materials for the suppression of hydration and removing soluble ions from pore solution. It was adapted for stopping carbonation to remove pore water, which is necessary for carbonation to occur (Lawrence 2006). Once the first sample was collected, it was immediately immersed in isopropanol $(CH_3)_2CHOH$ and stirred (about 50 ml of isopropanol for 5g sample), while the rest of the specimen was covered by a plastic bag. Immediately after the first sample was put in the isopropanol, the collection of the next sample started, and the procedure continued until the fourth sample in the shortest time possible (Figure 112 (d) and (e)). Each sample rested in the solution for at least 10 minutes. Afterward, starting from the first sample, each solution was filtered, to remove the excess isopropanol (Figure 112 (f)) and washed (still above the filter device) with ether (easily volatile solvent) to replace the isopropanol (Figure 112 (g)). Finally, each sample was wrapped in a plastic film and stored in a closed glass vessel (of a volume of about 0.25l) inside a controlled environment at 20±1°C and 60±5% RH (Figure 112 (h)). All the samples were tested within a maximum of two days from the beginning of the sampling process, for the sake of consistency. Before the execution of each DTA, the sample was removed from the container, furtherly ground with a ceramic bowl and pestle (Figure 112 (i)). The tests were performed according to the same order of collection and preparation of the samples. This allowed: i) repeatability of the procedure at the different ages; ii) assessing the effectiveness of the method applied to stop the carbonation, between samples 1 and 4.

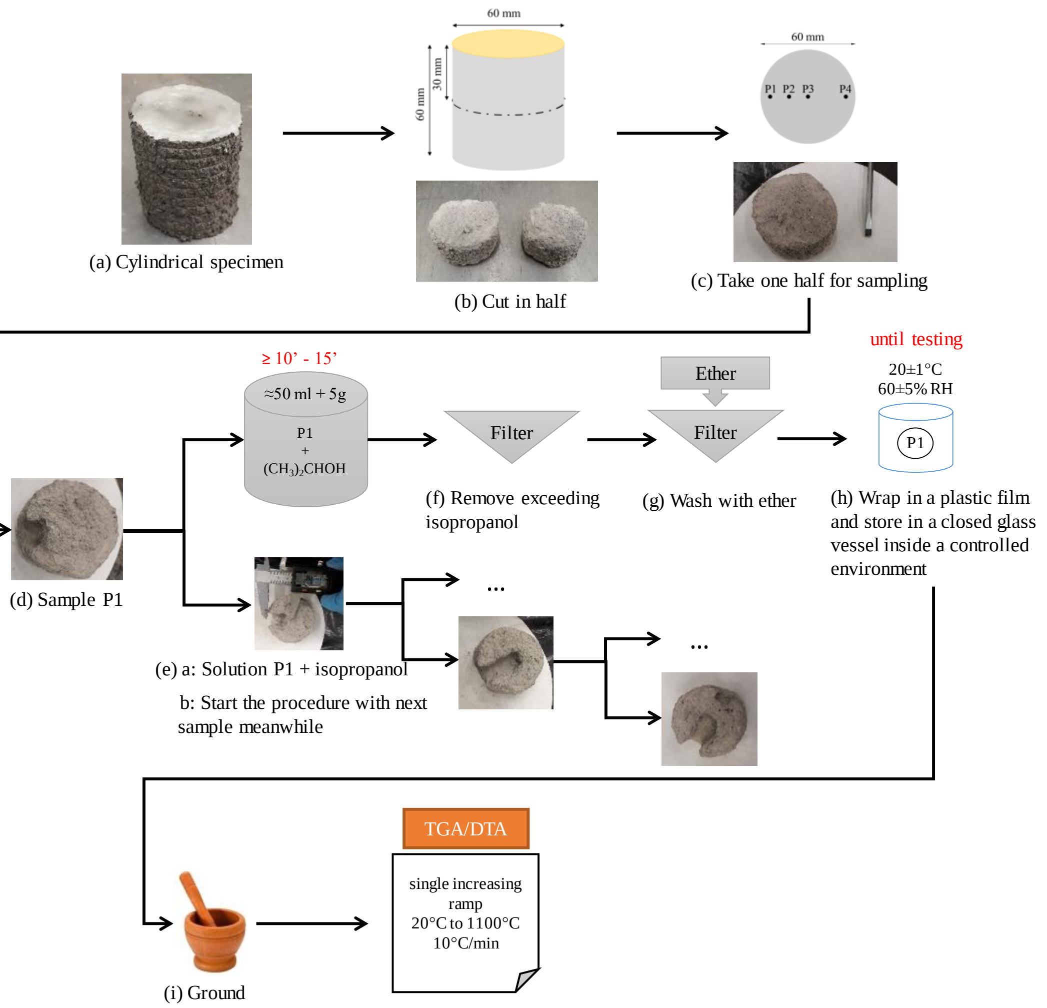

Figure 112. Procedure flow chart for DTA tests.

6.2. Discussion of the experimental results

6.2.1. Repeatability of results

To assess the repeatability of results obtained with the hand compaction method compared to mechanical compaction, Table 27 reports the mean values of ρ, V, f_f and f_c with the standard deviations and coefficients of variation (CoV) reported in brackets for hand compacted specimens and mechanically compacted ones, produced from the same batch of mortar (i.e. batch 3, as reported in Table 25). Despite a slight difference of results was detected between the two sets of specimens (i.e. ρ and V were higher in mechanically compacted specimens compared to hand compacted ones, the contrary happened for f and f_c), they were considered acceptable compared to the variation encountered in each of the individual tests, and also comparable with the variation encountered in the tests performed in experimental studies on aerial lime mortars (Garijo et al. 2019; Goldsworthy and Min 2008; Oliveira 2015). Indeed, the percentage differences between the results obtained did not exceed 5% for the bulk density and the ultrasonic pulse velocity, and about 10% for the flexural and compressive strength.

Table 27. Results of the tests performed for hand compacted specimens and mechanically compacted specimens, with standard deviation and coefficient of variation within brackets.

Batch	**Age [days]**	**Compaction method**	**ρ [kg/m³]**	**V [m/s]**	**f_f [MPa]**	**f_c [MPa]**
3	5	*Hand*	1850 (8) (0.5%)	1208 (66) (5%)	-	-
		Mechanical	1876 (15) (0.8%)	1229 (29) (2%)	-	-
	6	*Hand*	1797 (16) (0.9%)	1017 (39) (4%)	-	-
		Mechanical	1835 (16) (0.9%)	1023 (52) (5%)	-	-
	7	*Hand*	1741 (7) (0.4%)	1067 (45) (4%)	0.20 (0.01) (3%)	0.62 (0.08) (13%)
		Mechanical	1786 (11) (0.6%)	1023 (37) (4%)	0.18 (0.01) (3%)	0.57 (0.02) (3%)

A similar conclusion was reached as regards the repeatability of the results of specimens from different batches of mortar. Thus, Table 28 reports the mean values of ρ and V with the standard deviations and coefficients of variation reported in brackets for the specimens tested at different ages and for the reference specimens (i.e. the ones used for flexural and compression tests at 200 days as reported in Table 25). Indeed, the differences did not exceed 1% for the bulk density and 6% for the ultrasonic velocity.

Table 28. Bulk density and ultrasonic velocities of the specimens used for flexural and compression tests at each age and of the reference specimens, with standard deviation and coefficient of variation within brackets.

Age [days]	Batch	ρ [kg/m3]	V [m/s]
7	4	1775 (11) (0.6%)	1239 (50) (4%)
	8	1785 (13) (0.7%)	1323 (6) (0.4%)
28	5	1603 (7) (0.4%)	1601 (41) (3%)
	8	1605 (19) (3%)	1655 (55) (1%)
60	6	1610 (4) (0.2%)	1598 (68) (4%)
	8	1616 (18) (1%)	1679 (78) (5%)
90	7	1621 (5) (0.3%)	1686 (20) (1%)
	8	1620 (18) (1%)	1738 (33) (2%)

6.2.2. Flexural and compressive strength

Figure 113 reports the results of the strengths tests and their evolution in time. Note that the coefficients of variation are reported in brackets and the error bars in the graphs are the corresponding standard errors, calculated as the standard deviation divided by the square root of the number of experiments for each test. The flexural strength varied from 0.22 MPa to 0.56 MPa and the compressive strength varied from 0.78 MPa to 2.10 MPa. The tests showed similar development of flexural and compressive strength. Indeed, in both cases a substantial increase was showed between 7 and 28 days, then the increase was almost constant between 28 and 90 days, and finally, the increase was small between 90 and 200 days, with the flexural strength almost constant. These results indicated that the studied mixture developed its flexural and compressive strengths mainly in the first three months, then it slowly increased its compressive capacity up to six months. Similar trends were found in other studies on aerial lime mortars (Goldsworthy and Min 2008; Lawrence 2006; Moropoulou et al. 2005b).

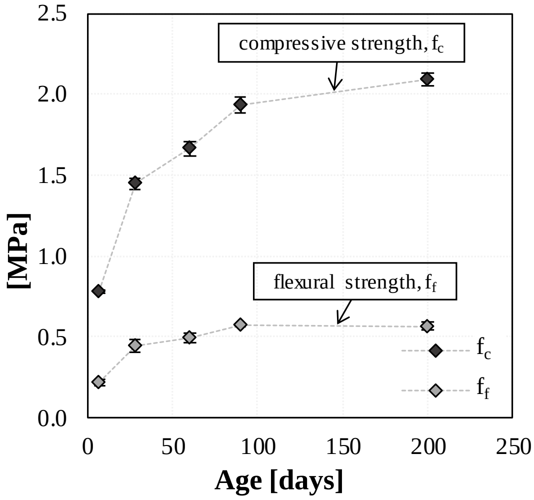

Age [days]	f_f [MPa]	f_c [MPa]
7	0.22 (14%)	0.78 (4%)
28	0.44 (15%)	1.45 (6%)
60	0.49 (9%)	1.67 (7%)
90	0.57 (0.2%)	1.93 (6%)
200	0.56 (8%)	2.10 (4%)

Figure 113. Evolution of the flexural and compressive strength.

6.2.3. Open porosity

The mean values of open porosity along with the coefficients of variation at each age are reported in Table 29. No significant variation of the open porosity with the time was detected, except for a slight reduction detected at 200 days. The mean value of the open porosity resulted in 39.6%, with CoV of 0.8%. However, a slightly decreasing trend was observed from 60 up to 200 days. These values and trends are consistent with the ones obtained on similar mortars by Faria et al. (Faria et al. 2008). Mortars made with lime putty typically have higher open porosity compared to mortars made with hydrated lime and lime-cement blended, due to the higher amount of water in such mixtures (Cizer 2009; Ramesh et al. 2019). Indeed, Cizer (Cizer 2009) found the open porosity of lime putty mortar at 90 days to be 4% to 7% higher than hydrated lime mortar for different curing conditions.

Table 29. Results of the open porosity tests.

Age [days]	7	28	60	90	200
Open porosity	39.8% (0.8%)	39.4% (0.8%)	39.9% (0.5%)	39.2% (1%)	38.3% (0.5%)

6.2.4. Ultrasonic pulse velocity and bulk density

The bulk density and ultrasonic velocity at each age for the reference specimens are reported in Figure 114. Note that the coefficients of variation are reported in brackets and the error bars in the graphs are the corresponding standard errors. The ultrasonic pulse velocity reduced between 5 and 6 days, then it increased up to 90 days and decreased again between 90 and 200 days. The higher velocity at 5 days compared to 6 days was probably related to the higher humidity of the specimens. Indeed, it is known that ultrasonic velocity is higher in water than in air, thus in water-saturated porous media (Vasanelli et al. 2015). After that, the increase up to 90 days, was probably related to the build-up of the solid skeleton. Indeed, it is also known that the ultrasonic velocity is higher in solids than in air (Vasanelli et al. 2015). Finally, the reduction of the velocity between 90 and 200 days was probably related to the loss of water in the specimens. As expected the bulk density showed a decreasing trend until 28 days, due to the evaporation of water, then a slight increase until 200 days, due to the carbonation process with the formation of calcium carbonate in place of calcium hydroxide, with a higher molar mass compared to the latter (Scrivener et al. 2018). This latter trend was consistent with the decrease observed for the open porosity and the subsequent increase of ultrasonic velocity. Both for bulk density and ultrasonic velocity the maximum variation was observed between 7 and 28 days, similarly to the flexural and compressive strength.

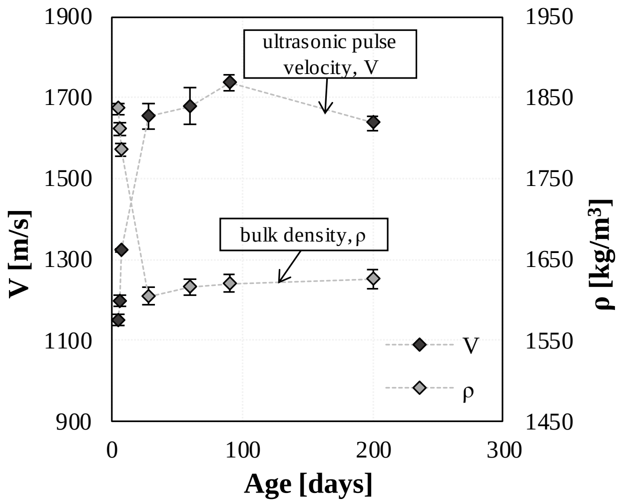

Age [days]	ρ [kg/m3]	V [m/s]
5	1836 (0.7%)	1266 (2%)
6	1811 (0.7%)	1239 (2%)
7	1785 (0.7%)	1323 (0.4%)
28	1605 (1%)	1655 (3%)
60	1616 (1%)	1679 (5%)
90	1620 (1%)	1738 (2%)
200	1625 (1%)	1637 (2%)

Figure 114. Evolution of the ultrasonic pulse velocity and bulk density.

6.2.5. Static elastic modulus

The mean static elastic modulus at each age is reported in Figure 115, with the coefficients of variation in brackets and the error bars in the graphs corresponding to the standard errors. The elastic modulus increased between 7 and 90 days from 0.70 GPa to

1.08 GPa. Aggelakopoulou (Aggelakopoulou et al. 2019) found lower static elastic modulus for lime putty mortars with siliceous and calcareous sand at 18 months of curing (i.e. 0.11 and 0.13 GPa). These different results could be related to the different aggregates used in the mixtures.

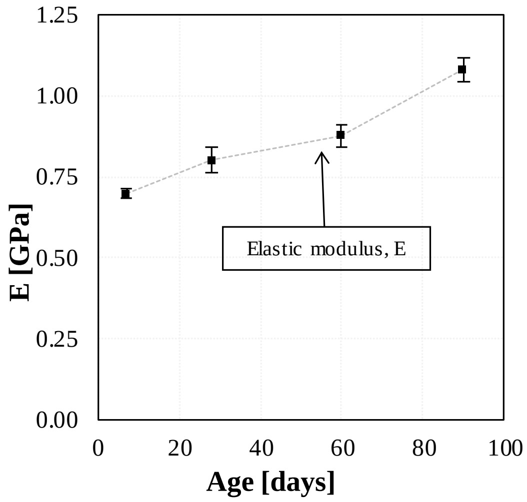

Age [days]	E [GPa]
7	0.70 (3%)
28	0.80 (8%)
60	0.88 (7%)
90	1.08 (6%)

Figure 115. Evolution of the elastic modulus with time.

6.2.6. Differential thermal analyses

Figure 116 shows DTA thermograms obtained from the sample P1 of each cylindrical specimen (i.e. from the surface of each specimen) at each age. A heat flow peak related to the dehydroxylation was evident at three days, getting smaller at 7 days and almost flattened from 28 days, meaning that the calcium hydroxide on the surface of the specimens was completely consumed at that age. A heat flow peak in the range of decarboxylation was observed from 3 days, with an increase in $CaCO_3$ content, alongside the reduction of $Ca(OH)_2$, indicating the evolution of carbonation. Meanwhile, a reduction of free water due to evaporation was observed. Moreover, the weight loss in the temperature range of 50-250°C from 3 days was further analyzed to investigate the occurrence of pozzolanic reactions related to the formation of hydrated phases (Cizer 2009; Moropoulou et al. 2004a). As no heat flow peaks were observed in that temperature range, this has led to conclude that such types of reactions were absent. Despite it was not possible to determine the reason for this unexpected outcome, this is an interesting result defining the behavior of this type of material.

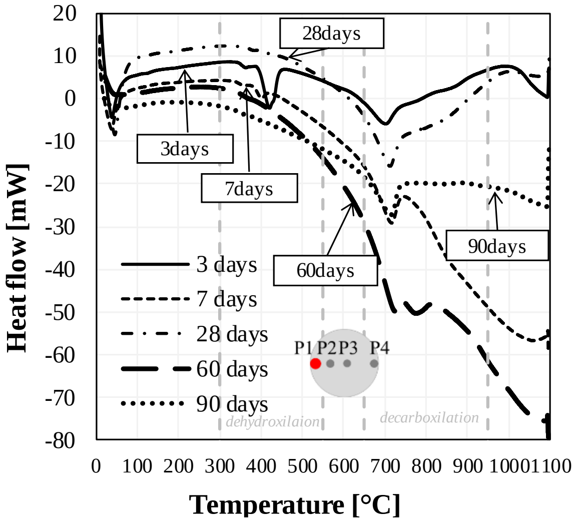

Figure 116. DTA curves of samples P1 (i.e. on the surface of each cylindrical specimen) at each age.

As regards the evolution of carbonation through the depth of the cylindrical specimens, DTA curves obtained from the samples P1, P2, P3 and P4 at 3, 7, 28, 60 and 90 days are reported in Figure 117. At 3 days, all the samples showed the heat flow peak in the range of dehydroxylation, while the heat flow peak in the range of decarboxylation was evident only for P1 and P4, meaning that at that age carbonation occurred only on the surface of the specimen (i.e. within a depth of about 12 mm). Similar behavior was shown at 7 days, while less evident peaks related to dehydroxylation in P1 and P4 were observed from 28 days. At 90 days, the heat flow peak in the range of dehydroxylation was observed in P2 and P3, while the peak in the range of decarboxylation was still not evident in P3. From that, it may be concluded that at that 90 days of age, carbonation was almost completed only at the edge of the specimen and was still in evolution within the core of the specimen. This was consistent with the results of thermogravimetric analyses performed by Lawrence et al. (Lawrence et al. 2006) and by literature values of carbonation depth in aerial lime mortar specimens evaluated through phenolphthalein (Lawrence 2006; Oliveira 2015).

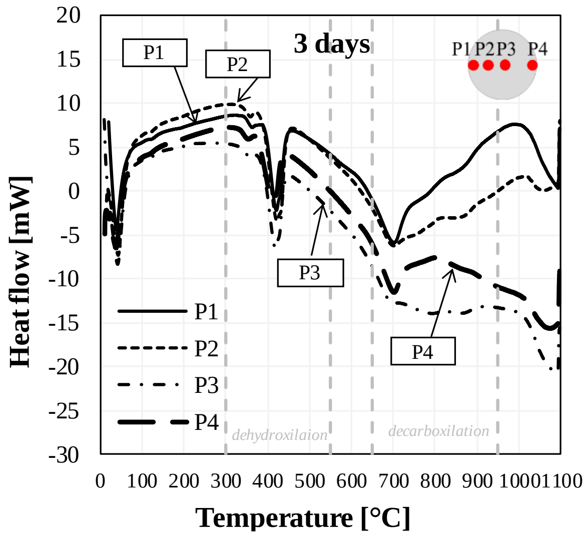
3 days
Heat flow [mW]
Temperature [°C]
P1
P2
P3
P4
P1 P2 P3 P4
dehydroxilaion
decarboxilation
20
15
10
5
0
-5
-10
-15
-20
-25
-30
0 100 200 300 400 500 600 700 800 900 1000 1100

(a)

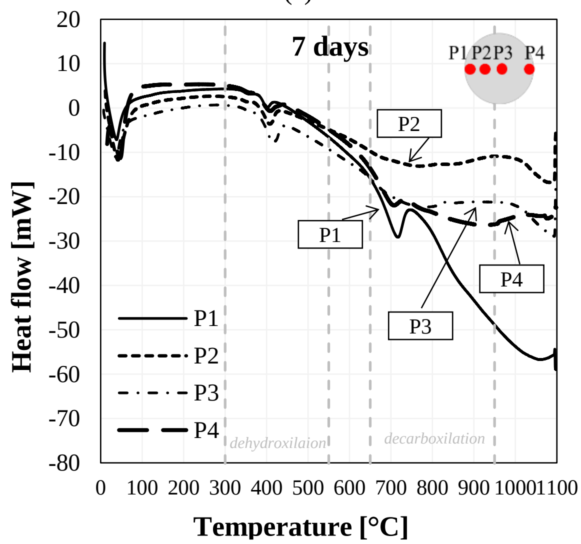
7 days
Heat flow [mW]
Temperature [°C]
P1
P2
P3
P4
P1 P2 P3 P4
dehydroxilaion
decarboxilation
20
10
0
-10
-20
-30
-40
-50
-60
-70
-80
0 100 200 300 400 500 600 700 800 900 1000 1100

(b)

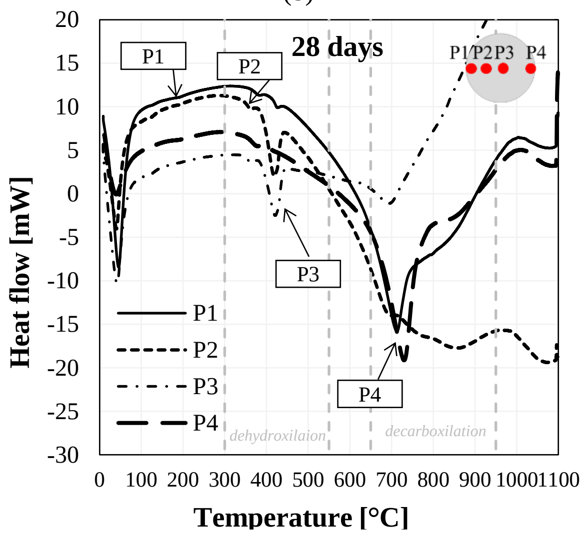
28 days
Heat flow [mW]
Temperature [°C]
P1
P2
P3
P4
P1 P2 P3 P4
dehydroxilaion
decarboxilation
20
15
10
5
0
-5
-10
-15
-20
-25
-30
0 100 200 300 400 500 600 700 800 900 1000 1100

(c)

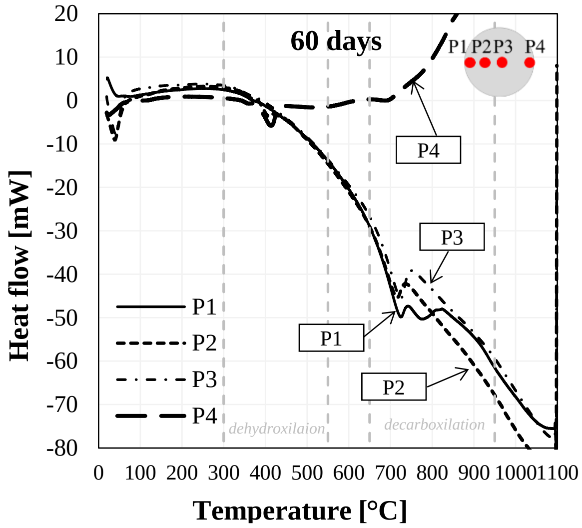

(d)

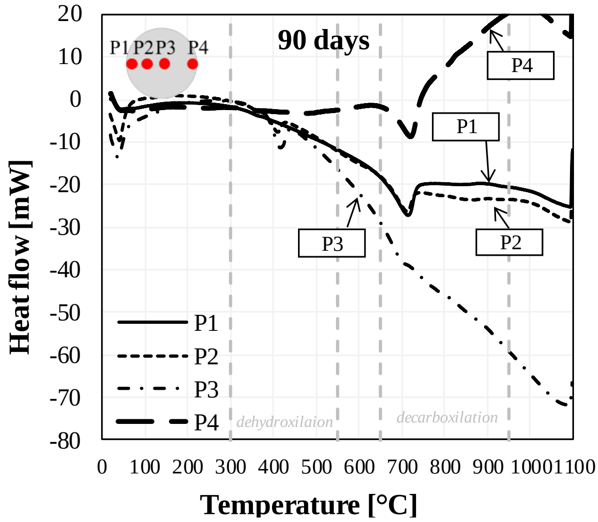

(e)

Figure 117. DTA curves for all the samples at 3 days (a), 7 days (b), 28 days (c), 60 days (d) and 90 days (e).

6.3.Comparative analysis of the obtained outcomes

A summary of the main mechanical and physical properties of the investigated mortar, with the coefficients of variation in brackets, is reported in Table 30.

Table 30. Summary of the investigated physical and mechanical properties.

Age [days]	f_f [MPa]	f_c [MPa]	open porosity [%]	ρ [kg/m^3]	V [m/s]	E [GPa]
5	-	-	-	1836 (0.7%)	1266 (2%)	-
6	-	-	-	1811 (0.7%)	1239 (2%)	-
7	0.22 (14%)	0.78 (4%)	39.8% (0.8%)	1785 (0.7%)	1323 (0.4%)	0.70 (3%)
28	0.44 (15%)	1.45 (6%)	39.4% (0.8%)	1605 (1%)	1655 (3%)	0.80 (8%)
60	0.49 (9%)	1.67 (7%)	39.9% (0.5%)	1616 (1%)	1679 (5%)	0.88 (7%)
90	0.57 (0.2%)	1.93 (6%)	39.2% (1%)	1620 (1%)	1738 (2%)	1.08 (6%)
200	0.56 (8%)	2.10 (4%)	38.3% (0.5%)	1625 (1%)	1637 (2%)	-

Low values of mechanical parameters were found to be consistent with other lime-based mixtures for repair interventions of historical masonries, ranging about 1MPa and 2.3MPa for the compressive strength and 0.5MPa and 0.6MPa for the flexural strength after 3 months of curing (Lindqvist et al. 2009; Moropoulou et al. 2005b; Oliveira 2015). In particular, the compressive strength was found to be compliant with the value targeted for lime-based mortar used in recent structural interventions at the Pompeii site (i.e. greater than 1.5 MPa at 28 days) (Calvanese and Zambrano 2021). The values found also comply with the requirement for mechanical compatibility with ancient mortars (Lindqvist and Sandström 2000; Maurenbrecher et al. 2001). Moreover, according to what was found by Faria et al. (Faria et al. 2008), the use of the lime putty in the mixture and the relatively high value of open porosity obtained may positively affect the durability of the mortar in terms of salt resistance, other than its workability. As regards the ultrasonic pulse velocity, despite it did not provide a direct correlation with the physical and mechanical properties of the mixture, its development trend was found to be a useful complementary method to follow the general development of the hardening process being consistent with the evolution of the hardened properties of the mortar.

Flexural and compressive strengths showed a similar evolution with time. The values of the flexural strength were compared with the compressive strength at each age as reported in Figure 118 (a). This could be a useful tool for a primary estimation of one of these parameters, known the other, being the flexural strength approximately equal to 30% of the compressive strength. A similar correlation was found by (Haach et al. 2011) for lime-cement blended mortars with different lime:cement proportions and type of aggregates.

Moreover, the compressive strength obtained at each age from the standard prisms' halves (i.e. the P-type specimens), f_c, were compared with the ones obtained from the cylindric specimens (i.e. Cyl_A-type), indicated as "f_c*", as reported in Figure 118 (b) and the relevant table. This correlation is particularly interesting from an engineering point of view since it is well known that the compressive strength of concrete and mortars is affected by the shape and size of the tested specimens. The ratio f_c^*/f_c was found to vary between 0.45 and 0.60. This was consistent with what found by Parsekian (Parsekian et al. 2014) according to whom mortars with a strength less than 4 MPa show a reduction of the strength of cylindrical specimens compared to prism halves between 37 and 49%, which is much lower than the usual relation adopted for concrete to relate cube and cylinder specimens.

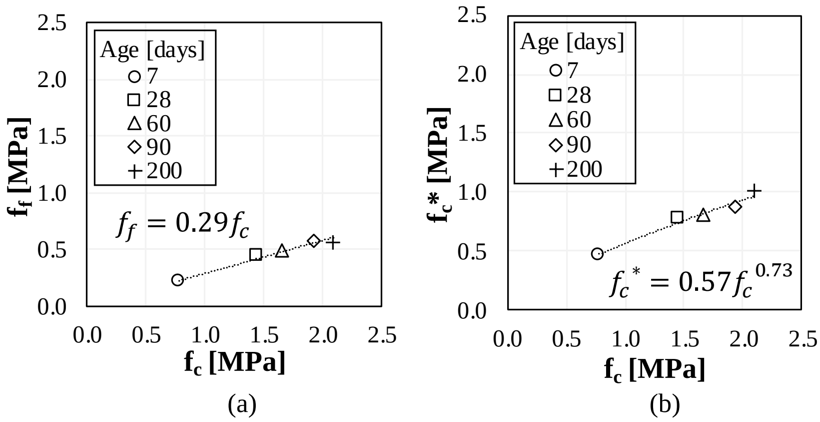

Age [days]	f_f/f_c	f_c^*/f_c
7	0.28	0.60
28	0.31	0.53
60	0.30	0.48
90	0.30	0.45
200	0.27	0.48

Figure 118. Relationship between the mean compressive strength obtained from prism halves, f_c, and the mean flexural strength, f_f, (a) and between the mean compressive strength f_c and the mean compressive strength obtained from cylindric specimens, f_c.*

The evolution of the stiffness of a mortar (elastic modulus) compared to the evolution of its load capacity (compressive strength) could be taken as an indicator of the development of its capacity to accommodate larger movements without cracking and could be useful for comparisons with other mortars. In the present study, the ratio E/f_c was found to vary in the range 900-500, with the highest value at 7 days, as shown in Figure 119. The figure also shows the comparison with the available data derived by literature concerning different types of mortar. In particular, data related to cement-aerial lime blended mortars (Ramesh et al. 2019), natural hydraulic lime mortars (Garijo et al. 2019) and cement-natural hydraulic lime blended mortars (Haach et al. 2011) were used for the comparison. Figure 119 also specifies the mix proportions for each mortar (Cement:Lime:Sand) and the water:binder ratio by volume. Note that as regards data from (Haach et al. 2011), mixtures made with fine coarse sand were considered. The mortar investigated here showed a lower value of the ratio E/f_c compared to the others and this may indicate a lower probability of cracking, which could be crucial in repair interventions, especially for constructions in archaeological sites which are typically characterized by a low strength capacity and high deformability.

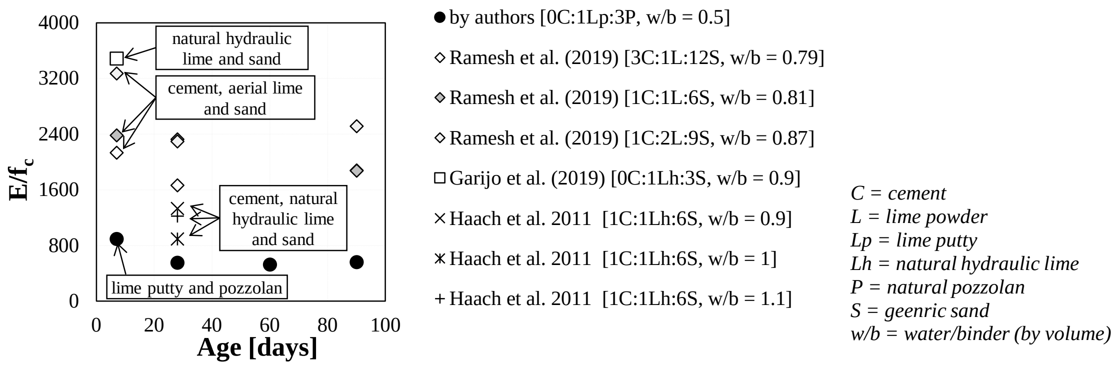

Figure 119. Evolution of the ratio of elastic modulus to the compressive strength with time and comparison with values presented in the literature concerning different types of mixtures.

6.4. Characterization of a repair mortar made with aggregate resulting from archaeological excavations

After wide and accurate characterization of putty lime and Phlegrean pozzolan mortar, a primary characterization of another mixture was performed involving DTA. This mixture was produced with the same lime putty used for the first mortar and a different aggregate. This latter was a volcanoclastic material as well, called “black sand” in what follows, generated from the Vesuvius’ eruption of 79 A.D. and brought to light during the new archaeological excavation works in *Regio V*. This material was abundant in that area of the archaeological site. Therefore, the possibility of using this material to produce repair mortars after assessing its compatibility and durability for restoration interventions was considered. However, due to logistic restrictions, it was not possible to arrange a complete experimental campaign similar to what was defined for the pozzolan-based mortar. Therefore, a limited set of tests was performed. In particular, DTA was performed on this other type of repair mortar at 3, 7, and 28 days according to the same protocol adopted for the first mortar.

The bulk density of the black sand was measured again according to the standard EN 1097-3 (CEN 1999b) and resulted in 1.21 g/cm^3. Its particle size distribution was evaluated according to the standard EN 933-1 (CEN 2012b) (Figure 120). Figure 121 shows the particle size distribution of the black sand in association with that of the pozzolan sand.

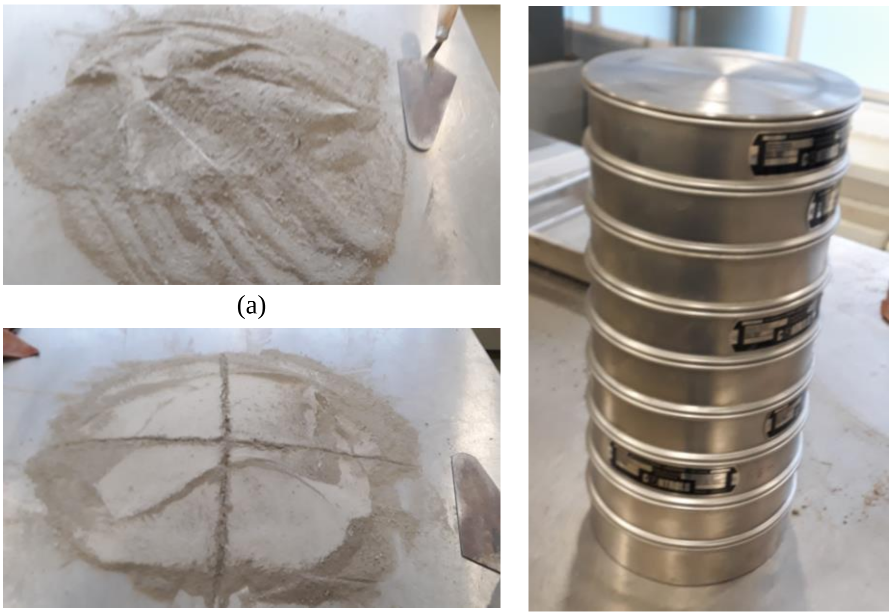

(a) (b) (c)

Figure 120. Determination of the particle size distribution of the black sand by sieving method: black sand after drying (a); preparation of the sample of sand (b); sieves (c).

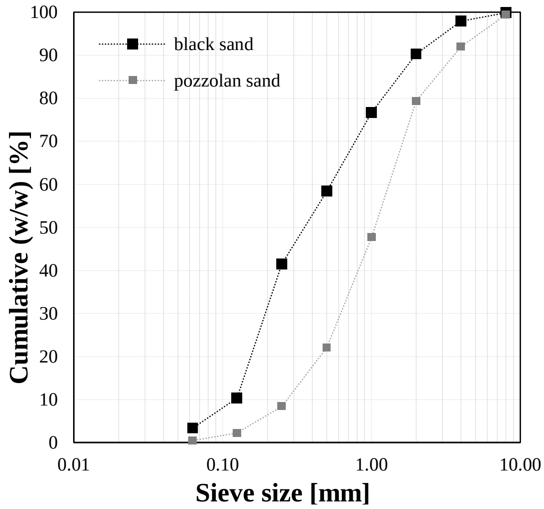

Figure 121. Particle size distribution of the black sand and pozzolana sand (0.063-8.0 mm).

DTA was performed at first on the single black sand, according to the same protocol defined for lime putty, pozzolan, and pozzolan-based mortar: a single increasing ramp, from 20°C to 1100°C, with a rate of 10°C/min. Figure 122 shows the DTA curve of the black sand, together with the ones of the lime putty and pozzolan sand. Different from the pozzolan sand, the black sand showed an evident heat flow peak in the range of decarboxylation. A slight heat flow peak corresponding to the presence of free water was visible in both the aggregates.

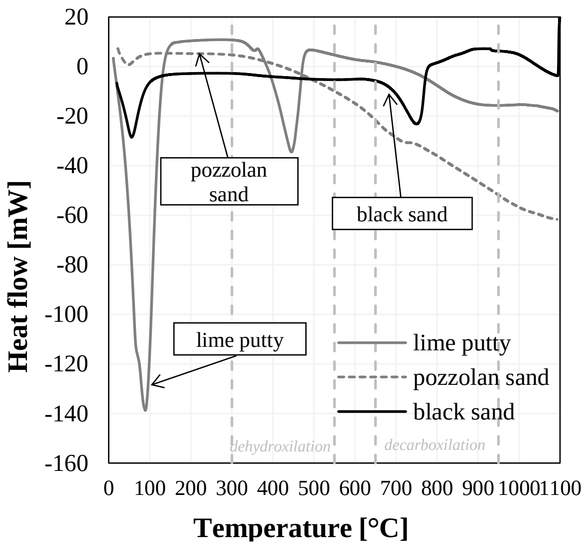

Figure 122. DTA curves of lime putty, pozzolan sand and the two samples of fresh mortar tested within two hours from the start of the mixing protocol.

For the execution of DTA, three specimen Cyl_A-type were produced. The mortar composition equal to 1:3:0.5 (i.e. binder:aggregate:water) by volume was defined, corresponding again to a plastic consistency according to the standard EN 1015-3:1999 (Figure 123). This resulted in a composition weight equal to 1000.0: 333.3: 135.0 g.

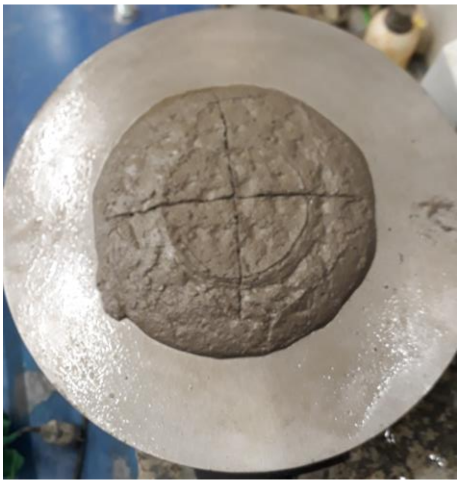

Figure 123. Black sand-based fresh mortarafter a flow test.

The mixing procedure was defined according to the standard EN 459-2 (CEN 2010). The specimens were compacted by hand, by filling the molds in two almost equal layers each one compacted by twenty-five strokes of a tamper, as indicated in the standard EN 1915-11 (CEN 2007a). The specimens were stored according to the type “B” method, as defined in the previous sections. In particular, after casting the specimens were completely sealed with plastic tape at the top and the bottom surfaces and stored at 20±1°C and 95±5%; then at two days the specimens were removed from the cylindric molds and the top and the bottom surfaces were completely sealed by putting paraffin layers on them. Thus the specimens were cured in a controlled environment at 20±1°C and 60±5% relative humidity. For the execution of DTA the procedure summarized in Figure 112 was applied. Thus, four samples of mortar collected from the cut surface of one cylindrical specimen at each age were tested. Figure 124 plots the DTA curves for the samples P1, P2, P3 and P4 of black sand-based mortar at 3 days (a), 7 days (b), and 28 days (c). Differently from the pozzolan-based mortar, heat flow peaks in the range of decarboxylation were visible in the black sand-based mortar already at 3 days. However, the presence of these peaks could be related to the nature of the black sand, which showed a similar peak (Figure 122). On the contrary, similarly to the pozzolan-based mortar, less intense peaks were observed in the range of dehydroxylation at 28 days, particularly for P1 and P4, showing that carbonation partially occurred on the surface of the specimen at that age, but it was still developing into greater depths.

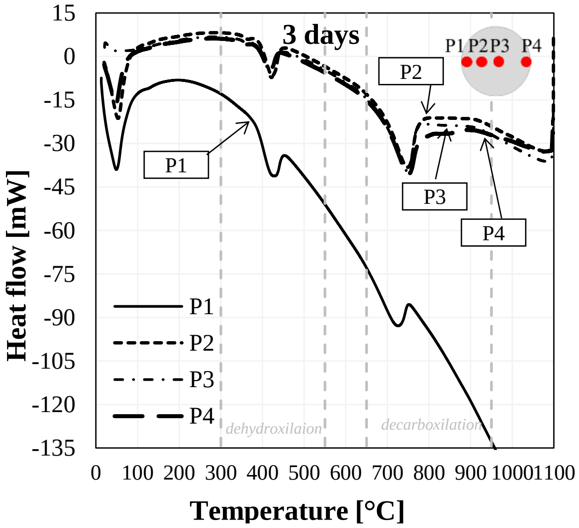

(a)

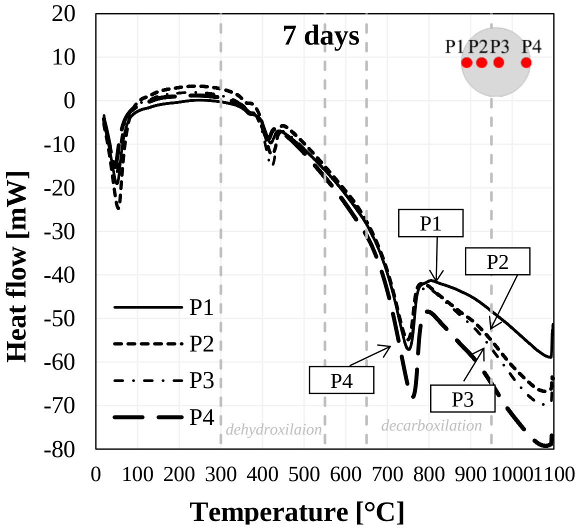

(b)

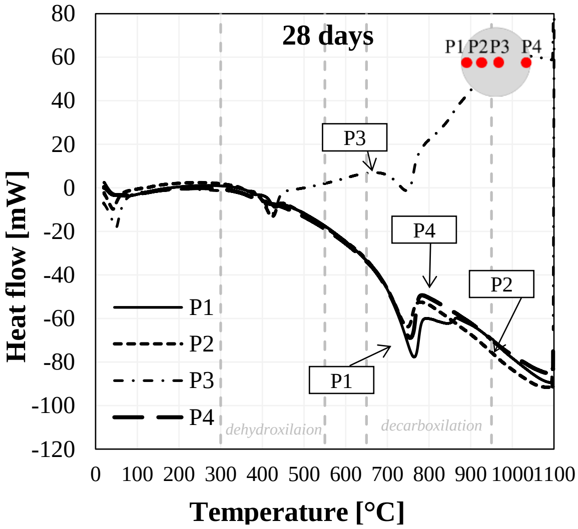

(c)

Figure 124. DTA curves for all the samples of black sand-based mortar at 3 days (a), 7 days (b), and 28 days (c).

CONCLUSIONS AND PROSPECTIVES

The conservation of ancient structures requires a deep and wide knowledge of their typological features, state of preservation and mechanical properties. However, due to technical, protection and logistic restrictions, suitable information in many historical and archeological contexts is still limited. The development of comprehensive and multidisciplinary knowledge is required. From a mechanical point of view, the diagnosis of heritage structures introduces difficult challenges related to the balancing of preservation requirements and technical issues. Therefore, the development of non-destructive investigation methods to achieve fundamental information on the structural behavior of ancient structures is strongly needed.

The archaeological site of Pompeii is an exceptional case study, related to both the outstanding value of its material and non-material asset and the special challenges occurring for its protection. These latter are related to the great extension of its built asset, the great variety of building materials and techniques, the presence of different forms of degradation and damage, the need to make the site safely accessible, other than ensuring its conservation.

The objective of this research was the development of a reliable path of knowledge and to provide valuable tools supporting the definition of appropriate choices and methodologies for the design and planning of suitable interventions on the archaeological structures. The adopted methodologies were defined taking into account on the one side conservation requirements and compatibility with the archaeological materials and structures, and the other side, standard testing procedures and commonly accepted scientific protocols. Indeed, information achieved in this study may be considered useful and applicable also in other archaeological and historical sites. The research was developed on the study of i) the most common masonry typology at the site, i.e. the *opus incertum*, and its typical constituent materials, ii) free-standing multidrum tuff columns and iii) compatible repair mortar for structural interventions. The choice for these topics was based on the representativeness of the studied structural elements and materials at the Pompeii site and similar contexts, and actual demands for conservation.

An extended and articulated investigation programme based on non-destructive and destructive tests was developed for the investigation of archaeological masonry structures. New archaeological excavations at *Regio V* allowed surveying and analyzing masonry structures and building materials that emerged for the first time since the Vesuvius eruption of 79 AD. Detailed surveys and *in situ* inspections of *opus incertum* structures allowed defining its typical geometrical and material characteristics. As a first stage of the research, archaeological specimens of stone units and masonry mortars were collected from masonry structures involved in the excavations at *Regio V*. This provided a unique opportunity to perform standard tests on archaeological materials. Typical rock typologies, namely travertine, lava, and foam lava, were characterized through non-destructive and destructive tests. It was found that they have different mechanical properties, with the lava showing the highest load capacity and the foam lava showing the lowest load capacity. A high scatter of results was also found for each typology, related to different weathering and natural defects of the stones. The non-destructive tests were found to correlate with a good matching the results of the destructive tests representing a sound tool to provide preliminary information on the mechanical properties of these traditional rock types. Compressive strength tests were performed on the original mortar specimens. These revealed the poor condition of the investigated mortars with a low value of the mean compressive strength and high scatter of the results.

Parallel to this, a qualitative non-destructive structural assessment was carried out on archaeological *opus incertum* masonry structures. This involved the execution of extensive sonic pulse velocity tests on masonry structures from different areas of the site (Villa of Diomedes and *Regio V*), with different ages (newly emerged from the excavations at *Regio V* or brought to light in the 19th century or 20th century) and with or without the presence of modern restoration interventions. These investigations led to a unique set of information for the qualitative structural assessment of the masonry under investigation and the enrichment of the existing available dataset concerning sonic test results on different typical ancient masonry typologies. It was found that sonic velocities of archaeological structures fall within the range of poor-quality masonry structures according to a typical classification adopted in the literature. Masonry structures subjected to modern partial mortar repointing showed mean velocities comparable to those attained on the newly emerged masonry structures without any modern interventions, meaning that a relevant improvement of the state of preservation of ancient masonry structures should involve the entire cross-section of the wall and not only the exterior surfaces. Also, factors typically encountered in historical and archaeological contexts, such as severely deteriorated masonry surfaces, available masonry portion located close to an opening or on partially collapsed walls, may lead to a reduction of the sonic velocities of about 25%.

The final stage of the investigation programme of *opus incertum* masonry structures involved the production of full-scale Pompeii-like masonry panels. This allowed carrying out standard destructive tests to the scale of the masonry assemblage. Moreover, sonic pulse velocity tests performed according to the same protocol used for the archaeological structures led to monitor the evolution of the hardening process of the panels and to assess useful correlations with the results of the destructive tests and with the results of the sonic tests performed on the archaeological structures. The panels were built by carefully following the ancient technique *opus incertum* and by using original stone units from the excavations at *Regio V* and putty lime and pozzolan-based mortar. *In situ* diagonal compression tests allowed obtaining essential information on the shear behavior of the panels, namely shear strength and modulus of elasticity, and axial compression tests performed allowed obtaining information on the normal behavior of the panels, namely compressive strength and modulus of elasticity. Despite available data are still not sufficient to deriver reliable analytical formulations providing the mechanical properties of *opus incertum* masonry structures from the results of sonic tests, the preliminary correlations defined in this study certainly represent a useful tool for an indicative assessment.

The study of free-standing multidrum tuff columns was aimed to improve the knowledge of such elements and provide a preliminary analysis of their seismic vulnerability. The relevance of this part of the study was related to the fact that these elements are very common within the Pompeii site and similar contexts and they are in many cases in a precarious state of conservation. Thus, the assessment of their most common characteristics, state of preservation and seismic stability is an crucial issue, especially considering the high seismic activity of the Mediterranean area. Indeed, despite consolidation and restoration interventions performed in the past, several tuff columns at Pompeii present nowadays cracks, material deterioration, detachments, and uneven profiles, affecting their stability and aesthetics. This part of the study at first focused on a detailed analysis of main mechanical properties and forms of degradation affecting the seismic response of a representative range of columns at the site. The study particularly focused on the aspect ratio, size, number of drums and completeness of the columns. It was found that the main critical issues that may affect the seismic response of columns under investigation were i) the weathering of tuff, cracks and detachment; ii) the initial tilting and partial lack of contact among the drums; iii) the presence of corroded metallic devices to connect drums and/or invasive post-excavation interventions. Based on fundamental findings from the literature, this systematic and detailed knowledge could provide a useful tool for identifying columns being potentially more vulnerable than others. The second part of the study of the multidrum columns was focused on a numerical simulation based on the Finite Element Method, FEM, of the seismic behavior of four columns for the *Casa del Fauno*, taking into account different real seismic records. It was found that i) the studied columns can show different dynamic responses for the different input motions, with low-frequency records leading to prevalent rocking and high-frequency ones leading to significant sliding and permanent relative displacements among the drums; ii) on the assumption of a good state of preservation, the columns can withstand notable seismic actions; iii) seismic records with higher predominant periods can be, in general, more dangerous than the ones with the higher frequencies. Approximate formulations for a simplified estimation of the stability of the multidrum columns towards the seismic risk were also provided. These criteria could be used for a primary assessment of multidrum columns and seismic inputs similar to those investigated in this study.

Finally, a deep and systematic study of repair mortars compatible with ancient materials was aimed to support the definition of appropriate interventions on archaeological structures. For that, a mixture was produced by using raw materials as similar as possible to the ancient ones and mix design consistent with traditional techniques. In particular, a precious and limitedly available Phlegrean natural pozzolan was used in the experiments allowing obtaining an exclusive mortar which is very similar to the archaeological ones. The production of the mortar and the experimental programme were carried out following carefully controlled procedures, to ensure the repeatability of the tests. The evolution with the time of fundamental mechanical and physical properties, namely flexural and compressive strength, elastic modulus, bulk density, open porosity and ultrasonic pulse velocity were monitored for up to 200 days, based on standard procedures. Moreover, the hardening process was monitored with Differential Thermal Analysis up to 90 days, through the evaluation of phase transitions associated with dehydroxylation and decarboxylation, considering different depths from the external surface of the mortar specimens. This allowed analyzing and comparing important information, most of which were still not available in the literature. In particular, it was found that the achieved mechanical properties were compatible with those of lime-based mixtures for repair interventions of ancient masonries. Moreover, the mortar was found to be well-suited to mitigate cracking, showing a low ratio between its stiffness and load capacity compared to other typologies of mortars used for masonry restoration. Also, the use of the ultrasonic pulse velocity test proved to be a reasonable complementary method to monitor the evolution of the hardened properties of the mortar, and, finally, the carbonation phenomenon was found to be still progressing at 90 days.

Possible future development of this research could involve: i) wider non-destructive investigations based on sonic pulse velocity tests of archaeological masonry structures by involving different masonry building techniques; ii) the production and characterization through destructive and non-destructive tests of further full-scale Pompeii like masonry panels, involving other traditional masonry building techniques found at the site; iii) further numerical analyses of the seismic behavior of multidrum columns, extended to different column typologies, further seismic inputs and/or parametric analyses on the effect of different geometrical and mechanical parameters on the columns’ response; iv) investigations of other compatible repair mortars, involving the use of other typical raw materials, parametric studies on the effect of variation in the mix design of the mortar, different preparation methods and/or curing conditions.

ANNEX 1)

Archaeological masonry summary sheets: survey and sonic test

(the following information refer exclusively to the investigated archaeological masonry structures at the Regio V*)*

ST1

<table>
<tr><th colspan="2">Masonry ID: ST1</th></tr>
<tr><th colspan="2">Masonry description</th></tr>
<tr><td colspan="2">Opus incertum masonry prevalently made of irregular travertine units, with few foam lava units and terracotta fragments, and mortar. The tested masonry portion was located between a door and a wall intersection.</td></tr>
<tr><th colspan="2">Localization</th></tr>
<tr><td colspan="2">Vico di M. L. Frontone, Regio V.</td></tr>
<tr><th colspan="2">State of preservation and deterioration</th></tr>
<tr><td colspan="2">The masonry surfaces were partially disintegrated, due to weathering. The mortar and the travertine units were friable and tendency to powder.</td></tr>
<tr><th colspan="2">Time of excavation</th></tr>
<tr><td colspan="2">20th century.</td></tr>
<tr><th colspan="2">Modern interventions</th></tr>
<tr><td colspan="2">Superficial repointing interventions with modern mortars were carried out after the excavation.</td></tr>
<tr><th colspan="2">Pictures</th></tr>
<tr><td>Hammer-side (S-W)
</td><td>Receiver-side (N-E)
</td></tr>
</table>

Geometric survey

Hammer-side (S-W)

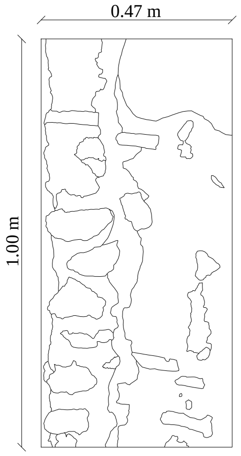

Receiver-side (N-E)

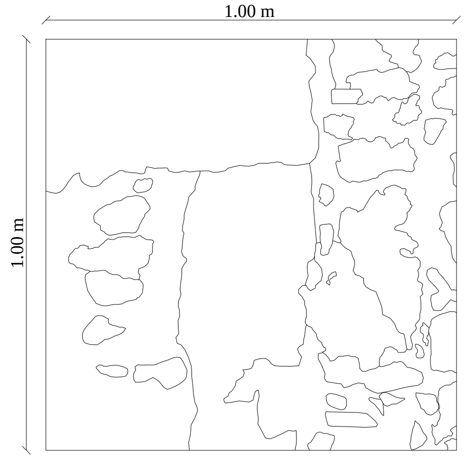

Material survey

Hammer-side (S-W)

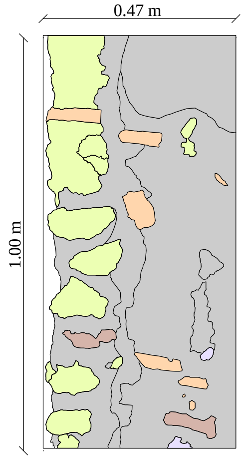

Receiver-side (N-E)

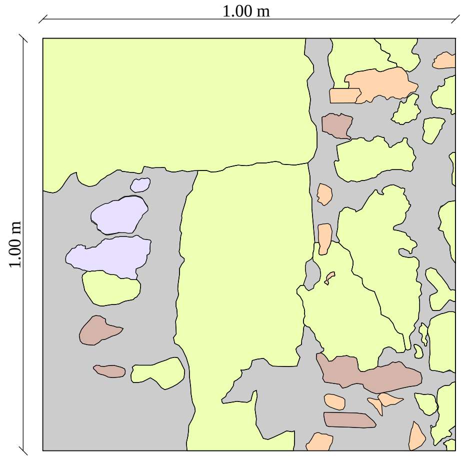

Travertine Lava Foam lava Terracotta Mortar Plaster

Soni test set-up

Wall thickness	Mesh area	Grid spacing	Number of points	Hammer side
0.42m	0.30m x 1.00m	0.10m x 0.10m	44	S-W

Sonic test statistics

V_{mean}	Standard deviation	CoV
390 m/s	593 m/s	48%

Histogram of the recorded velocities and probability density distribution

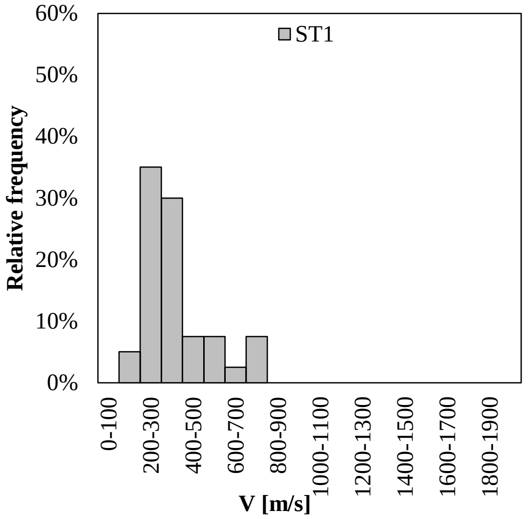

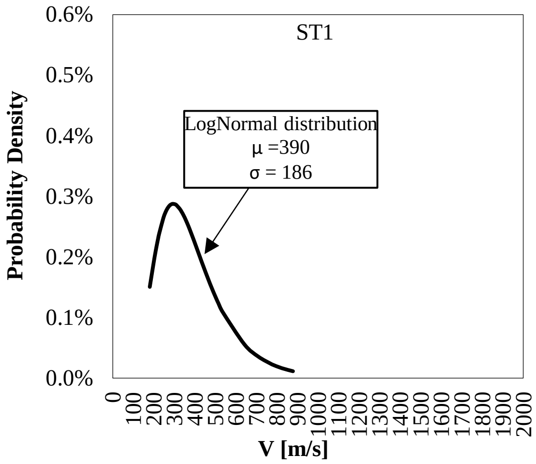

Velocity for each acquisition point

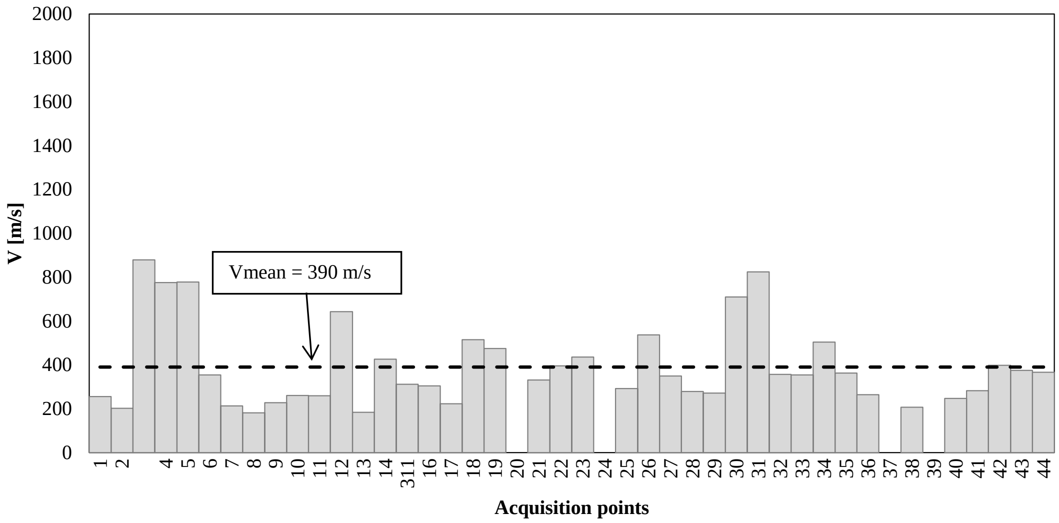

Velocity distribution map
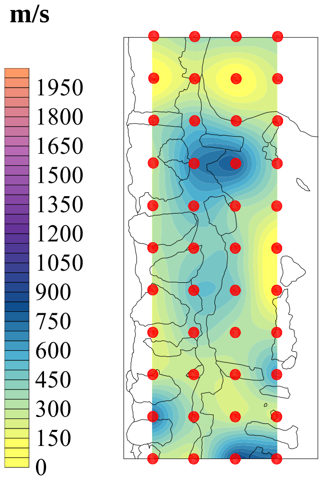

ST2

Masonry ID: ST2	
Masonry description	
Opus incertum masonry prevalently made of irregular travertine and foam lava units associated with horizontal courses of travertine ashlars alternated with terracotta tiles (*opus mixtum*) and squared pieces of travertine and foam lava diagonally aligned (*opus reticulatum*) and mortar. The investigated masonry portion was located between a window and a wall intersection.	
Localization	
Via delle Nozze d'Argento, *Regio V*.	
State of preservation and deterioration	
The masonry surfaces were partially disintegrated, due to weathering. The mortar and the travertine units were friable and tendency to powder. Widespread cracks are also evident.	
Time of excavation	
Newly emerged.	
Modern interventions	
None.	
Pictures	
Hammer-side (S-E)	Receiver-side (N-W)
	

Geometric survey

Hammer-side (S-E)

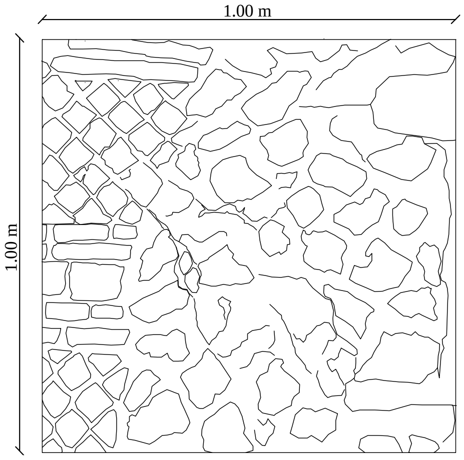

Receiver-side (N-W)

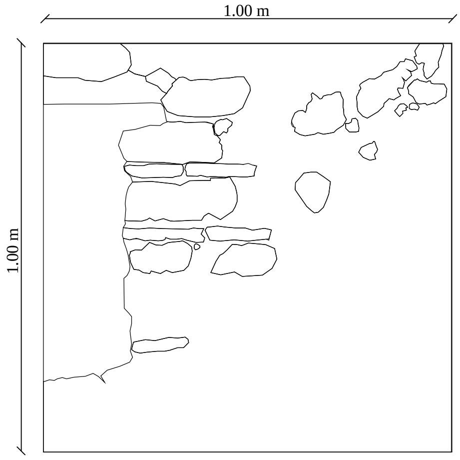

Material survey

Hammer-side (S-E)

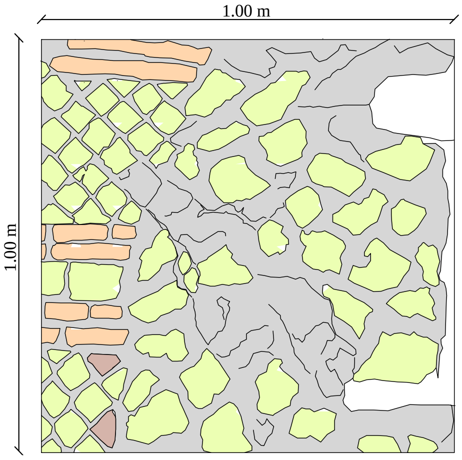

Receiver-side (N-W)

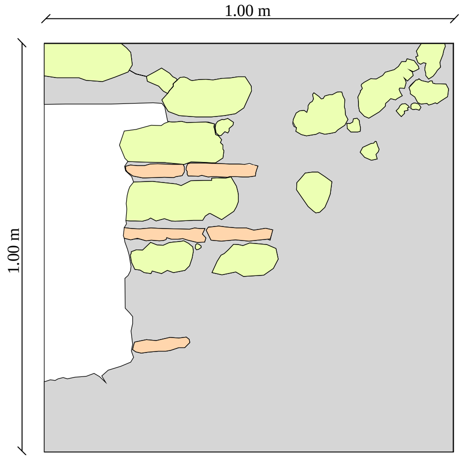

Travertine | Lava | Foam lava | Terracotta | Mortar | Plaster

Soni test set-up

Wall thickness	Mesh area	Grid spacing	Number of points	Hammer side
0.48m	0.60m x 1.00m	0.10m x 0.10m	77	S-E

Sonic test statistics

V_{mean}	Standard deviation	CoV
413 m/s	97 m/s	24%

Histogram of the recorded velocities and probability density distribution

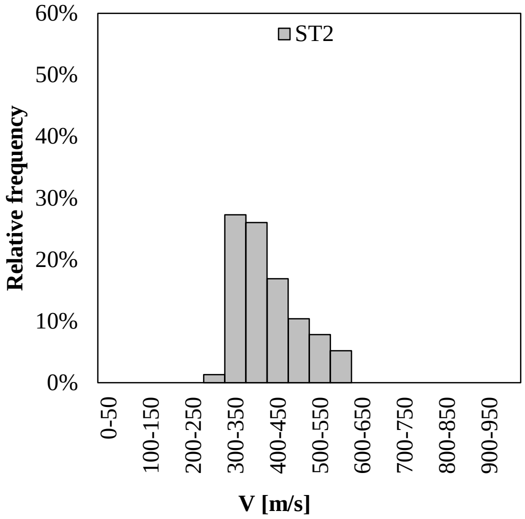

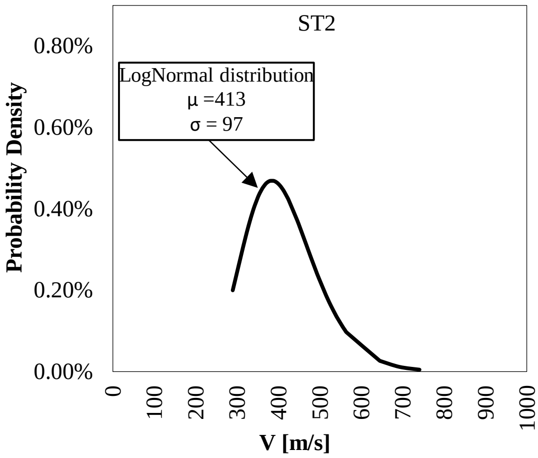

Velocity for each acquisition point

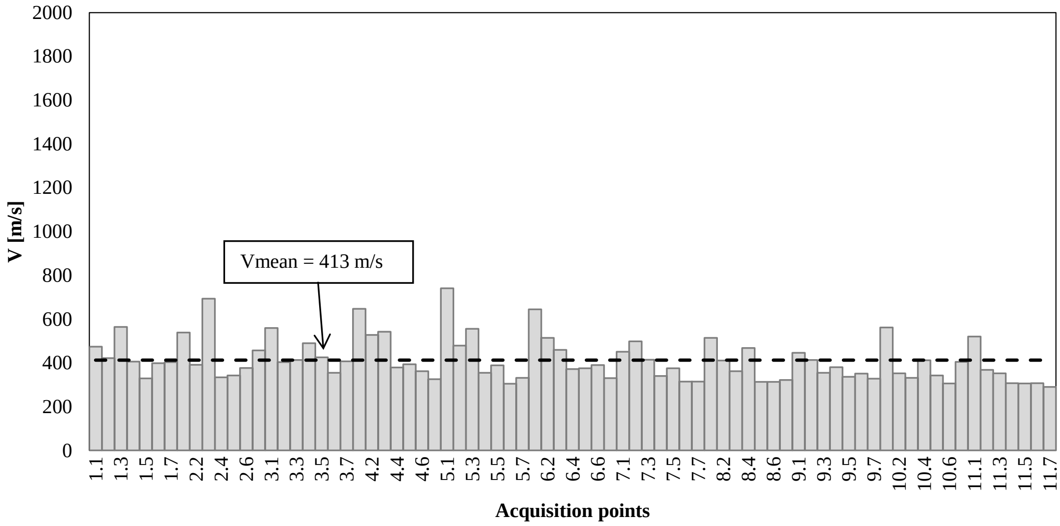

Velocity distribution map
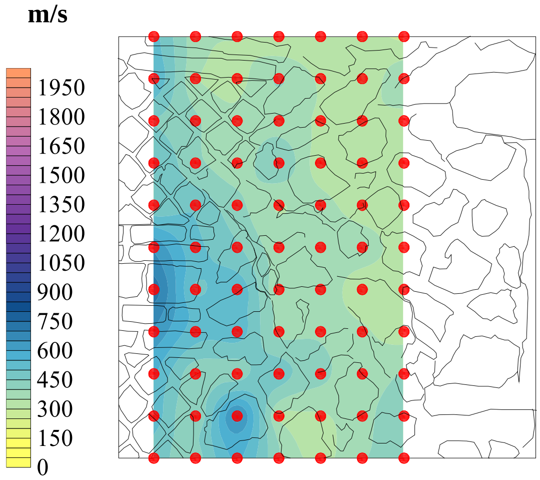

ST3

Masonry ID: ST3	
Masonry description	
Opus incertum masonry prevalently made of irregular travertine units and mortar.	
Localization	
Vicolo dei Balconi, Regio V.	
State of preservation and deterioration	
The masonry surfaces were partially disintegrated, due to weathering. The mortar and the travertine units were friable and tendency to powder.	
Time of excavation	
Newly emerged.	
Modern interventions	
None.	
Pictures	
Hammer-side (N-W)	Receiver-side (S-E)
	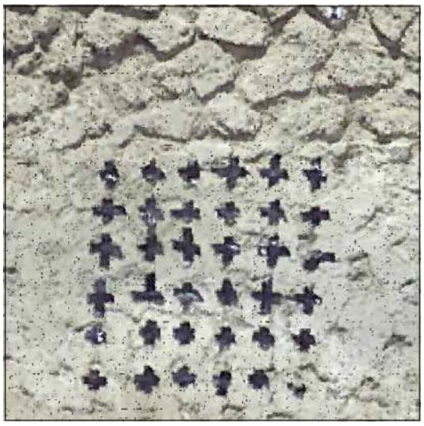

Geometric survey	
Hammer-side (N-W)	Receiver-side (S-E)
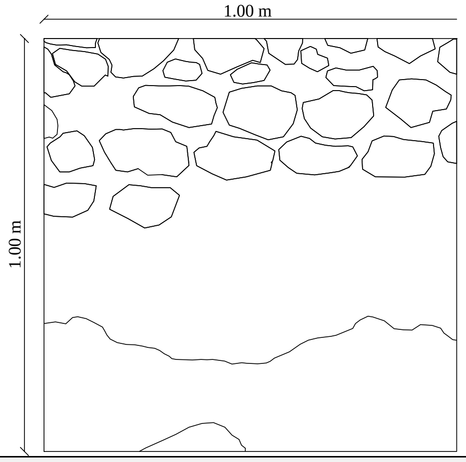	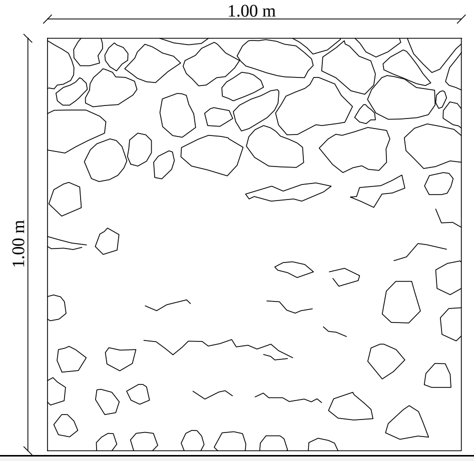

Material survey	
Hammer-side (N-W)	Receiver-side (S-E)
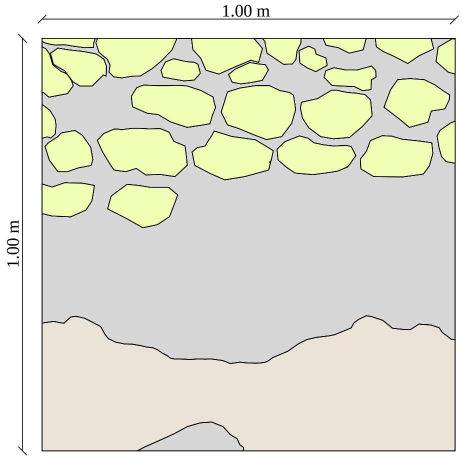	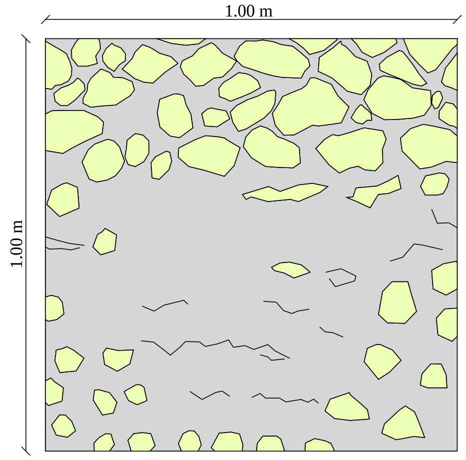

Travertine Lava Foam lava Terracotta Mortar Plaster

Soni test set-up

Wall thickness	Mesh area	Grid spacing	Number of points	Hammer side
0.33m	0.50m x 0.30m	0.10m x 0.10m	24	N-W

Sonic test statistics

V_{mean}	Standard deviation	CoV
518 m/s	190 m/s	37%

Histogram of the recorded velocities and probability density distribution

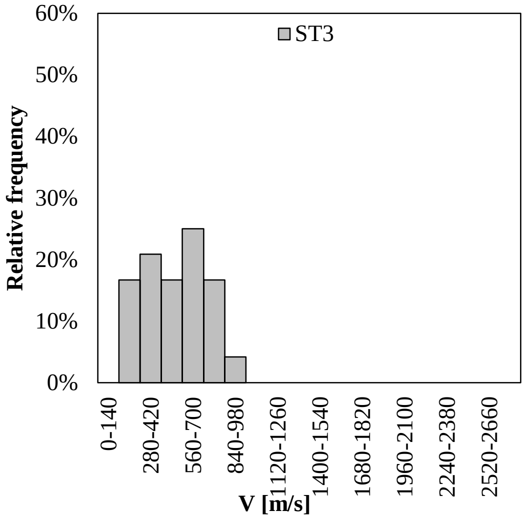

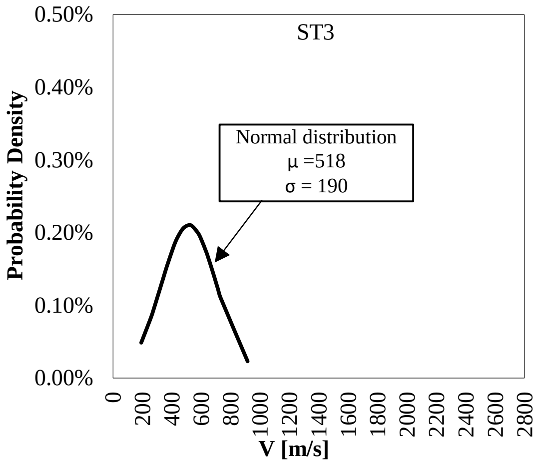

Velocity for each acquisition point

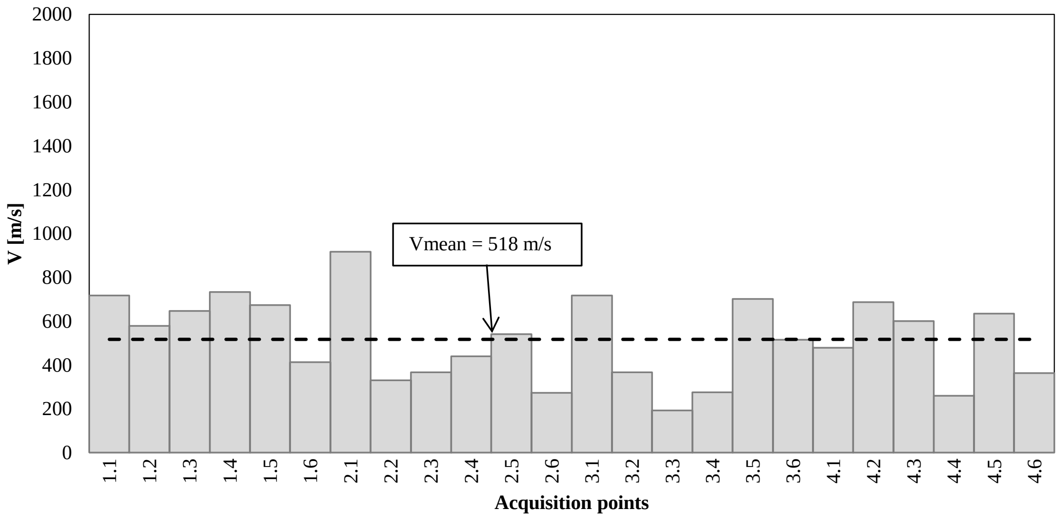

Velocity distribution map

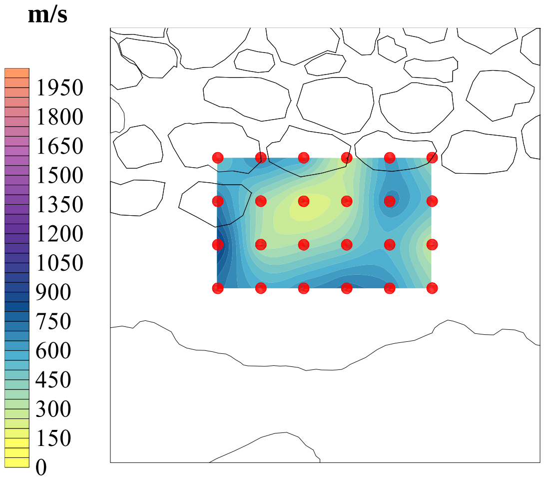

ST6

Masonry ID: ST6
Masonry description
Opus incertum masonry prevalently made of irregular travertine and lava units, with few foam lava units and mortar.
Localization
Vicolo dei Balconi, Regio V.
State of preservation and deterioration
The masonry surfaces were partially disintegrated, due to weathering. The mortar and the travertine units were friable and tendency to powder.
Time of excavation
Newly emerged.
Modern interventions
None.
Pictures

Hammer-side (N-E)

Receiver-side (S-W)

Geometric survey

Hammer-side (N-E)	Receiver-side (S-W)
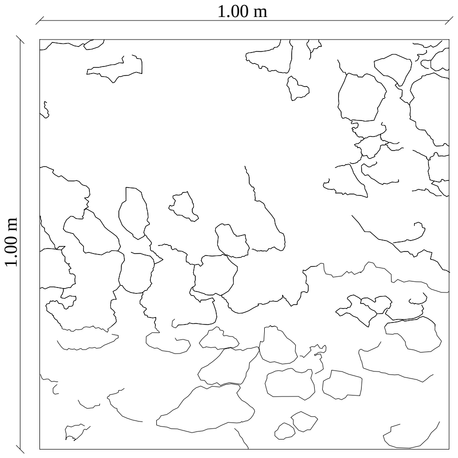	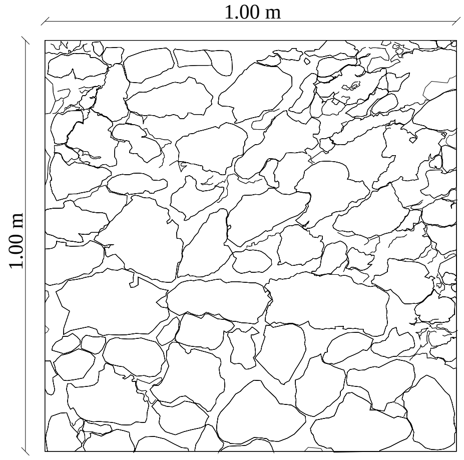

Material survey

Hammer-side (N-E)	Receiver-side (S-W)
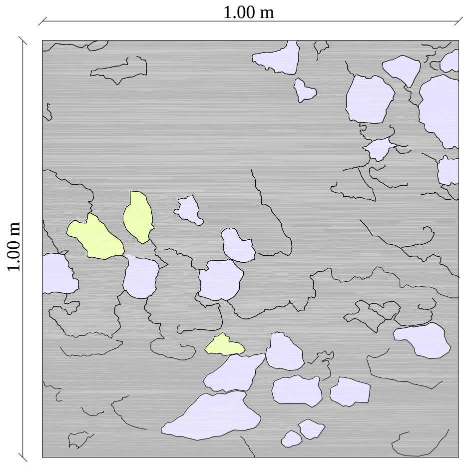	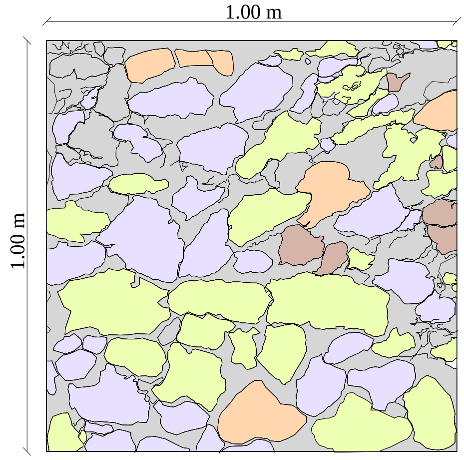

Travertine Lava Foam lava Terracotta Mortar Plaster

Soni test set-up

Wall thickness	Mesh area	Grid spacing	Number of points	Hammer side
0.44m	1.00m x 0.70m	0.10m x 0.10m	88	N-E

Sonic test statistics

V_{mean}	Standard deviation	CoV
591 m/s	165 m/s	28%

Histogram of the recorded velocities and probability density distribution

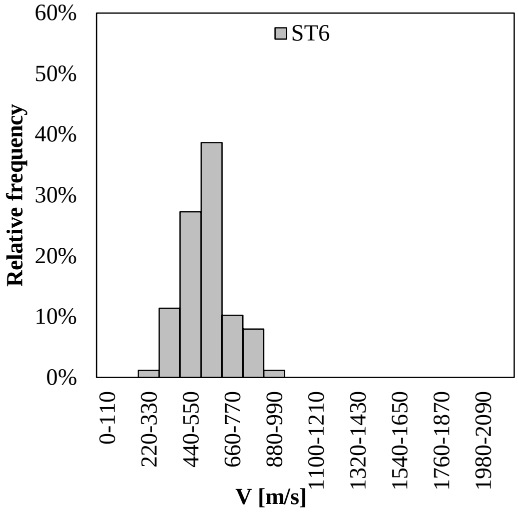

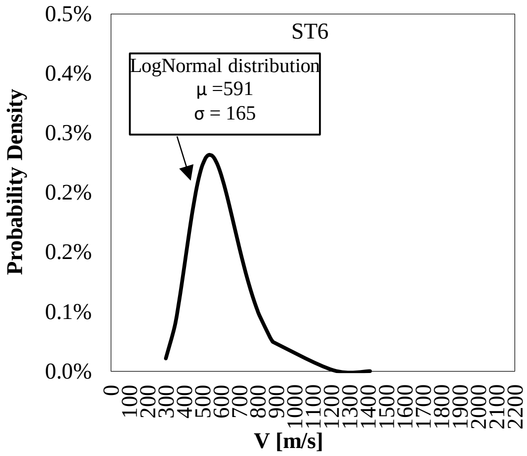

Velocity for each acquisition point

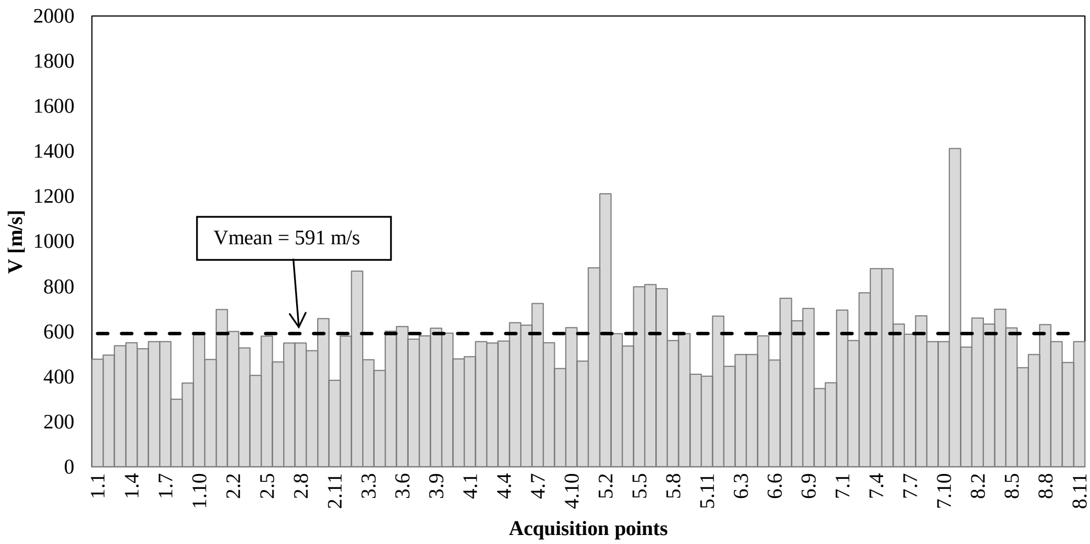

Velocity distribution map
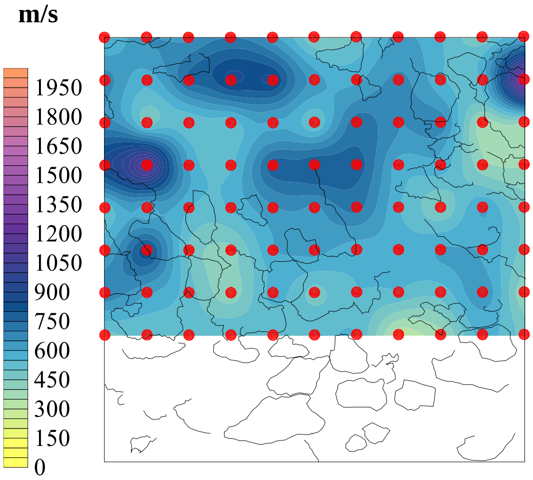

ST7

Masonry ID: ST7	
Masonry description	
Opus incertum masonry prevalently made of irregular travertine units, with few pieces of lava, foam lava units and terracotta fragments, and mortar.	
Localization	
Regio V, Insula 2.	
State of preservation and deterioration	
The masonry surfaces were partially disintegrated, due to weathering. The mortar and the travertine units were friable and tendency to powder.	
Time of excavation	
20th century.	
Modern interventions	
Superficial repointing interventions with modern mortars were carried out after the excavation.	
Pictures	
Hammer-side (S-W)	Receiver-side (N-E)
	

Geometric survey

Hammer-side (S-W)	Receiver-side (N-E)

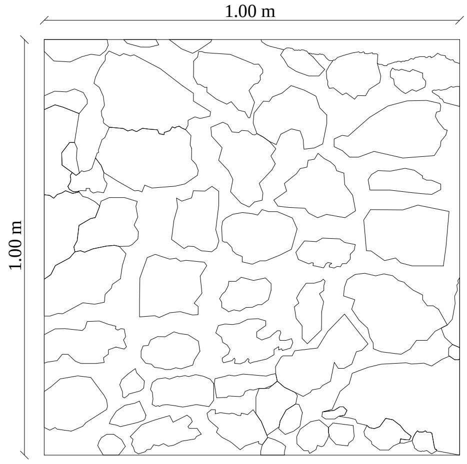

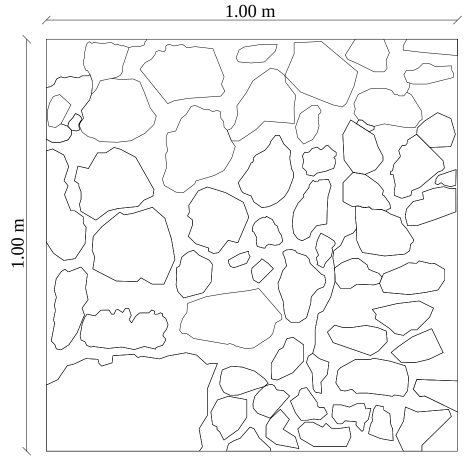

Material survey

Hammer-side (S-W)	Receiver-side (N-E)

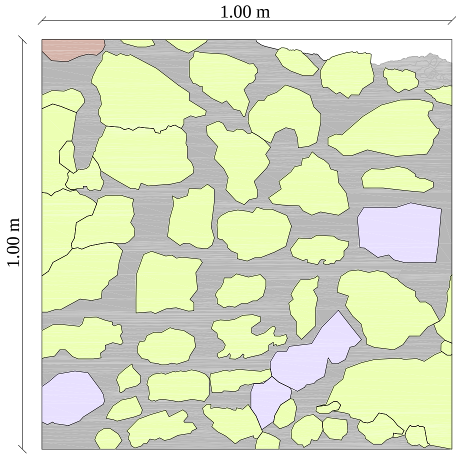

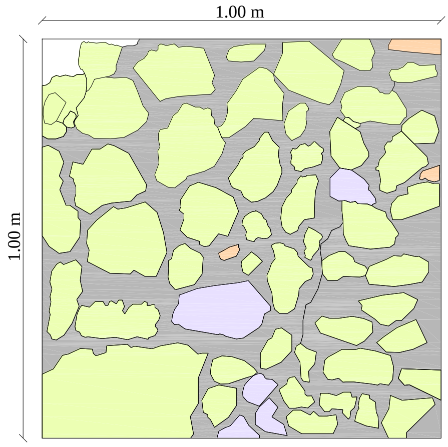

Travertine Lava Foam lava Terracotta Mortar Plaster

Soni test set-up

Wall thickness	Mesh area	Grid spacing	Number of points	Hammer side
0.39m	1.00m x 0.80m	0.10m x 0.10m	99	S-W

Sonic test statistics

V_{mean}	Standard deviation	CoV
669 m/s	438 m/s	65%

Histogram of the recorded velocities and probability density distribution

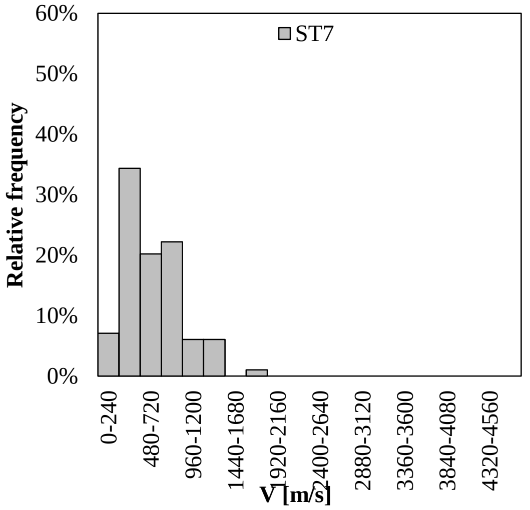

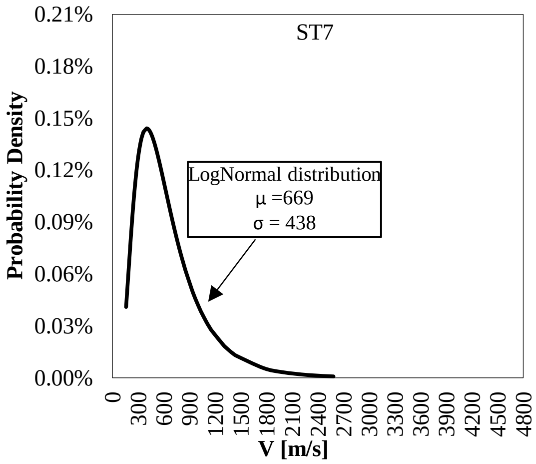

Velocity for each acquisition point

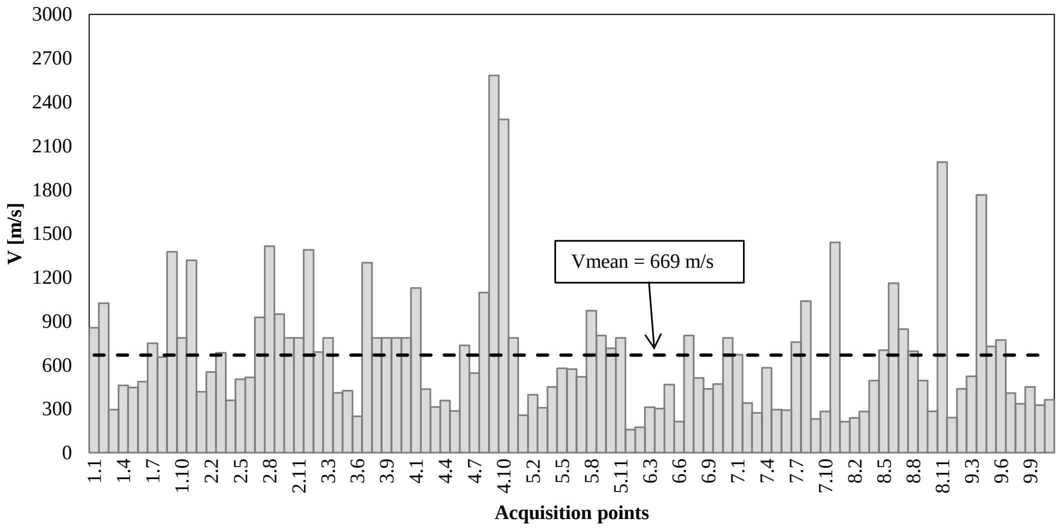

Velocity distribution map

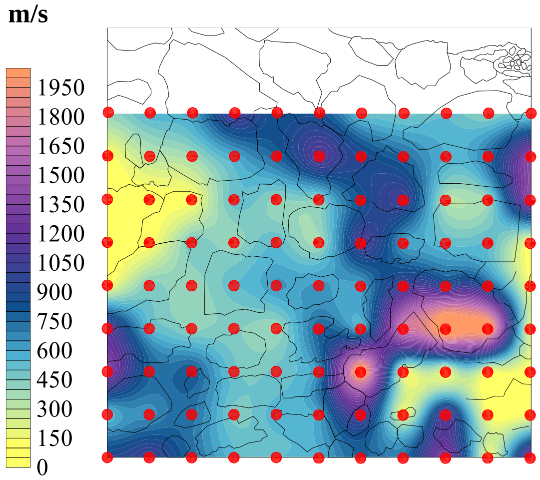

ST8

<table>
<tr><th colspan="2">Masonry ID: ST8</th></tr>
<tr><th colspan="2">Masonry description</th></tr>
<tr><td colspan="2">Opus incertum masonry prevalently made of irregular travertine and lava units, with few foam lava units and mortar.</td></tr>
<tr><th colspan="2">Localization</th></tr>
<tr><td colspan="2">Via del Vesuvio.</td></tr>
<tr><th colspan="2">State of preservation and deterioration</th></tr>
<tr><td colspan="2">The masonry surfaces were partially disintegrated, due to weathering. The mortar and the travertine units were friable and tendency to powder.</td></tr>
<tr><th colspan="2">Time of excavation</th></tr>
<tr><td colspan="2">Newly emerged.</td></tr>
<tr><th colspan="2">Modern interventions</th></tr>
<tr><td colspan="2">None.</td></tr>
<tr><th colspan="2">Pictures</th></tr>
<tr><td>Hammer-side (N-W)
</td><td>Receiver-side (S-E)
</td></tr>
</table>

Geometric survey

Hammer-side (N-W)	Receiver-side (S-E)

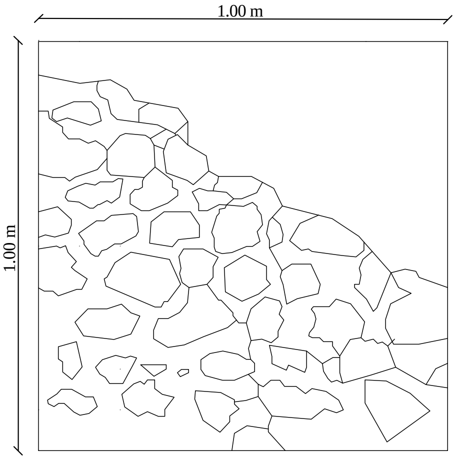

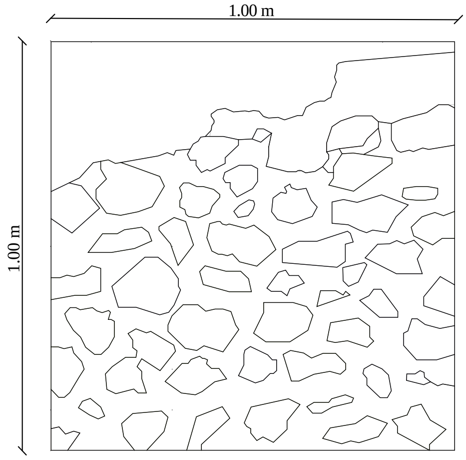

Material survey

Hammer-side (N-W)	Receiver-side (S-E)

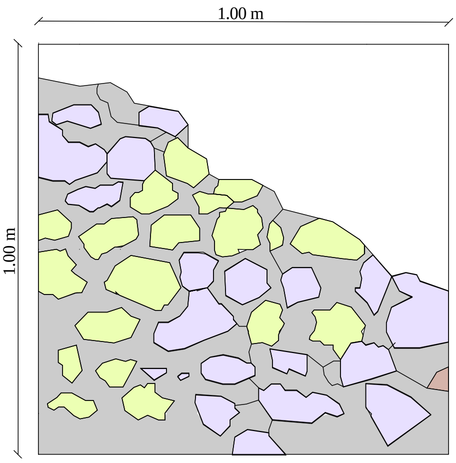

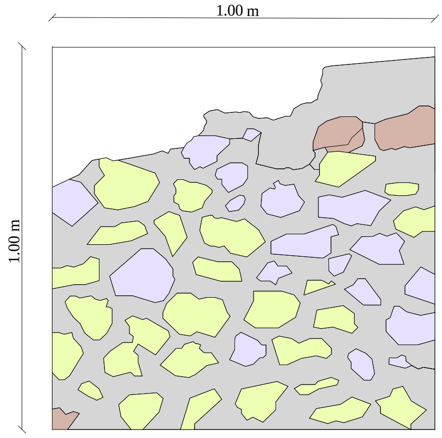

Travertine Lava Foam lava Terracotta Mortar Plaster

Soni test set-up

Wall thickness	Mesh area	Grid spacing	Number of points	Hammer side
0.46m	0.70m x 0.40m	0.10m x 0.10m	40	N-W

Sonic test statistics

V_{mean}	Standard deviation	CoV
742 m/s	255 m/s	34%

Histogram of the recorded velocities and probability density distribution

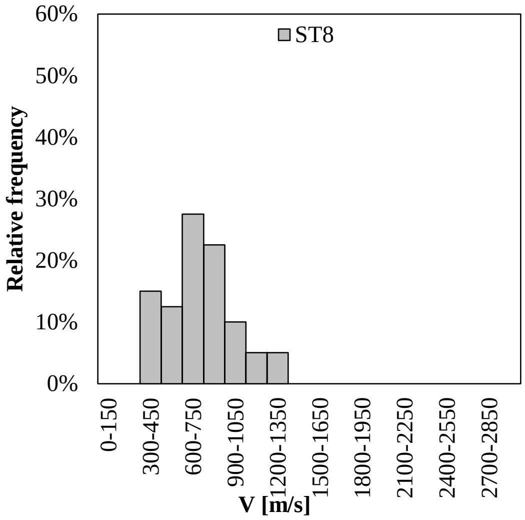

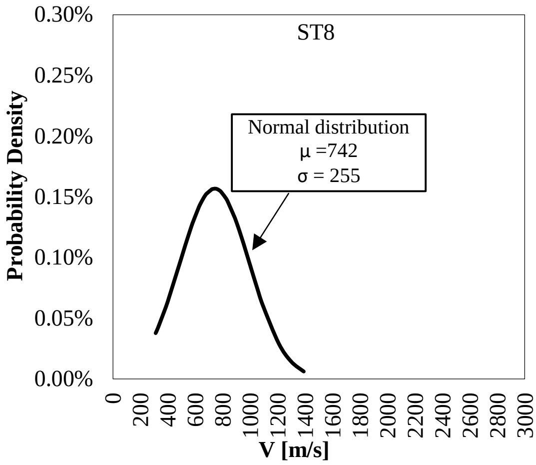

Velocity for each acquisition point

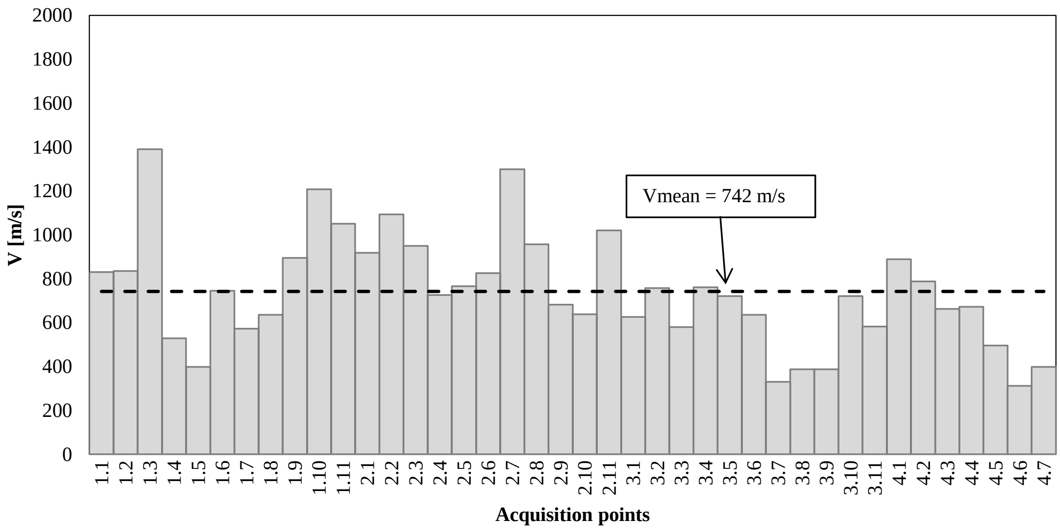

Velocity distribution map

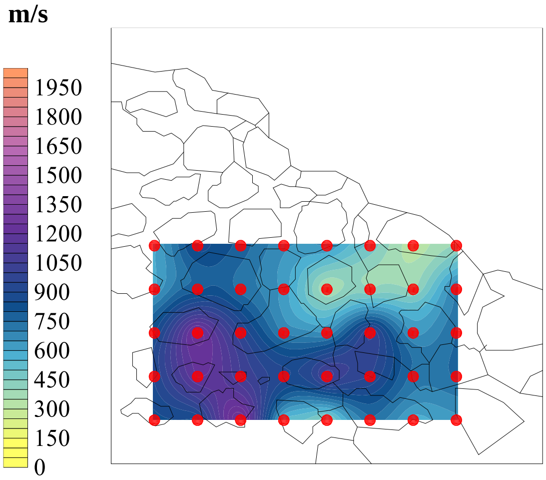

ST9

Masonry ID: ST9	
Masonry description	
Opus incertum masonry prevalently made of irregular travertine and lava units, with few foam lava units and mortar.	
Localization	
Regio V, Insula 3.	
State of preservation and deterioration	
The masonry surfaces were partially disintegrated, due to weathering. The mortar and the travertine units were friable and tendency to powder.	
Time of excavation	
Newly emerged.	
Modern interventions	
None.	
Pictures	
Hammer-side (S)	Receiver-side (N)
	

Geometric survey

Hammer-side (S)

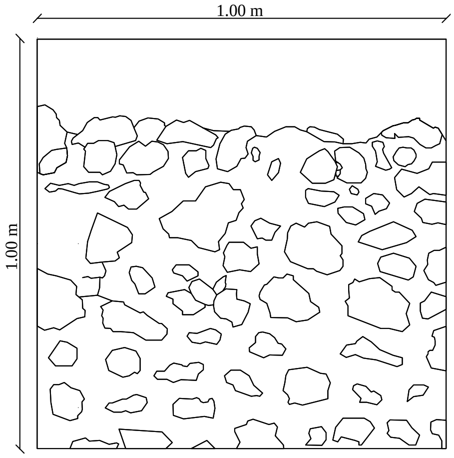

Receiver-side (N)

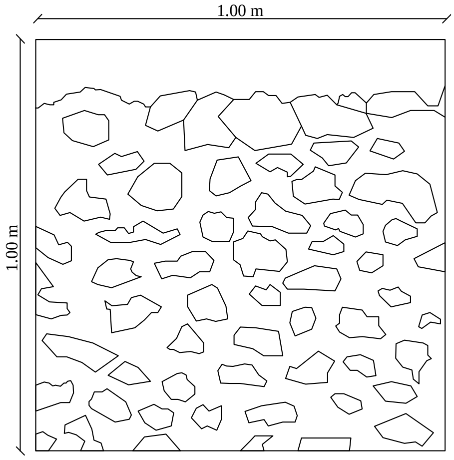

Material survey

Hammer-side (S)

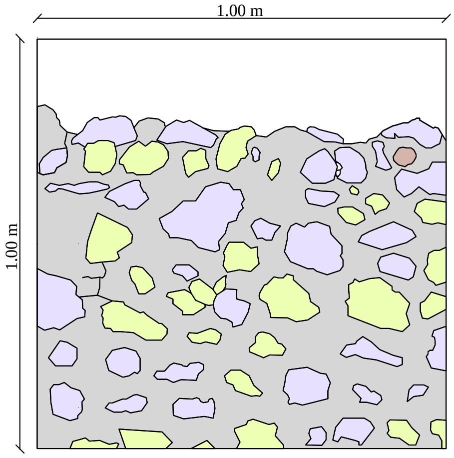

Receiver-side (N)

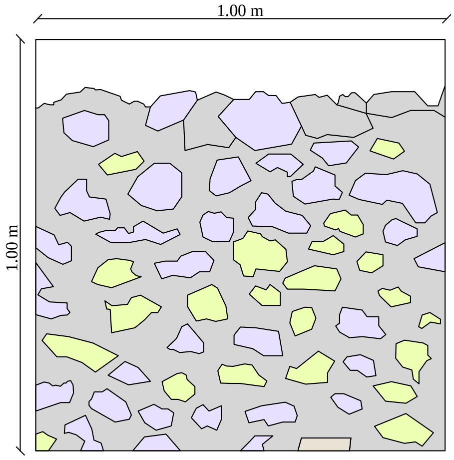

Travertine Lava Foam lava Terracotta Mortar Plaster

Soni test set-up

Wall thickness	Mesh area	Grid spacing	Number of points	Hammer side
0.36m	1.00m x 0.50m	0.10m x 0.10m	66	S

Sonic test statistics

V_{mean}	Standard deviation	CoV
747 m/s	262 m/s	35%

Histogram of the recorded velocities and probability density distribution

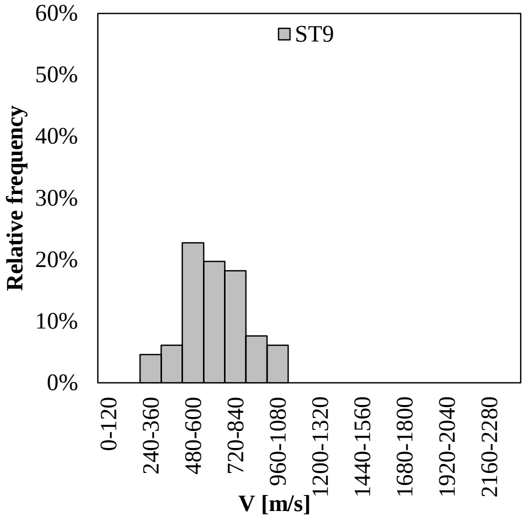

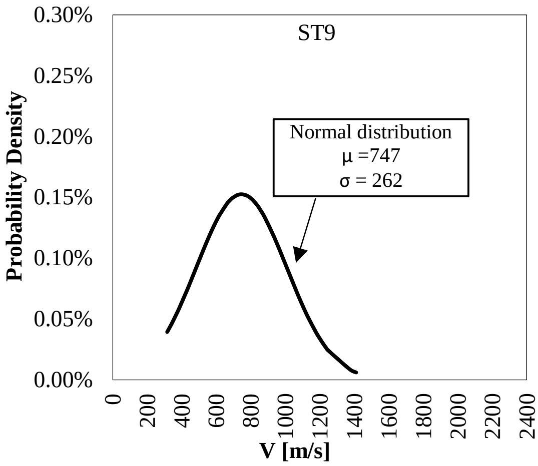

Velocity for each acquisition point

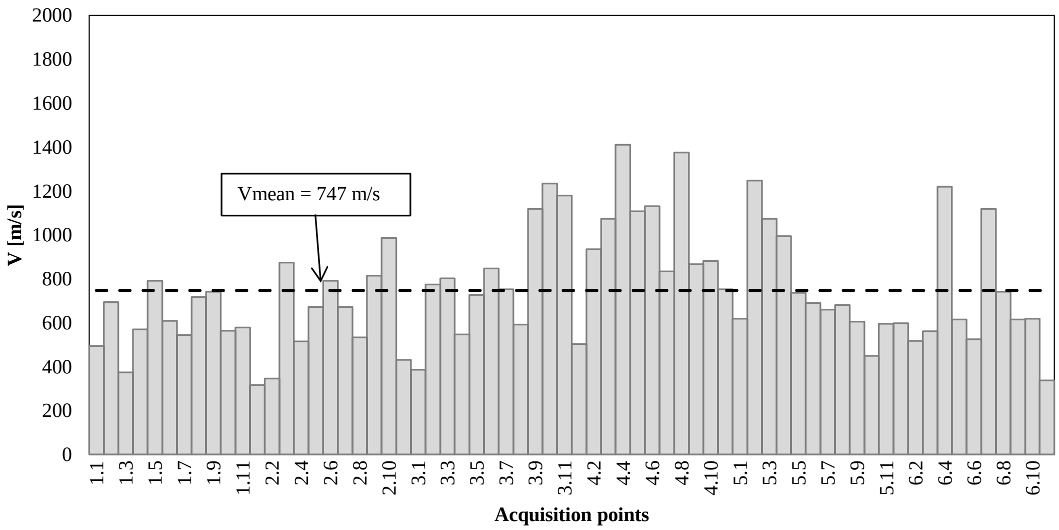

Velocity distribution map
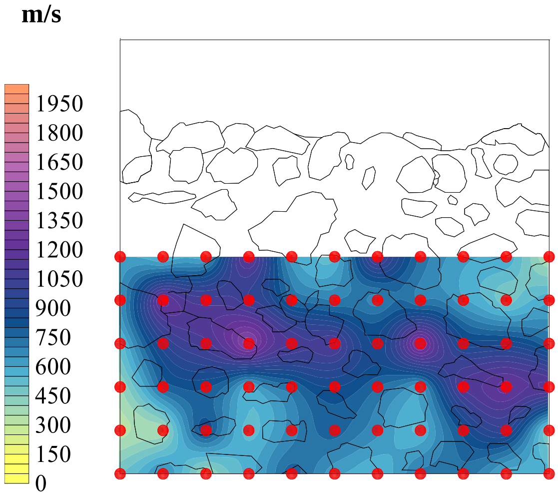

ST11

Masonry ID: ST11
Masonry description
Opus incertum masonry prevalently made of irregular travertine and lava units, with few foam lava units and mortar.
Localization
Vicolo dei Balconi.
State of preservation and deterioration
The masonry surfaces were partially disintegrated, due to weathering. The mortar and the travertine units were friable and tendency to powder.
Time of excavation
20^{th} century.
Modern interventions
The masonry portion was rebuilt after the excavation with modern mortar and original stones.
Pictures

Hammer-side (N-E)

Receiver-side (S-W)

Geometric survey

Hammer-side (N-E)	Receiver-side (S-W)
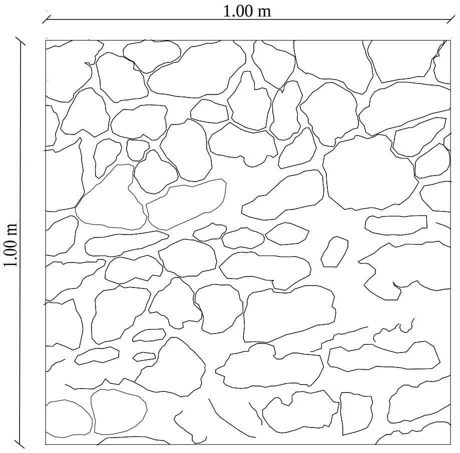	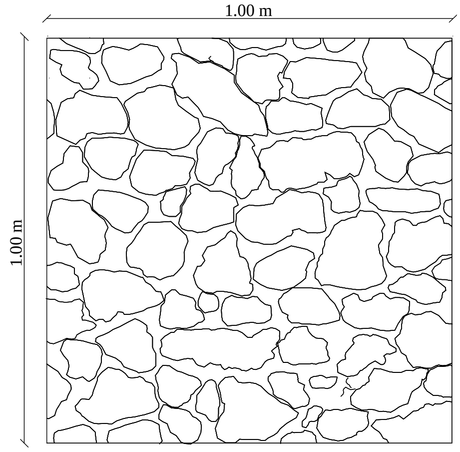

Material survey

Hammer-side (N-E)	Receiver-side (S-W)
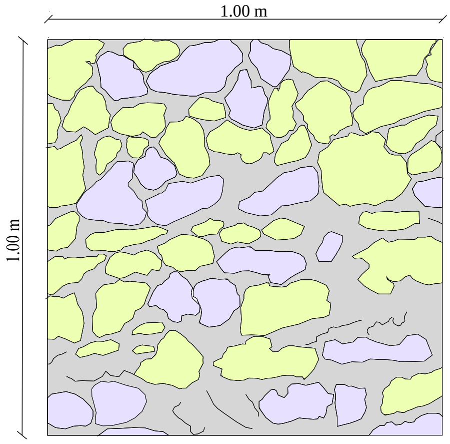	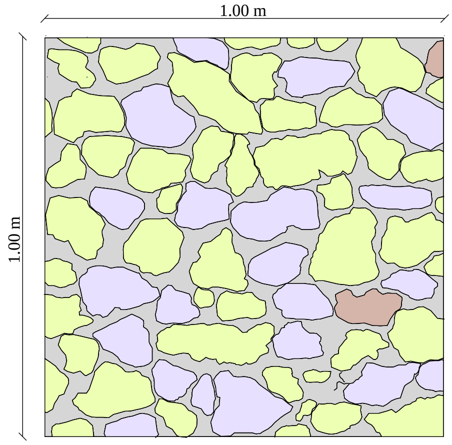

Travertine Lava Foam lava Terracotta Mortar Plaster

Soni test set-up

Wall thickness	Mesh area	Grid spacing	Number of points	Hammer side
0.41m	1.00m x 1.00m	0.10m x 0.10m	121	N-E

Sonic test statistics

V_{mean}	Standard deviation	CoV
1560 m/s	342 m/s	22%

Histogram of the recorded velocities and probability density distribution

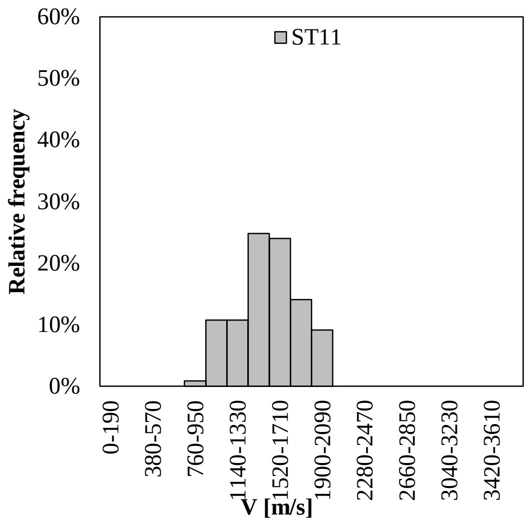

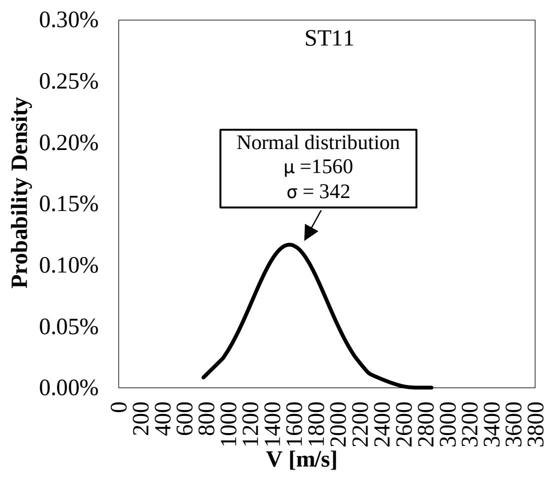

Velocity for each acquisition point

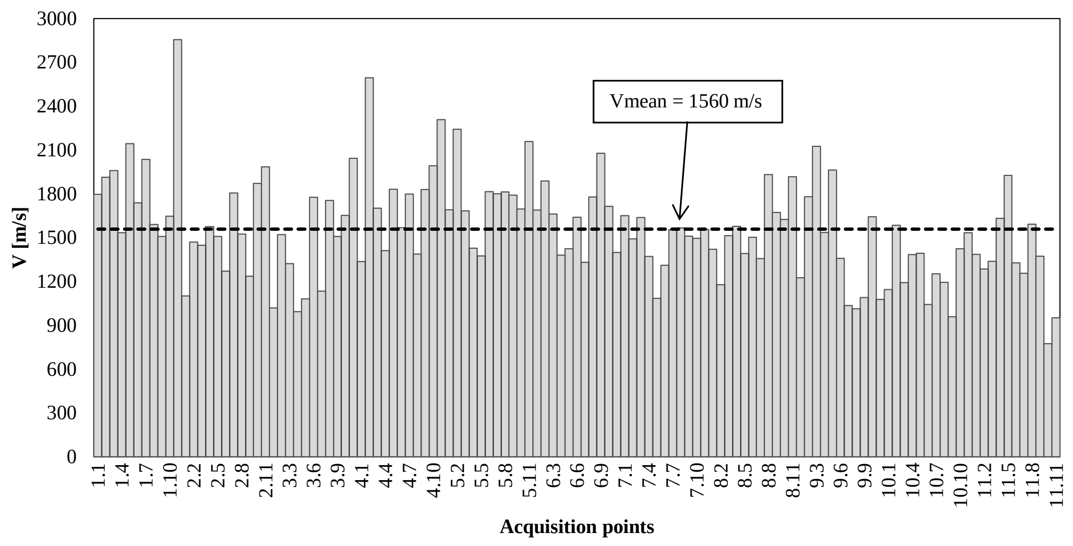

Velocity distribution map

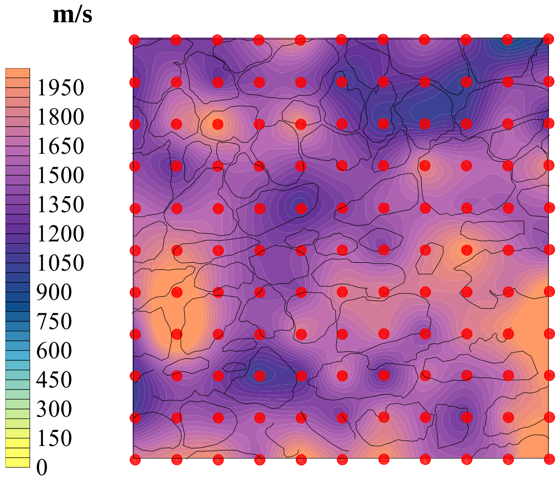

ANNEX 2)

Diagrams of velocities of columns from Casa del Fauno under eight seismic motions

Irpinia-Struno seismic record

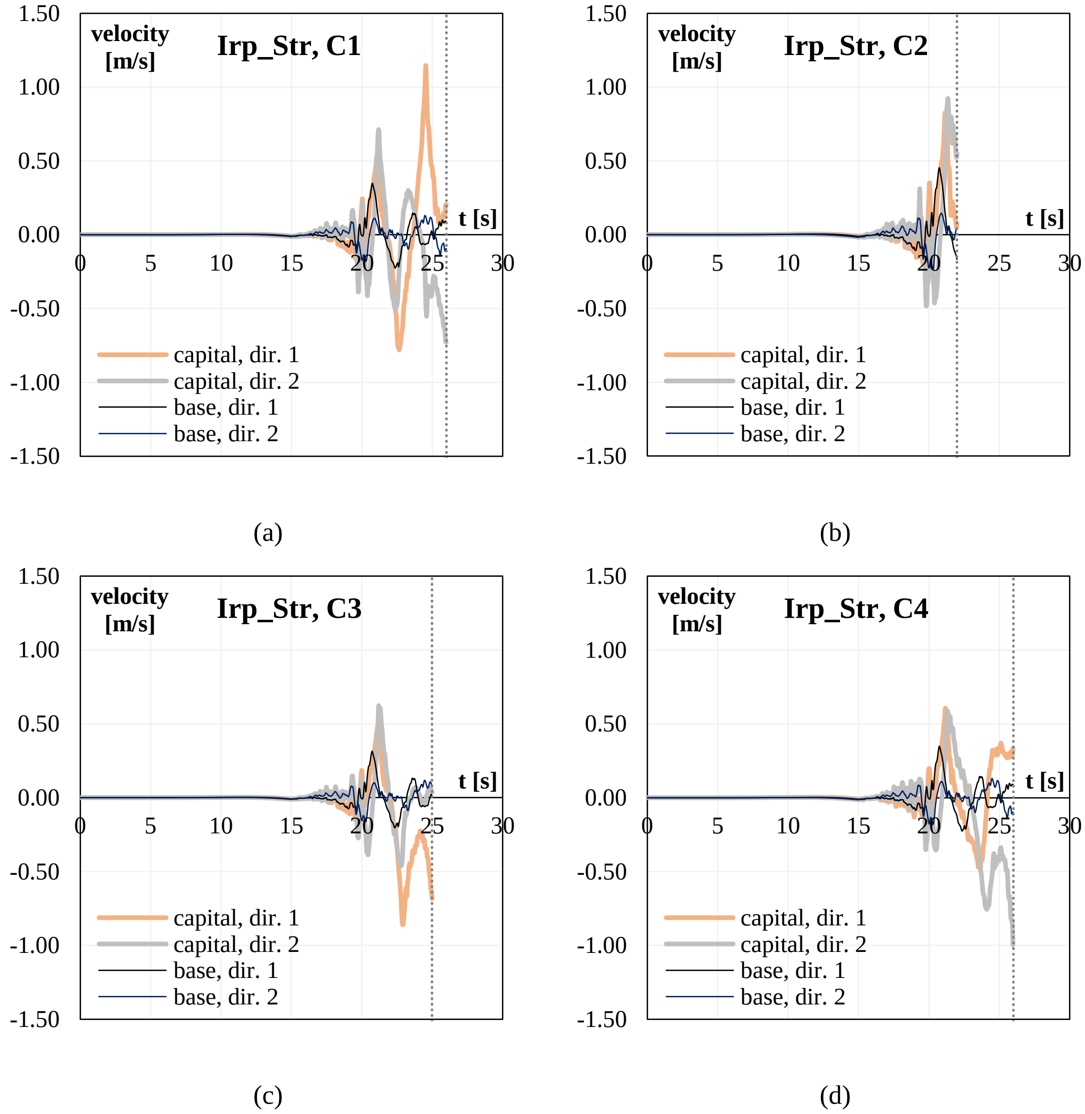

Diagrams of velocities in two orthogonal directions at the capital and base of columns 1 (a), 2 (b), 3 (c), and 4 (d) under the Irpinia-Struno input motion.

Irpinia-Torre del Greco seismic record

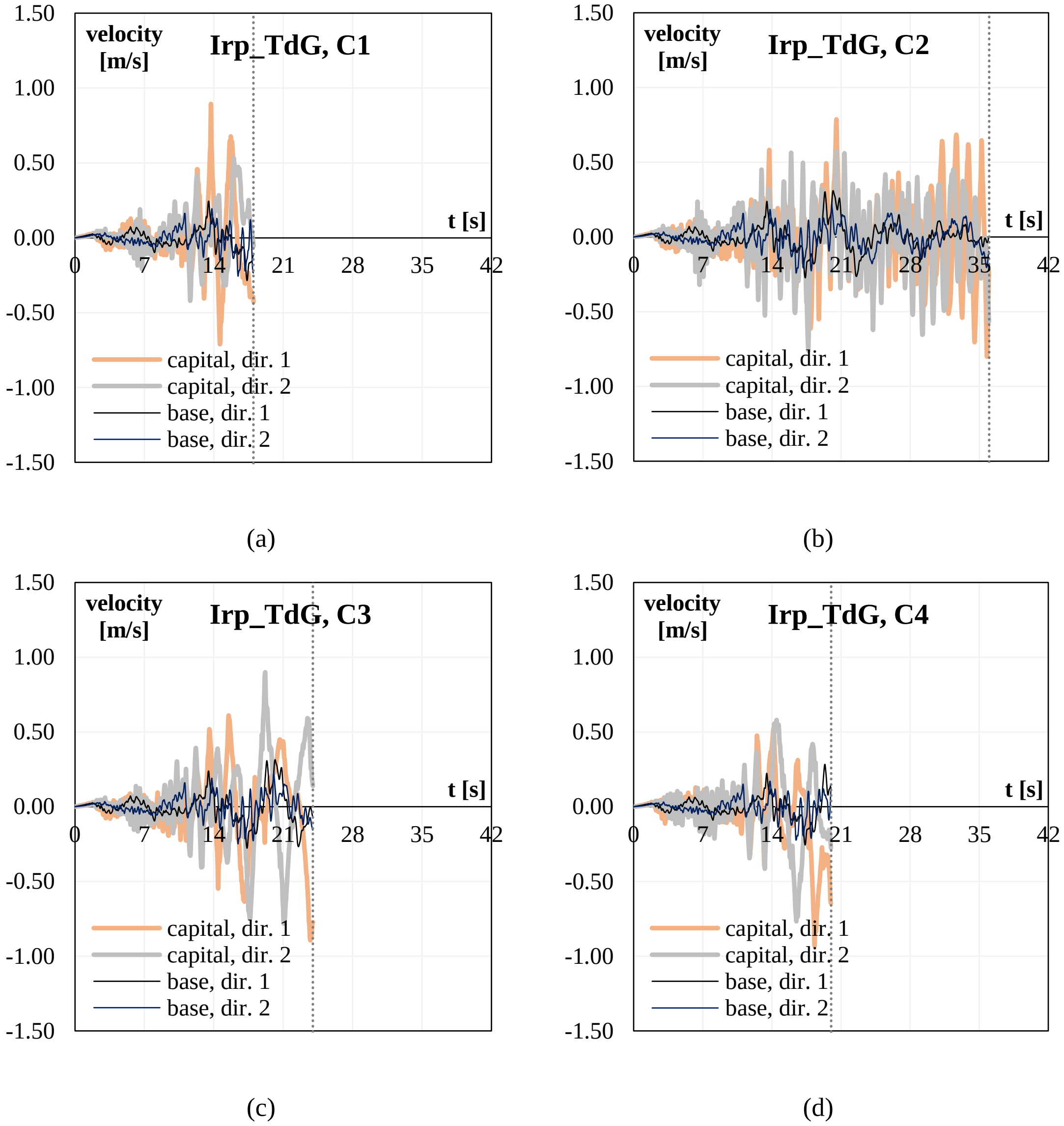

Diagrams of velocities in two orthogonal directions at the capital and base of columns 1 (a), 2 (b), 3 (c), and 4 (d) under the Irpinia-Torre del Greco input motion.

L’Aquila seismic record

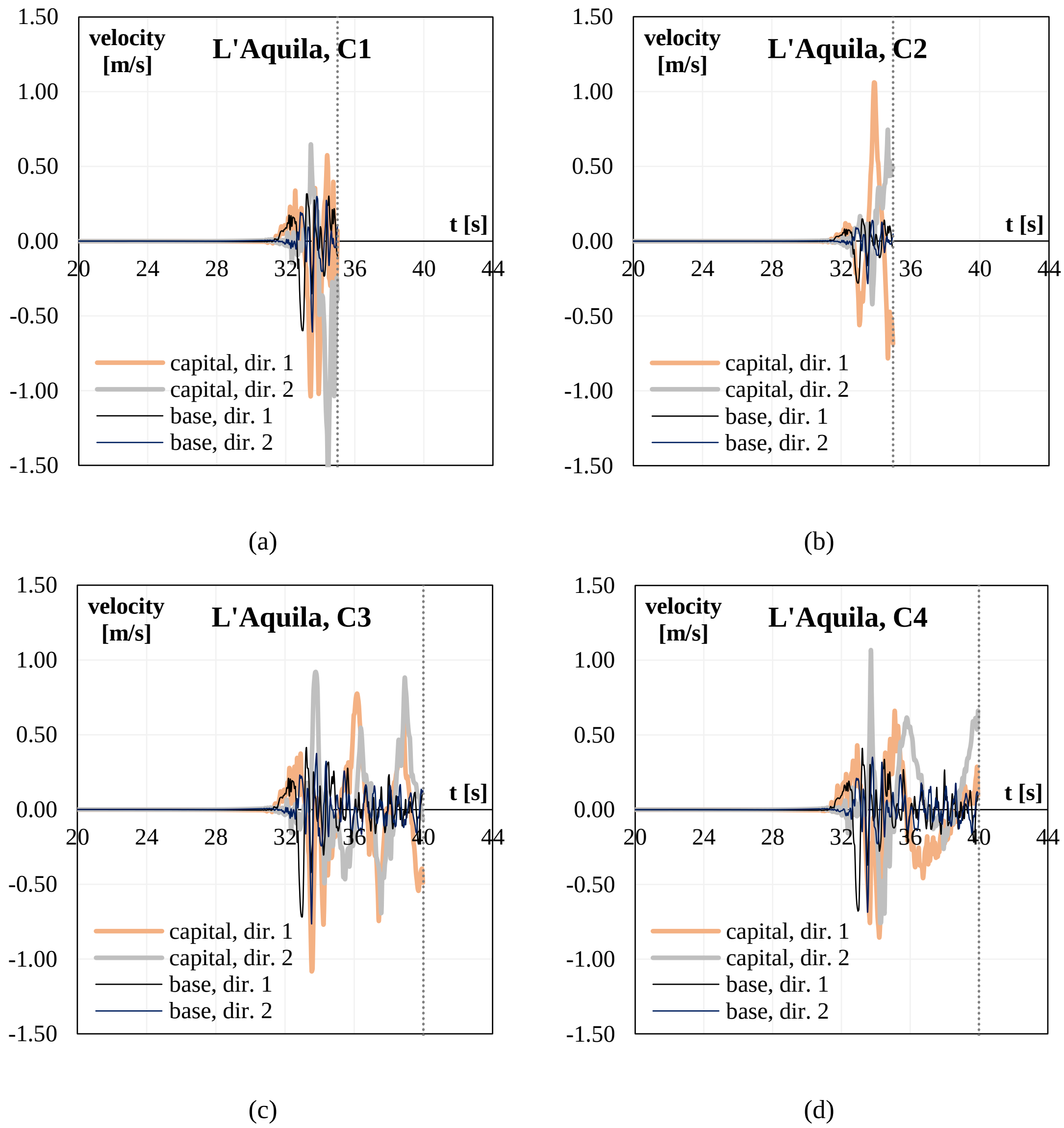

Diagrams of velocities in two orthogonal directions at the capital and base of columns 1 (a), 2 (b), 3 (c), and 4 (d) under the L’Aquila input motion.

Molise seismic record

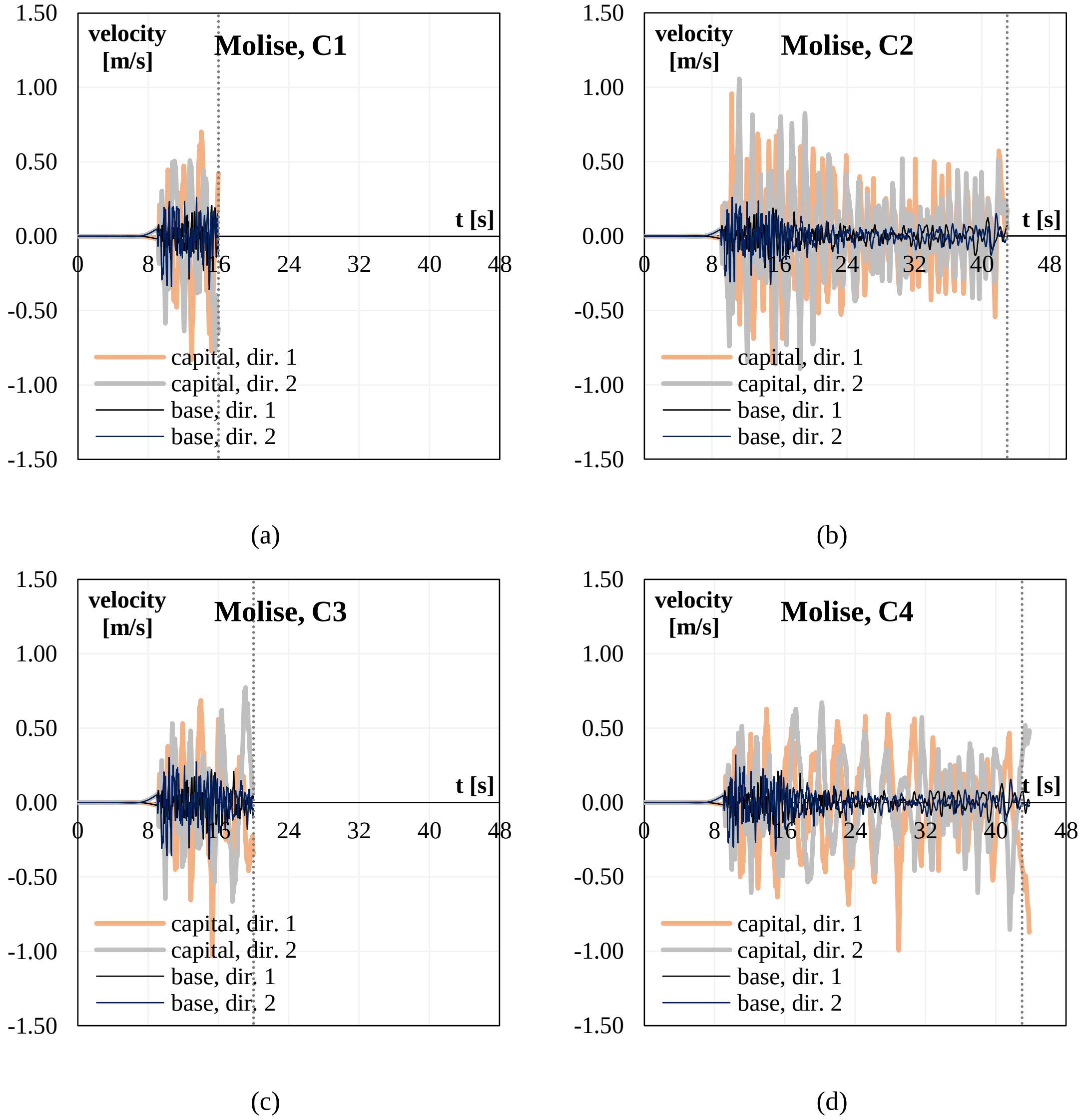

Diagrams of velocities in two orthogonal directions at the capital and base of columns 1 (a), 2 (b), 3 (c), and 4 (d) under the Molise input motion.

Kalamata seismic record

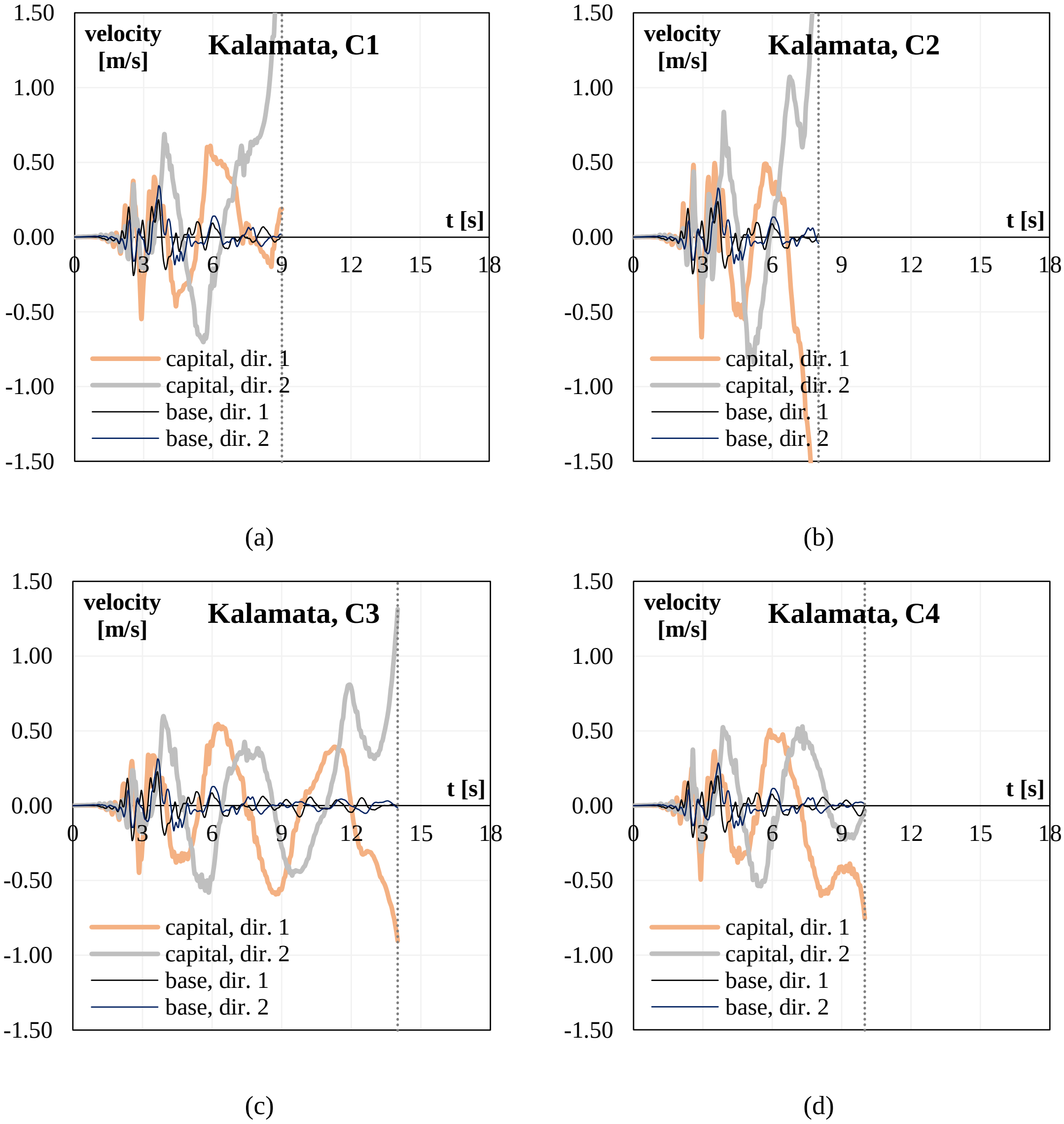

Diagrams of velocities in two orthogonal directions at the capital and base of columns 1 (a), 2 (b), 3 (c), and 4 (d) under the Kalamata input motion.

Edessa seismic record

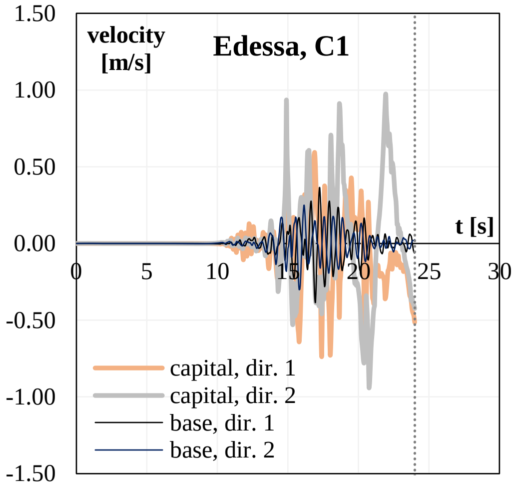

(a)

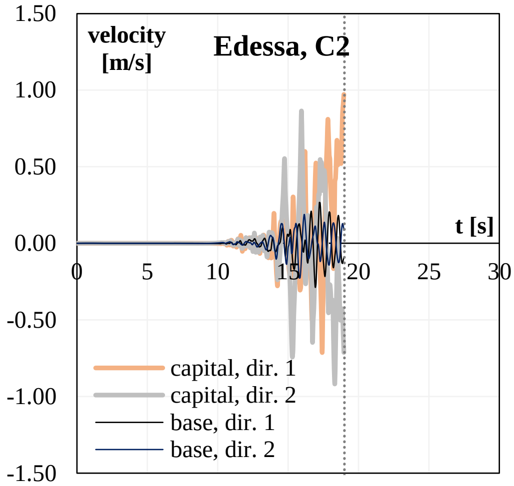

(b)

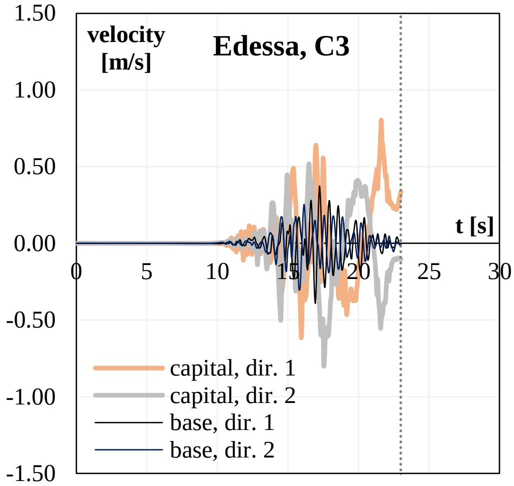

(c)

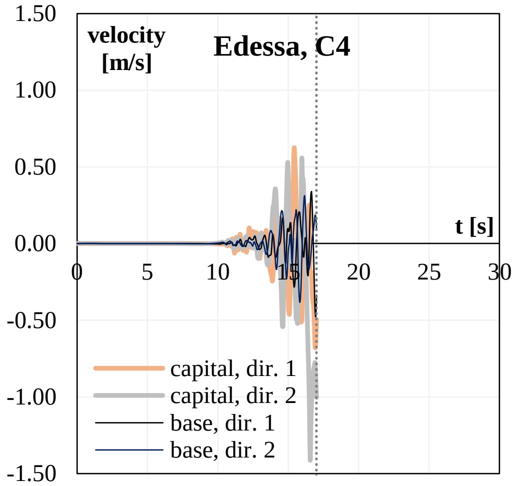

(d)

Diagrams of velocities in two orthogonal directions at the capital and base of columns 1 (a), 2 (b), 3 (c), and 4 (d) under the Edessa input motion.

Aigio seismic record

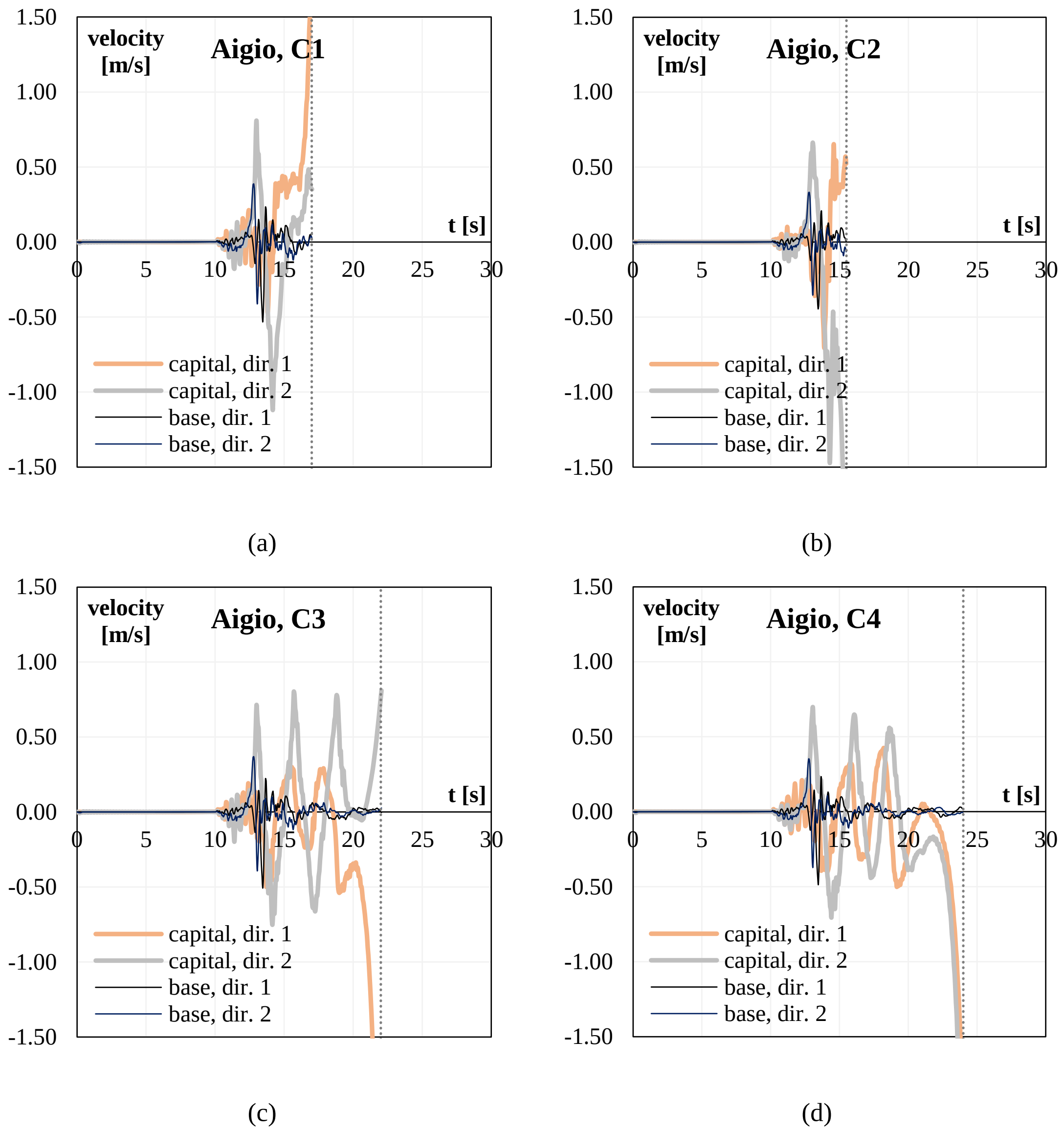

Diagrams of velocities in two orthogonal directions at the capital and base of columns 1 (a), 2 (b), 3 (c), and 4 (d) under the Aigio input motion.

Athens seismic record

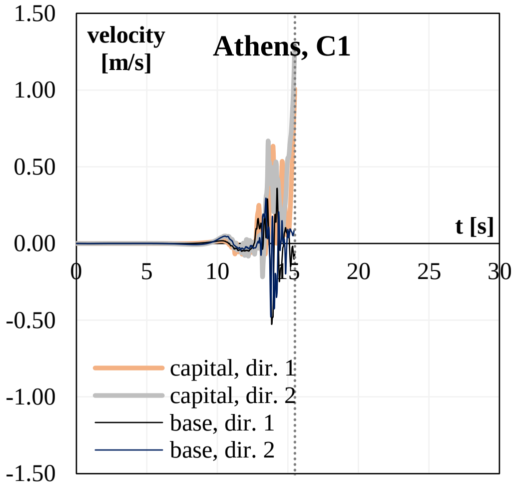

(a)

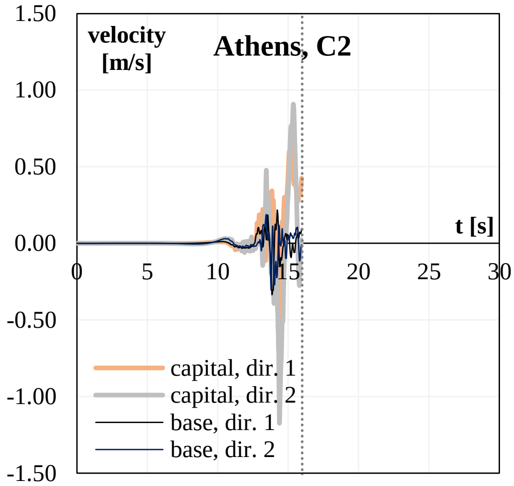

(b)

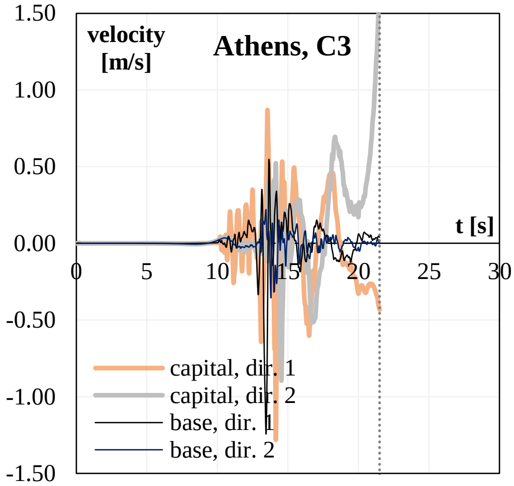

(c)

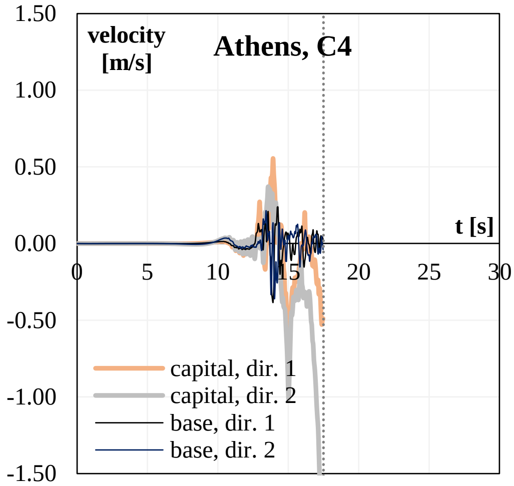

(d)

Diagrams of velocities in two orthogonal directions at the capital and base of columns 1 (a), 2 (b), 3 (c), and 4 (d) under the Athens input motion.

REFERENCES

ACI. (2003). “In-Place Methods to Estimate Concrete Strength.”

Adam, J.-P. (1986). “Observations techniques sur les suites du séisme de 62 à Pompéi.” *Tremblements de terre, éruptions volcaniques et vie des hommes dans la Campanie antique, Naples: Bibliothèque de l’Institut français de Naples, Centre Jean Bérard*, 67–87.

Adam, J. P. (2014). *L’arte di costruire presso i romani. Materiali e tecniche.* Milan.

Aggelakopoulou, E., Bakolas, A., and Moropoulou, A. (2019). “Lime putty versus hydrated lime powder: Physicochemical and mechanical characteristics of lime based mortars.” *Construction and Building Materials*, Elsevier Ltd, 225, 633–641.

ASTM. (1970). “D3148 - 02. Standard method of test for elastic moduli of rock core specimens in uniaxial compression.” *International society for rock mechanics*, 04(April 1997), 138–140.

ASTM. (1981). “D 5873 - 00. Determination of Rock Hardness by Rebound Hammer Method 1.” *Current*, 4–7.

ASTM. (2002). “E 519-02. Standard Test Method for Diagonal Tension (Shear) in Masonry Assemblages.” *American Society for Testing Materials*, 5.

ASTM. (2003). “C 597 - 02. Pulse Velocity Through Concrete.” *United States: American Society for Testing and Material.*, 04(02), 3–6.

ASTM. (2017). “D2845 - 08. Standard Test Method for Laboratory Determination of Pulse Velocities and Ultrasonic Elastic Constants of Rock.”

Atkinson, R. H., Bamford, W. E., Broch, E., Deere, D. U., Franklin, J. A., Nieble, C., Rummel, F., Tarkoy, P. J., and van Duyse, H. (1978). “Suggested Methods for Determining Hardness and Abrasiveness of Rocks.” *International Journal of Rock Mechanics and Mining Sciences*, 15(3), 89–97.

Balksten, K., and Steenari, B.-M. (2008). “A method to recreate historic mortars applied at Norrlanda church on the Island of Gotland , Sweden.” *Proceedings of Historical Mortars Conference HMC-2008, Lisbon, Portugal 2008*.

Baronio, G., and Binda, L. (1991). “EXPERIMENT AL APPROACH TO A PROCEDURE FOR THE INVESTIGATION OF HISTORIC MORTARS.” *9th Int. Brick-Block Masonry Conference*, 1397–1405.

Baronio, G., Binda, L., and Saisi, A. (1999). “Mechanical and Physical Behaviour of Lime Mortars Reproduced After the Characterisation of Historic Mortar.” *International RILEM Workshop on Historic Mortars: Characteristics and Tests*, 307–325.

Baronio, G., Binda, L., Tedeschi, C., and Tiraboschi, C. (2003). “Characterisation of the materials used in the construction of the Noto Cathedral.” *Construction and Building Materials*, 17(8), 557–571.

Binda, L. (2005). “2.4 Mechanical tests on mortars and assemblages.” (March), 57–76.

Binda, L., Cantini, L., Fernandes, F., Saisi, A., Tedeschi, C., and Zanzi, L. (2004). “Diagnostic Investigation on the Historical Masonry Structures of a Castle By the Complementary Use of Non Destructive.” *Brick and Block Masonry International Conference*, 1–10.

Binda, L., Saisi, A., and Tiraboschi, C. (2000). “Investigation procedures for the diagnosis of historic masonries.” *Construction and Building Materials*, 14(4), 199–233.

Binda, L., Saisi, A., and Tiraboschi, C. (2001). “Application of sonic tests to the diagnosis of damaged and repaired structures.” *NDT and E International*, 34(2), 123–138.

Binda, L., Saisi, A., and Zanzi, L. (2003). “Sonic tomography and flat-jack tests as complementary investigation procedures for the stone pillars of the temple of S. Nicolò 1’Arena (Italy).” *NDT and E International*, 36(4), 215–227.

Bonazzi, A., Santoro, S., and Mastrobattista, E. (2007). “Caratterizzazione archeometrica delle malte e degli intonaci dell’Insula del Centenario.” *Pompei. Insula del Centenario (IX, 8), I. Indagini diagnostiche geofisiche e analisi archeometriche*, Ante Quem, Bologna, 93-128.

Borri, A., Castori, G., Corradi, M., and Speranzini, E. (2011). “Shear behavior of unreinforced and reinforced masonry panels subjected to in situ diagonal compression tests.” *Construction and Building Materials*, Elsevier Ltd, 25(12), 4403–4414.

Brignola, A., Frumento, S., Lagomarsino, S., and Podestá, S. (2009). “Identification of shear parameters of masonry panels through the in-situ diagonal compression test.” *International Journal of Architectural Heritage*, 3(1), 52–73.

Calvanese, V., and Zambrano, A. (2021). “A Conceptual Design Approach for Archaeological Structures , a Challenging Issue between Innovation and Conservation : A Studied Case in Ancient Pompeii.”

Cantini, L. (2016). “The diagnostic investigations plan for historic masonry buildings: The role of sonic tests and other minor destructive techniques.” *Brick and Block Masonry – Trends, Innovations and Challenges*, C. Modena, F. Da Porto, and M. R. Valluzzi, eds., Taylor & Francis Group, Padua.

Capasso, G. (2002). *Viaggio a Pompei. Passeggiate virtuali nelle città perdute*. CAPWARE.

CEN. (1999a). “EN 1052-1. Methods of test for masonry - Part 1: Determination of compressive strength.” *European Committee for standardization*, 10969.

CEN. (1999b). “EN 1097-3:1998 Tests for mechanical and physical properties of aggregates - Part 3: Determination of loose bulk density and voids.”

CEN. (2003). “EN 1926:2000. Natural stone test methods - Determination of compressive strength.”

CEN. (2004). “EN 1015-3:1999 Methods of test for mortar for masonry - Part 3: Determination of consistence of fresh mortar (by flow table).”

CEN. (2005a). “EN 14579. Natural stone test methods - Determination of sound speed propagation.”

CEN. (2005b). “EN 12504-4. Testing concrete - Determination of pulse velocity.”

CEN. (2005c). “EN 196-1:2016 Methods of testing cement. Part 1: Determination of strength.” 3(August).

CEN. (2007a). “EN 1015-11:2019 Methods of test for mortar for masonry - Part 11: Determination of flexural and compressive strength of hardened mortar.”

CEN. (2007b). “EN 1015-6:1998 Methods of test for mortar for masonry - Part 6: Determination of bulk density of fresh mortar.”

CEN. (2010). “EN 459-2:2010 Building lime. Part 2: Test methods.”

CEN. (2012a). "EN 12504-2. Testing concrete in structures - Determination of rebound number."

CEN. (2012b). "EN 933-1:2012 Tests for geometrical properties of aggragates - Part 1: Determination of particle size distribution - Sieving method."

CEN. (2013). "EN 12390-13:2013 Testing hardened concrete. Part 13: Determination of secant modulus of elasticity in compression."

CEN. (2015). "EN 459-1:2015 Building lime - Part 1: Definitions, specifications and conformity criteria."

Cescatti, E., Rosato, L., Valluzzi, M. R., and Casarin, F. (2019). "An Automatic Algorithm for the Execution and Elaboration of Sonic Pulse Velocity Tests in Direct and Tomographic Arrangements." Springer International Publishing, 716–724.

Chiostrini, S., Galano, L., and Vignoli, A. (2000). "On the Determination of Strength of Ancient Masonry Walls via Experimental Tests." *12th World Conference on Earthquake Engineering*, 1–8.

Christaras, B. (1996). "Non destructive methods for investigation of some mechanical properties of natural stones in the protection of monuments." *Bulletin of the International Association of Engineering Geology*, 54(1), 59–63.

Cizer, O. (2009). "Competition between carbonation and hydration on the hardening of calcium hydroxide and calcium silicate binders." *Competition between carbonation and hydration on the hardening of calcium hydroxide and calcium silicate binders*, (Intergovernmental Panel on Climate Change, ed.), Cambridge University Press, Heverlee.

Colla, C., Das, P. C., McCann, D., and Forde, M. C. (1997). "Sonic, electromagnetic and impulse radar investigation of stone masonry bridges." *NDT and E International*, 30(4), 249–254.

D.Lgs 42. (2004). "Decreto Legislativo 22 gennaio 2004, n. 42. Codice dei beni culturali e del paesaggio, ai sensi dell'articolo 10 della legge 6 luglio 2002, n. 137."

D'Agostino, S., Cairoli Giuliani, F., Conforto, M. L., and Guidoboni, E. (2009). "Recommendations for drawing up projects and carrying out interventions for the conservation of the archaeological built heritage." 61–112.

DeJong, M. J., and Dimitrakopoulos, E. G. (2014). "Dynamically equivalent rocking structures." *Earthquake Engineering & Structural Dynamics*, 43(10), 1543–1563.

Dessales, H., Boust, C., Carrive, M., Cavero, J., Chapelin, G., Coutelas, A., Deiana, R., De Martino, G., Di Ludovico, M., Dubouloz, J., D'Harcourt, A., Letellier-Taillefer, Éloïse Lorenzoni, F., Maigret, A., Manfredi, G., Marchand-Beaulieu, F., Mauro, A., Milanese, A., Modena, C., Monier, F., Pimpaud, A.-B., Ponce, J., Prota, A., Rizzo, E., Rossi, A., Santoriellov, A., Tricoche, A., and Valluzzi, M. R. (2020). *The Villa of Diomedes. The making of a Roman villa in Pompeii*. (H. Dessales, ed.), Hermann, Paris.

Dessales, H., Ponce, J., Boust, C., Chapelin, G., Carrive, M., Cavero, J., Coutelas, A., Deiana, R., Ludovico, M. Di, Martino, G. De, Dubouloz, J., Letellier-taillefer, É., Maigret, A., Manfredi, G., Marchand-beaulieu, F., Milanese, A., Modena, C., Monier, F., Harcourt-péron, A., Pimpaud, A., Prota, A., Rizzo, E., Rossi, A., Santoriello, A., Tricoche, A., and Valluzzi, M. R. (2016). "Pompéi . Villa de Diomède. Campagne d'étude 2015." (August 2019).

Dobbins, J. J. (1994). "Problems of Chronology, Decoration, and Urban Design in the

Forum at Pompeii." *American Journal of Archaeology*, 98(4), 629.
Drdácký, M., Mašín, D., Mekonone, M., and Slížková, Z. (2008). "Compression tests on non-standard historic mortar specimens." *Proc. Historical Mortars Conference HMC08*.
Drosos, V., and Anastasopoulos, I. (2014). "Shaking table testing of multidrum columns and portals." *Earthquake Engineering & Structural Dynamics*, 43(11), 1703–1723.
Falcioni, C., Nosengo, S., and Pedemonte, S. (1995). "Valutazione della resistenza a compressione mono assiale di calcestruzzi e rocce mediante utilizzo degli sclerometri 'L' e 'N.'" *Revista Iberoamericana*, Professione geologo.
Faria, P., Henriques, F., and Rato, V. (2008). "Comparative evaluation of lime mortars for architectural conservation." *Journal of Cultural Heritage*, 9(3), 338–346.
Forde, M. C., Birjandi, K. F., and Batchelor, A. J. (1985). "Fault detection in stone masonry bridges by nondestructive testing." *Proc. 2nd International Conference Structural Faults & Repair*, Engineering Technics Press, Edinburgh, 373–379.
Garijo, L., Azenha, M., Ramesh, M., Lourenço, P. B., and Ruiz, G. (2019). "Stiffness evolution of natural hydraulic lime mortars at early ages measured through EMM-ARM." *Construction and Building Materials*, 216, 405–415.
Giuliani, C. F. (2007). *L'edilizia nell'antichità*.
Goldsworthy, H., and Min, Z. (2008). "Mortar Studies Towards the Replication of Roman Concrete." *Archaeometry*, 6(January 2008), 932–946.
Guidoboni, E., Ferrari, G., Mariotti, D., Comastri, A., Tarabusi, G., and Valensise, G. (2007). "Catalogue of Strong Earthquakes in Italy (461 B.C.-1997) and Mediterranean Area (760 B.C.-1500). INGV-SGA."
Haach, V. G., Vasconcelos, G., and Lourenço, P. B. (2011). "Influence of aggregates grading and water/cement ratio in workability and hardened properties of mortars." *Construction and Building Materials*, Elsevier Ltd, 25(6), 2980–2987.
Housner, G. W. (1963). "The behavior of inverted pendulum structures during earthquakes." *Bulletin of the Seismological Society of America*, 53(2), 403–417.
Hughes, J. J. (2012). "RILEM TC 203-RHM: Repair mortars for historic masonry. The role of mortar in masonry: an introduction to requirements for the design of repair mortars." *Materials and Structures/Materiaux et Constructions*, 45(9), 1287–1294.
ICOMOS. (2003). "Recommendations for the analysis, conservation and structural restoration of architectural heritage."
Italian Ministry of Cultural Heritage and Activities. (2010). "Linee guida per la valutazione e la riduzione del rischio sismico del patrimonio culturale con riferimento alle Norme tecniche per le costruzioni di cui al decreto del Ministero delle Infrastrutture e dei trasporti del 14 gennaio 2008."
Italian Presidency of the Council of Ministers. (2006). "Ordinance n. 3519. Criteri generali per l'individuazione delle zone sismiche e per la formazione e l'aggiornamento degli elenchi delle medesime zone, G.U. n.108 del 11/05/2006."
Izzo, F., Arizzi, A., Cappelletti, P., Cultrone, G., De Bonis, A., Germinario, C., Graziano, S. F., Grifa, C., Guarino, V., Mercurio, M., Morra, V., and Langella, A. (2016). "The art of building in the Roman period (89 B.C. - 79 A.D.): Mortars, plasters and mosaic floors from ancient Stabiae (Naples, Italy)." *Construction and Building Materials*, Elsevier Ltd, 117, 129–143.
Komodromos, P., Papaloizou, L., and Polycarpou, P. (2008). "Simulation of the response

of ancient columns under harmonic and earthquake excitations." *Engineering Structures*, 30(8), 2154–2164.

Konstantinidis, D., and Makris, N. (2005). "Seismic response analysis of multidrum classical columns." *Earthquake Engineering & Structural Dynamics*, 34(10), 1243–1270.

Lancaster, L. C. (2005). *Concrete vaulted construction in imperial Rome: Innovations in context*. *Concrete Vaulted Construction in Imperial Rome: Innovations in Context*.

Lancaster, L. C. (2015). *Innovative Vaulting in the Architecture of the Roman Empire*. *Innovative Vaulting in the Architecture of the Roman Empire*.

Lawrence, R. M. H. (2006). "A study of carbonation in non-hydraulic lime mortars." University of Bath.

Lawrence, R. M. H., Mays, T. J., Walker, P., and D'Ayala, D. (2006). "Determination of carbonation profiles in non-hydraulic lime mortars using thermogravimetric analysis." *Thermochimica Acta*, 444(2), 179–189.

Leone, G., De Vita, A., Magnani, A., and Rossi, C. (2016). "Characterization of archaeological mortars from Herculaneum." *Thermochimica Acta*, Elsevier B.V., 624, 86–94.

Lignola, G. P., Giamundo, V., and Cosenza, E. (2014). "Finite Element Modelling of the Archaeological Colonnade in Pompeii." *Civil-Comp Proceedings*.

Lindqvist, J. E., Balen, K. van, Bicer-Simsir, B., Binda, L., Bla¨uer, C., Elsen, J., Hansen, E., Hees, R. van, Henriques, F., Toumbakari, E. E., Konow, T. von, Lindqvist, J. E., Maurenbrecher, P., Middendorf, B., Papayanni, I., Simon, S., Subercaseaux, M., Tedeschi, C., Thompson, M., Valek, J., Valluzzi, M. R., Vanhellemont, Y., Veiga, R., and Waldum, A. (2009). "Rilem TC 203-RHM: Repair mortars for historic masonry. Testing of hardened mortars, a process of questioning and interpreting." *Materials and Structures/Materiaux et Constructions*, 42(7), 853–865.

Lindqvist, J. E., and Sandström, M. (2000). "Quantitative analysis of historical mortars using optical microscopy." *Materials and Structures*, 33(10), 612–617.

De Luca, R., Miriello, D., Pecci, A., Domínguez-Bella, S., Bernal-Casasola, D., Cottica, D., Bloise, A., and Crisci, G. M. (2015). "Archaeometric Study of Mortars from the Garum Shop at Pompeii, Campania, Italy." *Geoarchaeology*, 30(4), 330–351.

Magenes, G., Penna, A., Galasco, A., and Rota, M. (2010). "Experimental characterisation of stone masonry mechanical properties." *8th International Masonry Conference 2010*, (August 2015), 1–10.

Maiuri, A. (1942). *L'ultima fase edilizia di Pompei*. (ISTITUTO DI STUDI ROMANI - SEZIONE CAMPANA, ed.), Arte Tipografica, Naples.

de Martino, G., Giamundo, V., and Lignola, G. P. (2012). "Seismic vulnerability of the marble block colonnade of ancient forum in the archaeological site of Pompeii." *15th International Conference of Earthquake Engineering*, 4310–4323.

Masini, N., Sileo, M., Leucci, G., Soldovieri, F., D'Antonio, A., de Giorgi, L., Pecci, A., and Scavone, M. (2017). "Integrated In Situ Investigations for the Restoration: The Case of Regio VIII in Pompeii." 557–586.

Maurenbrecher, A. H. P., Trischuk, K., and Rousseau, M. Z. (2001). "Review of Factors Affecting the Durability of Repointing." *9th Canadian Masonry Symposium*, 1–12.

Mazzon, N. (2010). "Influence of grout injection on the dynamic behaviour of stone masonry buildings."

McCann, D. M., and Forde, M. C. (2001). "Review of NDT methods in the assessment of concrete and masonry structures." *NDT and E International*, 34(2), 71–84.

Milosevic, J., Gago, A. S., Lopes, M., and Bento, R. (2013a). "Experimental assessment of shear strength parameters on rubble stone masonry specimens." *Construction and Building Materials*, Elsevier Ltd, 47, 1372–1380.

Milosevic, J., Lopes, M., Gago, A. S., and Bento, R. (2013b). "Testing and modeling the diagonal tension strength of rubble stone masonry panels." *Engineering Structures*, Elsevier Ltd, 52, 581–591.

Minafò, G., Amato, G., and Stella, L. (2016). "Rocking Behaviour of Multi-Block Columns Subjected to Pulse-Type Ground Motion Accelerations." *The Open Construction and Building Technology Journal*, 10(1), 150–157.

Ministero della Pubblica Istruzione. (1972). "Carta italiana del restauro. Circolare n 117 del 6 aprile 1972 (in Italian)."

Miranda, L., Cantini, L., Guedes, J., Binda, L., and Costa, A. (2013). "Applications of sonic tests to masonry elements: Influence of joints on the propagation velocity of elastic waves." *Journal of Materials in Civil Engineering*, 25(6), 667–682.

Miranda, L. F., Rio, J., Miranda Guedes, J., and Costa, A. (2012). "Sonic Impact Method - A new technique for characterization of stone masonry walls." *Construction and Building Materials*, 36, 27–35.

Miriello, D., Barca, D., Bloise, A., Ciarallo, A., Crisci, G. M., De Rose, T., Gattuso, C., Gazineo, F., and La Russa, M. F. (2010). "Characterisation of archaeological mortars from Pompeii (Campania, Italy) and identification of construction phases by compositional data analysis." *Journal of Archaeological Science*, Elsevier Ltd, 37(9), 2207–2223.

Miriello, D., Bloise, A., Crisci, G. M., De Luca, R., De Nigris, B., Martellone, A., Osanna, M., Pace, R., Pecci, A., and Ruggieri, N. (2018a). "Non-destructive multi-analytical approach to study the pigments of wall painting fragments reused in mortars from the archaeological site of Pompeii (Italy)." *Minerals*, 8(4), 1–15.

Miriello, D., Bloise, A., Crisci, G. M., De Luca, R., De Nigris, B., Martellone, A., Osanna, M., Pace, R., Pecci, A., and Ruggieri, N. (2018b). "New compositional data on ancient mortars and plasters from Pompeii (Campania – Southern Italy): Archaeometric results and considerations about their time evolution." *Materials Characterization*, 146(September), 189–203.

Del Monte, E., and Vignoli, A. (2008). "IN SITU MECHANICAL CHARACTERIZATION OF THE MORTAR IN MASONRY BUILDINGS WITH DRMS." *SACoMaTiS 2008 International RILEM Conference*, 1–10.

Moradian, Z., and Behnia, M. (2009). "Predicting the Uniaxial Compressive Strength and Static Young's Modulus of Intact Sedimentary Rocks Using the Ultrasonic Test." *INTERNATIONAL JOURNAL OF GEOMECHANICS, vol. 9*, 14–19.

Moropoulou, A., Bakolas, A., and Aggelakopoulou, E. (2004a). "Evaluation of pozzolanic activity of natural and artificial pozzolans by thermal analysis." *Thermochimica Acta*, 420(1–2), 135–140.

Moropoulou, A., Bakolas, A., and Aggelakopoulou, E. (2004b). "Evaluation of pozzolanic activity of natural and artificial pozzolans by thermal analysis." *Thermochimica Acta*, Elsevier, 135–140.

Moropoulou, A., Bakolas, A., and Anagnostopoulou, S. (2005a). "Composite materials in ancient structures." *Cement and Concrete Composites*, 27(2), 295–300.

Moropoulou, A., Bakolas, A., Moundoulas, P., Aggelakopoulou, E., and Anagnostopoulou, S. (2005b). "Strength development and lime reaction in mortars for repairing historic masonries." *Cement and Concrete Composites,* 27(2), 289–294.

Mouzakis, H. P., Psycharis, I. N., Papastamatiou, D. Y., Carydis, P. G., Papantonopoulos, C., and Zambas, C. (2002). "Experimental investigation of the earthquake response of a model of a marble classical column." *Earthquake Engineering & Structural Dynamics,* 31(9), 1681–1698.

Negri, R. (2007). "Alla ricerca del 'saper fare' degli antichi nella Domus del Centenario." *Pompei. Insula del Centenario (IX, 8), I. Indagini diagnostiche geofisiche e analisi archeometriche,* Ante Quem, Bologna, 129–136.

De Nigris, B., and Previti, M. (2017). "L'affidabilità strutturale degli interventi di messa in sicurezza del patrimonio archeologico." *Ingegneria Forense, CRolli, Affidabilità Strutturale, Consolidamento,* N. Augenti and L. Jurina, eds., Dario Flaccovio Editore, Milan, 493–502.

Oliveira, M. A. N. (2015). "A Multi – Physics Approach Applied to Masonry Structures with Non – Hydraulic Lime Mortars." University of Minho.

Özkaya, Ö. A., and Böke, H. (2009). "Properties of Roman bricks and mortars used in Serapis temple in the city of Pergamon." *Materials Characterization*, Elsevier Inc., 60(9), 995–1000.

Ozlem Cizer. (2019). "COMPETITION BETWEEN CARBONATION AND HYDRATION ON THE HARDENING OF CALCIUM HYDROXIDE AND CALCIUM SILICATE BINDERS." *Journal of Chemical Information and Modeling*.

Papadopoulos, K., and Vintzileou, E. (2014). "Numerical Investigation of the Seismic Behaviour of Ancient Columns." *9th International Conference on Structural Analysis of Historical Constructions,* (October), 14–17.

Papadopoulos, K., Vintzileou, E., and Psycharis, I. N. (2019). "Finite element analysis of the seismic response of ancient columns." *Earthquake Engineering & Structural Dynamics*, 48(13), 1432–1450.

Papayanni, I., Pachta, V., Stefanidou, M., and Konopissi, S. (2012). "Survey of technological characteristics of structural mortars of different historical periods." *Structural Analysis of Historical Constructions*, J. Jasieńko, ed., Wrocław, 1248–1254.

Papayianni, I., and Hughes, J. (2019). "Testing properties governing the durability of lime-based repair mortars." *RILEM Technical Letters*, 3(2018), 135–139.

Papayianni, I., Pachta, V., and Stefanidou, M. (2013). "Analysis of ancient mortars and design of compatible repair mortars: The case study of Odeion of the archaeological site of Dion." *Construction and Building Materials*, Elsevier Ltd, 40, 84–92.

Pappas, A., da Porto, F., and Modena, C. (2016). "Seismic vulnerability assessment form for free-standing columns based on a simplified numerical analysis." *International Journal of Architectural Heritage*, Taylor & Francis, 10(2–3), 15583058.2015.1113336.

Pappas, A., Previato, C., Silva, B. Q., Porto, F., Bonetto, J., and Modena, C. (2014). "Multi-Parametric Seismic Vulnerability Assessment of Free-Standing Columns."

International Conference on Structural Analysis of Historical Constructions, (October), 14–17.

Parsekian, G. A., Fonseca, F. S., Pinheiro, G. L., and Camacho, J. S. (2014). "Properties of Mortar Using Cubes, Prism Halves, and Cylinder Specimens." *ACI Materials Journal*, 111(4).

Pesando, F. (2012). *Pompei. Le età di pompei*. 24 ORE Cultura srl, Milan.

Pesando, F., and Guidobaldi, M. P. (2006). *Pompei, Oplontis, Ercolano, Stabiae*. Laterza.

Picone, R. (2011). "Restauri di guerra a pompei. Le Case del Fauno e di Epidio Rufo." *Offese di guerra. Ricostruzione e restauri nel Mezzogiorno d'Italia*, S. Casiello, ed., Florence, 19–42.

Piovesan, R., Curti, E., Grifa, C., Maritan, L., and Mazzoli, C. (2009). "Petrographic and microstratigraphic analysis of mortar-based building materials from the Temple of Venus, Pompeii." *nterpreting Silent Artefacts: Petrographic Approaches to Archaeological Ceramics*, P. S. Quinn, ed., Archaeopress, Oxford, 65–79.

Pitilakis, K., and Tavouktsi, E. (2010). "Seismic Response of the Columns of Two Ancient Greek Temples in Rhodes and Lindos." *8th International Symposium on the Conservation of Monuments in the Mediterranean Basin, Patra.*, (1), Vol. 31.

Psycharis, I. N. (1990). "Dynamic behaviour of rocking two-block assemblies." *Earthquake Engineering & Structural Dynamics*, 19(4), 555–575.

Psycharis, I. N. (2018). "Seismic Vulnerability of Classical Monuments." *Recent Advances in Earthquake Engineering in Europe. 16th European Conference on Earthquake Engineering*, Thessaloniki, Greece, 563–582.

Psycharis, I. N., Lemos, J. V., Papastamatiou, D. Y., Zambas, C., and Papantonopoulos, C. (2003). "Numerical study of the seismic behaviour of a part of the Parthenon Pronaos." *Earthquake Engineering & Structural Dynamics*, 32(13), 2063–2084.

Psycharis, I. N., Papastamatiou, D. Y., and Alexandris, A. P. (2000). "Parametric investigation of the stability of classical columns under harmonic and earthquake excitations." *Earthquake Engineering & Structural Dynamics*, 29(8), 1093–1109.

Ramesh, M., Azenha, M., and Lourenço, P. B. (2019). "Quantification of impact of lime on mechanical behaviour of lime cement blended mortars for bedding joints in masonry systems." *Construction and Building Materials*, Elsevier Ltd, 229, 116884.

RILEM TC. (1994). "LUM B6 Diagonal tensile strength tests of small wall specimens, 1991." *RILEM Recommendations for the Testing and Use of Constructions Materials*, RILEM, ed., E & FN SPON, 488–489.

RILEM TC. (1996). "127- MS.D.1: Measurement of mechanical pulse velocity for masonry." *Materials and Structures*, 29, 463–466.

RILEM TC. (1998). "127- MS.D.2: Determination of masonry rebound hardness." *Materials and Structures*, 31, 363–377.

RILEM TC 25-PEM. (1980). "Recommended tests to measure the deterioration of stone and to assess the effectiveness of treatment methods." *Materials and Structures*, 13(75), 175–253.

Riva, G., Bettio, C., and Modena, C. (1997). "The use of sonic wave technique for estimating the efficiency of masonry consolidation by injection." *IB2MAC - 11h International Brick and Block Masonry Conference, Shanghai, China*, (October), 28–39.

La Russa, M. F., Ruffolo, S. A., Ricca, M., Rovella, N., Comite, V., De Buergo, M. A., Crisci, G. M., and Barca, D. (2015). "Archaeometric approach for the study of mortars from the underwater archaeological site of Baia (Naples) Italy: Preliminary results." *Periodico di Mineralogia*, 84(3A), 553–567.

Russlan, A. H., Sharkawi, A. M., and Abd Elnaby, S. F. M. (2018). "Performance of Modified Lime Mortar for Conservation of Ancient Buildings." *Second International Conference on Innovative Building Materials, IBMC18, HBRC,* Cairo, Egypt, IBMC (234).

Sarhosis, V., Lignola, G. P., and Asteris, P. G. (2016). "Seismic Vulnerability of Ancient Colonnade." *Civil and Environmental Engineering*, IGI Global, 950–974.

Scrivener, K., Snellings, R., and Lothenbach, B. (2018). *A Practical Guide to Microstructural Analysis of Cementitious Materials*. *A Practical Guide to Microstructural Analysis of Cementitious Materials*, (K. Scrivener, R. Snellings, and B. Lothenbach, eds.), CRC Press.

Silva, B., Dalla Benetta, M., Da Porto, F., and Valluzzi, M. R. (2014). "Compression and sonic tests to assess effectiveness of grout injection on three-leaf stone masonry walls." *International Journal of Architectural Heritage*, 8(3), 408–435.

Silva, B. L. (2012). "Diagnosis and Strengthening of Historical Masonry Structures: Numerical and Experimental Analysis."

Spanos, P. D., Roussis, P. C., and Politis, N. P. A. (2001). "Dynamic analysis of stacked rigid blocks." *Soil Dynamics and Earthquake Engineering*, 21(7), 559–578.

Spinazzola, V. (1953). *Pompei alla luce degli scavi nuovi di Via dell'Abbondanza (anni 1910-1923). Volume primo*. (S. Aurigemma, ed.), La Libreria dello Stato, Rome.

Toumbakari, E., and Psycharis, I. (2010). "Parametric investigation of the seismic response of a column of the Aphrodite Temple in Amathus , Cyprus." *14th European Conference on Earthquake Engineering*.

UNI EN 12372:2001. (2003). "Natural stone test methods - Determination of flexural strength under concentrated load." *Acustica*, 10969.

UNI EN 14580:2005. (2003). "Natural stone test methods - Determination of static elastic modulus." *Acustica*, 10969.

Válek, J., Hughes, J. J., and Groot, C. J. W. P. (2012). "Historic Mortars: Characterisation, Assessment and Repair. A State-of-the-Art Summary." *Historic Mortars. RILEM Bookseries, vol. 7,* J. Válek, J. J. Hughes, and C. J. W. P. Groot, eds., Springer, Dordrecht, 1–12.

Válek, J., and Veiga, R. (2005). "Characterisation of mechanical properties of historic mortars - Testing of irregular samples." *WIT Transactions on the Built Environment*, 83, 365–374.

Valluzzi, M. R. (2000). "Comportamento meccanico delle murature consolidate con materiali e tecniche a base di calce." Università degli studi di Trieste.

Valluzzi, M. R., Cescatti, E., Cardani, G., Cantini, L., Zanzi, L., Colla, C., and Casarin, F. (2018). "Calibration of sonic pulse velocity tests for detection of variable conditions in masonry walls." *Construction and Building Materials*, Elsevier Ltd, 192, 272–286.

Valluzzi, M. R., Lorenzoni, F., Deiana, R., Taffarel, S., and Modena, C. (2019). "Non-destructive investigations for structural qualification of the Sarno Baths, Pompeii." *Journal of Cultural Heritage*, Elsevier Masson SAS, 40, 280–287.

Vasanelli, E., Calia, A., Colangiuli, D., Miceli, F., and Aiello, M. A. (2016). "Assessing the reliability of non-destructive and moderately invasive techniques for the evaluation of uniaxial compression strength of stone masonry units." *Construction and Building Materials*, 124, 575–581.

Vasanelli, E., Colangiuli, D., Calia, A., Sileo, M., and Aiello, M. A. (2015). "Ultrasonic pulse velocity for the evaluation of physical and mechanical properties of a highly porous building limestone." *Ultrasonics*, Elsevier B.V., 60, 33–40.

Vasconcelos, G. F. M. (2005). "Experimental investigations on the mechanics of stone masonry: Characterization of granites and behavior of ancient masonry shear walls." *PhD Thesis*, 266.

Walker, R., and Pavía, S. (2011). "Physical properties and reactivity of pozzolans, and their influence on the properties of lime-pozzolan pastes." *Materials and Structures/Materiaux et Constructions*, 44(6), 1139–1150.

Yasar, E., and Erdogan, Y. (2004). "Correlating sound velocity with the density, compressive strength and Young's modulus of carbonate rocks." *International Journal of Rock Mechanics and Mining Sciences*, 41(5), 871–875.

WEB REFERENCES

www.cordis.europa.eu

www.ndt.net

www.niker.eu

www.stand4heritage.org

www.unipd.it

www.villadiomede.huma-num.fr

www.pompeiisites.org

www.whc.unesco.org

www.pompeiiperspectives.org

www.pompeiiinpictures.com

www.grandepompei.beniculturali.it

www.ponculturaesviluppo.beniculturali.it

www.uss-sisma2016.beniculturali.it

LEGISLATIVE FRAMEWORK AND RECOMMENDATIONS

Legislative Decree of 22 January 2004, no. 42, *Codice dei beni culturali e del paesaggio, ai sensi dell'articolo 10 della legge 6 luglio 2002, n. 137*

Directive of the President of the Council of Ministers of 9 February 2011, *Direttiva del Presidente del Consiglio dei Ministri 9 febbraio 2011. Linee guida per la valutazione e la riduzione del rischio sismico del patrimonio culturale con riferimento alle nuove Norme tecniche per le costruzioni di cui al decreto del Ministero delle infrastrutture e di trasporti del 14 gennaio 2008*

ICOMOS Charter, *Principles for the analysis, conservation and structural restoration of architectural heritage*, ratified by the ICOMOS 14th General Assembly in Victoria Falls, Zimbabwe, in 2003